Using simulation models to determine mechanisms driving outbreak dynamics and spatial distribution of environmentally transmitted pathogens

by

Amélie Coralie Dolfi

A dissertation submitted in partial fulfillment of

the requirements for the degree of

Doctor of Philosophy

(Forest and Wildlife Ecology)

at the

UNIVERSITY OF WISCONSIN-MADISON

2024

Date of final oral examination: August 7th, 2024

The dissertation is approved by the following members of the Final Examination Committee:

Wendy C. Turner, Research Professor, Forest and Wildlife Ecology
Timothy Van Deelen, Professor, Forest and Wildlife Ecology
Eliezer Gurarie, Affiliate Professor, Forest and Wildlife Ecology
Tony Goldberg, Professor, Pathobiological Sciences
Robin Russell, Research Scientist, US Fish and Wildlife Services, Colorado

"Remember that all models are wrong; the practical question is how wrong do they have to be to not be useful."

-- George P. Box

ACKNOWLEDGMENTS

For a starter, I want to thank my advisor Wendy Turner, for accepting me into a Ph.D. program in the USA. I have to admit, I had no idea what I was stepping into when I first applied; and here we are, 5 years later, and I am graduating from my Ph.D. So, I can never thank you enough, Wendy, for all the support you provided me along the road and for all the opportunities you opened. For all the trust you put in me. I feel lucky to have been one of your graduate students. I must also thank you for bringing Marie Gilbertson into the lab. Marie's guidance and help over the past years have been absolutely critical to my success and ability to finish my Ph.D. Thank you for making me a better scientist, for all the support you provided me, and for all the kind words you always finished our meetings with. I also want to thank each of my committee members, Tim VanDeelen, Elie Gurarie, Tony Goldberg, and Robin Russell, for accepting to be part of my Ph.D. journey while in the middle of a pandemic.

Next, I want to thank all the current and past members of the Turner Lab, especially Zoe Barandongo, Kimberlie Vera, Heather Inzalaco, Nurul Islam, Aaron Groves, Marie Gilbertson, Sunday Ochai, Yen-Hua Huang, Kristyna Rysava, Alizon Ketz, Ellen Brandell. Thanks for all the good times spent together, sharing a multitude of food delights over lab meetings. I also want to thank everyone in the anthrax research group, especially Pauline Kamath, Henriette Van Herdeen, and Kyree Kausrud. I am also very grateful to have been able to do fieldwork in Etosha National Park in Namibia (even if the pandemic delayed it by a few years!). I want to thank everyone at the Etosha Ecological Institute for being so kind and helpful, the rangers for their availability and flexibility, all the scientists who came through the research camp, and the Okaukuejo staff for the amazing time I had. I particularly want to thank Claudine Cloete, Werner Kilian, and Hendrina Joel for all the discussions we had around coffee and shortbread and all the field trips we went on.

I am also immensely grateful for the friends I made in the US, from all the karaoke friends in Albany to the sailing friends, climbing friends, baking and board gaming friends. I especially want to thank Riley, MacKenzie, Victor, Axel, Tatiana (my Ph.D. twin, as Zuzana once said!), Zakher, Quinn, Laura, Malena, Bijit, Celso, Tyler, Emma, Ewa, for their friendship and support, for all the moments we shared, and for all the amazing food we cooked and ate together. I am for sure going to miss all of you. I also want to thank my French friends, who have supported me in many ways, even with the 7-hour differences that separated us, especially Eliott, Laurie, Steven, et tous les foulafs, les anciens de La Martin, Bastien, Laura, Boris, Aline, Antoine, and Linda.

When I moved to Madison, I moved in with two strangers I met on Facebook market. Many people told me I was crazy, but this was the best decision I made! Cole and Austin, I will always be so thankful I moved in with you and not just two creepy guys! You have welcomed me with all your heart in the middle of the pandemic. Eddie and Clark were also a great bonus to our house! Thank you for all the evenings spent talking and playing and for the fabulous parties we had.

Martin, without you I have no idea in which state I would have finished this thesis. You helped me so much over these 5 years, even with all those kilometers that separated us. I have so many reasons to thank you, for all the support, the strength, the courage you gave me. Merci!

I have to switch to French now to thank my family. Je souhaite remercier ma famille pour son soutien inconditionnel, pour leur acceptation de me laisser partir seule dans un autre pays. Merci à mes parents, et merci à ma sœur et mon beau-frère pour leur soutien et pour m'avoir fait devenir tatie ! Merci pour tout.

Et maintenant s'ouvre un nouveau chapitre de ma vie !

And now a new chapter is opening in my life !

DISSERTATION ABSTRACT

Environmentally transmitted pathogens (ETPs) have been understudied despite their threats to the health of wildlife, domestic animals, and humans. These pathogens can survive for extended periods in the environment, and thus, understanding sources of variation in the off-host life stage is important for evaluating heterogeneity in host infection risk and outbreak dynamics. Variations among the three components of the epidemiological triangle (i.e., environment, host, and pathogen) may alter the timing, intensity, and spatial distribution of disease outbreaks. I first built a theoretical agent-based simulation model to assess how environmental characteristics, host behaviors, and ETP traits altered spatio-temporal patterns of disease dynamics. Model outcomes highlighted the dual roles of pathogen reservoir formation and host behavioral responses toward reservoirs in shaping the timing and intensity of outbreaks and the creation of high-risk pathogen hotspots on a landscape. I then applied this method to infection dynamics of *Bacillus anthracis*, the causative agent of anthrax. This widely distributed, multi-host pathogen must kill its host and be released into the environment where it forms persistent spores able to survive for years and transmit to new hosts. I focused on Etosha National Park, Namibia, where anthrax is endemic, unmanaged, and mostly affects mammalian herbivores. Combining a Poisson process model with long-term datasets on host behaviors and pathogen survival at reservoir sites, showed that early preference for foraging at infectious sites, combined with seasonality in spore concentrations at death, was a significant factor driving the number of secondary infections. Notably only wet-season formed reservoirs produced secondary infections. Finally, building an agent-based model of anthrax dynamics in Etosha, I showed that changes in host density, movement patterns, rainfall conditions, and pathogen persistence can significantly alter outbreak dynamics. In particular, smaller host range size, lower density and drought led to fewer host-pathogen encounters and

smaller outbreaks, while wetter conditions led to massive outbreaks, the intensity and timing depending on the host density. This dissertation highlights how variation in the environment, the hosts and the pathogens can profoundly modify ETP dynamics, emphasizing the necessity to study these three factors to infer the timing, intensity, and distribution of environmental diseases.

TABLE OF CONTENTS

LIST OF TABLES

LIST OF FIGURES

LIST OF PICTURES

LIST OF ABBREVIATIONS

ABM: Agent-based model

BA: *Bacillus anthracis*

CFU: Colony forming unit

CS: Continuous shedder

CWD: Chronic wasting disease

EEI: Etosha Ecological Institute

ETP: Environmentally transmitted pathogen

GPS: Global positioning system

LHS: Latin hypercube sampling

MAD: Month after death

NDVI: Normalized difference vegetation index

ODD: Overview, design concepts, and details

OK: Obligate-killer

PDF: Probability density function

PDP: Partial dependence plot

RSF: Resource selection function

SK: Shedder-killer

DISSERTATION INTRODUCTION

The recent COVID-19 pandemic shed a bright spotlight on the value of studying infectious disease dynamics. Indeed, infectious diseases—or those caused by pathogenic organisms that can spread among hosts within a population—are responsible for significant economic losses (Smith et al., 2019). They also pose a risk of spillover between wildlife, domestic animals, and/or humans (Plowright et al., 2017) and are a concern for species conservation as they can cause local extinction of wild populations (Smith et al., 2009). Studying disease dynamics is thus critical to better manage or mitigate the risk of disease outbreaks. To investigate disease outbreaks, we require knowledge about the pathogen itself, the hosts that the pathogen infects, and the environment in which host-pathogen interactions occur. These three components comprise the epidemiological triangle, which is essential to understanding how a disease moves through host populations and how pathogens survive (van Seventer and Hochberg, 2017).

One critical source of variation in pathogen transmission within a population depends upon the transmission mode. Two major transmission modes exist: direct and indirect. A directly transmitted pathogen requires close contact between an infected and a susceptible host to be transmitted. For example, the canine distemper virus spreads when animals cough or sneeze next to susceptible individuals (Martinez-Gutierrez and Ruiz-Saenz, 2016), the rabies virus is spread when an infected individual bites a susceptible one (Fisher et al., 2018), and chlamydia (*Chlamydia pecorum*) is transmitted during sexual intercourse (Burach et al., 2014). Indirect transmission happens when the pathogen can survive outside a host long enough to be transmitted to the next one, either through the external environment, or via a vector, i.e., an intermediary host that helps transmit the pathogen. Many vectors are arthropods, such as mosquitoes, ticks, and fleas, and

transmit numerous pathogens. The mosquito *Aedes aegypti,* can transmit dengue fever, yellow fever, chikungunya, and Zika viruses to humans (Leta et al., 2018). Ticks transmit Lyme disease, babesiosis, or tick-borne encephalitis, among others (Madison-Antenucci et al., 2020). When no vectors are required, transmission can occur from contact between a susceptible host and contaminated environments. For example, *Vibrio cholerae* (Rebaudet et al., 2013), *Salmonella* spp. (Holschbach and Peek, 2018), and *Escherichia coli* (Chekabab et al., 2013) are transmitted to humans by ingestion of contaminated food or water. While direct transmission represents the most common transmission mode, certain pathogens can combine multiple pathways, such as *Yersinia pestis*, the cause of the plague, which can be transmitted by fleas and from contaminated environments (Easterday et al., 2012), or chronic-wasting disease (CWD) caused by a prion, which can be transmitted from direct contact, and environmental reservoirs (Potapov et al., 2016). Theoretical studies have largely focused on directly transmitted diseases and more recently on vector-borne pathogens compared to environmentally transmitted diseases (Hollingsworth et al., 2015).

Environmentally transmitted pathogens (ETPs) have the particularity of surviving outside their hosts for extended periods, from hours to decades (Gerba, 2009). Persistent ETPs specifically can maintain diseases in an ecosystem and allow re-emergence of outbreaks long after they had seemingly faded out. Environmental reservoirs for avian influenza are believed to explain the re-emergence of the disease 2-4 years after it disappeared (Breban et al., 2009; Rohani et al., 2009). White-nose syndrome, caused by *Pseudogymnoascus destructans,* a fungus infecting hibernating bats, can survive within the roosting habitat while bats are away during the summer periods, allowing re-infection of bats every year (Hoyt et al., 2021). ETPs are often considered to be opportunistic pathogens as they are non-specific, do not require a host to survive and can become

pathogenic under certain conditions (Brown et al., 2012). This makes them harder to manage, as targeting the environment rather than a host is essential in these systems (Anttila et al., 2015, 2013; Samsing and Barnes, 2024). Different strategies have been observed to ensure pathogen survival in the external environment. Sporulation is a well-studied strategy among bacteria (*Bacillus* spp. and *Clostridium* spp. especially, [Swick et al., 2016]), but other pathogens such as fungi can sporulate to facilitate their survival in the environment (Huang and Hull, 2017). Spores are very resistant to unfavorable abiotic conditions and allow pathogens to survive for extended periods (Bressuire-Isoard et al., 2018; Nicholson et al., 2000). Certain pathogens are also able to grow in the environment, such as fungi like *Coccidioides* spp. (del Rocío Reyes-Montes et al., 2016) and *Pseudogymnoascus destructans* (Reynolds et al., 2015), or bacteria like the fish pathogen *Flavobacterium columnare* (Suomalainen et al., 2006). This external growth, often slow under unfavorable conditions, allows these microbes to be maintained between infections or until favorable conditions arise (Denham et al., 2019). Pathogens have also been observed in symbiotic relationships, notably in aquatic systems where associations with zooplankton have been observed (Perera et al., 2022). For example, the presence of copepods in water is associated with a longer survival of *Vibrio* spp. (Mueller et al., 2007; Nuttall and Moisander, 2023). Comprehending the mechanisms allowing ETPs to survive for extended periods in the environment is necessary, as differences in survival can impact disease dynamics and thus management strategies (Sinclair et al., 2012).

Depending on the pathogen, ETPs can be released into the environment in different patterns, which is likely to influence subsequent infection risk and its spatial distribution. Understanding the spatial distribution of ETPs is significant as this can alter the contact rate and thus, the number of infections. Certain pathogens are released by their hosts continuously or semi-

continuously in small quantities over the infection duration via urine (e.g. *Leptospira* spp. [Zaidi et al., 2018]), feces (e.g., *Campylobacter* spp. and *Salmonella* spp.; [Siembieda et al., 2011]), and other body fluids. Other ETPs, called obligate killers, must kill their hosts to be released into the environment and transmitted to the next host. Those pathogens are released in large quantities at the host death site (e.g., *Bacillus anthracis*, responsible for anthrax disease [Hugh-Jones and de Vos, 2002]; baculoviruses in Lepidoptera [Redman et al., 2016]; or *Metschnikowia bicuspidata* fungus in *Daphnia dentifera* [Sánchez et al., 2023]). Finally, pathogens can be released through both modes (e.g., CWD, which is shed in urine, feces, saliva, scent gland secretions, and upon host death [Haley et al., 2009; Schramm et al., 2006]; *Batrachochytrium salamandrivorans* released from skin and upon host death [Carter et al., 2024]; *Erysipelothrix rhusiopathiae*, a bacterium released in feces and upon host death infecting multiple hosts such as muskoxen (*Ovibos moschatus*) and swine [Mavrot et al., 2020; Ugochukwu et al., 2019]). Due to differences in how, where and when pathogens are released from infected hosts and differences in survival rates in the environment, it can be complex to study ETPs in free-ranging wildlife (Becker et al., 2023). Specifically, for highly persistent ETPs, determining temporal infection risk can be challenging as it may require years of intensive fieldwork (Barandongo et al., 2023; Turner et al., 2014).

Individual heterogeneity in hosts can also have important effects on disease dynamics and the spatial distribution of pathogens. Indeed, characteristics pertaining to host heterogeneity, such as age, physiology, and behaviors can alter host susceptibility and disease dynamics (Hawley and Altizer, 2011). For ETPs, behavioral modifications linked to visual cues of pathogen presence in an environment can alter the risk of contact and, thus, the dynamic of a disease (e.g., the landscape of disgust [Buck et al., 2018; Weinstein et al., 2018]). This has a particular implication for trying to obtain the basic reproduction number, R_0, of an ETP, which represents the average number of

individuals, in a fully susceptible population, an infected host may infect over its infectious period (Diekmann et al., 1990). This parameter has often been obtained for directly transmitted pathogens (Alimohamadi et al., 2020; Guerra et al., 2017), however, determining this parameter for an ETP proves challenging for multiple reasons (Blackburn et al., 2019). First, extended pathogen survival in the environment allows a time lag between the creation of environmental pathogen reservoirs and infection of secondary hosts (e.g., decadal anthrax outbreaks in Kruger National Park, South Africa, [Huang et al., 2022]). Second, host behavioral decisions to engage with a reservoir can evolve over time, as does the infectivity of the reservoir (Turner et al., 2014) adding more complexity to estimating the reproduction number of those pathogens. Third, the distribution of reservoirs in a heterogeneous environment can have consequences in terms of the number of encounters and initial risk of a reservoir (Gajewski et al., 2024). Specifically, fragmentation and resource distribution may affect host movements, altering both the contact risk and the spatial distribution of pathogens (Belasen et al., 2022; Suzán et al., 2008). Finally, differences in host susceptibility and immunity can have repercussions for both the distribution of pathogens in the environment and their initial infectivity potential. For example, super-shedder individuals can release an unexpectedly high quantity of pathogens into the environment (Chase-Topping et al., 2008; Matthews et al., 2009), contributing disproportionally to transmission risk by creating localized pathogen transmission risk hot spots. Understanding and managing ETPs is thus reliant upon unraveling the complex relationships arising from variation in the pathogens, hosts, and the environment, emphasizing the importance of studying all sides of the epidemiological triangle.

Mathematical models have been widely used to predict the risks that infectious diseases pose to human and animal populations and to determine how to reduce transmission. With the increased computational capacities and knowledge about disease transmission, model designs have

evolved toward the inclusion of more ecological complexity, going from, for example, non-spatially explicit compartmental models (Susceptible-Infected-Recovered models and their derivates, Stone et al., 2012) to reaction-diffusion models (Lou and Salako, 2023), contact network analysis (Craft, 2015), metapopulation approaches (Ball et al., 2015) and spatially explicit agent-based models (ABM, Tracey et al., 2014). Specifically, the use of ABMs in epidemiology has increased in the past decade largely due to their ability to model complex relationships between the environment, the host, and the pathogen (Carlos et al., 2023; Lane-deGraaf et al., 2013; Perez and Dragicevic, 2009; Strasburg and Christensen, 2024). ABMs allow modeling of individual organisms, called agents, moving in a spatially explicit environment that is able to change over time. By modeling at the individual level, ABMs facilitate the integration of different sources of heterogeneity and determination of the components most important for the disease dynamics. Indeed, each agent follows a set of pre-defined rules, allowing them to react depending on their surroundings and their individual characteristics (Railsback and Grimm, 2019). By computing complex relationships, these models can inform us about the underlying processes that allow an infectious disease to spread throughout a population and the direct and indirect consequences of disease management (Willem et al., 2017). For example, many ABMs were developed to understand transmission risks and spatial distribution of vector-borne diseases, notably by focusing on the role of human movement in the movement of vectors and ways to limit the spatial spread of the associated disease (e.g., dengue virus [Karl et al., 2014; Miksch et al., 2019]; malaria [Alam et al., 2017; Pizzitutti et al., 2018; Smith et al., 2018], or human African trypanosomiasis [Alderton et al., 2018; Grébaut et al., 2016]). ABMs for managing CWD in cervids through hunter-harvest decisions consider direct transmission only (Belsare et al., 2020; Belsare and Stewart, 2020). However, environmental transmission of CWD is believed to have a role in CWD spread when the

disease becomes endemic in a region (Thompson et al., 2024). Specifically, when environmental transmission occurs, ABMs can be very useful due to the ability to integrate individual host movement decisions, a major component to determine the number of encounters between hosts and reservoirs, a parameter necessary to estimate the risk of transmission for ETPs (Bonnell et al., 2018; Dougherty et al., 2018). While ABMs can be useful based on their capacity to include heterogeneity of hosts, pathogens and landscape, they are computationally time-consuming, and require substantial data input, calibration, and validation, making them very ecosystem specific (Niemann et al., 2021; Sun et al., 2016)..

In my dissertation, I used ABMs to study the mechanisms driving variation in timing, intensity, and spatial distribution of disease outbreaks caused by ETPs. Notably, I was interested in how the three sides of the epidemiological triangle—the pathogen, the host, and the environment—interact to create specific spatiotemporal disease dynamic patterns. ABMs are a useful methodology as they allow the inclusion of many variations in the pathogen, and in host ecology; as well as to re-create the emergence of specific host-pathogen interactions depending on the environmental properties, such as the landscape structure or the role of abiotic factors. By their capacity to be spatially-explicit and built around individual agents, information such as the number of contacts an individual has with a reservoir, the locations where infections occurred or when, and where pathogens are released can be obtained from ABM simulations. These are specifically important as they are directly linked to the spatial properties of ETPs, as well as the timing and intensity of outbreaks. While I started my research journey with a general approach to understanding ETPs, I specialized on anthrax transmission among its herbivorous hosts in Etosha National Park, Namibia (hereafter Etosha).

Anthrax, caused by the gram-positive bacterium *Bacillus anthracis* (BA), is an obligate-killer ETP found in all inhabited continents (Carlson et al., 2019). This pathogen has been studied for decades, in a very large variety of ecosystems and among different host species (Australia [Barro et al., 2016], Africa [Adesola et al., 2024], Asia [Sardar et al., 2023] Europe [Schmid and Kaufmann, 2002], or North America [Nekorchuk et al., 2019]). Thanks to the numerous studies among a large range of ecosystems and hosts, anthrax is a well-suited ETP for investigating the roles of environmental specificities, host ecology, and pathogen characteristics on emergence and maintenance of an ETP. Three natural exposure pathways to anthrax exist, including inhalation, a mostly uncommon pathway with the highest mortality risk; cutaneous, which has a low risk of mortality; and gastrointestinal, which has a relatively high mortality risk if untreated. For humans, the cutaneous pathway is most common, notably among farmers and butchers handling infected meat or animal products (Islam et al., 2013), inhalation is of greatest concern for bioterrorism (Goel, 2015), and a fourth transmission pathway specific to humans includes injectional anthrax from administration of contaminated intravenous drugs (Berger et al., 2014). In wildlife, gastrointestinal exposure is the main transmission pathway and occurs from different exposure ways such as from grazing, browsing, drinking, or bone-handling (Hugh-Jones and de Vos, 2002; Turner et al., 2014) (figure 1).

The anthrax bacterium has two life forms: vegetative cells and spores. Upon uptake by a host, BA spores germinate into vegetative cells, which proliferate and release toxins, causing septicemia and death within a few days (Beyer and Turnbull, 2009). At host death, blood fails to clot and hemorrhages, releasing vegetative cells into the environment, where they must sporulate or die (Dragon and Rennie, 1995). BA spores are highly resistant to abiotic factors and can survive for extended periods in the environment, usually decades (Barandongo et al., 2023; Dragon and

Rennie, 1995). The ability of BA spores to persist in the environment for long periods allows the disease to re-emerge after years without a single case recorded, creating regional epidemic anthrax outbreaks. For example, six outbreaks, killing thousands of wood bison (*Bison bison athabascae)* were recorded in the Canadian Northwest Territories between 1963 and 2006 (Dragon et al., 1999; Nishi et al., 2007). Similarly, major outbreaks in Kruger National Park, South Africa historically occurred at a decadal interval, with thousands of recorded cases (Huang et al., 2022; Pienaar, 1961). In contrast, certain ecosystems are considered anthrax endemic, due to the recurrent observation of usually small anthrax outbreaks, such as observed in Kenya (Muturi et al., 2018), Bangladesh (Chakraborty et al., 2012; Islam et al., 2016), Zambia (Munang'andu et al., 2012) or Namibia, especially Etosha (Lindeque and Turnbull, 1994).

Anthrax outbreaks in Etosha have been studied extensively for multiple decades and are unmanaged, allowing natural outbreak cycles to be observed (Barandongo et al., 2023; Cizauskas et al., 2014; Ebedes, 1976; Huang et al., 2021; Lindeque and Turnbull, 1994; Turner et al., 2013). BA is considered to have originated in southern Africa (Keim et al., 1997), and anthrax is endemic in Etosha, making this location a notable system for studying anthrax outbreaks. Etosha is a semi-arid savanna with outbreaks recorded yearly among mammalian herbivores (Turner et al., 2013). Anthrax is strongly seasonal and, in Etosha, cases peak during the end of the wet season (March-April) among the two most abundant grazers, plains zebra (*Equus quagga*) and blue wildebeest (*Connochaetes taurinus*) (Turner et al., 2013). Mixed-feeders (i.e., those consuming a mix of grasses and leaves of woody vegetation or browse) are the second most impacted species, especially the springbok (*Antidorcas marsupialis*) and African elephant (*Loxodonta africana*), the latter having most cases recorded during the dry season. Finally, browsers, although susceptible to the disease, are only seldom infected. Thanks to the availability of long-term datasets, the regular

and stable observations of outbreaks and the diversity of host species, Etosha is a prominent ecosystem to make inferences on the drivers of anthrax disease dynamics.

For my first chapter, I was interested in understanding how hosts' behavioral decisions, pathogens' dynamics, and landscape features alter ETPs' disease dynamics and spatial distribution. While theoretical models are abundant for direct and vector-borne diseases, they are lacking for ETPs. Thus, I developed a theoretical simulation ABM to determine which of the host behaviors, pathogen characteristics, and environmental features drive ETPs outbreak dynamics and spatial distribution. Establishment and maintenance of the disease was mostly influenced by host behavioral decisions when facing an environmental reservoir, the persistence of the pathogen in the environment, and the initial concentration of pathogen released into the environment. The spatial distribution of the ETPs in the landscape was most influenced by the pathogen release pattern from the infected host, with pathogens released upon death creating few highly infectious hotspots, while pathogens released from shedding created many low-infectivity risk zones. This theoretical model allowed us to emphasize the significant role of host decisions on disease dynamics, and of ETP release mechanisms on the spatial distribution of outbreaks.

Then, my overall goal was to adapt this simulation model to anthrax outbreaks in Etosha to understand how each side of the epidemiological triangle shapes the endemicity of anthrax outbreaks in this system. However, to develop and parameterize an ABM for anthrax in Etosha, some key parameters were still required, notably the exposure risk associated with anthrax reservoir encounters. Thus, my second chapter focused on determining the reproduction number of anthrax reservoirs in Etosha. I used a three-year camera trap dataset combined with a Poisson process model to simulate the reproduction number R of anthrax, defined as the number of hosts an anthrax reservoir may infect over its infectious period, considering a non-naïve population.

From the camera trap analysis, plains zebra and blue wildebeest seem to encounter anthrax reservoirs at random, but the probability of grazing on reservoirs was higher than on control sites. Upon effective contact with a reservoir, our model estimated that 10^7 to 10^8 spores needed to be ingested for a lethal infection to occur. Due to strong seasonality in anthrax reservoir infectivity, only reservoirs formed during the wet season resulted in secondary infections; dry-season formed reservoirs led to no additional cases. The temporal variation in BA spore concentration and host behavior towards environmental reservoirs were important for calculating the reproduction number of a reservoir, with most of the secondary infections occurring within three years of reservoir establishment. This study highlighted the challenge posed by persistent ETPs in recording the number of secondary infections arising from a single reservoir over its entire infectious period. It also highlighted the necessity of characterizing host behavior at environmental reservoirs, as behavioral choices can alter contact rates and thus the dynamics of a disease.

Finally, my third chapter consisted of integrating the insights obtained from my first two chapters and from the extensive research conducted on anthrax in Etosha to build an ABM to investigate the interplay among environmental variation, host ecology, and pathogen persistence on anthrax dynamics in Etosha. By varying rainfall conditions, the seasonality of outbreaks in Etosha was lost, both under drought and wetter conditions. However, under drought conditions, the number of cases recorded dropped rapidly, while under wetter conditions, the number of cases tended to be very high. Notably, when host density was high, we could simulate epidemic-like outbreaks, with large outbreaks causing a decline in the host population, leading to a substantial drop in cases thereafter. Varying host range sizes also significantly impacted outbreaks. Indeed, a smaller range size led to fewer cases due to a decline in reservoir encounters. This ABM specialized on anthrax unraveled the importance of the abiotic conditions on the maintenance of

anthrax outbreaks in the Etosha system. Indeed, changes in rainfall, and hence vegetation, had significant impact on the movement of herbivorous hosts, which altered exposure risk, leading to a drop in cases or to massive outbreaks. These results emphasize the necessity of including variation along the three sides of the epidemiological triangle, and the subsequent interactions that stem from modification of a single component.

By developing a theoretical ABM and then applying it to a specific system, I was able to unravel some key sources of variation in ETP outbreak dynamics and spatial distributions. Notably, host behavior when encountering a reservoir, specifically the decision to engage with it or not is a major component required to estimate the intrinsic risk a reservoir poses in an environment. For anthrax, while no direct attraction toward reservoirs on a landscape was observed, the probability of interacting with an infectious site once it was encountered was higher than for non-infectious sites, emphasizing the necessity of fine-scale behavioral data. Knowing pathogen survival rates in an environment and the associated pathogen concentration present at a reservoir over time proved to be an important component of understanding the timing and intensity of outbreaks. While BA can be detected a decade after host death at a carcass site, the risk of effective anthrax transmission was present only within the first few years of reservoir creation. Seasonality of cases was extremely important for anthrax, as during the unfavorable dry season of Etosha, the concentration of BA spores formed at carcass sites was for the most part below transmission levels. Finally, environmental conditions, mostly abiotic factors, were shown to be extremely important as they can alter host movements, which can then alter host-pathogen encounter rates, destabilizing the endemicity of anthrax in Etosha. To conclude, my dissertation emphasizes the importance of studying how hosts, pathogen and environment interact, and how variation in any side of the

epidemiological triangle may affect the disease dynamics in term of timing, intensity and spatial distribution.

Figures

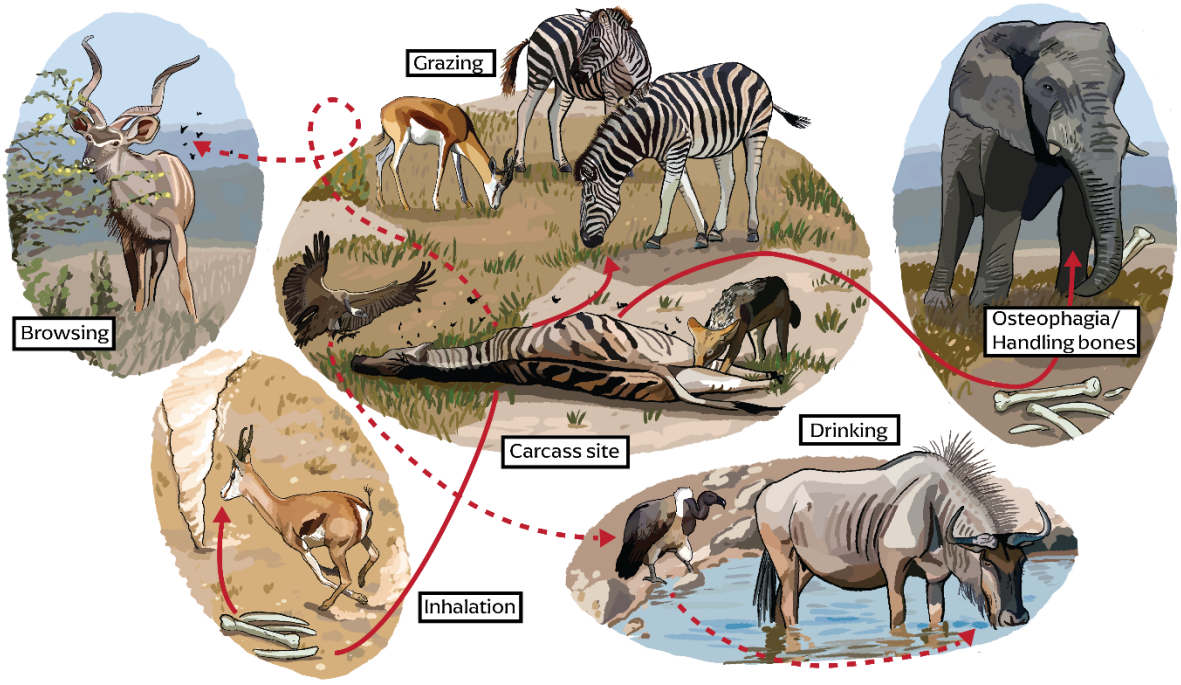

FIGURE 1: The main anthrax transmission pathways hypothesized for herbivorous wildlife. The main transmission mode for grazers is from grazing at infectious carcass sites. Browser species are infected when foraging on leaves that have been contaminated with *Bacillus anthracis* by blowflies after deposition of spores from their emesis and feces following the consumption of infected body fluids. Inhalation, while a possible pathway from dust exposure is likely uncommon. Osteophagia and bone handling may lead to anthrax transmission. Finally, drinking at water sources contaminated by anthrax carcasses or scavengers is a possible anthrax transmission pathway. Illustration from Huang et al., (2022), by Andi Kur, Sequential Potential.

References

Adesola, R.O., Okeke, V.C., Hamzat, A., Onawola, D.A., Arthur, J.F., 2024. Unraveling the binational outbreak of anthrax in Ghana and Nigeria: an in-depth investigation of epidemiology, clinical presentations, diagnosis, and plausible recommendations toward its eradication in Africa. Bull. Natl. Res. Cent. 48, 45. https://doi.org/10.1186/s42269-024-01203-4

Alam, Md.Z., Niaz Arifin, S.M., Al-Amin, H.M., Alam, M.S., Rahman, M.S., 2017. A spatial agent-based model of *Anopheles vagus* for malaria epidemiology: examining the impact of vector control interventions. Malar. J. 16, 432. https://doi.org/10.1186/s12936-017-2075-6

Alderton, S., Macleod, E.T., Anderson, N.E., Machila, N., Simuunza, M., Welburn, S.C., Atkinson, P.M., 2018. Exploring the effect of human and animal population growth on vector-borne disease transmission with an agent-based model of Rhodesian human African trypanosomiasis in eastern province, Zambia. PLoS Negl. Trop. Dis. 12, e0006905. https://doi.org/10.1371/journal.pntd.0006905

Alimohamadi, Y., Taghdir, M., Sepandi, M., 2020. Estimate of the basic reproduction number for COVID-19: A systematic review and meta-analysis. J. Prev. Med. Pub. Health 53, 151–157. https://doi.org/10.3961/jpmph.20.076

Anttila, J., Kaitala, V., Laakso, J., Ruokolainen, L., 2015. Environmental variation generates environmental opportunist pathogen outbreaks. PLOS ONE 10, e0145511. https://doi.org/10.1371/journal.pone.0145511

Anttila, J., Ruokolainen, L., Kaitala, V., Laakso, J., 2013. Loss of competition in the outside host environment generates outbreaks of environmental opportunist pathogens. PLOS ONE 8, e71621. https://doi.org/10.1371/journal.pone.0071621

Barandongo, Z.R., Dolfi, A.C., Bruce, S.A., Rysava, K., Huang, Y.-H., Joel, H., Hassim, A., Kamath, P.L., van Heerden, H., Turner, W.C., 2023. The persistence of time: the lifespan of *Bacillus anthracis* spores in environmental reservoirs. Res. Microbiol., Insights into the Bacillus anthracis cereus thuringiensis 2022 conference 174, 104029. https://doi.org/10.1016/j.resmic.2023.104029

Barro, A.S., Fegan, M., Moloney, B., Porter, K., Muller, J., Warner, S., Blackburn, J.K., 2016. Redefining the Australian anthrax belt: modeling the ecological niche and predicting the geographic distribution of *Bacillus anthracis*. PLoS Negl. Trop. Dis. 10, e0004689. https://doi.org/10.1371/journal.pntd.0004689

Becker, D.J., Eby, P., Madden, W., Peel, A.J., Plowright, R.K., 2023. Ecological conditions predict the intensity of Hendra virus excretion over space and time from bat reservoir hosts. Ecol. Lett. 26, 23–36. https://doi.org/10.1111/ele.14007

Belasen, A.M., Amses, K.R., Clemons, R.A., Becker, C.G., Toledo, L.F., James, T.Y., 2022. Habitat fragmentation in the Brazilian Atlantic Forest is associated with erosion of frog immunogenetic diversity and increased fungal infections. Immunogenetics 74, 431–441. https://doi.org/10.1007/s00251-022-01252-x

Belsare, A.V., Gompper, M.E., Keller, B., Sumners, J., Hansen, L., Millspaugh, J.J., 2020. An agent-based framework for improving wildlife disease surveillance: A case study of chronic wasting disease in Missouri white-tailed deer. Ecol. Model. 417, 108919. https://doi.org/10.1016/j.ecolmodel.2019.108919

Belsare, A.V., Stewart, C.M., 2020. OvCWD: An agent-based modeling framework for informing chronic wasting disease management in white-tailed deer populations. Ecol. Solut. Evid. 1, e12017. https://doi.org/10.1002/2688-8319.12017

Berger, T., Kassirer, M., Aran, A.A., 2014. Injectional anthrax - new presentation of an old disease. Eurosurveillance 19, 20877. https://doi.org/10.2807/1560-7917.ES2014.19.32.20877

Beyer, W., Turnbull, P.C.B., 2009. Anthrax in animals. Mol. Aspects Med., Anthrax 30, 481–489. https://doi.org/10.1016/j.mam.2009.08.004

Blackburn, J.K., Ganz, H.H., Ponciano, J.M., Turner, W.C., Ryan, S.J., Kamath, P., Cizauskas, C., Kausrud, K., Holt, R.D., Stenseth, N.C., Getz, W.M., 2019. Modeling R_0 for pathogens with environmental transmission: animal movements, pathogen populations, and local infectious zones. Int. J. Environ. Res. Public. Health 16, 954. https://doi.org/10.3390/ijerph16060954

Bonnell, T.R., Ghai, R.R., Goldberg, T.L., Sengupta, R., Chapman, C.A., 2018. Spatial configuration becomes more important with increasing habitat loss: a simulation study of environmentally-transmitted parasites. Landsc. Ecol. 33, 1259–1272. https://doi.org/10.1007/s10980-018-0666-4

Breban, R., Drake, J.M., Stallknecht, D.E., Rohani, P., 2009. The role of environmental transmission in recurrent avian influenza epidemics. PLOS Comput. Biol. 5, e1000346. https://doi.org/10.1371/journal.pcbi.1000346

Bressuire-Isoard, C., Broussolle, V., Carlin, F., 2018. Sporulation environment influences spore properties in *Bacillus*: evidence and insights on underlying molecular and physiological mechanisms. FEMS Microbiol. Rev. 42, 614–626. https://doi.org/10.1093/femsre/fuy021

Brown, S.P., Cornforth, D.M., Mideo, N., 2012. Evolution of virulence in opportunistic pathogens: generalism, plasticity, and control. Trends Microbiol. 20, 336–342. https://doi.org/10.1016/j.tim.2012.04.005

Buck, J.C., Weinstein, S.B., Young, H.S., 2018. Ecological and evolutionary consequences of parasite avoidance. Trends Ecol. Evol. 33, 619–632. https://doi.org/10.1016/j.tree.2018.05.001

Burach, F., Pospischil, A., Hanger, J., Loader, J., Pillonel, T., Greub, G., Borel, N., 2014. *Chlamydiaceae* and *Chlamydia*-like organisms in the koala (*Phascolarctos cinereus*)—Organ distribution and histopathological findings. Vet. Microbiol. 172, 230–240. https://doi.org/10.1016/j.vetmic.2014.04.022

Carlos, G.-C., Beatriz, M.-L., Carles, C., Raquel, C.-C., Emmanuel, S., Josep Maria, L.-M., Jordi, S.-C., Santiago, L., Jorge Ramón, L.-O., 2023. Assessing the epidemiological risk at the human-wild boar interface through a one health approach using an agent-based model in Barcelona, Spain. One Health 17, 100598. https://doi.org/10.1016/j.onehlt.2023.100598

Carlson, C.J., Kracalik, I.T., Ross, N., Alexander, K.A., Hugh-Jones, M.E., Fegan, M., Elkin, B.T., Epp, T., Shury, T.K., Zhang, W., Bagirova, M., Getz, W.M., Blackburn, J.K., 2019. The global distribution of *Bacillus anthracis* and associated anthrax risk to humans, livestock and wildlife. Nat. Microbiol. 4, 1337–1343. https://doi.org/10.1038/s41564-019-0435-4

Carter, E.D., DeMarchi, J.A., Wilber, M.Q., Miller, D.L., Gray, M.J., 2024. *Batrachochytrium salamandrivorans* is necronotic: carcasses could play a role in Bsal transmission. Front. Amphib. Reptile Sci. 2. https://doi.org/10.3389/famrs.2024.1284608

Chakraborty, A., Khan, S.U., Hasnat, M.A., Parveen, S., Islam, M.S., Mikolon, A., Chakraborty, R.K., Ahmed, B.-N., Ara, K., Haider, N., Zaki, S.R., Hoffmaster, A.R., Rahman, M., Luby, S.P., Hossain, M.J., 2012. Anthrax outbreaks in Bangladesh, 2009–2010. Am. J. Trop. Med. Hyg. 86, 703–710. https://doi.org/10.4269/ajtmh.2012.11-0234

Chase-Topping, M., Gally, D., Low, C., Matthews, L., Woolhouse, M., 2008. Super-shedding and the link between human infection and livestock carriage of *Escherichia coli* O157. Nat. Rev. Microbiol. 6, 904–912. https://doi.org/10.1038/nrmicro2029

Chekabab, S.M., Paquin-Veillette, J., Dozois, C.M., Harel, J., 2013. The ecological habitat and transmission of *Escherichia coli* O157:H7. FEMS Microbiol. Lett. 341, 1–12. https://doi.org/10.1111/1574-6968.12078

Cizauskas, C.A., Bellan, S.E., Turner, W.C., Vance, R.E., Getz, W.M., 2014. Frequent and seasonally variable sublethal anthrax infections are accompanied by short-lived immunity in an endemic system. J. Anim. Ecol. 83, 1078–1090. https://doi.org/10.1111/1365-2656.12207

Craft, M.E., 2015. Infectious disease transmission and contact networks in wildlife and livestock. Philos. Trans. R. Soc. B Biol. Sci. 370, 20140107. https://doi.org/10.1098/rstb.2014.0107

del Rocío Reyes-Montes, M., Pérez-Huitrón, M.A., Ocaña-Monroy, J.L., Frías-De-León, M.G., Martínez-Herrera, E., Arenas, R., Duarte-Escalante, E., 2016. The habitat of *Coccidioides* spp. and the role of animals as reservoirs and disseminators in nature. BMC Infect. Dis. 16, 550. https://doi.org/10.1186/s12879-016-1902-7

Denham, S.T., Wambaugh, M.A., Brown, J.C.S., 2019. How environmental fungi cause a range of clinical outcomes in susceptible hosts. J. Mol. Biol., Jekyll and Hyde: Bugs with

Double Personalities that Muddle the Distinction Between Commensal and Pathogen 431, 2982–3009. https://doi.org/10.1016/j.jmb.2019.05.003

Diekmann, O., Heesterbeek, J.A.P., Metz, J.A.J., 1990. On the definition and the computation of the basic reproduction ratio R0 in models for infectious diseases in heterogeneous populations. J. Math. Biol. 28, 365–382. https://doi.org/10.1007/BF00178324

Dougherty, E.R., Seidel, D.P., Carlson, C.J., Getz, W.M., 2018. Using movement data to estimate contact rates in a simulated environmentally-transmitted disease system. https://doi.org/10.1101/261198

Dragon, D.C., Elkin, B.T., Nishi, J.S., Ellsworth, T.R., 1999. A review of anthrax in Canada and implications for research on the disease in northern bison. J. Appl. Microbiol. 87, 208–213. https://doi.org/10.1046/j.1365-2672.1999.00872.x

Dragon, D.C., Rennie, R.P., 1995. The ecology of anthrax spores: tough but not invincible. Can. Vet. J. 36, 295–301.

Easterday, W.R., Kausrud, K.L., Star, B., Heier, L., Haley, B.J., Ageyev, V., Colwell, R.R., Stenseth, N.C., 2012. An additional step in the transmission of *Yersinia pestis*? ISME J. 6, 231–236. https://doi.org/10.1038/ismej.2011.105

Ebedes, H., 1976. Anthrax epizotics in Etosha National Park. Madoqua 10, 99–118.

Fisher, C.R., Streicker, D.G., Schnell, M.J., 2018. The spread and evolution of rabies virus: conquering new frontiers. Nat. Rev. Microbiol. 16, 241–255. https://doi.org/10.1038/nrmicro.2018.11

Gajewski, Z., McElmurray, P., Wojdak, J., McGregor, C., Zeller, L., Cooper, H., Belden, L.K., Hopkins, S., 2024. Nonrandom foraging and resource distributions affect the

relationships between host density, contact rates and parasite transmission. Ecol. Lett. 27, e14385. https://doi.org/10.1111/ele.14385

Gerba, C.P., 2009. Environmentally transmitted pathogens. Environ. Microbiol. 445–484. https://doi.org/10.1016/B978-0-12-370519-8.00022-5

Goel, A.K., 2015. Anthrax: A disease of biowarfare and public health importance. World J. Clin. Cases WJCC 3, 20–33. https://doi.org/10.12998/wjcc.v3.i1.20

Grébaut, P., Girardin, K., Fédérico, V., Bousquet, F., 2016. Simulating the elimination of sleeping sickness with an agent-based model. Parasite 23, 63. https://doi.org/10.1051/parasite/2016066

Guerra, F.M., Bolotin, S., Lim, G., Heffernan, J., Deeks, S.L., Li, Y., Crowcroft, N.S., 2017. The basic reproduction number (R0) of measles: a systematic review. Lancet Infect. Dis. 17, e420–e428. https://doi.org/10.1016/S1473-3099(17)30307-9

Haley, N.J., Mathiason, C.K., Zabel, M.D., Telling, G.C., Hoover, E.A., 2009. Detection of sub-clinical CWD infection in conventional test-negative deer long after oral exposure to urine and feces from CWD+ deer. PLOS ONE 4, e7990. https://doi.org/10.1371/journal.pone.0007990

Hawley, D.M., Altizer, S.M., 2011. Disease ecology meets ecological immunology: understanding the links between organismal immunity and infection dynamics in natural populations. Funct. Ecol. 25, 48–60. https://doi.org/10.1111/j.1365-2435.2010.01753.x

Hollingsworth, T.D., Pulliam, J.R.C., Funk, S., Truscott, J.E., Isham, V., Lloyd, A.L., 2015. Seven challenges for modelling indirect transmission: vector-borne diseases, macroparasites and neglected tropical diseases. Epidemics, Challenges in Modelling Infectious Disease Dynamics 10, 16–20. https://doi.org/10.1016/j.epidem.2014.08.007

Holschbach, C.L., Peek, S.F., 2018. Salmonella in dairy cattle. Vet. Clin. Food Anim. Pract. 34, 133–154. https://doi.org/10.1016/j.cvfa.2017.10.005

Hoyt, J.R., Kilpatrick, A.M., Langwig, K.E., 2021. Ecology and impacts of white-nose syndrome on bats. Nat. Rev. Microbiol. 19, 196–210. https://doi.org/10.1038/s41579-020-00493-5

Huang, M., Hull, C.M., 2017. Sporulation: how to survive on planet Earth (and beyond). Curr. Genet. 63, 831–838. https://doi.org/10.1007/s00294-017-0694-7

Huang, Y.-H., Kausrud, K., Hassim, A., Ochai, S.O., Van Schalkwyk, O.L., Dekker, E.H., Buyantuev, A., Cloete, C.C., Kilian, J.W., Mfune, J.K.E., Kamath, P.L., Van Heerden, H., Turner, W.C., 2022. Environmental drivers of biseasonal anthrax outbreak dynamics in two multihost savanna systems. Ecol. Monogr. 92, e1526. https://doi.org/10.1002/ecm.1526

Huang, Y.-H., Joel, H., Küsters, M., Barandongo, Z.R., Cloete, C.C., Hartmann, A., Kamath, P.L., Kilian, J.W., Mfune, J.K.E., Shatumbu, G., Zidon, R., Getz, W.M., Turner, W.C., 2021. Disease or drought: environmental fluctuations release zebra from a potential pathogen-triggered ecological trap. Proc. R. Soc. B Biol. Sci. 288, 20210582. https://doi.org/10.1098/rspb.2021.0582

Hugh-Jones, M.E., de Vos, V., 2002. Anthrax and wildlife. Rev. Sci. Tech. Int. Off. Epizoot. 21, 359–383. https://doi.org/10.20506/rst.21.2.1336

Islam, Md.S., Hossain, M.J., Mikolon, A., Parveen, S., Khan, M.S.U., Haider, N., Chakraborty, A., Titu, A.M.N., Rahman, M.W., Sazzad, H.M.S., Rahman, M., Gurley, E.S., Luby, S.P., 2013. Risk practices for animal and human anthrax in Bangladesh: an exploratory study. Infect. Ecol. Epidemiol. 3, 21356. https://doi.org/10.3402/iee.v3i0.21356

Islam, S., Castellan, D., Akhter, A., Hossain, M., Hasan, Md.Z., 2016. Animal anthrax in Sirajganj district of Bangladesh from 2010 to 2012. Asian J. Med. Biol. Res. 1, 387. https://doi.org/10.3329/ajmbr.v1i3.26444

Karl, S., Halder, N., Kelso, J.K., Ritchie, S.A., Milne, G.J., 2014. A spatial simulation model for dengue virus infection in urban areas. BMC Infect. Dis. 14, 447. https://doi.org/10.1186/1471-2334-14-447

Keim, P., Kalif, A., Schupp, J., Hill, K., Travis, S.E., Richmond, K., Adair, D.M., Hugh-Jones, M., Kuske, C.R., Jackson, P., 1997. Molecular evolution and diversity in *Bacillus anthracis* as detected by amplified fragment length polymorphism markers. J. Bacteriol. 179, 818–824. https://doi.org/10.1128/jb.179.3.818-824.1997

Lane-deGraaf, K.E., Kennedy, R.C., Arifin, S.N., Madey, G.R., Fuentes, A., Hollocher, H., 2013. A test of agent-based models as a tool for predicting patterns of pathogen transmission in complex landscapes. BMC Ecol. 13, 35. https://doi.org/10.1186/1472-6785-13-35

Leta, S., Beyene, T.J., De Clercq, E.M., Amenu, K., Kraemer, M.U.G., Revie, C.W., 2018. Global risk mapping for major diseases transmitted by *Aedes aegypti* and *Aedes albopictus*. Int. J. Infect. Dis. 67, 25–35. https://doi.org/10.1016/j.ijid.2017.11.026

Lindeque, P.M., Turnbull, P.C.B., 1994. Ecology and epidemiology of anthrax in the Etosha National Park, Namibia.

Lou, Y., Salako, R.B., 2023. Mathematical analysis of the dynamics of some reaction-diffusion models for infectious diseases. J. Differ. Equ. 370, 424–469. https://doi.org/10.1016/j.jde.2023.06.018

Madison-Antenucci, S., Kramer, L.D., Gebhardt, L.L., Kauffman, E., 2020. Emerging tick-borne diseases. Clin. Microbiol. Rev. 33, 10.1128/cmr.00083-18. https://doi.org/10.1128/cmr.00083-18

Martinez-Gutierrez, M., Ruiz-Saenz, J., 2016. Diversity of susceptible hosts in canine distemper virus infection: a systematic review and data synthesis. BMC Vet. Res. 12, 78. https://doi.org/10.1186/s12917-016-0702-z

Matthews, L., Reeve, R., Woolhouse, M.E.J., Chase-Topping, M., Mellor, D.J., Pearce, M.C., Allison, L.J., Gunn, G.J., Low, J.C., Reid, S.W.J., 2009. Exploiting strain diversity to expose transmission heterogeneities and predict the impact of targeting supershedding. Epidemics 1, 221–229. https://doi.org/10.1016/j.epidem.2009.10.002

Mavrot, F., Orsel, K., Hutchins, W., Adams, L.G., Beckmen, K., Blake, J.E., Checkley, S.L., Davison, T., Francesco, J.D., Elkin, B., Leclerc, L.-M., Schneider, A., Tomaselli, M., Kutz, S.J., 2020. Novel insights into serodiagnosis and epidemiology of *Erysipelothrix rhusiopathiae*, a newly recognized pathogen in muskoxen (*Ovibos moschatus*). PLOS ONE 15, e0231724. https://doi.org/10.1371/journal.pone.0231724

Miksch, F., Jahn, B., Espinosa, K.J., Chhatwal, J., Siebert, U., Popper, N., 2019. Why should we apply ABM for decision analysis for infectious diseases?—An example for dengue interventions. PLOS ONE 14, e0221564. https://doi.org/10.1371/journal.pone.0221564

Mueller, R.S., McDougald, D., Cusumano, D., Sodhi, N., Kjelleberg, S., Azam, F., Bartlett, D.H., 2007. *Vibrio cholerae* strains possess multiple strategies for abiotic and biotic surface colonization. J. Bacteriol. 189, 5348–5360. https://doi.org/10.1128/jb.01867-06

Munang'andu, H.M., Banda, F., Siamudaala, V.M., Munyeme, M., Kasanga, C.J., Hamududu, B., 2012. The effect of seasonal variation on anthrax epidemiology in the upper Zambezi

floodplain of western Zambia. J. Vet. Sci. 13, 293–298. https://doi.org/10.4142/jvs.2012.13.3.293

Muturi, M., Gachohi, J., Mwatondo, A., Lekolool, I., Gakuya, F., Bett, A., Osoro, E., Bitek, A., Thumbi, S.M., Munyua, P., Oyas, H., Njagi, O.N., Bett, B., Njenga, M.K., 2018. Recurrent anthrax outbreaks in humans, livestock, and wildlife in the same locality, Kenya, 2014–2017. Am. J. Trop. Med. Hyg. 99, 833–839. https://doi.org/10.4269/ajtmh.18-0224

Nekorchuk, D.M., Morris, L.R., Asher, V., Hunter, D.L., Ryan, S.J., Blackburn, J.K., 2019. Potential *Bacillus anthracis* risk zones for male plains bison (*Bison bison bison*) in Southwestern Montana, USA. J. Wildl. Dis. 55, 136–141. https://doi.org/10.7589/2017-09-234

Nicholson, W.L., Munakata, N., Horneck, G., Melosh, H.J., Setlow, P., 2000. Resistance of *Bacillus* endospores to extreme terrestrial and extraterrestrial environments. Microbiol. Mol. Biol. Rev. 64, 548–572. https://doi.org/10.1128/mmbr.64.3.548-572.2000

Niemann, J.-H., Winkelmann, S., Wolf, S., Schütte, C., 2021. Agent-based modeling: population limits and large timescales. Chaos Interdiscip. J. Nonlinear Sci. 31, 033140. https://doi.org/10.1063/5.0031373

Nishi, J.S., Ellsworth, T.R., Lee, N., Dewar, D., Elkin, B.T., Dragon, D.C., An outbreak of anthrax (*Bacillus anthracis*) in free-roaming bison in the Northwest Territories, June–July 2006. 2007. Can. Vet. J. 48, 37–38.

Nuttall, R.A., Moisander, P.H., 2023. *Vibrio cyclitrophicus* population-specific biofilm formation and epibiotic growth on marine copepods. Environ. Microbiol. 25, 2534–2548. https://doi.org/10.1111/1462-2920.16483

Perera, I.U., Fujiyoshi, S., Nishiuchi, Y., Nakai, T., Maruyama, F., 2022. Zooplankton act as cruise ships promoting the survival and pathogenicity of pathogenic bacteria. Microbiol. Immunol. 66, 564–578. https://doi.org/10.1111/1348-0421.13029

Perez, L., Dragicevic, S., 2009. An agent-based approach for modeling dynamics of contagious disease spread. Int. J. Health Geogr. 8, 50. https://doi.org/10.1186/1476-072X-8-50

Pienaar, U., 1961. A second outbreak of anthrax amongst game animals in the Kruger National Park. 5th June to 11th October, 1960. Koedoe Afr. Prot. Area Conserv. Sci. 4. https://doi.org/10.4102/koedoe.v4i1.824

Pizzitutti, F., Pan, W., Feingold, B., Zaitchik, B., Álvarez, C.A., Mena, C.F., 2018. Out of the net: an agent-based model to study human movements influence on local-scale malaria transmission. PLOS ONE 13, e0193493. https://doi.org/10.1371/journal.pone.0193493

Plowright, R.K., Parrish, C.R., McCallum, H., Hudson, P.J., Ko, A.I., Graham, A.L., Lloyd-Smith, J.O., 2017. Pathways to zoonotic spillover. Nat. Rev. Microbiol. 15, 502–510. https://doi.org/10.1038/nrmicro.2017.45

Potapov, A., Merrill, E., Pybus, M., Lewis, M.A., 2016. Chronic wasting disease: transmission mechanisms and the possibility of harvest management. PLOS ONE 11, e0151039. https://doi.org/10.1371/journal.pone.0151039

Railsback, S.F., Grimm, V., 2019. Agent-based and individual-based modeling: a practical introduction, Second Edition. Princeton University Press.

Rebaudet, S., Sudre, B., Faucher, B., Piarroux, R., 2013. Environmental determinants of cholera outbreaks in inland Africa: a systematic review of main transmission foci and propagation routes. J. Infect. Dis. 208, S46–S54. https://doi.org/10.1093/infdis/jit195

Redman, E.M., Wilson, K., Cory, J.S., 2016. Trade-offs and mixed infections in an obligate-killing insect pathogen. J. Anim. Ecol. 85, 1200–1209. https://doi.org/10.1111/1365-2656.12547

Reynolds, H.T., Ingersoll, T., Barton, H.A., 2015. Modeling the environmental growth of *Pseudogymnoascus destructans* and its impact on the white-nose syndrome epidemic. J. Wildl. Dis. 51, 318–331. https://doi.org/10.7589/2014-06-157

Rohani, P., Breban, R., Stallknecht, D.E., Drake, J.M., 2009. Environmental transmission of low pathogenicity avian influenza viruses and its implications for pathogen invasion. Proc. Natl. Acad. Sci. 106, 10365–10369. https://doi.org/10.1073/pnas.0809026106

Samsing, F., Barnes, A.C., 2024. The rise of the opportunists: What are the drivers of the increase in infectious diseases caused by environmental and commensal bacteria? Rev. Aquac. https://doi.org/10.1111/raq.12922

Sánchez, K.F., Zhong, B., Agudelo, J.A., Duffy, M.A., 2023. Infectivity of the parasite *Metschnikowia bicuspidata* is decreased by time spent as a transmission spore, but exposure to phycotoxins in the water column has no effect. Freshw. Biol. 68, 1020–1030. https://doi.org/10.1111/fwb.14082

Sardar, N., Aziz, M.W., Mukhtar, N., Yaqub, T., Anjum, A.A., Javed, M., Ashraf, M.A., Tanvir, R., Wolfe, A.J., Schabacker, D.S., Forrester, S., Khemmani, M., Aqel, A.A., Warraich, M.A., Shabbir, M.Z., 2023. One Health assessment of *Bacillus anthracis* incidence and detection in anthrax-endemic areas of Pakistan. Microorganisms 11, 2462. https://doi.org/10.3390/microorganisms11102462

Schmid, G., Kaufmann, A., 2002. Anthrax in Europe: its epidemiology, clinical characteristics, and role in bioterrorism. Clin. Microbiol. Infect. 8, 479–488. https://doi.org/10.1046/j.1469-0691.2002.00500.x

Schramm, P.T., Johnson, C.J., Mathews, N.E., McKenzie, D., Aiken, J.M., Pedersen, J.A., 2006. Potential role of soil in the transmission of prion disease. Rev. Mineral. Geochem. 64, 135–152. https://doi.org/10.2138/rmg.2006.64.5

Siembieda, J.L., Miller, W.A., Byrne, B.A., Ziccardi, M.H., Anderson, N., Chouicha, N., Sandrock, C.E., Johnson, C.K., 2011. Zoonotic pathogens isolated from wild animals and environmental samples at two California wildlife hospitals. https://doi.org/10.2460/javma.238.6.773

Sinclair, R.G., Rose, J.B., Hashsham, S.A., Gerba, C.P., Haas, C.N., 2012. Criteria for selection of surrogates used to study the fate and control of pathogens in the environment. Appl. Environ. Microbiol. 78, 1969–1977. https://doi.org/10.1128/AEM.06582-11

Smith, K.F., Acevedo-Whitehouse, K., Pedersen, A.B., 2009. The role of infectious diseases in biological conservation. Anim. Conserv. 12, 1–12. https://doi.org/10.1111/j.1469-1795.2008.00228.x

Smith, K.M., Machalaba, C.C., Seifman, R., Feferholtz, Y., Karesh, W.B., 2019. Infectious disease and economics: The case for considering multi-sectoral impacts. One Health 7, 100080. https://doi.org/10.1016/j.onehlt.2018.100080

Smith, N.R., Trauer, J.M., Gambhir, M., Richards, J.S., Maude, R.J., Keith, J.M., Flegg, J.A., 2018. Agent-based models of malaria transmission: a systematic review. Malar. J. 17, 299. https://doi.org/10.1186/s12936-018-2442-y

Stone, L., Hilker, F., Katriel, G., 2012. SIR models, in: Hastings, A., Gross, L. (Eds.), Encyclopedia of theoretical ecology. University of California Press, Berkeley, pp. 648–658.

Strasburg, M., Christensen, S., 2024. Evaluating the interaction of emerging diseases on white-tailed deer populations using an agent-based modeling approach. Pathogens 13, 545. https://doi.org/10.3390/pathogens13070545

Sun, Z., Lorscheid, I., Millington, J.D., Lauf, S., Magliocca, N.R., Groeneveld, J., Balbi, S., Nolzen, H., Müller, B., Schulze, J., Buchmann, C.M., 2016. Simple or complicated agent-based models? A complicated issue. Environ. Model. Softw. 86, 56–67. https://doi.org/10.1016/j.envsoft.2016.09.006

Suomalainen, L.-R., Kunttu, H., Valtonen, E.T., Hirvelä-Koski, V., Tiirola, M., 2006. Molecular diversity and growth features of *Flavobacterium columnare s*trains isolated in Finland. Dis. Aquat. Organ. 70, 55–61. https://doi.org/10.3354/dao070055

Suzán, G., Marcé, E., Giermakowski, J.T., Armién, B., Pascale, J., Mills, J., Ceballos, G., Gómez, A., Aguirre, A.A., Salazar-Bravo, J., Armién, A., Parmenter, R., Yates, T., 2008. The effect of habitat fragmentation and species diversity loss on hantavirus prevalence in Panama. Ann. N. Y. Acad. Sci. 1149, 80–83. https://doi.org/10.1196/annals.1428.063

Swick, M.C., Koehler, T.M., Driks, A., 2016. Surviving between hosts: sporulation and transmission in virulence mechanisms of bacterial pathogens. John Wiley & Sons, Ltd, pp. 567–591. https://doi.org/10.1128/9781555819286.ch20

Thompson, N.E., Butts, D.J., Murillo, M.S., O'Brien, D.J., Christensen, S.A., Porter, W.F., Roloff, G.J., 2024. An individual-based model for direct and indirect transmission of

chronic wasting disease in free-ranging white-tailed deer. Ecol. Model. 491, 110697. https://doi.org/10.1016/j.ecolmodel.2024.110697

Tracey, J.A., Bevins, S.N., VandeWoude, S., Crooks, K.R., 2014. An agent-based movement model to assess the impact of landscape fragmentation on disease transmission. Ecosphere 5, art119. https://doi.org/10.1890/ES13-00376.1

Turner, W.C., Imologhome, P., Havarua, Z., Kaaya, G.P., Mfune, J.K.E., Mpofu, I.D.T., Getz, W.M., 2013. Soil ingestion, nutrition and the seasonality of anthrax in herbivores of Etosha National Park. Ecosphere 4, art13. https://doi.org/10.1890/ES12-00245.1

Turner, W.C., Kausrud, K.L., Krishnappa, Y.S., Cromsigt, J.P.G.M., Ganz, H.H., Mapaure, I., Cloete, C.C., Havarua, Z., Küsters, M., Getz, W.M., Stenseth, N.Chr., 2014. Fatal attraction: vegetation responses to nutrient inputs attract herbivores to infectious anthrax carcass sites. Proc. R. Soc. B Biol. Sci. 281, 20141785. https://doi.org/10.1098/rspb.2014.1785

Ugochukwu, I.C.I., Samuel, F., Orakpoghenor, O., Nwobi, O.C., Anyaoha, C.O., Majesty-Alukagberie, L.O., Ugochukwu, M.O., Ugochukwu, E.I., 2019. Erysipelas, the opportunistic zoonotic disease: history, epidemiology, pathology, and diagnosis—a review. Comp. Clin. Pathol. 28, 853–859. https://doi.org/10.1007/s00580-018-2856-5

van Seventer, J.M., Hochberg, N.S., 2017. Principles of infectious diseases: transmission, diagnosis, prevention, and control. Int. Encycl. Public Health 22–39. https://doi.org/10.1016/B978-0-12-803678-5.00516-6

Weinstein, S.B., Buck, J.C., Young, H.S., 2018. A landscape of disgust. Science 359, 1213–1214. https://doi.org/10.1126/science.aas8694

Willem, L., Verelst, F., Bilcke, J., Hens, N., Beutels, P., 2017. Lessons from a decade of individual-based models for infectious disease transmission: a systematic review (2006-2015). BMC Infect. Dis. 17, 612. https://doi.org/10.1186/s12879-017-2699-8

Zaidi, S., Bouam, A., Bessas, A., Hezil, D., Ghaoui, H., Ait-Oudhia, K., Drancourt, M., Bitam, I., 2018. Urinary shedding of pathogenic Leptospira in stray dogs and cats, Algiers: A prospective study. PLOS ONE 13, e0197068. https://doi.org/10.1371/journal.pone.0197068

CHAPTER ONE: Pathogen transmission, host movement, and landscape features alter the spatial distribution of environmentally transmitted pathogens

Contributing authors: Amélie C. Dolfi, Marie L. J. Gilbertson, Lauren A. White, Wendy C. Turner

PICTURE 1: Plains zebra (*Equus quagga*) in Etosha National Park, Namibia, standing and bleeding from the nose (left) and carcass of the same individual found the next day (right) after being scavenged. Photos by Amélie Dolfi, May 2022

1.1 Abstract

Environmentally transmitted pathogen (ETP) dynamics can be complex to characterize, often due to discrepancies in the spatial and temporal scales of the infectious environment and host movement. To manage ETP outbreaks, it is critical to understand which variables pertaining to the host, pathogen, and landscape are most relevant to the disease dynamic. However, persistent ETPs can be challenging to study in free-ranging wildlife due to the difficulty of recording infections, infection duration, and pathogen release events. Thus, we developed a theoretical agent-based simulation model to examine the role of pathogen transmission mode, environmental survival and infectivity; host movement and behavior; and landscape quality and fragmentation on disease prevalence and spatial distribution. The model explores three pathogen release pathways: (i) continuous shedding (e.g., via saliva or feces), (ii) at host death, or (iii) through both shedding and death. Depending on host movement behavior and habitat selection, hosts either created 'hot spots' for transmission risk by aggregating pathogens in the environment or they widely dispersed the pathogen across the landscape. In each case, the pathogen distribution in the environment will be shaped by the host's decisions and subsequent transmission events. Parameters linked to host behavioral response when facing environmental reservoirs (avoidance-attraction), the duration of environmental persistence, and the infectivity of reservoirs were most relevant to determine the establishment and maintenance of the disease over time for all pathogen-releasing modes. The spatial distribution of exposure risk depended on the pathogen release mode, with pathogens released upon the host death creating fewer more infectious hot spots, while continuous shedding led to a larger spatial extent of low-risk infection by creating many low-risk hot spots. Attraction and avoidance of reservoirs led to a greater proportion of the environment infected, with higher variance under avoidance. Surprisingly, landscape structure did not appear to be a significant

parameter. Our results shed light on how ETP characteristics and host behavior interact to shape outbreak dynamics and the emergence of environmental infection risk "hot spots." Future empirical ETP research could further explore the effects of host avoidance-attraction of environmental pathogen reservoirs on disease dynamics.

Keywords: simulation model, environmentally transmitted pathogen, resource-selection function, spatial disease risk, individual-based model, spatial heterogeneity, movement ecology, environmental reservoir

1.2 Introduction

For infectious pathogens transmitted to mobile hosts, infection risk can be heterogeneous across a landscape. Understanding how this spatial heterogeneity emerges is critical for predicting disease dynamics and mapping transmission risk (Hagenaars et al., 2004). Spatial heterogeneity in disease risk has been well studied for directly transmitted and vector-borne pathogens, notably by studying hosts' movement and interactions. However, the study of the spatial distribution of environmentally transmitted pathogens (ETPs) has been lagging. These pathogens can be particularly challenging to study due to the difficulty in accurately recording pathogen presence in the environment (Bellan et al., 2013), and in determining the associated transmission risk (Becker et al., 2023). Long-term pathogen monitoring remains sparse, especially for persistent ETPs where decades can be required to record the spatiotemporal risk. Monitoring these pathogens proves field-intensive (Barandongo et al., 2023), emphasizing the necessity to combine empirical field

study and theoretical models to better comprehend long-term ecological implications (Lindenmayer et al., 2012).

Many mathematical models have been developed to understand and predict disease outbreak risk and to map the spatial distribution of transmission risk (White et al., 2018a). Knowing the spatial distribution of infection risk is essential for mitigating outbreak emergence and predicting spillover risks (Plowright et al., 2017; Washburne et al., 2019). Some pathogens, mostly directly and vector-borne transmitted, have been particularly well studied over their spatiotemporal distribution, such as rabies outbreaks (Blanton et al., 2012; Bonilla-Aldana et al., 2022), tuberculosis (Chang et al., 2023; Shaweno et al., 2018) or dengue fever (Andrioli et al., 2020; Hazrin et al., 2016). Those models emphasize the importance of mapping disease risk to better respond to and control disease emergence by targeting the most at-risk areas and hosts. However, because ETPs rely on the environment for transmission and can survive outside hosts for extended periods (Gerba, 2009), understanding where they are distributed and the risks they pose upon contact with a host is an especially important but significant gap in current knowledge. In this study, we used spatially explicit simulation models to make inferences about ETP disease dynamics, focusing on how different pathogen release modes by infected hosts affect spatial patterns of pathogen clustering in the environment and, hence, infection risk.

Spatial risk dynamics are dependent on landscape features and structure (Bonnell et al., 2018; Leach et al., 2016; White et al., 2018b), host characteristics and movement (e.g., heterogeneity in behavior, susceptibility [VanderWaal and Ezenwa, 2016]; movement [Dougherty et al., 2018] and responses to environmental cues [White et al., 2020]), and pathogen characteristics (e.g., survival in the environment [Mitchell et al., 2007]). From a landscape perspective, factors such as habitat quality, fragmentation, and the distribution of specific

resources (e.g., water; Ostfeld et al., 2005) can have significant impacts on the spatial heterogeneity of transmission risk. For example, habitat quality can shape transmission risk by attracting hosts toward high-quality habitats, increasing the risk of transmission from increased direct contact (VerCauteren et al., 2018) or increased contact with infectious environments (Leach et al., 2016). Habitat fragmentation can have contrasting effects depending on the pathogen studied. Indeed, fragmentation can increase the risk of disease transmission, as reported for human risk for Lyme disease (Allan et al., 2003; Heylen et al., 2019) or for infection by *Giardia intestinalis* among chimpanzees (*Pan troglodytes verus*) and red colobus (*Piliocolobus rufomitratu*s) (Gillespie and Chapman, 2008; Sá et al., 2013). However, fragmentation can also reduce disease pressure: higher habitat fragmentation can reduce tsetse fly (*Glossina* spp.) abundance, reducing *Trypanosoma congolense* transmission risk (Van den Bossche et al., 2010). Further, for many pathogens such as bovine tuberculosis (*Mycobacterium bovis*), host aggregation at localized resources like waterholes and baited sites can act as transmission hot spots, enhancing transmission between domestic and wildlife hosts (Cowie et al., 2016; Miller et al., 2003; Payne et al., 2017). Landscape plays an essential role in understanding pathogen transmission. For ETPs which rely upon the environment for transmission, defining habitat quality and fragmentation is necessary to understand the landscape connectivity for the hosts and, in turn, the contact risks.

Layered on top of these landscape factors are heterogeneities in host and pathogen characteristics. Together, these elements shape where infected hosts shed pathogens into the environment, the transmissibility and survival of pathogens in those environments, and where and how susceptible individuals later uptake those pathogens (Wilber et al., 2022). In the first of these processes, infected hosts can release pathogens into the environment, creating patches of infection risk, hereafter referred to as environmental reservoirs. The release mode depends upon the

pathogen-host combination but can be simplified based on the release timing relative to infection and host death. When hosts are infectious before death, shedding releases pathogens on a regular or semi-regular basis via urine (e.g., leptospirosis [Levett et al., 2001], Hendra virus [Edson et al., 2015]), feces (e.g., gastrointestinal nematodes [Zajac and Garza, 2020]), saliva (e.g., Marburg virus [Amman et al., 2021]), or other tissues or bodily fluids. Obligate killer pathogens, on the other hand, release pathogens all at once upon host death (e.g., *Bacillus anthracis*, responsible for anthrax disease [Hugh-Jones and de Vos, 2002]; baculoviruses in Lepidoptera [Redman et al., 2016]; or *Metschnikowia bicuspidata* fungus in *Daphnia dentifera* [Sánchez et al., 2023]). Parasites can also be released through both modes (e.g., chronic wasting disease, CWD, can be shed via urine, feces, saliva, scent glands secretions, and upon host death [Haley et al., 2009; Schramm et al., 2006]; *Batrachochytrium salamandrivorans* can be released in ponds from shedding and upon host death [Carter et al., 2024], *Erysipelothrix rhusiopathiae*, a bacterium released in feces and upon host death [Mavrot et al., 2020; Ugochukwu et al., 2019]). ETP release mode significantly affects the spatial distribution of pathogens as continuous shedding will increase the spatial extent of the pathogen due to the pathogen being released in multiple environmental locations. In contrast, a strictly obligate killer pathogen will only be released at the death site. Similarly, transmission mode may impact the virulence-transmission relationship of pathogens (Turner et al., 2021) and thus cause different disease dynamics.

Once in the environment, transmission dynamics are affected by pathogen survival and transmissibility, which can vary through time (e.g., seasonally; Koelle et al., 2005) and space (e.g., increased survival in some habitats; Alegbeleye and Sant'Ana, 2020). Susceptible hosts may then contact ETPs through ingestion of contaminated water or forage (e.g., guinea worm transmission during drinking events [Garrett et al., 2020]); using infectious environments (e.g.,

Batrachochytrium dendrobatidis transmission in ponds [Rumschlag et al., 2022]; white-nose syndrome transmitted in bat roosting habitat [Hoyt et al., 2021]); or from contact with infected environmental features such as smelling, licking, or touching contaminated material (e.g., white-tailed deer (*Odocoileus virginianus*) interactions at scent-marking sites may transmit CWD [Egan et al., 2023]).

However, hosts may exhibit a range of behavioral responses to infectious environments that affect disease dynamics, including avoidance or attraction to infectious sites. For example, the 'landscape of disgust' concept proposes that individuals tend to avoid spending time close to sick individuals or unappealing environments (Buck et al., 2018; Weinstein et al., 2018a). Both direct and indirect cues can help hosts avoid parasites. Indirect cues such as feces, carcasses, or scents can be associated with parasite risk, for example, herbivores avoid foraging near feces (Hutchings et al., 2001) and mandrills (*Mandrillus sphinx*) use olfaction to avoid grooming infected conspecifics (Poirotte et al., 2017). Direct cues are also used to avoid parasite risk, such as animals avoiding habitats with biting flies (Belanger et al., 2020). On the other hand, attraction to infectious sites may occur and enhance risk transmission. For example, indirect attraction of rats (*Rattus* spp.) to raccoon (*Procyon lotor*) latrines can enhance rat risk of infection with raccoon roundworm, *Baylisascariasis procyonis* (Weinstein et al., 2018b). Supplemental feeding and bait can concentrate hosts, enhancing the risk of direct and indirect parasite transmission (Sorensen et al., 2014), e.g., bovine tuberculosis and brucellosis (*Brucella abortus*) transmission between cattle (*Bos taurus*) and elk (*Cervus canadensis)* (Brook et al., 2013; Cross et al., 2010).

When attraction to sites contaminated with ETPs occurs, those sites may become ecological traps—defined in the disease context as habitats that do not maximize host fitness due to the presence of infectious pathogens (Schlaepfer et al., 2002). Habitat quality and environmental

survival of ETP are expected to be important factors determining the creation of ecological traps in a landscape. Notably, high-quality habitats can facilitate direct and indirect transmission, while low-quality habitats can act as refugia due to the lower host density and lower infection risk (Leach et al., 2016). However, it is still unclear how landscape structure, host movement, behavior and infection duration, and the persistence and infectivity of pathogens with different release modes alter disease dynamics and spatial parasite distribution. This knowledge gap is important as more and more habitat fragmentation and land use changes occur worldwide, leading to animal movement and behavior disruptions, which can increase outbreak emergence and spill-over risk (Altizer et al., 2013; Gottdenker et al., 2014).

We developed a theoretical simulation agent-based model to examine the role of landscape features, host behaviors and ETP characteristics on disease dynamics and spatial distribution of environmental reservoirs after introducing a single infected individual in a closed population. The landscape features considered included fragmentation and aggregation. Among ETP characteristics, we assessed the role of pathogen release patterns from infected hosts, the environmental persistence, and the infectivity risk of the pathogen upon release into the environment. Finally, for the host characteristics, we examined the strength of selection for resource quality and for environmental reservoirs (specifically attraction, avoidance, or neutrality towards environmental reservoirs), and the duration of infection. Our results shed light on the effect of host-pathogen interactions for different types of ETPs on disease dynamics and spatial distribution of infection risk, which may inform disease management efforts.

1.3 Materials and Methods

1.3.1 Model description

Following the models from (White et al., 2020, 2018b), we developed a stochastic, Susceptible-Infected-Removed agent-based model (ABM) for ETPs in a closed population (i.e., no immigration, emigration, birth, or natural death) in a spatially explicit discrete lattice landscape, where resources varied in quality (medium or high). For a full description of the model following the overview, design concepts, and details (ODD) protocol of Grimm et al. (2020) for describing individual-based models, see Appendix A. We modeled three *transmission scenarios* where pathogens are released into the environment (i.e., in a cell of the landscape) *(i)* at host death, referred to as the Obligate-killer scenario (OK), *(ii)* shed over the infectious period, referred to as the Continuous-shedder scenario (CS), or *(iii)* both shed over time and at host death, referred to as the Shedder-killer scenario (SK). Each simulation began with one infected individual introduced into a fully susceptible population composed of N individuals, with N an assigned parameter per simulation (Table 1.1). In all scenarios, when infected individuals reached their maximum infectious period, they were removed from the simulation. This can be seen as either individuals dying (OK and SK scenarios) or being fully immune to the disease (CS).

Binary landscapes were generated using the midpoint displacement algorithm (Turner and Gardner, 2015). The landscapes varied in their proportion of high-quality resources available (p) and their degree of resource aggregation (Hurst exponent, H). Four 33 x 33 cell landscapes were generated and used for simulations: (i) medium resource availability with low aggregation: p = 0.5; H = 0.5; (ii) high resource availability with low aggregation: p = 0.8, H = 0.5; (iii) medium resource availability with high aggregation: p = 0.5, H = 0.8; and (iv) high resource availability

with high aggregation: p = 0.8, H = 0.8 (Appendix A figure A1). The landscapes assumed a torus shape (i.e., wrapped boundaries) to avoid movement edge effects.

The ABM was composed of four sub-models occurring in the following order (figure 1.1): (i) host movement, (ii) new infection of susceptible hosts, (iii) pathogen release from infected hosts, and (iv) decay of environmental (cell) infectivity.

1.3.1.a Host movement

Host movement was modeled using a resource selection function (RSF) with movement choices weighted by the habitat quality and presence of pathogens. Each of the *N* hosts could move only one cell at a time, in a Von Neumann neighborhood (i.e., the eight cells surrounding the current cell [Kari, 2005]), or stay in their current cell. A 2D movement kernel and RSF were used following White et al., (2018b). The probability of a host moving from its current location, *a,* to a new location, *b*, is:

$$P = \frac{\phi(a,b) \cdot \omega_b}{\sum_{k=1}^{9}[\phi(a,c_k) \cdot \omega_k]} \quad (1.1)$$

Where $\phi(.)$ is a 2D movement kernel, c_k represents the center point of each grid cell accessible by the individuals, and ω_b and ω_k are RSFs governing a host's movement preference for cells *b* and *k*, respectively. The RSF of any given cell *j* is $\omega_j = \exp(\beta * R_j + \beta_1 * P_j)$, with R_j representing the resource quality and Pj representing the presence of an environmental reservoir. The coefficients β and β_1 represent the strength of selection. When coefficient β_1 is negative, it represents an avoidance of reservoir sites (e.g., "landscape of disgust"), and when it is positive, it represents an attraction (e.g., rat attraction to raccoon latrines).

For the 2D movement kernel, we assumed the simplest case of a uniform circular distribution:

$$\phi(r) = \frac{1}{2\pi r^2} \quad (1.2)$$

where the movement kernel is inversely proportional to radial distance (r) from the center point of the current grid cell such that:

$$r = \sqrt{(x_a - x_c)^2 + (y_a - y_c)^2} \quad (1.3)$$

To account for a uniform circular distribution, we multiplied the inverse distance weight (i.e., 1/r) by the kernel's circumference (i.e., 1/2πr).

1.3.1.b Pathogen release from infected hosts

If shedding occurs prior to death (*CS* and *SK* scenarios), pathogens were released into cells at each step for the entire period that individuals were infected. At each step, infected individuals either died or recovered from infection at rate γ. If an individual died from infection (*OK* and *SK* scenarios), they released pathogens into the cell in which they died before their removal from the simulation.

Upon pathogen release, the initial infectivity of cell c, denoted by the parameter ρ_c, is the probability of infection given effective contact (e.g., foraging) between the host and the environmental cell. This probability differs depending on the type of pathogen release. We expected pathogen loads released during continual shedding to be lower than those released from an infectious carcass at death. For CWD, it is assumed that CWD-prions shed in excreta by live deer would be far lower than the prions available in a carcass (Chen et al., 2010; Mathiason et al., 2010). As such, if the pathogen was released during a shedding event, its initial infectivity was denoted ρ_S, and was defined as ten times lower than ρ_D, the initial infectivity from pathogens released upon death. We assumed that pathogens accumulate in the cell when multiple release events happen in the same cell and over time. Thus, if a cell already had a positive infectivity, the

value of ρ_D and ρ_S is added for each pathogen release event in that cell. We make the simplifying assumption that the cell infectivity probability is directly proportional to the pathogen load in the environment. Hence, infectivity increased additively with pathogen release, decreased exponentially over time, and was bound between 0 and 1.

1.3.1.c Infectivity decay

We allowed infectivity of a cell to decay over time, assuming that the infectivity ρ of cell c, at time $t+1$ followed an exponential law:

$$\rho_{c,t+1} = \rho_{c,t} \cdot e^{-\mu} \quad (1.4)$$

where μ is the decay rate.

We removed reservoirs from the environment (cell infectivity returned to zero) when we considered their infectivity to be below a minimum level necessary for transmission (as in a minimum infectious dose). This level was based on the initial infectivity of the shed pathogen parameter (ρ_S) and the pathogen decay rate (μ), such that minimum infectivity, ρ_{min} was the infectivity achieved after two half-lives of ρ_S:

$$\rho_{min} = (\rho_S \cdot e^{-\mu})^{\frac{2 \cdot \ln(2)}{\mu}} \quad (1.5)$$

with a decay rate, μ. This approach allowed us to vary ρ_S and ρ_D without changing the duration of infectivity in the environment, which was then solely controlled by μ.

1.3.1.d Disease transmission

Every susceptible host present on an environmental reservoir (i.e., an infectious cell) was at risk of infection. The probability of infection depended on the probability of having a contact with the pathogen that resulted in transmission (*i.e.*, an effective contact), ξ, and of the cell infectivity (see

1.3.1.b and 1.3.1.c for cell infectivity details). For example, in the case of an ingested pathogen, an effective contact could represent the probability of foraging at the reservoir, which would depend on the resource quality (Owen-Smith et al., 2010). In our model, we assumed that ξ depended on resource quality, with effective contacts being twice as likely in high-resource habitats as in medium-resource habitats. When a host effectively had contact with a reservoir, the probability of transmission also depended on the cell's infectivity. The probability of transmission was contingent on an effective contact with a reservoir, and depended on the cell's infectivity.

1.3.1.e Model parameters

In total, eight parameters were varied for each of the three transmission scenarios (parameters in Table 1.1 and the four different landscapes described above). To evaluate the role of each parameter in shaping infection prevalence and the spatial distribution of pathogens in the environment, we used a Latin Hypercube Sampling (LHS) design to obtain 250 parameter sets (Balakrishnan, 2012, package 'FME, v.1.3.6.3, [Soetaert and Petzoldt, 2010]). We chose an LHS over a factorial design due to the high number of parameter sets required by the factorial design. Each parameter set was tested on each transmission scenario, leading to 750 parameter sets. We ran the simulations for each parameter set until we obtained 100 successful simulations, defined as a minimum of five subsequent infections, capping the number of failed simulations at 10,000. Each simulation ran for a maximum of 10,000 steps. Simulations ended when no more susceptible individuals were present in the environment or when the disease faded out (no infected hosts or environmental cells).

The model and subsequent analysis were coded using the R software, version 4.3.2 (R Core Team 2023), using the packages 'dplyr' (v.1.1.3; Wickham et al., 2023), 'tidyr' (v.1.3.0; Wickham et al., 2019), and 'extraDistr' (v.1.9.1; Wolodzko, 2023).

1.3.2 Analysis

For each simulation, we recorded the number of susceptible and infected hosts, the number of cells infected per time step, as well as the infectivity and location of each infected cell every 150 steps.

1.3.2.a Disease dynamics

We assessed the disease dynamics by computing seven summary statistics. Three of these were computed at the parameter set level: (i) the percentage of simulations where the pathogen went extinct before the end of the simulation (referred to as pathogen fade-out), (ii) the percentage of simulations where the population went extinct / was fully immune before the end of the simulation (referred to as susceptible die-out), and (iii) the proportion of successful simulations (at least five subsequent infections). The other four summary statistics obtained for each simulation included: (iv) the proportion of environmental cells that were infectious at least once, (v) the proportion of the host population that was ever infected, (vi) the maximum number of continuous temporal steps with at least one infection occurring, and (vii) the maximum number of consecutive temporal steps between two infections.

For each summary statistic, we conducted a variable importance analysis by fitting random forests (Breiman, 2001). Partial dependence plots (PDPs) were obtained to visualize each parameter's effect. Random forests and variable importance analysis were done using the package 'randomForest' (v.4.7-1.1; Liaw and Wiener, 2002), and the PDPs were created using the package 'pdp' (v.0.8.1; Greenwell, 2017).

1.3.3 Pathogen spatial distribution

To estimate environmental pathogen spatial distribution, we conducted tests for global spatial autocorrelation and local clustering. We computed Moran's I index to determine the global spatial autocorrelation of pathogen reservoirs in the environment using the 'ape' package (v.5.7-1;

Paradis and Schliep, 2019). Moran's I values are bounded between -1 and 1, with -1 designating perfect dispersion of reservoirs in the environment, 0 full randomness, and 1 perfect clustering of environmental reservoirs. We obtained this index every 150 steps of each simulation, then compared between simulations using the median value per simulation. We also conducted a local spatial cluster analysis to identify regions of high environmental infectivity using the software SaTScan (v.10.1.2, https://www.satscan.org/; Kulldorff, 1997) with the R package 'rsatscan' (v.1.0.7; Kleinman, 2023). The analysis ran using a normal distribution on a purely spatial model and a requirement of at least two cells per cluster. We calculated the "infectivity risk" within a cluster by dividing the "risk within" a cluster as SaTScan estimated by the cluster's area. For each simulation, we ran SaTScan every 600 steps, starting at step 300, and recorded the number of unique clusters of high environmental infectivity created over the simulation period. Clusters were considered unique if they overlapped by less than 50% of their area.

We conducted additional variable importance analyses for our metrics of pathogen spatial distribution using random forests and corresponding PDPs. We conducted these analyses with (i) the global clustering of reservoirs (median Moran's I per simulation), (ii) the number of unique clusters created over a simulation, (iii) the mean peak cluster infectivity risk per simulation, and (iv) the mean cluster radius.

1.4 Results

1.4.1 Disease dynamic

Globally, the disease dynamics observed for the OK and SK scenarios were quite similar, suggesting that the deposition of pathogens at death contributes more to shaping the disease dynamics than continuous shedding for diseases when both transmission modes occur. However,

regarding pathogen spatial distributions, the two modes with shedding, SK and CS, were more similar.

Eighteen of the 750 parameter sets did not reach the number of successful simulations required (i.e., fewer than five infections occurred). Of those 18 scenarios, 13 were from the CS scenario, four from the OK, and one from the SK. Using a random forest analysis, we see that for all transmission modes, an increase in reservoir attractivity, β_1, in initial cell infectivity at pathogen shedding, ρ, and a slower pathogen decay rate, μ, led to a higher proportion of successful outbreaks (Table1.2, Appendix Table A1, figure A2). Table 1.2 summarizes the values of the main significant parameters for the variable importance analysis, and Table A1 shows all parameters.

When simulations were successful, four types of outbreaks were observed (figure 1.2). The first outbreak type showed infection of all susceptible hosts before the end of the simulation. The infection was often fast, happening within as few as 1,128 (mean ± standard deviation given for all following results: 5,221 ± 2,127; OK); 821 (5,089 ± 2,292; CS), and 493 steps (4,117 ± 2,080; SK). Second, we could observe a rapid pathogen fade-out, with only a few individuals infected before fade-out, happening as fast as 2,208 (6,463 ± 2,094; OK), 1,536 (5,722 ± 2,329; CS), and 2,282 steps (6,984 ± 1,956; SK). When infections and susceptible hosts were maintained for the entire simulation, these had two different presentations, with either sporadic infections occurring across the simulation, with long periods between consecutive infections, or by having regular infections of only a few individuals at a time (i.e., short periods between consecutive infections).

Overall, the pathogen faded out in 22% of the successful simulations, and the entire population died out or became fully immune in 25%. Specifically, the risk of pathogen fade-out was higher for the CS (29%) compared to the OK (19%) and SK (20%) scenarios. The susceptible hosts died out in 19% of CS simulations, compared to 21% for the OK and 34% for the SK scenarios. From

the simulations where the pathogen faded out, an average of 35% of the population was infected before it faded out. For the CS scenario, 31 parameter sets had a 100% risk of pathogen fade-out, compared to 13 for the OK scenario and only 4 for the SK scenario. The main parameter explaining pathogen fade-out for all transmission scenarios was the pathogen decay rate μ, with an increase in the decay rate leading to an increase in fade-out (figure A3). In contrast, the susceptible hosts died out more often when the pathogen decay rate μ was lower, the reservoir site attracted the hosts (positive β_1), and the initial pathogen infectivity ρ was higher (figure A4).

The differences between sporadic and regular infections were most apparent in the maximum periods of continuous infections and non-infections. Both periods were similar between the three transmission scenarios, with an average of 2.7 (± 1.2) steps with continuous infection and an average of 1,133 (± 961) steps between two infections. With simulations capped at 10,000 steps, some scenarios reached up to 8,839 steps (CS), 9,066 steps (OK), and even 9,697 steps (SK) between infections (figure 1.3a), emphasizing the importance of ETP's ability to spark new outbreaks long after they seemingly died off. For all transmission modes, a decrease in initial reservoir infectivity ρ or pathogen decay μ, and avoidance of reservoir sites (negative β_1) led to longer periods of continuous non-infection (figure A5). Opposite to this, an attraction toward reservoir sites (positive β_1) and an increase in ρ led to longer periods of continuous infection for all three scenarios. Specifically for OK, an increase in the number of susceptible individuals N, and for CS, a longer infection duration γ also increased the periods of continuous infections (figure A6).

While few individuals were typically infected simultaneously, pathogens still often reached high proportions of the host population and the environment. The proportion of the population infected during the simulations varied from 5 individuals (the minimum to be considered a “successful”

simulation) to the entire population. The proportion of infected hosts within a simulation was often high, CS having the lowest proportion with a median of 84.4% (quantile 25%-75%: 2.5%-99.4%), followed by OK with 93.9% (11.6%-99.7%) for OK, and final SK with the highest infection 98.8% (70.0%-100%) for SK. Host attraction to reservoir sites (positive β_1) and higher initial reservoir infectivity ρ were the most important parameters that increased host infection (figure A7).

The proportion of the environmental cells infected at least once over the simulation varied widely, from 0.1% to 98.3% (15.8% ± 17.7%, figure 1.3b). While the minimum number of cells infected was similar for all three transmission scenarios, OK had fewer cells infected at the maximum, with only 46.0% (12.1% ± 9.2%). For this scenario, initial infectivity ρ, the number N of susceptible individuals, and the attraction of reservoirs on host movement β_1 were the most important parameters, with an increase in any of those three increasing the number of cells infected. The CS scenario reached a maximum of 97.3% of the environment infected (14.4% ± 18.9%), and the SK scenario reached 98.3 % (27.6% ± 19.4%). For those scenarios, an increase in the infection duration γ, the initial infectivity of the reservoir ρ, and the number N of susceptible individuals in the simulation led to a higher proportion of environmental cells infected. It is worth noting that reservoir attractivity has a parabolic effect, with both avoidance and very high attractivity leading to a lower spatial extent of environmental infection. This was particularly marked in the SK scenario (figure A8).

1.4.2 Disease spatial distribution

For all scenarios, the median Moran's I for the entire simulation time varied from -0.73 to 0.83, with a mean of 0.03 ± 0.09. The OK scenario drove those extremes, while SK and CS had a minimum and maximum Moran of -0.51 – 0.55 and -0.55 – 0.78, respectively (figure 1.4b). For all transmission modes, the strength of host selection for reservoir sites, β_1, was the main parameter

of importance, followed by the decay rate μ and the initial reservoir infectivity, ρ (figure A9). The spatial autocorrelation always began as negative for all scenarios (i.e., more evenly distributed). For all scenarios, increased avoidance of reservoir sites leads to a Moran's I close to 0, meaning that no spatial autocorrelation of the environmental reservoir is observed (figure 1.4a). When reservoir attraction was present, CS had the highest autocorrelation (i.e., clustering of reservoirs) compared to SK and OK scenarios, and the autocorrelation of SK and OK scenarios peaked earlier than that of CS. Once the peak was reached, spatial autocorrelation was maintained when the pathogen decay rate was low (figure 1.4a.b), but it quickly decreased toward random distribution of environmental reservoirs with the pathogen decay rate (figure 1.4).

When focusing on the local clustering, CS scenarios developed more unique clusters (2.1 ± 1.2) of lower infectivity risk ($9.5 \times 10^{-4} \pm 3.2 \times 10^{-3}$), compared to SK (1.7 ± 0.8 unique cluster with peak infectivity of $4.5 \times 10^{-3} \pm 8.1 \times 10^{-3}$) and OK (1.3 ± 0.6 unique clusters with peak infectivity of $2.7 \times 10^{-3} \pm 8.4 \times 10^{-3}$) scenarios (figure 1.5). However, CS and OK scenarios had similar mean cluster sizes (CS: 3.0 ± 1.7 cell radius; OK: 2.9 ± 2.3), compared to SK (3.5 ± 2.0), but OK clusters reached a maximum radius of up to 34.7 cells, while SK and CS reached a maximum radius of 28.0 and 27.6 respectively.

Depending on the transmission mode, variables explaining the number of unique clusters differed. For SK, the infection duration γ, the proportion of high-resource habitat, p, and the number of susceptible hosts N were most important. For OK, the pathogen decay rate, μ, N, and β_1 were most important. For CS, μ, γ, and β_1 were most important. The parameters μ and β_1 had a parabolic effect, with a minimum number of clusters created at each extreme value (figure 1.5b). This means that neutrality toward the reservoir site and a relatively moderate decay rate led to more high-infectivity clusters. An increase in p and a decrease in N and γ decreased the number of clusters

(figure A10). For all transmission scenarios, the peak infectivity risk within a cluster depended primarily on ρ, β_1, and μ, with an increase in ρ and β_1 and a decrease in μ leading to an increase in the relative risk (figure 1.5a, figure A11). Lastly, parameter importance for cluster size varied by scenario. OK depended on β_1, γ, and ρ; SK on γ, N, and μ; while CS depended on γ, μ and ρ. An increase in N and γ led to larger clusters in all scenarios (figure 1.5). However, the attraction to reservoirs led to bigger clusters for CS but smaller clusters for SK and OK (figure 1.5). An increase in the pathogen decay rate led to smaller clusters in CS but larger clusters in OK. A more parabolic effect was present for SK, with larger clusters at either low or very high decay rates. Finally, an increase in the initial reservoir infectivity increased the cluster size for CS and SK, while larger clusters were recorded at low and high ρ for the OK scenario (figure A12).

1.5 Discussion

Our study aimed to determine how the mode of pathogen release from infected hosts affected the dynamics of ETP outbreaks and their spatial distribution. Our simulations underscore the pivotal role of several key parameters, including the strength of host selection for environmental reservoirs, β_1, the pathogen environmental decay rate, μ, the initial infectivity at pathogen release, ρ, and the infection duration, γ. The density of susceptible hosts emerged as a more influential factor for the spatial distribution of reservoirs than for outbreak dynamics. Surprisingly, the landscape structure played only a minor role in the spatial distribution of the reservoirs, with the aggregation of resources and their effect on host movement not proving to be significant parameters, and the proportion of high-resource habitat only slightly impacted the number of high-infectivity clusters created during an outbreak. The lack of landscape importance may be due to the landscape design not differing enough per simulations or because the landscape variables are categorical, so they could not stand out in the variable importance analysis. This point will be

considered with further analysis. Curiously, the probability of effective contact between hosts was consistently found to be a non-significant factor. We assume that the strong effect of host selection toward reservoir sites, β_1, probably obscured any effect of effective contacts. That parameter was assumingly able to regulate the number of encounters with reservoir sites. The outbreak sizes of the SK scenarios were more similar to those of the OK. In contrast, the spatial distribution of reservoirs for the SK scenario resembles more that of the CS scenario. This suggests that the higher infectivity of reservoirs created from death events matters more for initiating and maintaining outbreaks, while pathogen shedding over the infection period ensures a larger spatial extent of pathogen presence and their connectivity in the environment.

An extended period between two consecutive infections could be observed for every transmission mode, emphasizing the importance of environmental pathogen persistence in sparking outbreaks in places where it had seemingly faded out long previously. Interestingly, a lower pathogen decay rate and lower initial infectivity led to longer periods between consecutive infections. These could be seen as opposite as a slower decay rate leads to more environmental pathogens over time, while a lower initial risk means fewer pathogens in the environmental reservoir. While the concentrations of pathogens released in the environment start at very different numbers, the exponential nature of the decay function means the number of pathogens declines quickly early on, and then pathogens persist at lower numbers for a long time. This may obscure large differences in initial infectivity if exposures do not occur in the earliest steps after reservoir formation. The extended survival of pathogens at low concentrations manifests the ability of low environmental pathogenicity to spark new host infections even when the risk of infections seems below the transmission level. This reinforces the significant threat posed by persistent pathogens as stochasticity and time can lead to the infection of a single unlucky host that can potentially spark a new outbreak (e.g., anthrax

outbreaks can emerge after multiple years gaps [Gachohi et al., 2019; Liskova et al., 2021]). Persistent pathogens complicate the definition of a disease outbreak due to the ability of a single reservoir to re-infect new hosts over long periods. Here, we defined an outbreak as the clustering of infections in space and time, and for persistent pathogens, a single reservoir site can cause multiple outbreaks over time. For migrating species susceptible to environmental pathogens, mostly ectoparasites or those transmitted from fecal-oral transmission, long-distance movements are presumed to lower the disease pressure by allowing them to evade infectious habitats (Altizer et al., 2011). However, the persistence of pathogens in the environment permits re-infection when individuals return.

When pathogens enter the environment through continuous shedding, the spatial extent of environmental contamination is higher than for pathogens released via death events. When only one pathogen release mode is present, a CS scenario creates more infection clusters of lower infectivity than an OK scenario, which creates fewer infectious clusters of higher infectivity. For CS, this translates into a higher spatial autocorrelation among cases, most notably when the infection duration increases and shedding occurs in localized habitats. When the duration of infection increases, but movement decisions toward reservoirs are random or show avoidance, shedding across the landscape leads to a higher percentage of the environment being infectious. This more heterogeneous pathogen distribution under CS can increase the number of contacts between susceptible hosts and the low-risk environmental reservoirs, which translates into a higher number of secondary infections due to higher reservoir encounters. On the other hand, OK makes fewer high-risk hotspots, which have fewer secondary infections; this may be because fewer infectious sites lead to fewer encounters. It appears that for OK, any attraction, even small, toward reservoir sites, high infectivity, and long environmental persistence are necessary to produce a

surge in infection cases instead of sporadic infections over time because the number of contacts between hosts and reservoir may be increased, as well as the risk when contact is effective. For CS to create high-risk hot spots, we can expect attraction to and shedding at specific sites to enhance the risk. For example, scent-marking sites for deer (Huang et al., 2024) and roosting sites for bats (Hoyt et al., 2021) can become high-infectivity hot spots due to continual shedding at these locations.

The model also points out the parabolic effect of β_I and μ on the number of clusters and β_I on the spatial extent of environmental infectivity. Host avoidance of reservoirs and fast pathogen decay lead to few infectivity clusters due to reduced infection risk and shorter survival of the reservoir. However, attraction to the pathogen reservoirs led to fewer clusters and to lower spatial infection extent, probably due to the accumulation of pathogens within the same clustered environmental cells, reducing the spreading of pathogens in the landscape but emphasizing the role of site attraction in creating fewer clusters of higher infectivity. Our model highlights the importance of estimating pathogen risk in the environment, notably to determine where pathogens can accumulate and create infection risk hot spots. While it is not an easy task for ETPs (Becker et al., 2023), focusing on sampling sites where shedding and exposure are more likely to occur would be influential in better estimating and preventing disease transmission risks.

When focusing on landscape infectivity, it was surprising that OK had the lowest spatial autocorrelation with the highest variation in Moran's I. This was most notable when avoidance or neutrality to reservoirs was present and with faster pathogen decay. This may come from the stochasticity in movement decisions, mostly when neutrality toward the reservoir was present, which leads to the highest variation in spatial autocorrelation. Conversely, for pathogens released by CS, spatial autocorrelation was often present, notably when hosts avoided reservoirs and

pathogen reservoirs decayed slowly. For these pathogens, reservoir avoidance pushed individuals to move away from the infectious environment and to deposit parasites in the uninfected landscape, increasing the spatial extent of the pathogen. This was heightened by a slow pathogen decay, which allowed pathogens to be present in the entirety of the landscape at different infectivity levels.

Our general modeling framework allowed us to explore the relative importance of transmission mode, environmental persistence, and the infectivity of environmental reservoirs on ETP outbreak dynamics and spatial distribution. We made some simplifying assumptions to balance computational feasibility and generality in order to reflect most of our knowledge about ETPs. First, the initial infectivity at pathogen release was fixed during a simulation. However, we know that the quantity of pathogen shed by infected hosts may depend on the hosts' sex, age, physiology, and seasons (Altizer et al., 2006). Including variability in the initial infectivity would allow accounting for super-shedding events, which could alter the spatial distribution of the risk, increasing effective transmission contact (Chase-Topping et al., 2008; Matthews et al., 2009). It would also be worth including seasonality in future models as it can alter the transmission risk by altering a reservoir's initial infectivity and pathogen survival. Notably, many pathogens show differential infection per season (Nyerere et al., 2020; Perez-Saez et al., 2022; Pittiglio et al., 2022). Thus, including seasonality could allow periods of the year when few to no infections are present, permitting the visualization and understanding of the main drivers behind the seasonal dynamics. For example, the quantity of anthrax bacterium released by hosts infected during the dry season can be lower by 1.36 orders of magnitude than during the wet season, which subsequently leads to no risk of anthrax transmission from a reservoir created during the dry season (Barandongo et al., 2023; Dolfi et al., 2024). Similarly, eggs of the gastrointestinal nematodes *Haemonchus contortus* and *Trichostrongylus* spp. could not survive when they were deposited during the dry

season (Chiejina et al., 1989). Seasonality can also alter the probability of effective contact with the pathogen due to host behavioral modification, such as changes in habitat quality modifying the contact rate (Breban et al., 2009; Kessler et al., 2018). It can also alter the concentration of pathogens within a reservoir and thus the transmission risk due to climatic events, such as floodings or extreme temperatures (Lau et al., 2010).

To simplify our model, we assumed that hosts would have a fixed response (e.g., avoidance, neutrality, attraction) to environmental reservoirs for the entire duration of a given simulation. However, host responses to environmental reservoirs might vary through time. An initial avoidance might occur when pathogens are released from blood, feces, or dead bodies. However, nutrients released in body fluids may enhance the site attractivity after the environmental cues disappear, while the pathogen concentration is still relevant for transmission. For example, *Bacillus anthracis* can facilitate grass seed germination (Ganz et al., 2014), which may further enhance plant growth and greening up from nutrients released from zebra carcass sites during the following year (Turner et al., 2014), attracting herbivores to the infectious environment. Including this more versatile role of the reservoir on host movement by fluctuating the attraction and repulsion over time could be an important extension of our model.

In this study, we do not simulate any change in behavioral response post-infection. However, pathogens can modify the behavior of individuals, notably as clinical stages of infections develop. For instance, CWD-infected mule deer (*Odocoileus hemionus*) tend to move more slowly and utilize different landscapes, with more individuals dying closer to rivers (Barrile et al., 2024); wolves (*Canis lupus*) infected by sarcoptic mange (*Sarcoptes scabiei*) reduce their daily movement (Cross et al., 2016); and amphibians infected by *Batrachochytrium dendrobatidis* selected warmer and drier open habitat (Barrile et al., 2021). Including behavioral modification

post-infection in our model could be an important factor in better visualizing the pathogens' spatial distribution.

While we only modeled indirect environmental transmission, many diseases can have multiple transmission pathways: environment, vector-borne, and direct contact, the latter arguably being the more common mode of transmission. For example, multiple transmission pathways exist for CWD (Miller et al., 2004; Miller and Williams, 2003), avian influenza (Mata et al., 2019), plague (Russell et al., 2021), or *Batrachochytrium salamandrivorans* (Islam et al., 2021). Persistent environmental pathogens have been shown to maintain and spark new outbreaks long after direct pathogen transmission disappears, and specifically for avian influenza, environmental transmission can be important in starting outbreaks, allowing direct transmission to take over and create intense outbreaks (Breban et al., 2009; Mata et al., 2019; Rohani et al., 2009). For CWD, environmental accumulation of prions within the early phase of the disease introduction, enhanced by direct transmission, may lead to a dominance of indirect transmission in the future due to the long persistence of prions (Almberg et al., 2011). Thus, future models could include the different pathogen transmission modes and unravel the importance of each transmission mode depending on the scale of the outbreak by determining which transmission mode is most important for maintaining an acute outbreak compared to the outbreak initiation.

This study aimed to explore how transmission mode, pathogens characteristics, host movement decisions, and landscape structures alter ETP outbreak dynamics and spatial distribution of environmental reservoirs. Our findings highlight how the different pathogen release modes contribute differently to the outbreaks: death events are more important for the disease dynamics, while continuous shedding events ensure the spatial extent of environmental reservoirs. The host's behavioral response toward the environmental reservoir was consistently a significant factor of

interest; avoidance of the reservoir reduced the intensity of outbreaks but increased the spatial extent of pathogens, while attraction increased the intensity of outbreaks, reducing the spatial extent of the pathogen but increasing the number of high infectivity hotspots. While it can be arduous to determine the role of environmental reservoirs on host behavior, this seems to be an important factor to target in future empirical studies. Notably, future empirical research would benefit from determining specific local environmental sites where hosts are most at risk of shedding pathogens and having effective contact with them. A better understanding of local environmental pathogens and hosts behavioral responses would improve the ability to respond to the emergence of diseases.

1.6 Acknowledgments

We acknowledge the Center for High Throughput Computing at the University of Wisconsin-Madison for providing resources that contributed to the research results reported within this paper (https://chtc.cs.wisc.edu/). This work was funded by the U.S. National Science Foundation grant DEB-1816161/DEB2106221 and the Department of Agriculture, National Institute of Food and Agriculture grant 2022-05138, both through the NSF-NIH-USDA Ecology and Evolution of Infectious Diseases program.

1.7 Tables

TABLE 1-1: Parameter levels used in the simulation, their role in the model, and biological relevance. *Note: The parameter sets tested in the model were obtained using a Latin Hypercube Sample*. RSF = Resource Selection Function.

Parameter	Range	Role in the model	Biological relevance
		Initialization	
N	300 - 800	Number of hosts in the environment	Host density threshold is important in epidemiology (Lloyd-Smith et al., 2005)
		Pathogen dynamic	
ρ_D ρ_S	0.0025 - 0.025 0.00025 - 0.0025	Infectivity of environmental reservoirs upon pathogen release at death (D) or continuous shedding (S)	Quantity of pathogen released, linked to dose-response function (Ng et al., 2022)
μ	0.0002 - 0.002	Pathogen decay rate in the environment	Short vs. Long-lived organisms (Walther and Ewald, 2004)
γ	0.7 - 0.95	Host infection duration	Speed at which animal dies or recovers. Shapes the duration and spatial extent of pathogen shedding and the distance a host may travel before dying (White et al., 2020)
		Host movement and behavior	
β	0 - 6	Strength of selection for habitat quality	Attraction toward better habitat; if high-quality habitat is also more likely to be infectious, ecological traps may form (Leach et al., 2016)
β_I	-1 - 1	Strength of selection/avoidance for environmental reservoirs	Host can be neutral, attracted (Cross et al., 2010), or avoid reservoir cells (Hutchings et al., 2001), shaping the risk of infection

ξ	0.4 – 0.8	Probability of transmission relevant contact in high-quality resource cell	Host may engage more with the environment when in high-quality habitat, which impacts their risk of effective contact with pathogens (Owen-Smith et al., 2010)

TABLE 1-2: Variable importance analysis for the six main parameters of importance (see Appendix Table A1 for all parameters). Values represent the mean decrease in accuracy. The top 3 variables of importance are in bold, and the number of stars shows their order of important *** = most important parameter, ** = 2nd most important, and * = 3rd most important. Values have been scaled for each variable to facilitate their visualization. OK = Obligate-killer; CS = Continuous-shedder; SK = Shedder-Killer. N is the initial population size, β_1 is the host strength of selection for environmental reservoir, γ represents the infection duration; μ is the pathogen decay rate, ρ_D and ρ_S are the initial infectivity at pathogen release for death (D) and shed (S) events.

	Scenario	N	β1	γ	μ	ρ_D	ρ_S
Proportion of successful simulations	OK	-0.42	**1.77*** **	-0.54	**1.30***	**1.69****	
	CS	-0.45	**2.40*** **	0.29	**1.54***		**1.90****
	SK	-0.61	**0.92*** **	-0.70	**0.60****	**0.27***	0.23
Simulations with disease fade out	OK	-0.37	**0.02****	-0.18	**2.41*** **	**-0.14***	
	CS	-0.20	**0.60****	-0.24	**3.75*** **		**0.10***
	SK	-0.31	**-0.05****	-0.41	**2.38*** **	**-0.24***	**-0.24***
Simulations with susceptible die off	OK	-0.62	**1.54*** **	-0.55	**1.38****	**0.92***	
	CS	-0.50	**0.72***	0.42	**1.33*** **		**0.73****
	SK	-0.42	**1.84****	-0.20	**2.38*** **	**0.92***	0.91
Period of continuous non-infection	OK	-0.06	**1.40****	-0.61	**0.88***	**1.73*** **	
	CS	-0.03	**1.30****	0.10	**3.30*** **		**1.27***
	SK	-0.43	**0.73*** **	-0.28	0.28	**0.50***	**0.43****

Period of continuous infection	OK	**0.39***	**2.18*****	-0.35	-0.25	**1.41****	
	CS	0.34	**2.66*****	**1.12***	0.08		**1.70****
	SK	0.28	**1.43*****	-0.14	-0.25	**0.45****	**0.35***
Proportion of infected population	OK	-0.32	**2.41*****	-0.54	**0.13***	**1.70****	
	CS	-0.24	**2.79*****	**0.43***	0.34		**1.88****
	SK	-0.50	**1.31*****	-0.61	-0.05	**0.38***	**0.39****
Proportion of infected cells	OK	**-0.42****	**-0.53***	-0.65	-0.72	**-0.09*****	
	CS	**0.61***	0.41	**3.08*****	0.25		**1.48****
	SK	**1.06****	0.49	**2.54*****	0.22	0.81	**0.87***
Median Moran's Index	OK	-0.41	**0.89*****	-0.67	**0.10****	**0.02***	
	CS	-0.02	**3.60*****	1.17	**1.43***		**1.62****
	SK	-0.34	**1.70*****	-0.36	**0.56****	**-0.06***	**-0.06***
Number of high-infectivity clusters	OK	**-0.64****	**-0.68***	-0.73	**-0.61*****	-0.71	
	CS	1.34	**2.09***	**2.70****	**2.75*****		1.10
	SK	-0.16	**-0.04****	**-0.03*****	-0.16	-0.49	-0.49
Mean relative cluster infectivity	OK	-0.03	**1.04***	0.30	**1.45****	**3.92*****	
	CS	-0.73	**-0.57****	-0.75	**-0.63***		**-0.32*****
	SK	-0.33	**0.60***	0.32	0.34	**1.43****	**1.44*****
Mean cluster size	OK	-0.55	**3.01*****	**1.70****	0.55	**0.71***	
	CS	-0.11	-0.52	**1.19*****	**0.26****		**0.09***
	SK	**0.75****	-0.06	**2.16*****	**0.65***	-0.32	-0.33

1.8 Figures

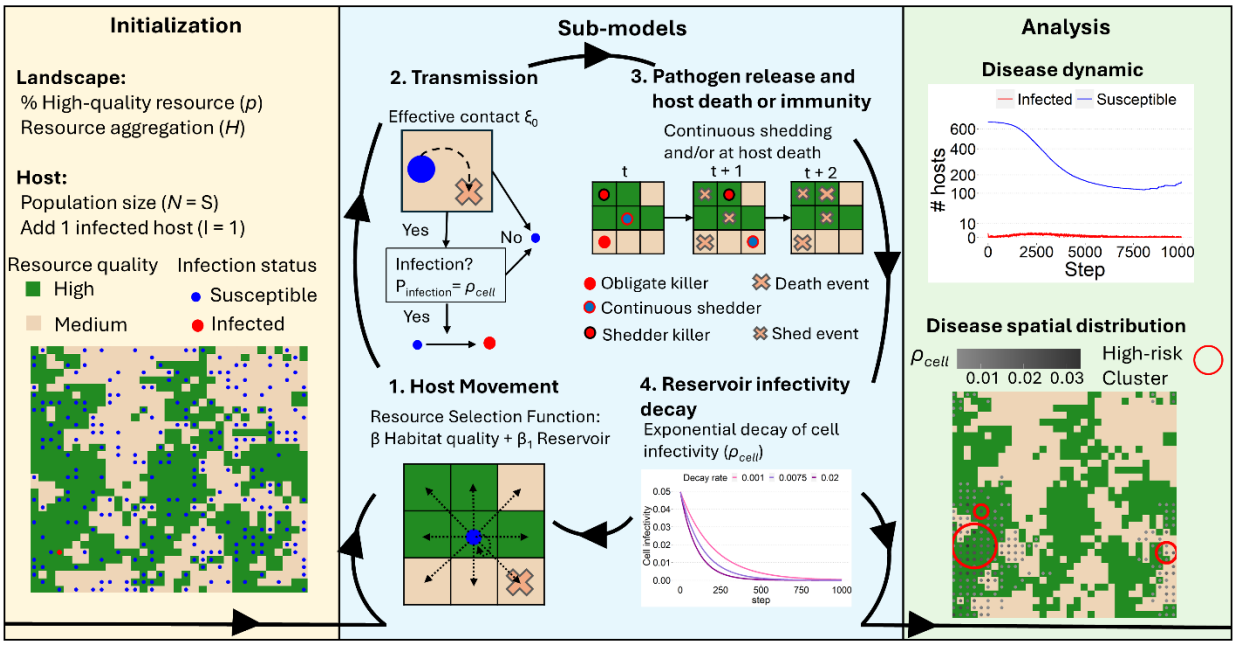

FIGURE 1.1: Overview of the agent-based model process and scheduling. We start by initializing the model. Then, we simulate the host movement, transmission, pathogen release, and cell infectivity for up to 10,000 steps. Finally, we record and analyze the disease dynamics and spatial distribution of the pathogens, by recording the number of high-risk clusters.

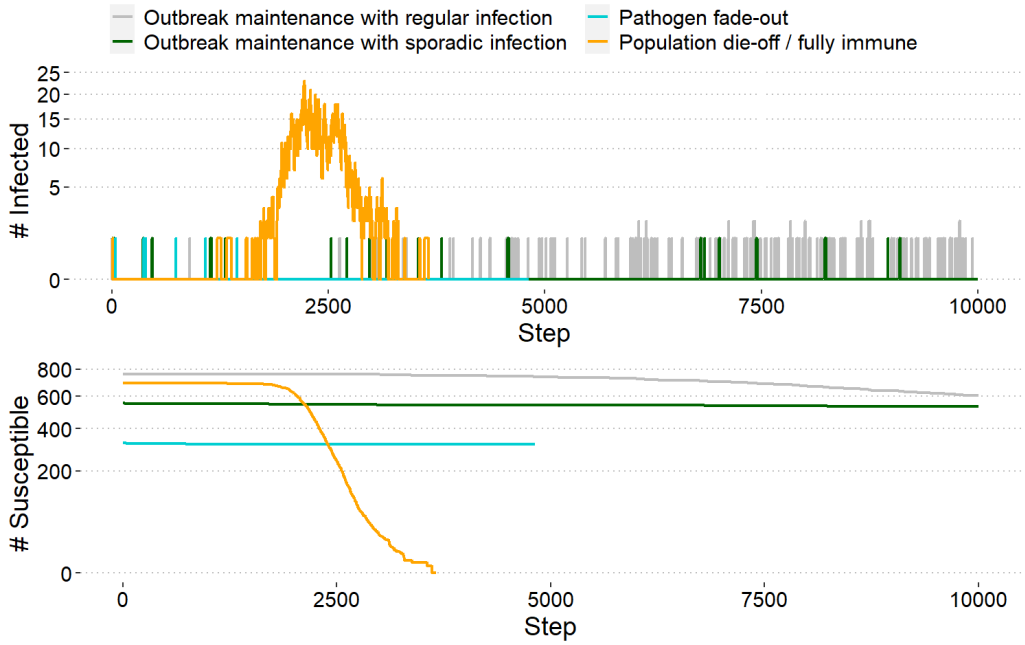

FIGURE 1.2: Four outbreak dynamic types were observed during the simulations. The dynamics represented in this figure represent an example of simulation observed. The top plot represents the number of infected individuals per time step, and the bottom plot shows the number of susceptible individuals. Individuals lose their infected status by either dying from the infection or becoming fully immune; in each case, they are removed from the environment. The four outbreak types are shown in colors: Grey represents outbreaks maintained throughout the simulation, with regular infections occurring. Green represents outbreaks maintained through simulation with only a few sporadic cases. Turquoise shows pathogen fading out after 500 steps. Orange shows the population fully dying/ immune after about 3,500 steps, following a surge in infection, peaking around step 2,500.

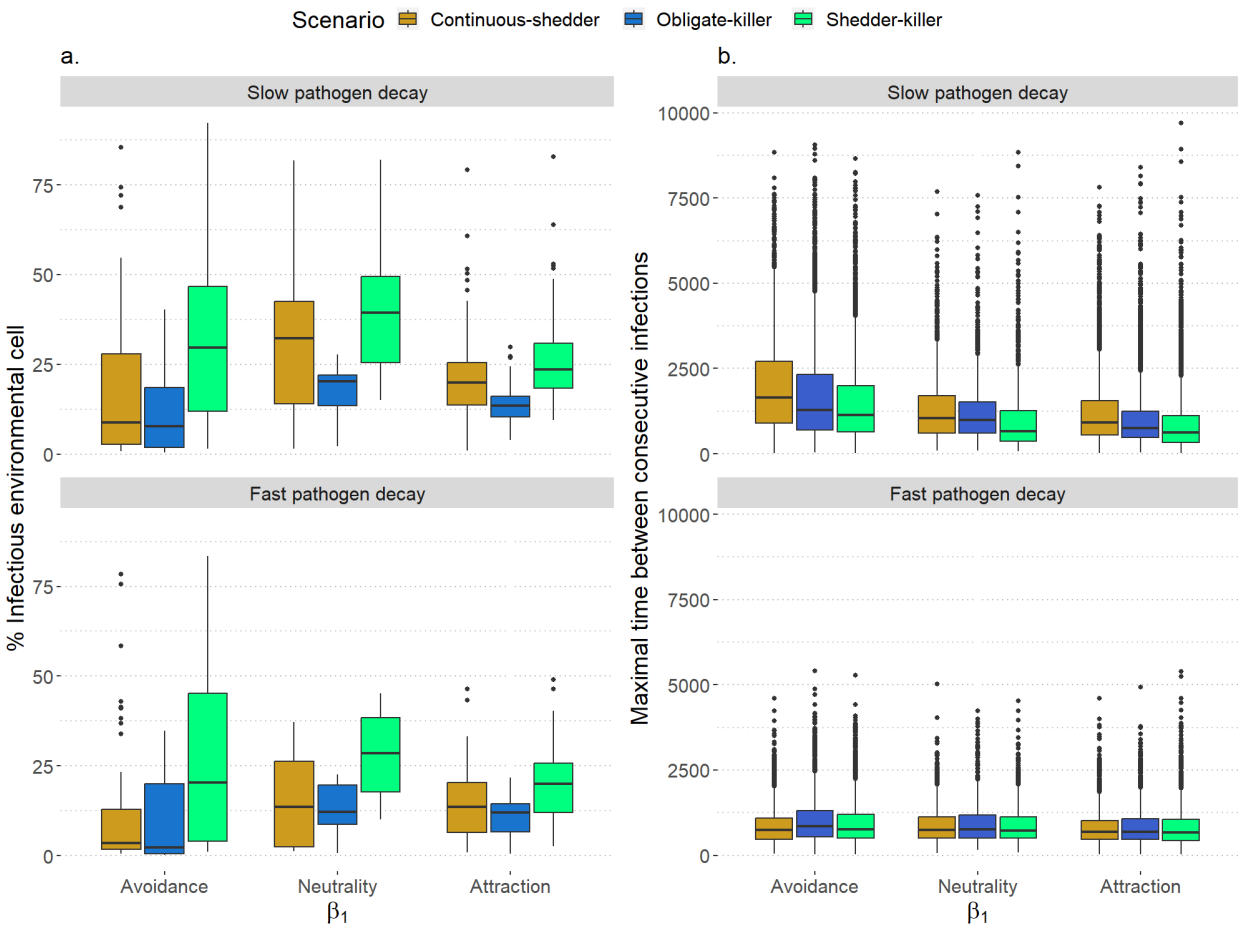

FIGURE 1.3: a. Maximum number of steps between two consecutive infections, and b. percentage of environmental cells that were infectious at least once during the simulation, per simulation depending on the pathogen decay rate (slow decay: $\mu < 7.7 \times 10^{-4}$; fast decay: $\mu > 7.7 \times 10^{-4}$); the transmission mode (yellow: continuous-shedder (CS), blue: obligate-killer (OK); green: shedder-killer (SK)) and the strength of host selection for reservoir sites β_1 (avoidance, neutrality, or attraction). Note that the simulations were capped at 10,000 steps.

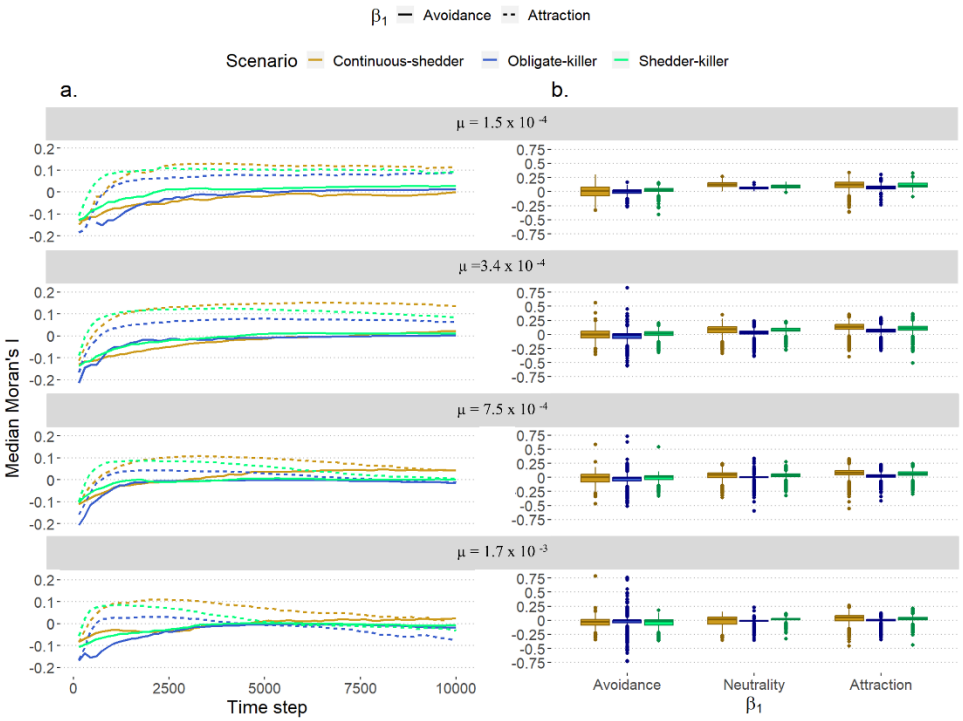

FIGURE 1.4: a. Temporal evolution of the median Moran's I over the 10,000 simulation time steps, and b. Moran's I median per parameter sets. Each plot is split by the pathogen decay rate μ (slowest to fastest decay rate from top to bottom), the strength of host selection for reservoir sites, β_1 (continuous line: avoidance; dashed line: attraction), and the transmission mode (yellow: Continuous-shedder (CS); blue: Obligate-killer (OK), green: Shedder-killer (SK)). A faster decay rate leads to no autocorrelations (Moran's I close to 0) observed for each transmission mode and selection strength. OK presents the highest variation, notably under reservoir avoidance and fast pathogen decay.

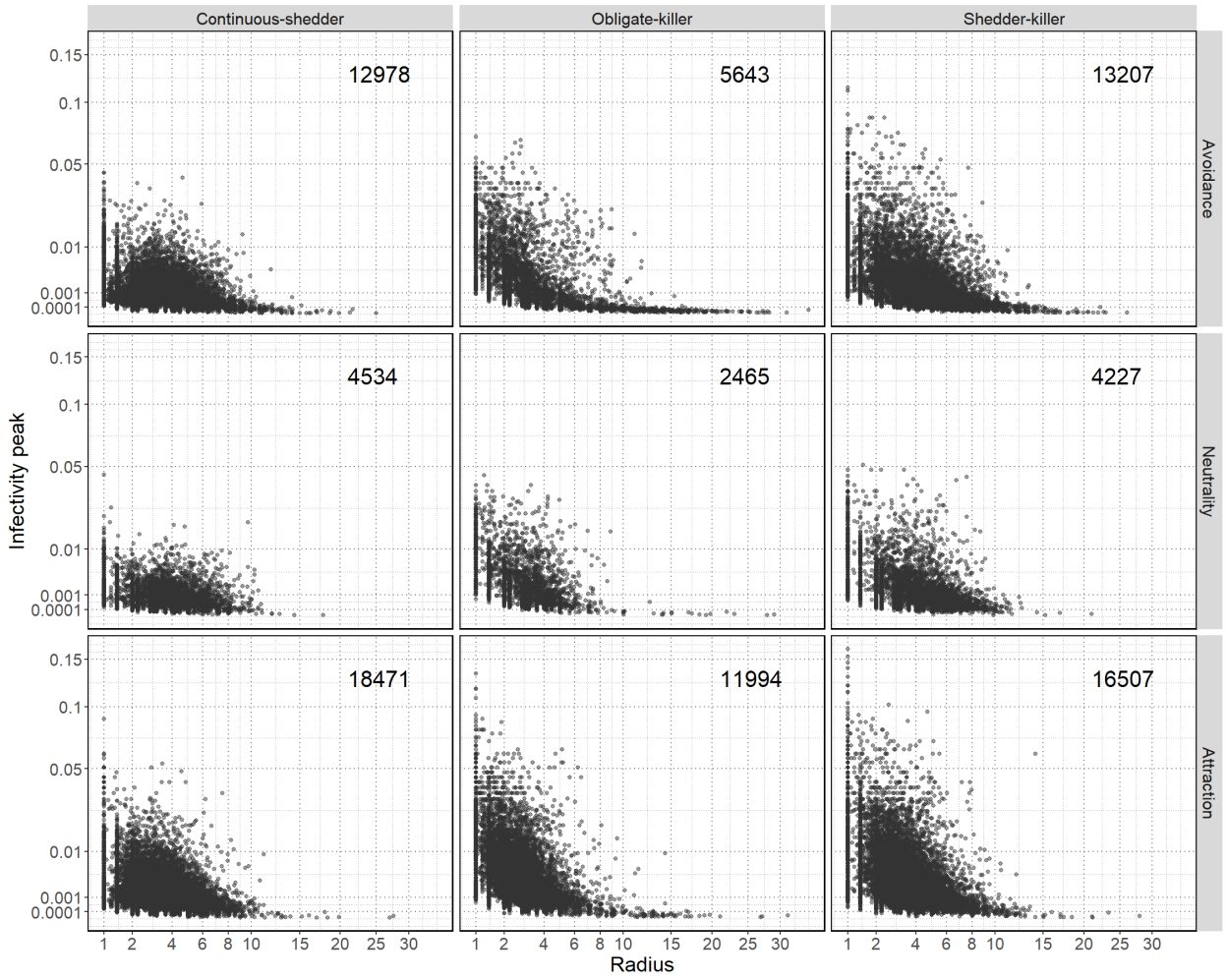

FIGURE 1.5: Scatterplot of the transmission risk clusters peak infectivity depending on the radius. Each panel represents all simulations for the specific pathogen release mode (from left to right: continuous-shedder, obligate-killer, shedder-killer) and for the effect of reservoirs on host movement decisions (from top to bottom: avoidance, neutrality, attraction). The numbers in each panel represent the total number of unique clusters recorded for all simulations. The x and y-axis are square-transformed to facilitate visualization.

1.9 References

Alegbeleye, O.O., Sant'Ana, A.S., 2020. Manure-borne pathogens as an important source of water contamination: An update on the dynamics of pathogen survival/transport as well as practical risk mitigation strategies. Int. J. Hyg. Environ. Health 227, 113524. https://doi.org/10.1016/j.ijheh.2020.113524

Allan, B.F., Keesing, F., Ostfeld, R.S., 2003. Effect of forest fragmentation on Lyme disease risk. Conserv. Biol. 17, 267–272. https://doi.org/10.1046/j.1523-1739.2003.01260.x

Almberg, E.S., Cross, P.C., Johnson, C.J., Heisey, D.M., Richards, B.J., 2011. Modeling routes of chronic wasting disease transmission: environmental prion persistence promotes deer population decline and extinction. PLOS ONE 6, e19896. https://doi.org/10.1371/journal.pone.0019896

Altizer, S., Bartel, R., Han, B.A., 2011. Animal migration and infectious disease risk. Science 331, 296–302. https://doi.org/10.1126/science.1194694

Altizer, S., Dobson, A., Hosseini, P., Hudson, P., Pascual, M., Rohani, P., 2006. Seasonality and the dynamics of infectious diseases. Ecol. Lett. 9, 467–484. https://doi.org/10.1111/j.1461-0248.2005.00879.x

Altizer, S., Ostfeld, R.S., Johnson, P.T.J., Kutz, S., Harvell, C.D., 2013. Climate change and infectious diseases: from evidence to a predictive framework. Science 341, 514–519. https://doi.org/10.1126/science.1239401

Amman, B.R., Schuh, A.J., Albariño, C.G., Towner, J.S., 2021. Marburg virus persistence on fruit as a plausible route of bat to primate filovirus transmission. Viruses 13, 2394. https://doi.org/10.3390/v13122394

Andrioli, D.C., Busato, M.A., Lutinski, J.A., 2020. Spatial and temporal distribution of dengue in Brazil, 1990 - 2017. PLOS ONE 15, e0228346. https://doi.org/10.1371/journal.pone.0228346

Balakrishnan, N., 2012. Methods and applications of statistics in the atmospheric and earth sciences. John Wiley & Sons.

Barandongo, Z.R., Dolfi, A.C., Bruce, S.A., Rysava, K., Huang, Y.-H., Joel, H., Hassim, A., Kamath, P.L., van Heerden, H., Turner, W.C., 2023. The persistence of time: the lifespan of *Bacillus anthracis* spores in environmental reservoirs. Res. Microbiol., Insights into the Bacillus anthracis cereus thuringiensis 2022 conference 174, 104029. https://doi.org/10.1016/j.resmic.2023.104029

Barrile, G.M., Chalfoun, A.D., Walters, A.W., 2021. Infection status as the basis for habitat choices in a wild amphibian. Am. Nat. 197, 128–137. https://doi.org/10.1086/711927

Barrile, G.M., Cross, P.C., Stewart, C., Malmberg, J., Jakopak, R.P., Binfet, J., Monteith, K.L., Werner, B., Jennings-Gaines, J., Merkle, J.A., 2024. Chronic wasting disease alters the movement behavior and habitat use of mule deer during clinical stages of infection. Ecol. Evol. 14, e11418. https://doi.org/10.1002/ece3.11418

Becker, D.J., Eby, P., Madden, W., Peel, A.J., Plowright, R.K., 2023. Ecological conditions predict the intensity of Hendra virus excretion over space and time from bat reservoir hosts. Ecol. Lett. 26, 23–36. https://doi.org/10.1111/ele.14007

Belanger, R.J., Edwards, M.A., Carbyn, L.N., Nielsen, S.E., 2020. Evaluating trade-offs between forage, biting flies, and footing on habitat selection by wood bison (*Bison bison athabascae*). Can. J. Zool. 98, 254–261. https://doi.org/10.1139/cjz-2019-0201

Bellan, S.E., Gimenez, O., Choquet, R., Getz, W.M., 2013. A hierarchical distance sampling approach to estimating mortality rates from opportunistic carcass surveillance data. Methods Ecol. Evol. 4, 361–369. https://doi.org/10.1111/2041-210x.12021

Blanton, J.D., Dyer, J., McBrayer, J., Rupprecht, C.E., 2012. Rabies surveillance in the United States during 2011. J. Am. Vet. Med. Assoc. 241, 712–722. https://doi.org/10.2460/javma.241.6.712

Bonilla-Aldana, D.K., Jimenez-Diaz, S.D., Barboza, J.J., Rodriguez-Morales, A.J., 2022. Mapping the spatiotemporal distribution of Bovine rabies in Colombia, 2005–2019. Trop. Med. Infect. Dis. 7, 406. https://doi.org/10.3390/tropicalmed7120406

Bonnell, T.R., Ghai, R.R., Goldberg, T.L., Sengupta, R., Chapman, C.A., 2018. Spatial configuration becomes more important with increasing habitat loss: a simulation study of environmentally-transmitted parasites. Landsc. Ecol. 33, 1259–1272. https://doi.org/10.1007/s10980-018-0666-4

Breban, R., Drake, J.M., Stallknecht, D.E., Rohani, P., 2009. The role of environmental transmission in recurrent Avian Influenza epidemics. PLOS Comput. Biol. 5, e1000346. https://doi.org/10.1371/journal.pcbi.1000346

Breiman, L., 2001. Random Forests. Mach. Learn. 45, 5–32. https://doi.org/10.1023/A:1010933404324

Brook, R.K., Wal, E.V., van Beest, F.M., McLachlan, S.M., 2013. Evaluating use of cattle winter feeding areas by elk and white-tailed deer: Implications for managing bovine tuberculosis transmission risk from the ground up. Prev. Vet. Med. 108, 137–147. https://doi.org/10.1016/j.prevetmed.2012.07.017

Buck, J.C., Weinstein, S.B., Young, H.S., 2018. Ecological and evolutionary consequences of parasite avoidance. Trends Ecol. Evol. 33, 619–632. https://doi.org/10.1016/j.tree.2018.05.001

Carter, E.D., DeMarchi, J.A., Wilber, M.Q., Miller, D.L., Gray, M.J., 2024. *Batrachochytrium salamandrivorans* is necronotic: carcasses could play a role in Bsal transmission. Front. Amphib. Reptile Sci. 2. https://doi.org/10.3389/famrs.2024.1284608

Chang, Y., Hartemink, N., Byrne, A.W., Gormley, E., McGrath, G., Tratalos, J.A., Breslin, P., More, S.J., de Jong, M.C.M., 2023. Inferring bovine tuberculosis transmission between cattle and badgers via the environment and risk mapping. Front. Vet. Sci. 10, 1233173. https://doi.org/10.3389/fvets.2023.1233173

Chase-Topping, M., Gally, D., Low, C., Matthews, L., Woolhouse, M., 2008. Super-shedding and the link between human infection and livestock carriage of *Escherichia coli* O157. Nat. Rev. Microbiol. 6, 904–912. https://doi.org/10.1038/nrmicro2029

Chen, B., Morales, R., Barria, M.A., Soto, C., 2010. Estimating prion concentration in fluids and tissues by quantitative PMCA. Nat. Methods 7, 519–520. https://doi.org/10.1038/nmeth.1465

Chiejina, S.N., Fakae, B.B., Eze, P.I., 1989. Development and survival of free-living stages of gastrointestinal nematodes of sheep and goats on pasture in the Nigerian derived savanna. Vet. Res. Commun. 13, 103–112. https://doi.org/10.1007/BF00346720

Cowie, C.E., Hutchings, M.R., Barasona, J.A., Gortázar, C., Vicente, J., White, P.C.L., 2016. Interactions between four species in a complex wildlife: livestock disease community: implications for *Mycobacterium bovis* maintenance and transmission. Eur. J. Wildl. Res. 62, 51–64. https://doi.org/10.1007/s10344-015-0973-x

Cross, P.C., Almberg, E.S., Haase, C.G., Hudson, P.J., Maloney, S.K., Metz, M.C., Munn, A.J., Nugent, P., Putzeys, O., Stahler, D.R., Stewart, A.C., Smith, D.W., 2016. Energetic costs of mange in wolves estimated from infrared thermography. Ecology 97, 1938–1948. https://doi.org/10.1890/15-1346.1

Cross, P.C., Heisey, D.M., Scurlock, B.M., Edwards, W.H., Ebinger, M.R., Brennan, A., 2010. Mapping Brucellosis increases relative to elk density using hierarchical Bayesian models. PLOS ONE 5, e10322. https://doi.org/10.1371/journal.pone.0010322

Dolfi, A.C., Kausrud, K., Rysava, K., Champagne, C., Huang, Y.-H., Barandongo, Z.R., Turner, W.C., 2024. Season of death, pathogen persistence and wildlife behaviour alter number of anthrax secondary infections from environmental reservoirs. Proc. R. Soc. B Biol. Sci. 291, 20232568. https://doi.org/10.1098/rspb.2023.2568

Dougherty, E.R., Seidel, D.P., Carlson, C.J., Getz, W.M., 2018. Using movement data to estimate contact rates in a simulated environmentally-transmitted disease system. https://doi.org/10.1101/261198

Edson, D., Field, H., McMichael, L., Jordan, D., Kung, N., Mayer, D., Smith, C., 2015. Flying-fox roost disturbance and Hendra virus spillover risk. PLOS ONE 10, e0125881. https://doi.org/10.1371/journal.pone.0125881

Egan, M.E., Pepin, K.M., Fischer, J.W., Hygnstrom, S.E., VerCauteren, K.C., Bastille-Rousseau, G., 2023. Social network analysis of white-tailed deer scraping behavior: Implications for disease transmission. Ecosphere 14, e4434. https://doi.org/10.1002/ecs2.4434

Gachohi, J.M., Gakuya, F., Lekolool, I., Osoro, E., Nderitu, L., Munyua, P., Ngere, I., Kemunto, N., Bett, B., Otieno, F., Muturi, M., Mwatondo, A., Widdowson, M.A., Njenga, M.K.,

2019. Temporal and spatial distribution of anthrax outbreaks among Kenyan wildlife, 1999–2017. Epidemiol. Infect. 147, e249. https://doi.org/10.1017/S0950268819001304

Ganz, H.H., Turner, W.C., Brodie, E.L., Kusters, M., Shi, Y., Sibanda, H., Torok, T., Getz, W.M., 2014. Interactions between *Bacillus anthracis* and plants may promote anthrax transmission. PLoS Negl. Trop. Dis. 8, e2903. https://doi.org/10.1371/journal.pntd.0002903

Garrett, K.B., Box, E.K., Cleveland, C.A., Majewska, A.A., Yabsley, M.J., 2020. Dogs and the classic route of guinea worm transmission: an evaluation of copepod ingestion. Sci. Rep. 10, 1430. https://doi.org/10.1038/s41598-020-58191-4

Gerba, C.P., 2009. Environmentally transmitted pathogens. Environ. Microbiol. 445–484. https://doi.org/10.1016/B978-0-12-370519-8.00022-5

Gillespie, T.R., Chapman, C.A., 2008. Forest fragmentation, the decline of an endangered primate, and changes in host–parasite interactions relative to an unfragmented forest. Am. J. Primatol. 70, 222–230. https://doi.org/10.1002/ajp.20475

Gottdenker, N.L., Streicker, D.G., Faust, C.L., Carroll, C.R., 2014. Anthropogenic land use change and infectious diseases: a review of the evidence. EcoHealth 11, 619–632. https://doi.org/10.1007/s10393-014-0941-z

Greenwell, B., M., 2017. pdp: An R package for constructing partial dependence plots. R J. 9, 421. https://doi.org/10.32614/RJ-2017-016

Grimm, V., Railsback, S.F., Vincenot, C.E., Berger, U., Gallagher, C., DeAngelis, D.L., Edmonds, B., Ge, J., Giske, J., Groeneveld, J., Johnston, A.S.A., Milles, A., Nabe-Nielsen, J., Polhill, J.G., Radchuk, V., Rohwäder, M.-S., Stillman, R.A., Thiele, J.C., Ayllón, D., 2020. The ODD protocol for describing agent-based and other simulation

models: a second update to improve clarity, replication, and structural realism. J. Artif. Soc. Soc. Simul. 23, 7. https://doi.org/10.18564/jasss.4259

Hagenaars, T.J., Donnelly, C.A., Ferguson, N.M., 2004. Spatial heterogeneity and the persistence of infectious diseases. J. Theor. Biol. 229, 349–359. https://doi.org/10.1016/j.jtbi.2004.04.002

Haley, N.J., Mathiason, C.K., Zabel, M.D., Telling, G.C., Hoover, E.A., 2009. Detection of sub-clinical CWD infection in conventional test-negative deer long after oral exposure to urine and feces from CWD+ deer. PLOS ONE 4, e7990. https://doi.org/10.1371/journal.pone.0007990

Hazrin, M., Hiong, H.G., Jai, N., Yeop, N., Hatta, M., Paiwai, F., Joanita, S., Othman, W., 2016. Spatial distribution of dengue incidence: a case study in Putrajaya. J. Geogr. Inf. Syst. 8, 89–97. https://doi.org/10.4236/jgis.2016.81009

Heylen, D., Lasters, R., Adriaensen, F., Fonville, M., Sprong, H., Matthysen, E., 2019. Ticks and tick-borne diseases in the city: role of landscape connectivity and green space characteristics in a metropolitan area. Sci. Total Environ. 670, 941–949. https://doi.org/10.1016/j.scitotenv.2019.03.235

Hoyt, J.R., Kilpatrick, A.M., Langwig, K.E., 2021. Ecology and impacts of white-nose syndrome on bats. Nat. Rev. Microbiol. 19, 196–210. https://doi.org/10.1038/s41579-020-00493-5

Huang, M.H.J., Demarais, S., Banda, A., Strickland, B.K., Welch, A.G., Hearst, S., Lichtenberg, S., Houston, A., Pepin, K.M., VerCauteren, K.C., 2024. Expanding CWD disease surveillance options using environmental contamination at deer signposts. Ecol. Solut. Evid. 5, e12298. https://doi.org/10.1002/2688-8319.12298

Hugh-Jones, M.E., de Vos, V., 2002. Anthrax and wildlife. Rev. Sci. Tech. Int. Off. Epizoot. 21, 359–383. https://doi.org/10.20506/rst.21.2.1336

Hutchings, M.R., Gordon, I.J., Kyriazakis, I., Jackson, F., 2001. Sheep avoidance of faeces-contaminated patches leads to a trade-off between intake rate of forage and parasitism in subsequent foraging decisions. Anim. Behav. 62, 955–964. https://doi.org/10.1006/anbe.2001.1837

Islam, M.R., Gray, M.J., Peace, A., 2021. Identifying the dominant transmission pathway in a multi-stage infection model of the emerging fungal pathogen *Batrachochytrium Salamandrivorans* on the eastern newt. Infectious Diseases and Our Planet. Springer International Publishing, Cham, pp. 193–216. https://doi.org/10.1007/978-3-030-50826-5_7

Kari, J., 2005. Theory of cellular automata: a survey. Theor. Comput. Sci. 334, 3–33. https://doi.org/10.1016/j.tcs.2004.11.021

Kessler, M.K., Becker, D.J., Peel, A.J., Justice, N.V., Lunn, T., Crowley, D.E., Jones, D.N., Eby, P., Sánchez, C.A., Plowright, R.K., 2018. Changing resource landscapes and spillover of henipaviruses. Ann. N. Y. Acad. Sci. 1429, 78–99. https://doi.org/10.1111/nyas.13910

Kleinman, K., 2023. rsatscan: Tools, classes, and methods for interfacing with "SaTScan" stand-alone software_. R package version 1.0.7,.

Koelle, K., Pascual, M., Yunus, M., 2005. Pathogen adaptation to seasonal forcing and climate change. Proc. R. Soc. B Biol. Sci. 272, 971–977. https://doi.org/10.1098/rspb.2004.3043

Kulldorff, M., 1997. A spatial scan statistic. Commun. Stat. - Theory Methods. https://doi.org/10.1080/03610929708831995

Lau, C.L., Smythe, L.D., Craig, S.B., Weinstein, P., 2010. Climate change, flooding, urbanisation and leptospirosis: fuelling the fire? Trans. R. Soc. Trop. Med. Hyg. 104, 631–638. https://doi.org/10.1016/j.trstmh.2010.07.002

Leach, C.B., Webb, C.T., Cross, P.C., 2016. When environmentally persistent pathogens transform good habitat into ecological traps. R. Soc. Open Sci. 3, 160051. https://doi.org/10.1098/rsos.160051

Levett, P.N., Branch, S.L., Whittington, C.U., Edwards, C.N., Paxton, H., 2001. Two methods for rapid serological diagnosis of acute Leptospirosis. Clin. Diagn. Lab. Immunol. 8, 349–351. https://doi.org/10.1128/cdli.8.2.349-351.2001

Liaw, A., Wiener, M., 2002. Classification and regression by randomForest 2.

Lindenmayer, D.B., Likens, G.E., Andersen, A., Bowman, D., Bull, C.M., Burns, E., Dickman, C.R., Hoffmann, A.A., Keith, D.A., Liddell, M.J., Lowe, A.J., Metcalfe, D.J., Phinn, S.R., Russell-Smith, J., Thurgate, N., Wardle, G.M., 2012. Value of long-term ecological studies. Austral Ecol. 37, 745–757. https://doi.org/10.1111/j.1442-9993.2011.02351.x

Liskova, E.A., Egorova, I.Y., Selyaninov, Y.O., Razheva, I.V., Gladkova, N.A., Toropova, N.N., Zakharova, O.I., Burova, O.A., Surkova, G.V., Malkhazova, S.M., Korennoy, F.I., Iashin, I.V., Blokhin, A.A., 2021. Reindeer anthrax in the Russian arctic, 2016: climatic determinants of the outbreak and vaccination effectiveness. Front. Vet. Sci. 8. https://doi.org/10.3389/fvets.2021.668420

Lloyd-Smith, J.O., Cross, P.C., Briggs, C.J., Daugherty, M., Getz, W.M., Latto, J., Sanchez, M.S., Smith, A.B., Swei, A., 2005. Should we expect population thresholds for wildlife disease? Trends Ecol. Evol. 20, 511–519. https://doi.org/10.1016/j.tree.2005.07.004

Mata, M.A., Greenwood, P., Tyson, R., 2019. The relative contribution of direct and environmental transmission routes in stochastic avian flu epidemic recurrence: an approximate analysis. Bull. Math. Biol. 81, 4484–4517. https://doi.org/10.1007/s11538-018-0414-6

Mathiason, C.K., Hayes-Klug, J., Hays, S.A., Powers, J., Osborn, D.A., Dahmes, S.J., Miller, K.V., Warren, R.J., Mason, G.L., Telling, G.C., Young, A.J., Hoover, E.A., 2010. B Cells and platelets harbor prion infectivity in the blood of deer infected with chronic wasting disease. J. Virol. 84, 5097–5107. https://doi.org/10.1128/jvi.02169-09

Matthews, L., Reeve, R., Woolhouse, M.E.J., Chase-Topping, M., Mellor, D.J., Pearce, M.C., Allison, L.J., Gunn, G.J., Low, J.C., Reid, S.W.J., 2009. Exploiting strain diversity to expose transmission heterogeneities and predict the impact of targeting supershedding. Epidemics 1, 221–229. https://doi.org/10.1016/j.epidem.2009.10.002

Mavrot, F., Orsel, K., Hutchins, W., Adams, L.G., Beckmen, K., Blake, J.E., Checkley, S.L., Davison, T., Francesco, J.D., Elkin, B., Leclerc, L.-M., Schneider, A., Tomaselli, M., Kutz, S.J., 2020. Novel insights into serodiagnosis and epidemiology of *Erysipelothrix rhusiopathiae*, a newly recognized pathogen in muskoxen (*Ovibos moschatus*). PLOS ONE 15, e0231724. https://doi.org/10.1371/journal.pone.0231724

Miller, M.W., Williams, E.S., 2003. Horizontal prion transmission in mule deer. Nature 425, 35–36. https://doi.org/10.1038/425035a

Miller, M.W., Williams, E.S., Hobbs, N.T., Wolfe, L.L., 2004. Environmental sources of prion transmission in mule deer. Emerg. Infect. Dis. 10, 1003–1006. https://doi.org/10.3201/eid1006.040010

Miller, R., Kaneene, J.B., Fitzgerald, S.D., Schmitt, S.M., 2003. Evaluation of the influence of supplemental feeding of white-tailed deer (*Odocoileus virginianus*) on the tuberculosis in the Michigan deer population. J. Wildl. Dis. 39, 84–95. https://doi.org/10.7589/0090-3558-39.1.84

Mitchell, K.M., Churcher, T.S., Garner, T.W.J., Fisher, M.C., 2007. Persistence of the emerging pathogen *Batrachochytrium dendrobatidis* outside the amphibian host greatly increases the probability of host extinction. Proc. R. Soc. B Biol. Sci. 275, 329–334. https://doi.org/10.1098/rspb.2007.1356

Ng, W.H., Myers, C.R., McArt, S.H., Ellner, S.P., 2022. Pathogen transport amplifies or dilutes disease transmission depending on the host dose-response relationship. Ecol. Lett. 25, 453–465. https://doi.org/10.1111/ele.13932

Nyerere, N., Luboobi, L.S., Mpeshe, S.C., Shirima, G.M., 2020. Modeling the impact of seasonal weather variations on the infectiology of Brucellosis. Comput. Math. Methods Med. 2020, 8972063. https://doi.org/10.1155/2020/8972063

Ostfeld, R.S., Glass, G.E., Keesing, F., 2005. Spatial epidemiology: an emerging (or re-emerging) discipline. Trends Ecol. Evol. 20, 328–336. https://doi.org/10.1016/j.tree.2005.03.009

Owen-Smith, N., Fryxell, J.M., Merrill, E.H., 2010. Foraging theory upscaled: the behavioural ecology of herbivore movement. Philos. Trans. R. Soc. B Biol. Sci. 365, 2267–2278. https://doi.org/10.1098/rstb.2010.0095

Paradis, E., Schliep, K., 2019. ape 5.0: an environment for modern phylogenetics and evolutionary analyses in R. Bioinformatics 35, 526–528. https://doi.org/10.1093/bioinformatics/bty633

Payne, A., Philipon, S., Hars, J., Dufour, B., Gilot-Fromont, E., 2017. Wildlife interactions on baited places and waterholes in a French area infected by bovine tuberculosis. Front. Vet. Sci. 3. https://doi.org/10.3389/fvets.2016.00122

Perez-Saez, J., Lessler, J., Lee, E.C., Luquero, F.J., Malembaka, E.B., Finger, F., Langa, J.P., Yennan, S., Zaitchik, B., Azman, A.S., 2022. The seasonality of cholera in sub-Saharan Africa: a statistical modelling study. Lancet Glob. Health 10, e831–e839. https://doi.org/10.1016/S2214-109X(22)00007-9

Pittiglio, C., Shadomy, S., El Idrissi, A., Soumare, B., Lubroth, J., Makonnen, Y., 2022. Seasonality and ecological suitability modelling for anthrax (*Bacillus anthracis*) in Western Africa. Animals 12, 1146. https://doi.org/10.3390/ani12091146

Plowright, R.K., Parrish, C.R., McCallum, H., Hudson, P.J., Ko, A.I., Graham, A.L., Lloyd-Smith, J.O., 2017. Pathways to zoonotic spillover. Nat. Rev. Microbiol. 15, 502–510. https://doi.org/10.1038/nrmicro.2017.45

Poirotte, C., Massol, F., Herbert, A., Willaume, E., Bomo, P.M., Kappeler, P.M., Charpentier, M.J.E., 2017. Mandrills use olfaction to socially avoid parasitized conspecifics. Sci. Adv. 3, e1601721. https://doi.org/10.1126/sciadv.1601721

R Core Team, 2023. R: A language and environment for statistical computing. R Foundation for Statistical Computing, Vienna, Austria.

Redman, E.M., Wilson, K., Cory, J.S., 2016. Trade-offs and mixed infections in an obligate-killing insect pathogen. J. Anim. Ecol. 85, 1200–1209. https://doi.org/10.1111/1365-2656.12547

Rohani, P., Breban, R., Stallknecht, D.E., Drake, J.M., 2009. Environmental transmission of low pathogenicity avian influenza viruses and its implications for pathogen invasion. Proc. Natl. Acad. Sci. 106, 10365–10369. https://doi.org/10.1073/pnas.0809026106

Rumschlag, S.L., Roth, S.A., McMahon, T.A., Rohr, J.R., Civitello, D.J., 2022. Variability in environmental persistence but not per capita transmission rates of the amphibian chytrid fungus leads to differences in host infection prevalence. J. Anim. Ecol. 91, 170–181. https://doi.org/10.1111/1365-2656.13612

Russell, R.E., Walsh, D.P., Samuel, M.D., Grunnill, M.D., Rocke, T.E., 2021. Space matters: host spatial structure and the dynamics of plague transmission. Ecol. Model. 443, 109450. https://doi.org/10.1016/j.ecolmodel.2021.109450

Sá, R.M., Petrášová, J., Pomajbíková, K., Profousová, I., Petrželková, K.J., Sousa, C., Cable, J., Bruford, M.W., Modrý, D., 2013. Gastrointestinal symbionts of chimpanzees in Cantanhez National Park, guinea-bissau with respect to habitat fragmentation. Am. J. Primatol. 75, 1032–1041. https://doi.org/10.1002/ajp.22170

Sánchez, K.F., Zhong, B., Agudelo, J.A., Duffy, M.A., 2023. Infectivity of the parasite *Metschnikowia bicuspidata* is decreased by time spent as a transmission spore, but exposure to phycotoxins in the water column has no effect. Freshw. Biol. 68, 1020–1030. https://doi.org/10.1111/fwb.14082

Schlaepfer, M.A., Runge, M.C., Sherman, P.W., 2002. Ecological and evolutionary traps. Trends Ecol. Evol. 17, 474–480. https://doi.org/10.1016/S0169-5347(02)02580-6

Schramm, P.T., Johnson, C.J., Mathews, N.E., McKenzie, D., Aiken, J.M., Pedersen, J.A., 2006. Potential role of soil in the transmission of prion disease. Rev. Mineral. Geochem. 64, 135–152. https://doi.org/10.2138/rmg.2006.64.5

Shaweno, D., Karmakar, M., Alene, K.A., Ragonnet, R., Clements, A.C., Trauer, J.M., Denholm, J.T., McBryde, E.S., 2018. Methods used in the spatial analysis of tuberculosis epidemiology: a systematic review. BMC Med. 16, 193. https://doi.org/10.1186/s12916-018-1178-4

Soetaert, K., Petzoldt, T., 2010. Inverse modelling, sensitivity and Monte Carlo analysis in *R* using package FME. J. Stat. Softw. 33. https://doi.org/10.18637/jss.v033.i03

Sorensen, A., van Beest, F.M., Brook, R.K., 2014. Impacts of wildlife baiting and supplemental feeding on infectious disease transmission risk: a synthesis of knowledge. Prev. Vet. Med. 113, 356–363. https://doi.org/10.1016/j.prevetmed.2013.11.010

Turner, M.G., Gardner, R.H., 2015. Landscape ecology in theory and practice: pattern and process. Springer New York, New York, NY. https://doi.org/10.1007/978-1-4939-2794-4

Turner, W.C., Kamath, P.L., van Heerden, H., Huang, Y.-H., Barandongo, Z.R., Bruce, S.A., Kausrud, K., 2021. The roles of environmental variation and parasite survival in virulence–transmission relationships. R. Soc. Open Sci. 8, 210088. https://doi.org/10.1098/rsos.210088

Turner, W.C., Kausrud, K.L., Krishnappa, Y.S., Cromsigt, J.P.G.M., Ganz, H.H., Mapaure, I., Cloete, C.C., Havarua, Z., Küsters, M., Getz, W.M., Stenseth, N.Chr., 2014. Fatal attraction: vegetation responses to nutrient inputs attract herbivores to infectious anthrax carcass sites. Proc. R. Soc. B Biol. Sci. 281, 20141785. https://doi.org/10.1098/rspb.2014.1785

Ugochukwu, I.C.I., Samuel, F., Orakpoghenor, O., Nwobi, O.C., Anyaoha, C.O., Majesty-Alukagberie, L.O., Ugochukwu, M.O., Ugochukwu, E.I., 2019. Erysipelas, the

opportunistic zoonotic disease: history, epidemiology, pathology, and diagnosis—a review. Comp. Clin. Pathol. 28, 853–859. https://doi.org/10.1007/s00580-018-2856-5

Van den Bossche, P., de La Rocque, S., Hendrickx, G., Bouyer, J., 2010. A changing environment and the epidemiology of tsetse-transmitted livestock trypanosomiasis. Trends Parasitol. 26, 236–243. https://doi.org/10.1016/j.pt.2010.02.010

VanderWaal, K.L., Ezenwa, V.O., 2016. Heterogeneity in pathogen transmission: mechanisms and methodology. Funct. Ecol. 30, 1606–1622.

VerCauteren, K.C., Lavelle, M.J., Campa, H., 2018. Persistent spillback of bovine tuberculosis from white-tailed deer to cattle in Michigan, USA: status, strategies, and needs. Front. Vet. Sci. 5. https://doi.org/10.3389/fvets.2018.00301

Walther, B.A., Ewald, P.W., 2004. Pathogen survival in the external environment and the evolution of virulence. Biol. Rev. 79, 849–869. https://doi.org/10.1017/S1464793104006475

Washburne, A.D., Crowley, D.E., Becker, D.J., Manlove, K.R., Childs, M.L., Plowright, R.K., 2019. Percolation models of pathogen spillover. Philos. Trans. R. Soc. B Biol. Sci. 374, 20180331. https://doi.org/10.1098/rstb.2018.0331

Weinstein, S.B., Buck, J.C., Young, H.S., 2018a. A landscape of disgust. Science 359, 1213–1214. https://doi.org/10.1126/science.aas8694

Weinstein, S.B., Moura, C.W., Mendez, J.F., Lafferty, K.D., 2018b. Fear of feces? Tradeoffs between disease risk and foraging drive animal activity around raccoon latrines. Oikos 127, 927–934. https://doi.org/10.1111/oik.04866

White, L.A., Forester, J.D., Craft, M.E., 2018a. Dynamic, spatial models of parasite transmission in wildlife: Their structure, applications and remaining challenges. J. Anim. Ecol. 87, 559–580. https://doi.org/10.1111/1365-2656.12761

White, L.A., Forester, J.D., Craft, M.E., 2018b. Disease outbreak thresholds emerge from interactions between movement behavior, landscape structure, and epidemiology. Proc. Natl. Acad. Sci. 115, 7374–7379. https://doi.org/10.1073/pnas.1801383115

White, L.A., VandeWoude, S., Craft, M.E., 2020. A mechanistic, stigmergy model of territory formation in solitary animals: Territorial behavior can dampen disease prevalence but increase persistence. PLOS Comput. Biol. 16, e1007457. https://doi.org/10.1371/journal.pcbi.1007457

Wickham, H., Averick, M., Bryan, J., Chang, W., McGowan, L.D., François, R., Grolemund, G., Hayes, A., Henry, L., Hester, J., Kuhn, M., Pedersen, T.L., Miller, E., Bache, S.M., Müller, K., Ooms, J., Robinson, D., Seidel, D.P., Spinu, V., Takahashi, K., Vaughan, D., Wilke, C., Woo, K., Yutani, H., 2019. Welcome to the Tidyverse. J. Open Source Softw. 4, 1686. https://doi.org/10.21105/joss.01686

Wickham, H., Francois, R., Henry, L., Müller, K., Vaughan, D., 2023. dplyr: A grammar of data manipulation_. R package version 1.1.4.

Wilber, M.Q., Yang, A., Boughton, R., Manlove, K.R., Miller, R.S., Pepin, K.M., Wittemyer, G., 2022. A model for leveraging animal movement to understand spatio-temporal disease dynamics. Ecol. Lett. 25, 1290–1304. https://doi.org/10.1111/ele.13986

Wolodzko, T., 2023. extraDistr: Additional univariate and multivariate distributions_. R package version 1.10.0.

Zajac, A.M., Garza, J., 2020. Biology, Epidemiology, and control of gastrointestinal nematodes of small ruminants. Vet. Clin. North Am. Food Anim. Pract., Ruminant Parasitology 36, 73–87. https://doi.org/10.1016/j.cvfa.2019.12.005

CHAPTER TWO: Season of death, pathogen persistence and wildlife behaviour alter number of anthrax secondary infections from environmental reservoirs

Dolfi AC, Kausrud K, Rysava K, Champagne C, Huang Y-H, Barandongo ZR, Turner WC. 2024 Season of death, pathogen persistence and wildlife behaviour alter number of anthrax secondary infections from environmental reservoirs. Proc. R. Soc. B 291: 20232568. https://doi.org/10.1098/rspb.2023.2568

PICTURE 2: Left: A female blue wildebeest (*Connochaetes taurinus*) grazing in the grassland. Right: A herd of six plains zebra (*Equus quagga*) grazing next to Rietfontein waterhole. Three black-faced impala (*Aepyceros melampus petersi*) and one zebra can be observed on the other side of the waterhole and birds are flying above the water. Photos by Amélie Dolfi, June 2022, Etosha National Park, Namibia

2.1 Abstract

An important part of infectious disease management is predicting factors that influence disease outbreaks, such as *R*, the number of secondary infections arising from an infected individual. Estimating R is particularly challenging for environmentally transmitted pathogens given time lags between cases and subsequent infections. Here, we calculated *R* for *Bacillus anthracis* infections arising from anthrax carcass sites in Etosha National Park, Namibia. Combining host behavioural data, pathogen concentrations and simulation models, we show that *R* is spatially and temporally variable, driven by spore concentrations at death, host visitation rates and early preference for foraging at infectious sites. While spores were detected up to a decade after death, most secondary infections occurred within 2 years. Transmission simulations under scenarios combining site infectiousness and host exposure risk under different environmental conditions led to dramatically different outbreak dynamics, from pathogen extinction ($R < 1$) to explosive outbreaks ($R > 10$). These transmission heterogeneities may explain variation in anthrax outbreak dynamics observed globally, and more generally, the critical importance of environmental variation underlying host–pathogen interactions. Notably, our approach allowed us to estimate the lethal dose of a highly virulent pathogen non-invasively from observational studies and epidemiological data, useful when experiments on wildlife are undesirable or impractical.

Keywords: *Bacillus anthracis*, disease transmission, environmentally transmitted pathogen, host–pathogen contact, reproduction number

2.2 Introduction

Environmentally transmitted pathogens (ETPs) represent a large proportion of the most burdensome infectious disease agents globally (Hopkins et al., 2022). Understanding their

epidemiology often proves very challenging as they are difficult to detect, and for some, the environmental reservoirs are still poorly known (Martinez-Bakker et al., 2015; Rohani et al., 2009). Persistence in the environment is highly dependent on the traits of the pathogen and the characteristics of the environment. *Brucella abortus* bacteria can persist 20–80 days (Aune et al., 2012), *Toxoplasma gondii* oocytes can survive for months (Shapiro et al., 2019), and the prion responsible for scrapie can survive for at least 16 years (Georgsson et al., 2006). Persistent pathogens in the environment can extend existing outbreaks or initiate 'new' outbreaks years into the future. For example, avian influenza outbreaks emerge in North America every 2–4 years, with emergence sparked by ingestion of virions from environmental reservoirs established in previous outbreaks (Breban et al., 2009; Martin et al., 2018). Here, we estimate the number of secondary infections arising from pathogen reservoirs for a highly persistent ETP and how environmental variation affecting pathogen survival and host behaviours alters host–pathogen contact rates and, ultimately, transmission.

For directly transmitted pathogens, the basic reproduction number R_0 is an estimate of the average number of secondary cases produced from a single infectious individual introduced into a susceptible population and is often used as a key epidemiological parameter (Diekmann et al., 1990). However, the assumption of a naive population is not met for diseases in endemic areas, and estimating R_0 for ETPs is arduous due to the extended infectious time in the environment, variation in the spatial extent of pathogen reservoirs, and heterogeneity in host movement, behaviour and susceptibility (Blackburn et al., 2019; VanderWaal and Ezenwa, 2016). In cases where ETPs are only released into the environment at host death (i.e. obligate killer pathogens [Ebert and Weisser, 1997]), one host mortality will form one infectious reservoir 'patch' in the environment. We can assess the reproduction number R, which does not assume a naive

population, defined here for ETPs as the average number of secondary infections produced by one infectious patch over its infectious period. This novel formulation of the reproduction number acknowledges that the population may not be entirely susceptible, without needing to know the susceptible proportion of the population to calculate the effective reproduction number R_e. For persistent ETPs, patches can remain infectious spanning multiple, seemingly independent, outbreak events and monitoring of pathogen reservoirs is thus needed to identify how pathogen concentrations affect transmission risk over time (McCallum et al., 2017).

In addition to pathogen persistence, information on host movement and behaviour is essential to identify contacts with pathogen reservoirs in heterogeneous landscapes that vary in exposure risk. Movement ecology studies of host locations can be combined with pathogen location data to estimate host–pathogen contact rates (Dougherty et al., 2022; Manlove et al., 2022). However, the temporal scales of host telemetry studies are often too coarse to determine an encounter with infectious patches present at a fine spatial extent. Fine-scale behavioural information like direct observation is needed to identify contacts with infectious patches in heterogeneous environments. For terrestrial vertebrates, the infectious sites often represent a small part of the host range, such as a water source or specific pasture sites (Barasona et al., 2017; Titcomb et al., 2021), depending on how and where pathogens are released from hosts. Thus, reservoir-focused sampling techniques to monitor host behaviours and transmission risk can fill a gap in our understanding of transmission for ETPs.

Hosts may modulate their behaviour based on cues suggesting the presence of infectious patches. Exposure may be reduced if hosts avoid detectable cues associated with infection risk such as faeces, carcasses or macroparasites (Hart, 1990), a response now called the ‘landscape of disgust’ (Buck et al., 2018; Weinstein et al., 2018). Conversely, exposure risk can be enhanced by

attraction toward contaminated water or nutrient-rich foraging sites, leading to ingestion of pathogens with forage or water (Titcomb et al., 2021; Turner et al., 2014). Because behaviour can depend on the state of the reservoir site, quantifying host–environment contact is crucial to assess disease transmission potential at heterogeneous environmental reservoirs.

Bacillus anthracis is a bacterial pathogen with two life forms; infectious spores that are maintained in the environment, and vegetative cells that multiply and cause disease inside mammalian hosts (Baillie and Read, 2001). Spores at carcass sites can be found on grasses for several years (Turner et al., 2014) and in exposed surface soils for up to a decade (Turner et al., 2014). A new case occurs when a host ingests spores while grazing at a carcass site (Huang et al., 2022; Turner et al., 2014), if the exposure exceeds the lethal dose threshold (Turner et al., 2016; WHO, 2008). If exposed to a lethal dose, the host will die within a few days, and the site of death becomes a new infectious patch in the soil (an area less than 20 m^2 [Turner et al., 2014]). For *B. anthracis*, estimating *R* is made conceptually tractable with this ETP being an obligate killer, where one host fatality generates one infectious patch that can then cause secondary infections. We aimed to estimate *R* for *B. anthracis*, incorporating variation in the three sides of the epidemiological triangle: host, pathogen and environment. We assessed host individual and population-level attraction to infectious sites using camera traps at anthrax carcass sites and paired controls sites, and quantified foraging behaviour of two host species, plains zebra (*Equus quagga*, hereafter zebra) and blue wildebeest (*Connochaetes taurinus*, hereafter wildebeest). We then estimated pathogen concentrations on soil and grasses at reservoir sites over a decade using interpolation and extrapolation from empirical datasets on soil and grass spore concentrations. Finally, we developed a simulation model to determine the exposure risk of the two host species to *B. anthracis* by estimating *R*, defined as the number of individuals a single anthrax infectious

site may infect over its decadal lifespan. Knowing *R* and its duration for ETPs may inform wildlife disease management decisions, such as assessing spatial overlap with appropriate time lags at the interface between livestock and wildlife.

2.3 Materials and Methods

2.3.1 Study area

Etosha National Park (hereafter Etosha) is a 22 270 km^2 nature reserve in northern Namibia containing a large salt pan surrounded by grasslands, shrublands and woodlands (Turner et al., 2022). Etosha encompasses a sub-tropical, semi-arid savannah biome with a single wet season (January–April) and a long dry season (cool dry season, May–August and hot dry season, September-December). In Etosha, anthrax occurs mainly during wet seasons, through ingestion of spores by grazing herbivores (Cizauskas et al., 2014; Havarua et al., 2014; Turner et al., 2013). The two main host species are plains zebra and blue wildebeest which represent 50.3%, and 16.2% of all confirmed anthrax cases recorded 1968–2020, respectively (2150 anthrax cases among all hosts; Etosha Ecological Institute; all data from this institute were communicated by Claudine Cloete in 2023). The population density of zebras is more than six times higher than wildebeests (estimate of 16 174 zebras and 2 482 wildebeests, [Turner et al., 2014]), and population estimates of both species have been fairly stable over the last 30 years (Turner et al., 2022). Additional information about heterogeneities in anthrax dynamics within this study area is available (Barandongo et al., 2023; Huang et al., 2022, 2021).

2.3.2 Camera site data collection

Motion-sensing remote camera traps were used to collect animal behavioural data at carcass sites (study design and camera placement described in Turner et al., 2014). In brief, 13 rock-delimited 2.5 m radius zones at anthrax carcass sites (from 12 zebras and one wildebeest) paired with 13

control sites situated 100 m away were monitored between March 2010 and March 2013, totalling 14 779 days of observation (figure B1). The sites were situated within the same habitat, thus, we assumed that visitation would not differ between the carcass and control sites. Motion-triggered cameras took 10 pictures at 1s intervals continuously when movement was detected. Vegetation greenness for each site pair was obtained from the normalized difference vegetation index (NDVI) at a resolution of 250 m^2 every 8 days (Global Inventory Modeling and Mapping Studies [Pinzon and Tucker, 2014]).

Site visitation was recorded from photographs when animals entered the rock-delimited zones. The information recorded included date, time, species, age (juvenile: less than 1-year-old; sub-adult: 1–2 years old; adult: greater than 2 years old), sex, total time spent on site and time spent grazing in seconds. Age, sex, location in the image and coat patterns (Appendix B1) were used to ensure whether the same individual was assessed across triggers proximate in time, defined as a gap of a few minutes. Depending on the position of the animal and the lighting of the image, age and sex could not always be determined, so the confidence of age/sex observations was ranked from 0 (impossible to identify) to 3 (certain), with confidence scores of 0 and 1 removed from relevant analyses. Two observers manually coded host demographics from images (C.C. and A.C.D.).

2.3.3 Host parameter analysis

We assessed the attractiveness of carcass sites to zebra and wildebeest from camera trap data, defining three behavioural response variables for both species, for each site: (i) monthly average number of visitations, (ii) monthly average probability of grazing given visitation and (iii) time spent grazing given grazing occurred (Appendix B1). We investigated how the treatment (carcass or control), the number of months after death (MAD), environmental factors (NDVI and season), demographic variables (age and sex), and spatial variables (distance to the closest perennial water

and distance to an edge of the main Etosha salt pan; Table B1) affected each of the three behavioural response variables, using generalized linear models. All analyses and models were conducted using the R software (R Core Team, 2018), with packages lme4 (Bates et al., 2015), and glmmTMB (Brooks et al., 2017). Only months with at least 20 days of recording for both cameras at a site (carcass and control) were included in the analysis. Out of the 546 individual camera-months sampled, 438 met this inclusion criterion. For included months with missing data, these had an average of 2.5 days missing (Appendix B1, figure B2). The monthly visitation was analysed using a zero-truncated negative-binomial model, the proportion of monthly grazing events was analysed using a binomial model, and the time spent grazing using a log-transformed linear mixed model. Interactions between season and distance to water, as well as between treatment and MAD were included. In each model, we kept treatment, age and sex as fixed effects and site ID as a random factor. Model selection was made using the Akaike Information Criterion. For each response variable, 16 models were tested (Table B2), totalling 48 models per species.

2.3.4 Pathogen parameter estimation

Pathogen concentrations on grasses and soil, measured as colony-forming units (CFUs) per gram of dry matter, were obtained at zebra anthrax carcass sites (sampling method and data in Turner et al., [2014] and Barandongo et al., [2023]). Concentrations of spores on grasses were recorded at 23 sites up to 4 years after death. Two measurements were obtained from grasses, the concentration of pathogen on the aboveground material (i.e. everything above the roots), or in the upper portion of the aboveground material (the aboveground component after removal of 1 cm at the base of the plant which can collect soil; this upper grass portion is hereafter referred to as the ‘grass’ component ingested in simulations). Soil spore concentrations were recorded for up to 12 years at 40 carcass sites, but no spores were detected after 10 years (Barandongo et al., 2023).

To obtain estimates of spore concentrations on grasses and in soil over the full time series, we interpolated the soil CFU for all missing values (156 out of 442) at the 40 sites using the log-linear model from Barandongo et al. (2023), with site age as a predictor. Then, we extrapolated the concentration of spores on grasses for all 40 sites over 10 years using two steps. We first fit a loglinear model using the soil CFU and age of sites to obtain the concentration of spores on the aboveground grass components:

$$log_{10}(CFU_{aboveground,s,t} + 1) = log_{10}(CFU_{soil,s,t} + 1) + \beta * Age_s + \varepsilon_{s,t} \qquad (2.1)$$

where β is the regression coefficient, ε is the error at site z and time after death t. Then, we extrapolated the expected values of CFU on the grass tops, using a log-linear model based on the aboveground CFU only.

2.3.5 Reproduction number estimation: infection risk simulation

We estimated the reproduction number, *R*, as the number of lethal infections occurring at an infectious site over a decade by simulating host exposure to the pathogen. To simulate host behaviour, we drew the number of animals visiting an infectious patch, the probability of grazing, and grazing time from empirical probability density functions (PDFs). Then, to simulate individual host–pathogen exposure we estimated the quantity of spores ingested based on time spent grazing and seasonal patterns of soil ingestion (Turner et al., 2013). We only considered an exposure to be an infection if the number of spores ingested, at one visitation, exceeded a fixed lethal dose; we did not consider multiple exposures. The estimated *B. anthracis* lethal dose by ingestion is between 10^5 and 10^8 spores (Turner et al., 2016), so we considered four threshold doses (10^5,10^6,10^7 and 10^8) to estimate which threshold matched the anthrax dynamic observed. Each model iteration simulated each season of each post-death year 0–10. A visual representation of the model is presented in figure 2.1. We ran each simulation 100 times to account for stochasticity. The host

empirical PDFs were built using the 3-year period of camera trap data and were subdivided using the significant variables obtained from the statistical analyses, mainly season, year after death and distance to water or salt pan (see main text result; Appendix B2, figures B3–B8). Using a subdivided dataset allowed us to consider how host visitation and behaviours vary under a range of environmental conditions. We used PDFs rather than model predictions as we wanted to draw values from a distribution which encompasses the extreme values present in the data, better representing the stochasticity present in the system. From the statistical analysis, carcass sites influenced host visitations and grazing during the first 24 months, after which carcass and control sites did not differ. We assumed that behaviours at control sites, and at older carcass sites (i.e. greater than 2 years old, after the attraction signal has faded), were plausible estimates for visitation rates and behaviours at older carcass sites (i.e. 2–10 years in the simulation). To account for this temporal signal in host behaviour, we separated the datasets into three time periods: year 0, year 1 and years 2–10. To estimate host parameters for years 0 and 1, we used data from carcass sites for years 0 and 1 after death, respectively. For host parameters in years 2–10, we pooled data from control sites and for carcass sites over 2 years old. Individual pathogen exposure was simulated by estimating the amount of forage ingested, then calculating the associated spore intake using empirical data. The number of grams ingested, $ngram_i$, by individual i,is

$$ngram_i = T_i * Bn_s * Bw_s \quad (2.2)$$

where T_i is the time spent grazing by individual i, B_{ns} is the number of bites per second and B_{ws} is the weight of a bite for species s. Foraging zebras take bites of about two grams and an average of 27 bites min^{-1} (Chen et al., 2021; Okello et al., 2002) while wildebeest take bites averaging 1 g $bite^{-1}$ and 26 bites min^{-1} (Chen et al., 2021; Okello et al., 2002). To estimate the number of spores ingested by each individual, we randomly selected one of the 40 carcass sites for which we have

spore concentrations as the site of foraging. Because zebra and wildebeest ingest not just grass, but also soil and roots when grazing (Arthur and Alldredge, 1979; Collas et al., 2019), and because spore concentrations are higher in soil/roots than on grasses (Turner et al., 2014), we modelled the ingested spore concentration as a mix of grass and soil ingestion. The quantity of soil ingested while grazing at infectious patches is unknown, however, we expect hosts primarily consume grass when grazing. We assume that if soil was ingested, it would represent 10% of intake mass (Turner et al., 2016). To denote this, we included a parameter β representing the portion of soil ingested per bite ($\beta = 0.1$ if soil ingestion occurs, $\beta = 0$ otherwise). For each gram ingested, we treated the concentration of spores in the grass and in the soil as a Poisson process (to counterbalance errors that arise from extrapolation without accounting for variance in this step, as in Turner et al., (2016), and we assumed that the concentration of pathogen at the site is not modified by grazing. Thus, we calculate the number of spores ingested, $D_{i,z,t}$, by individual i, at infectious site z, of age t as

$$D_{i,z,t} = \sum_{n=1}^{ngram_i}((1-\beta)\, Pois\left[CFU_{grass,z,t}\right] + \beta\, Pois[CFU_{soil,z,t}]) \qquad (2.3)$$

where $ngram_i$ is the number of grams of food ingested, β is the proportion of soil ingested and $CFU_{z,t}$ is the number of spores ingested from grass and soil components. Because herbivores ingest soil more often during the wet season than the dry season (Turner et al., 2013), we included a weight ω_{wet} and ω_{dry} representing seasonal differences in the proportion of individuals that ingest soil while grazing, while others ingest grass only. We tested all combinations with ω_{wet} and ω_{dry} varying from 0 to 1, by 0.1 increments. For example, a simulation with the proportion $\omega_{wet} = 0.4$ and $\omega_{dry} = 0$ would simulate that 40% of grazing individuals ingest grass and soil while 60% ingest grass only during the wet season, and all grazing individuals ingest only grass during the dry season. Based on host foraging ecology (Havarua et al., 2014; Turner et al., 2013), we assumed that the most likely parameter space for Etosha is within 0–40% of individuals ingesting soil when

grazing, with a higher percentage during the wet versus dry season. To further explore the role of environmental variability on *R*, we repeated simulations considering seasonality in the timing of reservoir formation and interannual variation in host foraging behaviour. The concentration of spores in soil reservoirs is over an order of magnitude lower when individuals die in dry seasons versus wet seasons (Barandongo et al., 2023). Thus, to understand how the season of death impacts secondary infections, we separated infectious sites formed in dry seasons (five sites) from infectious sites formed in wet seasons (35 sites). Similarly, to explore interannual variation in *R*, we simulated the wet season under drought conditions using dry season behavioural data and under average rainfall conditions using wet season behavioural data. The camera trap data were collected during average to above-average rainfall years, however, in Etosha, zebras are less at risk of anthrax during drought due to changing habitat selection reducing exposure risk (Huang et al., 2021). Under drought conditions, 'wet season' habitat use mirrors habitat use observed in dry seasons. With these changes, we considered five different data combination: (i) all data from hosts and infectious sites; (ii) all data from hosts and wet season formed infectious sites, (iii) all data from hosts and dry season formed infectious sites, (iv) data from hot dry host behaviour and wet season formed infectious sites and (v) data from hot dry host behaviour and dry season formed infectious sites. Finally, to investigate which lethal dose threshold best represented anthrax dynamics in the system, we simulated the number of cases that would be produced over 100 years, using infection model results combining zebra and wildebeest. We initialized the simulation using zebra and wildebeest anthrax mortality data from 2003 to 2013, representing 235 cases (Etosha Ecological Institute). For each time step, we obtained the number of yearly new cases by drawing the number of new infections occurring at each of the 235 sites from the infection model result, discriminating the sites by age. A maximum of 10 000 new infections per year was fixed, as it

represents the average population of zebra and wildebeest present in Etosha (Etosha Ecological Institute). We used the model combination using all host and infectious sites to simulate this prediction. This is a simple model, used to inform where the lethal dose threshold might fall in free-ranging wildlife populations.

2.4 Results

2.4.1 Host parameters

Of 119 226 triggers of the camera traps, 5196 contained zebras and 1043 contained wildebeests. Based on sequential triggers clustered in time, we identified visitations by 3838 zebras and 830 wildebeests. At visits to carcass sites, 37.2% of zebras grazed and 60.3% of wildebeests grazed, while at visits to control sites only 24.6% of zebras and 42.0% of wildebeests grazed. For both species, most recorded individuals were adult females (figure 2.2a.b; all statistical results in Appendix B2). Among zebras, more individuals were recorded on sites closer to permanent water ($p < 0.05$), during the hot dry season ($p < 0.0001$) and at control sites ($p < 0.05$, figure 2.2a). For wildebeests, sites nearer the salt pan ($p < 0.01$) as well as carcass sites ($p = 0.01$) had more visitations (figure 2.2b). Despite small visitation differences at carcass and control sites, the probability of grazing was significantly higher at carcass sites for both species ($p < 0.0001$; figure 2.2a,b). In addition, for zebra, the probability of grazing was higher for females ($p < 0.0001$), adults ($p < 0.05$), during the cool dry season ($p < 0.05$) and under higher NDVI ($p < 0.0001$). The probability of grazing at carcass sites significantly decreased the older the site ($p < 0.001$). Wildebeest grazing was similarly affected by NDVI ($p < 0.05$), and sites farther from permanent water significantly increased the probability of grazing during the dry season ($p < 0.05$). Finally, given that grazing occurred, the time spent grazing for both species did not differ between site treatments. However, season played a major role in foraging time. Zebra grazed for longer times

during both dry seasons ($p < 0.001$) than the wet season, while wildebeest spent longer times grazing during the cool dry season ($p < 0.0001$; figure 2.2c.d).

2.4.2 Pathogen estimation

For the 40 monitored carcass sites, we obtained a yearly concentration of spores per gram of soil or grass. For the soil pathogen concentrations, 35% of the data came from the model interpolation, while all the data presented for the grass tops came from the extrapolation. The concentration of spores on grasses was much lower than in soil, starting nearly three orders of magnitude lower (figure 2.3). Our data suggest that after 5 years, spores are absent from the grass, despite persisting in the soil.

2.4.3 *R* estimation

Across models, zebra had more anthrax infections than wildebeest, matching patterns observed in disease surveillance data. Since otherwise both species showed similar trends, we only show zebra results, and report wildebeest in Appendix B. There was variability in *R* estimation due to the high heterogeneity in visitations, the proportion of individuals ingesting soil while grazing, and the lethal dose threshold considered (figure 2.4; Appendix figures B9–B11). From our simulations, the lethal dose threshold most likely to match the dynamics observed in Etosha is between 10^7 and 10^8 spores for both species. Indeed, for a lethal dose threshold of 10^5,10^6 and 10^7, the estimated *R*, for our parameter space, is above two and we predict an exponential increase in anthrax cases over time, while, for a lethal dose of 10^8, *R* is below one and we simulated pathogen extinction occurring after 70 years, on average (figure 2.5). If the lethal dose falls between 10^7 and 10^8 spores, extrapolating from our models, a host would need to ingest between 687 and 6878 g of grass only, or between 1.5 and 14.8 g of grass with soil (when soil is 10% of intake biomass) to become infected at a newly infectious site. The former is unlikely to occur based on site size and host

behaviour, emphasizing the critical importance of soil ingestion for transmission risk. Seasonality played a pivotal role in anthrax epidemiology and infectious site heterogeneity. In general, a larger proportion of individuals ingesting soil led to more infections, but the magnitude of this effect varied seasonally. For the same proportion of individuals ingesting soil during the dry or the wet season, more infections occurred during the dry season, possibly due to seasonal behavioural differences, with longer grazing times recorded during the dry season (compare R above versus below the diagonals, figure 2.4b; figure B11b). Infectious sites formed in the wet season drove disease dynamics in this system (figure 2.4c.e; figure B11c,e); and dry season formed infectious patches contributed no cases (all $R = 0$, figure 2.4d.f; figure B11d.f), probably due to the lower spore concentrations found at dry season formed sites. Similarly, seasonality in host visitation rates played an important role in the number of individuals infected, with fewer infections during drought conditions (figure 2.4e; figure B11e) than average rainfall conditions (figure 2.4c; B11c), probably due to fewer visits and grazing events.

The risk of infection diminished rapidly with site age (figure 2.6; figure B12). If individuals only consumed grass, no infections were predicted after 3 years regardless of the lethal dose threshold or host species (figures B13 and B14). However, when at least some individuals ingested soil when grazing, infections continued for longer. The higher the proportion of individuals ingesting soil, the higher the number of infections, occurring over a longer time since death. For a lethal dose threshold of 10^5, infections occurred throughout the 10 years of simulation, while for thresholds of 10^6,10^7 and 10^8, no infections were recorded after years 9, 5 and 4, respectively.

2.5 Discussion

Determining fine-scale transmission dynamics for ETPs can be complex due to the difficulties in characterizing contact locations, reservoir infectiousness and frequency of interactions in

heterogeneous environments. This study used simulation models combining long-term monitoring data of a pathogen in its environmental reservoir with fine-scale host behavioural data to estimate the number of secondary infections arising from infectious patches of an ETP. Together with knowledge of the long-term epidemiology of this system, this method has allowed us to evaluate variation in the number of secondary infections, *R*, arising from heterogeneities along the three sides of the epidemiological triangle (host, pathogen, and environment). Our results suggest ecological mechanisms for why anthrax disease dynamics and seasonality can vary so dramatically in different ecosystems and offers a perspective on how ETP heterogeneities alter outbreak dynamics.

Investigating host individual behaviours at infectious reservoir sites revealed how fine-scale behavioural variation scales up to altered disease dynamics. Both host species had similar visitation rates between site treatments (at times even higher for zebra at control sites) and the time spent grazing did not differ between site treatments by age or sex. The critical difference in behaviour was that, over the study period, a higher proportion of animals chose to graze when encountering a carcass site: zebra by 1.5 times and wildebeest by 1.4 times. Notably, individuals were most likely to graze at infectious sites within 2 years after creation, when higher pathogen concentrations are more likely to result in a fatal exposure. This pattern goes against what would be expected under the landscape of disgust theory (Weinstein et al., 2018), as we see an increase in risky behaviour at infectious sites. Carcasses are known to enhance the nutrient content and palatability of the grasses at the site of death (Towne, 2000; van Klink et al., 2020), and *B. anthracis* spores may further promote plant growth (Ganz et al., 2014), increasing the chances of spores being ingested by a potential host. However, when focusing on the seasonality of anthrax infections, visitations and grazing probabilities were often higher during dry seasons than the wet

season, suggesting a higher risk of infection during the dry seasons, contrary to what we observe in the system. The key difference in risk between seasons thus arises from soil contact, since herbivores ingest significantly more soil in wet than dry seasons (Turner et al., 2013). *Bacillus anthracis* being a soil-borne pathogen, the quantity of soil a host ingests when grazing is a major component of transmission risk. Thus, one limit of our model comes from uncertainty in our estimate of the amount of soil ingested during foraging at an infectious patch (β parameter of equation (2.3)). While the quantity will vary depending on host and environmental factors, our estimate for this parameter was based on the faecal analysis from Turner et al. (2013) and does not account for seasonal differences in forage digestibility. However, by varying the proportion of individuals ingesting soil, we explore the effect of spore exposure from soil in addition to spore exposure from grasses on R, and how this varies in different seasons. A finer assessment of the proportion of individuals ingesting soil at reservoir patches, the quantity of soil ingested, and the impact of seasonality on those variables across ecosystems would be important to increase our understanding of the disease transmission risk.

At the host population level, these behavioural patterns demonstrate two important findings. First, high variation in visitation rates suggests that encounters with infectious patches occur somewhat randomly at a local scale. Forage choice at the smallest spatial and temporal scales is an important driver of pathogen exposure; however, larger-scale factors such as proximity to desirable landscape features and seasonal changes in habitat selection affect the number of individuals available in an area to encounter infectious sites. Second, the expected R varies based on environmental conditions, which led to dramatically different disease dynamics in simulation models. Environment affects site infectiousness and host encounters, as well as spatio-temporal patterns in when and where host mortality occurs. Infectious sites created during the wet season

have higher spore concentrations than those formed in the dry season season (Barandongo et al., 2023), and in Etosha, dry seasons and drought shift hosts out of the high-risk area into habitat with lower anthrax risk (Huang et al., 2021; Zidon et al., 2017); but see pattern in Tanzania, (Aminu et al., 2022). Infectious patches formed during the dry season did not contribute any new cases and host behaviours under drought-simulated conditions (based on dry season behaviours) significantly decreased *R* compared to average to wetter conditions, patterns that match disease outbreak dynamics in this ecosystem (Hampson et al., 2011; Huang et al., 2022). Thus, environmental variation in both infection potential of reservoir patches and host behaviour reinforces the wet season timing of anthrax in this ecosystem, where mortalities occurring in preferred wet season habitats are more likely to contribute secondary infections than mortalities occurring in dry season habitats.

The seasonality of anthrax outbreaks across the global range of *B. anthracis* varies from outbreaks associated with wet seasons or high rainfall events, to large, intermittent outbreaks often associated with dry seasons or droughts (Clegg et al., 2007). Our simulation results suggest underlying mechanisms that could drive variation in seasonality of outbreaks across ecosystems. For example, soil ingestion occurring during the dry season led to bigger outbreaks than during the wet season. This matches patterns observed across locations; outbreaks occurring during dry seasons are more epidemic-like, compared to the outbreaks occurring in the wet season that are typically smaller and more endemic-like (Hampson et al., 2011; Huang et al., 2022). This pattern could be explained by a seasonal behavioural change, with higher visitation rates during the end of the dry season increasing the exposed population, combined with longer times spent grazing, increasing individual exposure risk. We could then expect that extreme weather events such as drought could impact the disease dynamics in different ways. For environments where anthrax deaths peak during

the dry season, drought would accelerate exposures and outbreak sizes, while for environments where anthrax deaths peak during the wet season, drought would lead to a lower infection risk.

The intensity and frequency of anthrax outbreaks likewise vary across the global range of *B. anthracis*. In areas like Etosha where regular, small outbreaks maintain endemicity, contacts occur annually but are seasonally constrained, reducing the number of exposures occurring at sites. However, for ecosystems where outbreaks occur infrequently (e.g., decadal periods in Kruger National Park, South Africa [Huang et al., 2022]; sporadic events in Ruaha National Park, Tanzania, [Stears et al., 2021]; re-emergence after 70 years in Northwest Siberia, [Ezhova et al., 2021]), understanding the cause of disease emergence with such a long time-lag between the last recorded case is more difficult to understand. While anthrax can survive for decades in the soil, the concentration of spores is reduced and the risk of an effective contact resulting in anthrax mortality is low. Environmental perturbations may drive outbreaks with time lags that exceed the lifespan we detected for surface soils of reservoirs. Extreme events such as droughts, floods, or permafrost melting may impact host–pathogen contact rates, exposure doses or host susceptibility. Anthropogenic disturbances can also enhance exposure risk, such as when soil scarification brought *B. anthracis* spores from historic burial grounds protected in deeper soil layers for 45 years—to the surface, causing anthrax cases (Turnbull et al., 1996). Outbreak emergence decades after the last recorded case may be due to a 'series of unfortunate events' that result in infections when contact rates and exposure dose are relatively low or improbable (similar to the alignment of conditions promoting disease spillover Plowright et al., 2017]).

The lethal dose required to kill a host in natural settings varies with individual susceptibility and behaviour (Turner et al., 2016). Using host behaviour combined with pathogen concentrations and knowledge of long-term outbreak patterns, we were able to refine our estimation of the lethal dose

of *B. anthracis* in free-ranging wildlife. Anthrax persists endemically and from estimates of the frequency at which animals are exposed to different doses of the pathogen, we can infer lethal doses, in this case between 10^7 and 10^8 spores that would give a frequency of infection matching the observed dynamics. This information would otherwise be difficult to determine without expensive and impractical animal trials on large, long-lived wildlife species. Our models assumed infection occurs after a single exposure, without considering previous exposures, and that the lethal dose is fixed over the simulation for all individuals. Lethal doses may vary among and within individuals, depending on factors that alter immune function such as age, sex, reproductive status, nutrition or other infections (Cizauskas et al., 2015). Herbivores show evidence of exposure to sublethal doses of *B. anthracis* (Cizauskas et al., 2014; Ochai et al., 2022); however, whether these sublethal exposures confer immune protection or how the timing of previous exposures alters susceptibility to subsequent exposures in wild populations remains unknown. If previous exposure builds resistance (Caraco and Turner, 2018; Gutting et al., 2016), this would reduce the *R* by increasing the lethal dose required for mortality. For inhalational anthrax, experimental daily exposure of New-Zealand white rabbits (*Oryctolagus cuniculus*) to low spore concentrations resulted in death when an accumulated dose, lower than required for a single exposure (Gutting et al., 2016), was reach over a three-week study period (Taft et al., 2020). Adding multiple exposures would complicate the computation of *R* as grazing at multiple infectious sites may occur before infections take place, making it harder to track the number of secondary infections occurring from a single infectious site.

By assessing the *R* for *B. anthracis* infectious patches, we show that heterogeneities in hosts, pathogen, and environment are highly interconnected, leading to strong temporal variation in disease dynamics. Variation in these interactions may explain outbreak differences observed in

different ecosystems, where host–pathogen exposure rates under dry versus wet conditions change due to herbivore foraging behaviour altered by rainfall variability and vegetation dynamics overlaid upon a landscape of variable pathogen risk. Estimating *R* using multiple data sources demonstrated how heterogeneity of the disease system, notably the variability in the transmission potential of infectious sites, altered epidemiological dynamics. Understanding this heterogeneity may be of importance for risk estimates and control efforts in animal husbandry and conservation in anthrax-prone areas. Future work on how the lethal dose may be connected to recurrent sublethal exposures and general animal health may further explain anthrax dynamics in arid areas worldwide.

Recent studies have recognized the importance of linking fine-scale host movement to disease transmission (Albery et al., 2022; Manlove et al., 2022), where excluding individuals' movement decisions can then lead to incorrect predictions (Dougherty et al., 2022; Roever et al., 2014). Simulation models showed that including feedback into wild boar (*Sus scrofa*) movement decisions led to significantly different results about persistence of classical swine fever, which has severe consequences for disease management (Scherer et al., 2020). For ETPs specifically, infectious patches can be quite small compared to host ranges (Huang et al., 2023) and correctly characterizing contacts between host and pathogen is crucial to better inform disease transmission risk. Connecting the three sides of the epidemiological triangle, i.e. connecting how environmental changes affect pathogens, hosts and host–pathogen contacts in heterogeneous landscapes may be of high importance to increase accuracy in disease risks predictions (Manlove et al., 2022). For Hendra virus (*Hendra henipavirus*), spillover from Australian flying foxes, or fruit bats (*Pteropup* spp*.)* to horses to humans, is associated with habitat loss and food shortages caused by land use change and climate change (Eby et al., 2023). These changes shift bat movements and foraging

behaviours, increasing spillover events. Similarly, our study emphasizes the importance of the environmental compartment, notably how seasonality affected pathogen reservoir infectivity and host movements and foraging decisions, with implications for disease transmission risk at seasonal and interannual scales.

2.6 Acknowledgments

We thank the Ministry of Environment and Tourism in Namibia for providing permission to conduct this research. We greatly appreciate the scientific staff and managers at the Etosha Ecological Institute for logistical support and assistance, particularly to W. Kilian, C. Cloete and G. Shatumbu. We thank all of those who assisted with data collection, in particular H. Joel. This work was supported by NSF Grant DEB-1816161/DEB2106221 through the NSF-NIH-USDA Ecology and Evolution of Infectious Diseases program. Data were collected under the NSF grant OISE-1103054. Any use of trade, firm or product names is for descriptive purposes only and does not imply endorsement by the US Government.

2.7 Author contribution

Authors' contributions. A.C.D.: conceptualization, formal analysis, investigation, methodology, writing—original draft; K.K.: conceptualization, methodology, supervision, writing—review and editing; K.R.: formal analysis, methodology, writing—review and editing; C.C.: data curation, writing—review and editing; Y.-H.H.: data curation, writing—review and editing; Z.R.B.: data curation, writing—review and editing; W.C.T.: conceptualization, data curation, funding acquisition, supervision, writing—review and editing. All authors gave final approval for publication and agreed to be held accountable for the work performed therein.

2.8 Data availability

The data and codes used in this manuscript are available on Dryad (Dolfi *et al*., 2024), and at

https://github.com/ameliedolfi/Reproduction_number

2.9 Figures

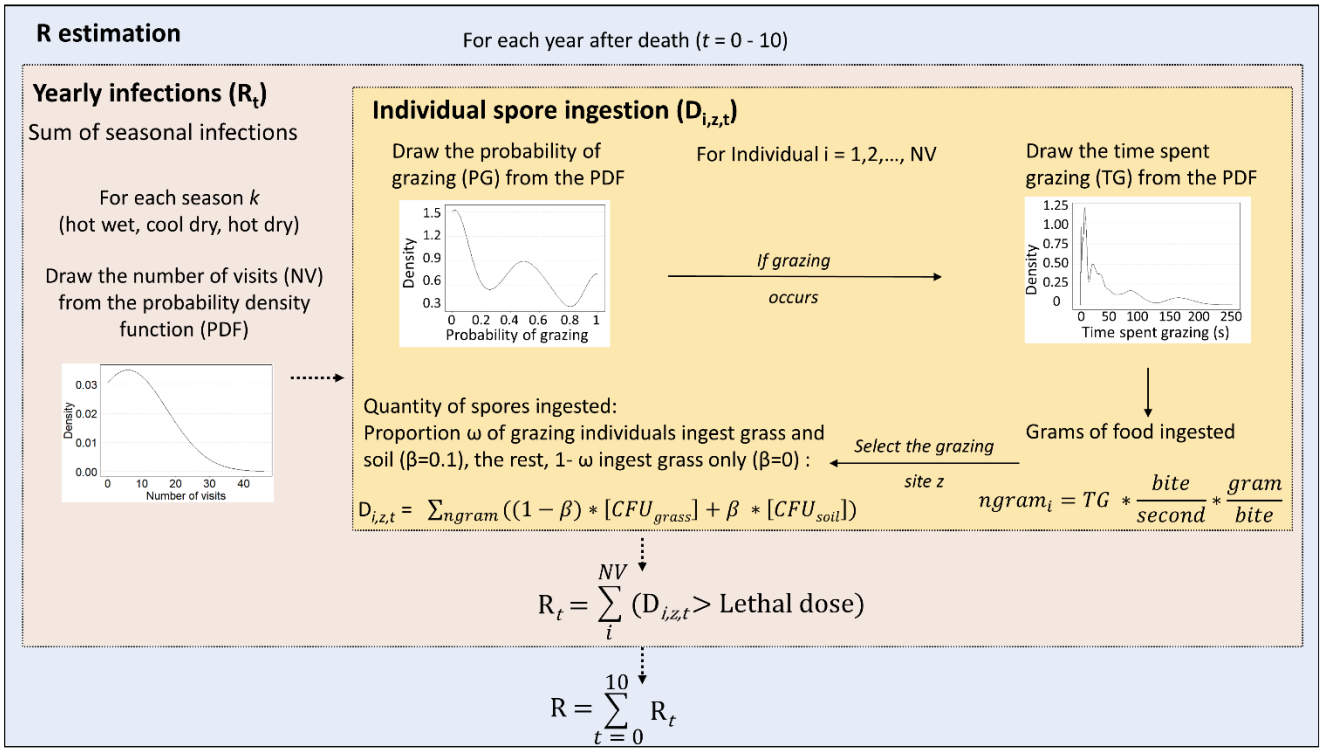

FIGURE 2.1: Model visualization for the estimation of the reproduction number *R* of anthrax in Etosha National Park, Namibia. Each simulation ran over 10 years and was repeated 100 times. Each year is separated into three seasons (*k*), the hot wet, cool dry and hot dry seasons. Each probability density function (PDF) is obtained using the camera trap data. During the hot wet season, the proportion of animals ingesting grass and soil ω is ω_{wet}, while it is ω_{dry} during the cool and hot dry seasons. The yearly reproduction number R_t is the sum of the number of infections occurring during each of the three seasons *k* of year *t*. The reproduction number *R* is the sum of the yearly reproduction number.

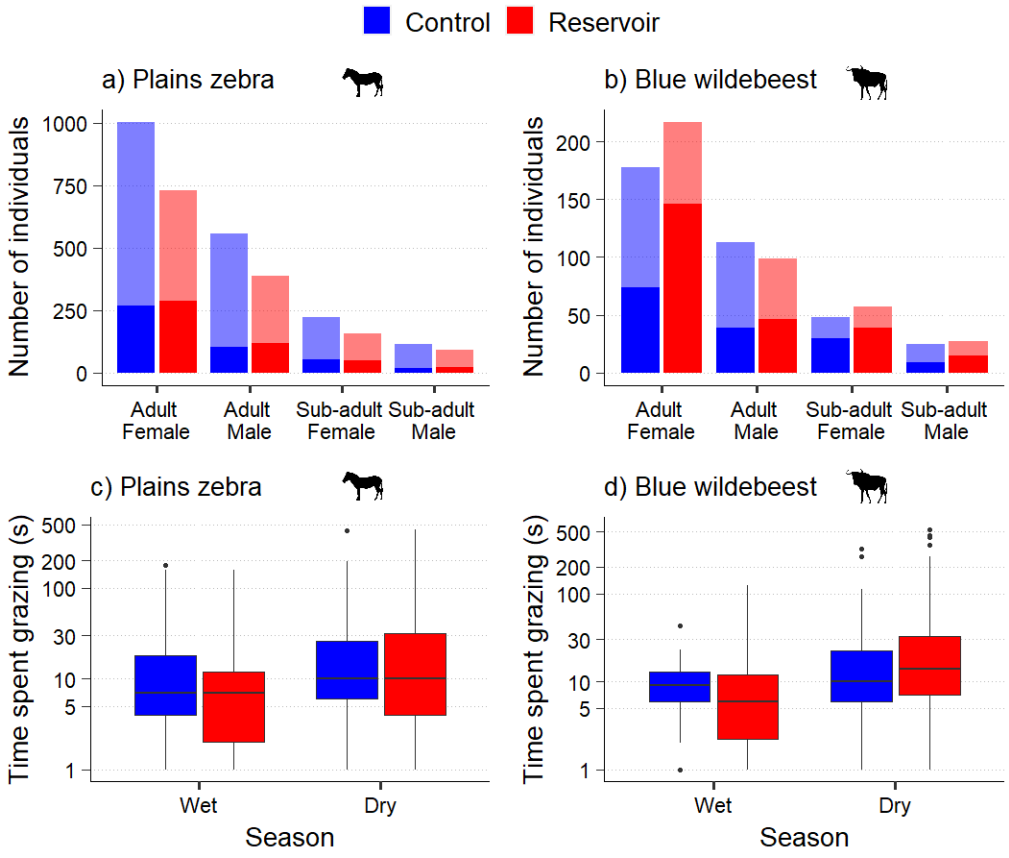

FIGURE 2.2: Total number of individuals by age and sex recorded visiting (lighter colours) and grazing (darker colours) at anthrax carcass sites (a,b), and the time spent grazing (in seconds) by season, at control (blue) and carcass (red) sites (c,d), for plains zebra (*Equus quagga*: a,c) and blue wildebeest (*Connochaetes taurinus*: b,d) in Etosha National Park, Namibia.

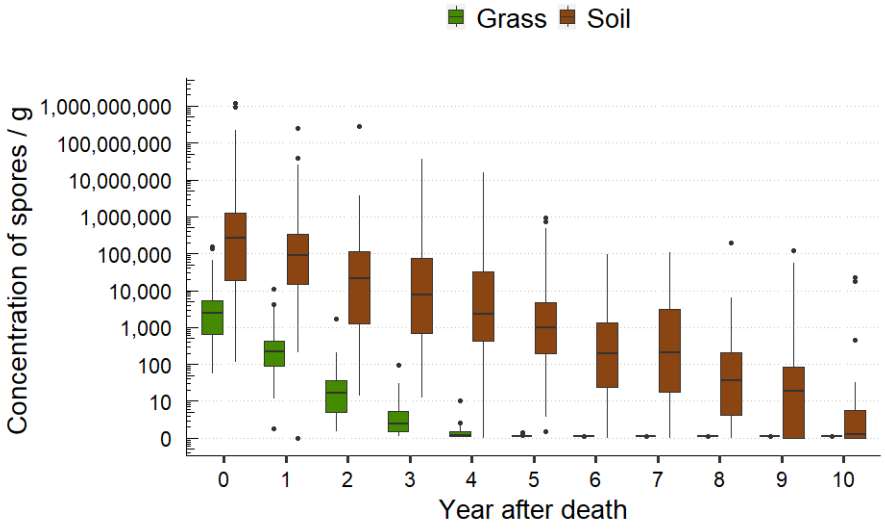

FIGURE 2.3: Decline in *Bacillus anthracis* spore concentrations at 40 anthrax carcass sites in Etosha National Park, Namibia, over time, on grass tops (green) and in surface soils (brown). Grass concentrations were obtained from extrapolation of the soil concentrations (equation 2.1).

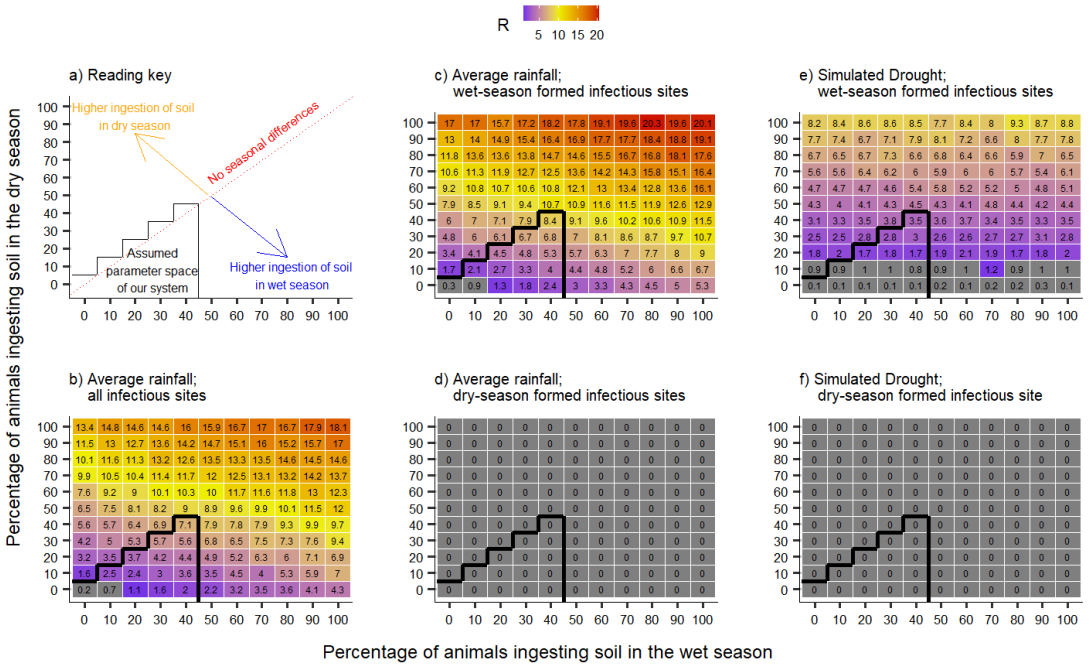

FIGURE 2.4: Variation in the reproduction number, *R*, for plains zebras (*Equus quagga*) at anthrax carcass sites, for a lethal dose threshold of 10^7 *Bacillus anthracis* spores based on differences in seasonality of host visitation, season of reservoir formation, and percentage of individuals ingesting soil during grazing, estimated over the 10-year lifetime of a *B. anthracis* reservoir site. The percentage of animals ingesting soil while grazing is varied from 0% to 100%. In all cases, animals are ingesting 10% soil, 90% grass (by weight) if soil is consumed. Soil contact during foraging is considered for two seasons, wet season (numbers below the diagonal) and dry season (numbers above the diagonal). The *R* values falling along the diagonal represent no difference in soil exposure by season. The black line represents the most likely parameter space for the study system, according to host foraging literature (Havarua et al., 2014; Turner et al., 2013). The grey tiles represent an $R < 1$, then a colour gradient is used for $R > 1$. (a) reading key; (b) all host and reservoir data; (c) visitation rates under good rainfall, wet season reservoirs; (d) visitation rates under good rainfall, dry season reservoirs; (e) visitation rates under simulated drought, wet season reservoirs; (f) visitation rates under simulated drought, dry season reservoirs.

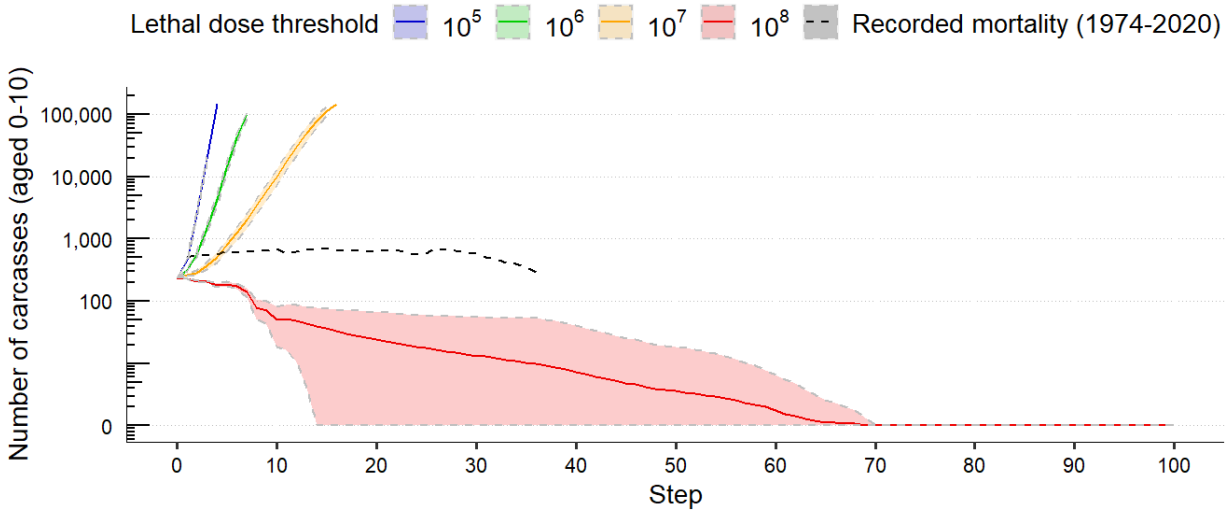

FIGURE 2.5: Prediction of the number of anthrax cases recorded over 100 years depending on lethal dose thresholds of 10^5,10^6,10^7 and 10^8. The shaded area represents the standard deviation over the 100 simulations. The black dashed line represents the recorded mortality in Etosha National Park, Namibia from 1974 to 2020. Each simulation started with the recorded mortality data from a decade (2003–2013). The x-axis represents the total number of potentially infectious carcass sites present in the environment (each site 'disappears' after 10 years). Predictions were made using the simulation model output, with a limit of 10 000 new cases. The lethal doses 10^5,10^6 and 10^7 lead to an explosion of cases, while the lethal dose of 10^8 leads to extinction. Lethal doses maintaining a relatively stable number of cases over time would be between 10^7 and 10^8. The y-axis is log-transformed

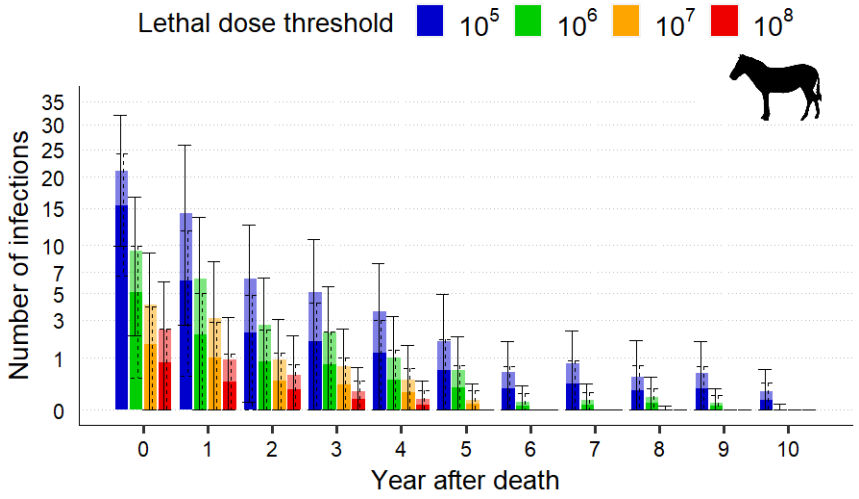

FIGURE 2.6: Variation in the average number of plains zebra (*Equus quagga*) secondary anthrax mortalities occurring per year after death at an anthrax carcass site, depending on the lethal dose threshold of *Bacillus anthracis* spores ingested. Opaque colours and dotted error bars represent the average number of infections within the assumed parameter space of our study system, i.e., the percentage of animals ingesting soil while grazing varied from 0% to 40%. The transparent bars and solid error bars represent the average number of secondary infections for the entire parameter space, i.e. the percentage of animals ingesting soil while grazing varied from 0% to 100%. The y-axis is square root transformed to better visualize small numbers. Error bars represent standard deviation.

2.10 References

Albery, G.F., Sweeny, A.R., Becker, D.J., Bansal, S., 2022. Fine-scale spatial patterns of wildlife disease are common and understudied. Funct. Ecol. 36, 214–225. https://doi.org/10.1111/1365-2435.13942

Aminu, O.R., Forde, T.L., Ekwem, D., Johnson, P., Nelli, L., Mmbaga, B.T., Mshanga, D., Shand, M., Shirima, G., Walsh, M., Zadoks, R.N., Biek, R., Lembo, T., 2022. Participatory mapping identifies risk areas and environmental predictors of endemic anthrax in rural Africa. Sci. Rep. 12, 10514. https://doi.org/10.1038/s41598-022-14081-5

Arthur, W.J., Alldredge, A.W., 1979. Soil ingestion by mule deer in Northcentral Colorado. J. Range Manag. 32, 67. https://doi.org/10.2307/3897389

Aune, K., Rhyan, J.C., Russell, R., Roffe, T.J., Corso, B., 2012. Environmental persistence of *Brucella abortus* in the Greater Yellowstone Area. J. Wildl. Manag. 76, 253–261. https://doi.org/10.1002/jwmg.274

Baillie, L., Read, T.D., 2001. *Bacillus anthracis*, a bug with attitude! Curr. Opin. Microbiol. 4, 78–81. https://doi.org/10.1016/S1369-5274(00)00168-5

Barandongo, Z.R., Dolfi, A.C., Bruce, S.A., Rysava, K., Huang, Y.-H., Joel, H., Hassim, A., Kamath, P.L., van Heerden, H., Turner, W.C., 2023. The persistence of time: the lifespan of *Bacillus anthracis* spores in environmental reservoirs. Res. Microbiol. 104029. https://doi.org/10.1016/j.resmic.2023.104029

Barasona, J.A., Vicente, J., Díez-Delgado, I., Aznar, J., Gortázar, C., Torres, M.J., 2017. Environmental presence of *Mycobacterium tuberculosis* complex in aggregation points at the wildlife/livestock interface. Transbound. Emerg. Dis. 64, 1148–1158. https://doi.org/10.1111/tbed.12480

Bates, D., Mächler, M., Bolker, B., Walker, S., 2015. Fitting linear mixed-effects models using lme4. J. Stat. Softw. 67. https://doi.org/10.18637/jss.v067.i01

Blackburn, J.K., Ganz, H.H., Ponciano, J.M., Turner, W.C., Ryan, S.J., Kamath, P., Cizauskas, C., Kausrud, K., Holt, R.D., Stenseth, N.C., Getz, W.M., 2019. Modeling R0 for pathogens with environmental transmission: Animal movements, pathogen populations, and local infectious zones. Int. J. Environ. Res. Public. Health 16, 954. https://doi.org/10.3390/ijerph16060954

Breban, R., Drake, J.M., Stallknecht, D.E., Rohani, P., 2009. The role of environmental transmission in recurrent avian influenza epidemics. PLoS Comput. Biol. 5, e1000346. https://doi.org/10.1371/journal.pcbi.1000346

Brooks, M., E., Kristensen, K., Benthem, K., J. ,van, Magnusson, A., Berg, C., W., Nielsen, A., Skaug, H., J., Mächler, M., Bolker, B., M., 2017. glmmTMB balances speed and flexibility among packages for zero-inflated generalized linear mixed modeling. R J. 9, 378. https://doi.org/10.32614/RJ-2017-066

Buck, J.C., Weinstein, S.B., Young, H.S., 2018. Ecological and evolutionary consequences of parasite avoidance. Trends Ecol. Evol. 33, 619–632. https://doi.org/10.1016/j.tree.2018.05.001

Caraco, T., Turner, W.C., 2018. Pathogen transmission at stage-structured infectious patches: Killers and vaccinators. J. Theor. Biol. 436, 51–63. https://doi.org/10.1016/j.jtbi.2017.09.029

Chen, A., Reperant, L., Fischhoff, I.R., Rubenstein, D.I., 2021. Increased vigilance of plains zebras (*Equus quagga*) in response to more bush coverage in a Kenyan savanna. Clim. Change Ecol. 1, 100001. https://doi.org/10.1016/j.ecochg.2021.100001

Cizauskas, C.A., Turner, W.C., Pitts, N., Getz, W.M., 2015. Seasonal patterns of hormones, macroparasites, and microparasites in wild African ungulates: The interplay among stress, reproduction, and disease. PLOS ONE 10, e0120800. https://doi.org/10.1371/journal.pone.0120800

Cizauskas, C.A., Turner, W.C., Wagner, B., Küstersrs, M., Vance, R.E., Getz, W.M., 2014. Gastrointestinal helminths may affect host susceptibility to anthrax through seasonal immune trade-offs. BMC Ecol. 14, 1–15. https://doi.org/10.1186/s12898-014-0027-3

Clegg, S.B., Turnbull, P.C.B., Foggin, C.M., Lindeque, P.M., 2007. Massive outbreak of anthrax in wildlife in the Malilangwe Wildlife Reserve, Zimbabwe. Vet. Rec. 160, 113–118. https://doi.org/10.1136/vr.160.4.113

Collas, C., Mahieu, M., Tricheur, A., Crini, N., Badot, P.-M., Archimède, H., Rychen, G., Feidt, C., Jurjanz, S., 2019. Cattle exposure to chlordecone through soil intake. The case-study of tropical grazing practices in the French West Indies. Sci. Total Environ. 668, 161–170. https://doi.org/10.1016/j.scitotenv.2019.02.384

Dannock, R., 2016. Understanding the behavioural trade-offs made by blue wildebeest (*Connochaetes taurinus*): the importance of resources, predation and the landscape (PhD Thesis). The University of Queensland. https://doi.org/10.14264/uql.2016.861

Diekmann, O., Heesterbeek, J.A., Metz, J.A., 1990. On the definition and the computation of the basic reproduction ratio R0 in models for infectious diseases in heterogeneous populations. J. Math. Biol. 28, 365–382. https://doi.org/10.1007/BF00178324

Dougherty, E.R., Seidel, D.P., Blackburn, J.K., Turner, W.C., Getz, W.M., 2022. A framework for integrating inferred movement behavior into disease risk models. Mov. Ecol. 10, 31. https://doi.org/10.1186/s40462-022-00331-8

Dolfi AC, Kausrud K, Rysava K, Champagne C, Huang Y-H, Barandongo ZR, Turner WC. 2024 Season of death, pathogen persistence and wildlife behaviour alter number of anthrax secondary infections from environmental reservoirs: R scripts, input and output data [Dataset]. Dryad. (doi:10.5061/dryad. 3n5tb2rqt)

Ebert, D., Weisser, W.W., 1997. Optimal killing for obligate killers: the evolution of life histories and virulence of semelparous parasites. Proc. R. Soc. Lond. B Biol. Sci. 264, 985–991. https://doi.org/10.1098/rspb.1997.0136

Eby, P., Peel, A.J., Hoegh, A., Madden, W., Giles, J.R., Hudson, P.J., Plowright, R.K., 2023. Pathogen spillover driven by rapid changes in bat ecology. Nature 613, 340–344. https://doi.org/10.1038/s41586-022-05506-2

Ezhova, E., Orlov, D., Suhonen, E., Kaverin, D., Mahura, A., Gennadinik, V., Kukkonen, I., Drozdov, D., Lappalainen, H.K., Melnikov, V., Petäjä, T., Kerminen, V.-M., Zilitinkevich, S., Malkhazova, S.M., Christensen, T.R., Kulmala, M., 2021. Climatic factors influencing the anthrax outbreak of 2016 in Siberia, Russia. EcoHealth 18, 217–228. https://doi.org/10.1007/s10393-021-01549-5

Ganz, H.H., Turner, W.C., Brodie, E.L., Kusters, M., Shi, Y., Sibanda, H., Torok, T., Getz, W.M., 2014. Interactions between *Bacillus anthracis* and plants may promote anthrax transmission. PLoS Negl. Trop. Dis. 8, e2903. https://doi.org/10.1371/journal.pntd.0002903

Georgsson, G., Sigurdarson, S., Brown, P., 2006. Infectious agent of sheep scrapie may persist in the environment for at least 16 years. J. Gen. Virol. 87, 3737–3740. https://doi.org/10.1099/vir.0.82011-0

Gutting, B.W., Rukhin, A., Marchette, D., Mackie, R.S., Thran, B., 2016. Dose-response modeling for inhalational anthrax in rabbits following single or multiple exposures: Dose-response modeling for inhalational anthrax. Risk Anal. 36, 2031–2038. https://doi.org/10.1111/risa.12564

Hampson, K., Lembo, T., Bessell, P., Auty, H., Packer, C., Halliday, J., Beesley, C.A., Fyumagwa, R., Hoare, R., Ernest, E., Mentzel, C., Metzger, K.L., Mlengeya, T., Stamey, K., Roberts, K., Wilkins, P.P., Cleaveland, S., 2011. Predictability of anthrax infection in the Serengeti, Tanzania: Predicting anthrax infection in the Serengeti. J. Appl. Ecol. 48, 1333–1344. https://doi.org/10.1111/j.1365-2664.2011.02030.x

Hart, B.L., 1990. Behavioral adaptations to pathogens and parasites: Five strategies. Neurosci. Biobehav. Rev. 14, 273–294. https://doi.org/10.1016/S0149-7634(05)80038-7

Havarua, Z., Turner, W.C., Mfune, J.K.E., 2014. Seasonal variation in foraging behaviour of plains zebra (*Equus quagga*) may alter contact with the anthrax bacterium (*Bacillus anthracis*). Can. J. Zool. 92, 331–337. https://doi.org/10.1139/cjz-2013-0186

Hopkins, S.R., Jones, I.J., Buck, J.C., LeBoa, C., Kwong, L.H., Jacobsen, K., Rickards, C., Lund, A.J., Nova, N., MacDonald, A.J., Lambert-Peck, M., De Leo, G.A., Sokolow, S.H., 2022. Environmental persistence of the world's most burdensome infectious and parasitic diseases. Front. Public Health 10.

Huang, Y.-H., Joel, H., Küsters, M., Barandongo, Z.R., Cloete, C.C., Hartmann, A., Kamath, P.L., Kilian, J.W., Mfune, J.K.E., Shatumbu, G., Zidon, R., Getz, W.M., Turner, W.C., 2021. Disease or drought: environmental fluctuations release zebra from a potential pathogen-triggered ecological trap. Proc. R. Soc. B. https://doi.org/10.1098/rspb.2021.0582

Huang, Y.-H., Kausrud, K., Hassim, A., Ochai, S.O., van Schalkwyk, O.L., Dekker, E.H., Buyantuev, A., Cloete, C.C., Kilian, J.W., Mfune, J.K.E., Kamath, P.L., van Heerden, H., Turner, W.C., 2022. Environmental drivers of biseasonal anthrax outbreak dynamics in two multihost savanna systems. Ecol. Monogr. 92, e1526. https://doi.org/10.1002/ecm.1526

Huang, Y.-H., Owen-Smith, N., Henley, M.D., Kilian, J.W., Kamath, P.L., Ochai, S.O., Van Heerden, H., Mfune, J.K.E., Getz, W.M., Turner, W.C., 2023. Variation in herbivore space use: comparing two savanna ecosystems with different anthrax outbreak patterns in southern Africa. Mov. Ecol. 11, 46. https://doi.org/10.1186/s40462-023-00385-2

Manlove, K., Wilber, M., White, L., Bastille-Rousseau, G., Yang, A., Gilbertson, M.L.J., Craft, M.E., Cross, P.C., Wittemyer, G., Pepin, K.M., 2022. Defining an epidemiological landscape that connects movement ecology to pathogen transmission and pace-of-life. Ecol. Lett. 25, 1760–1782. https://doi.org/10.1111/ele.14032

Martin, G., Becker, D.J., Plowright, R.K., 2018. Environmental persistence of influenza H5N1 is driven by temperature and salinity: insights from a Bayesian meta-analysis. Front. Ecol. Evol. 6, 131. https://doi.org/10.3389/fevo.2018.00131

Martinez-Bakker, M., King, A.A., Rohani, P., 2015. Unraveling the transmission ecology of polio. PLOS Biol. 13, e1002172. https://doi.org/10.1371/journal.pbio.1002172

McCallum, H., Fenton, A., Hudson, P.J., Lee, B., Levick, B., Norman, R., Perkins, S.E., Viney, M., Wilson, A.J., Lello, J., 2017. Breaking beta: deconstructing the parasite transmission function. Philos. Trans. R. Soc. B Biol. Sci. https://doi.org/10.1098/rstb.2016.0084

Murray, M.G., Brown, D., 1993. Niche separation of grazing ungulates in the Serengeti: An experimental test. J. Anim. Ecol. 62, 380. https://doi.org/10.2307/5369

Ochai, S.O., Crafford, J.E., Hassim, A., Byaruhanga, C., Huang, Y.-H., Hartmann, A., Dekker, E.H., Van Schalkwyk, O.L., Kamath, P.L., Turner, W.C., Van Heerden, H., 2022. Immunological evidence of variation in exposure and immune response to *Bacillus anthracis* in herbivores of Kruger and Etosha National Parks. Front. Immunol. 13, 814031. https://doi.org/10.3389/fimmu.2022.814031

Okello, M.M., Wishitemi, R.E.L., Muhoro, F., 2002. Forage intake rates and foraging efficiency of free-ranging zebra and impala 32.

Pinzon, J.E., Tucker, C.J., 2014. A non-stationary 1981–2012 AVHRR NDVI3g time series. Remote Sens. 6, 6929–6960. https://doi.org/10.3390/rs6086929

Plowright, R.K., Parrish, C.R., McCallum, H., Hudson, P.J., Ko, A.I., Graham, A.L., Lloyd-Smith, J.O., 2017. Pathways to zoonotic spillover. Nat. Rev. Microbiol. 15, 502–510. https://doi.org/10.1038/nrmicro.2017.45

R Core Team, 2018. R A language and environment for statistical computing. R Foundation for Statistical Computing, Vienna. - References - Scientific Research Publishing. https://www.R-project.org (accessed 3.15.23).

Roever, C.L., Beyer, H.L., Chase, M.J., van Aarde, R.J., 2014. The pitfalls of ignoring behaviour when quantifying habitat selection. Divers. Distrib. 20, 322–333. https://doi.org/10.1111/ddi.12164

Rohani, P., Breban, R., Stallknecht, D.E., Drake, J.M., 2009. Environmental transmission of low pathogenicity avian influenza viruses and its implications for pathogen invasion. PNAS. https://doi.org/10.1073/pnas.0809026106

Scherer, C., Radchuk, V., Franz, M., Thulke, H., Lange, M., Grimm, V., Kramer-Schadt, S., 2020. Moving infections: individual movement decisions drive disease persistence in spatially structured landscapes. Oikos 129, 651–667. https://doi.org/10.1111/oik.07002

Shapiro, K., Bahia-Oliveira, L., Dixon, B., Dumètre, A., de Wit, L.A., VanWormer, E., Villena, I., 2019. Environmental transmission of *Toxoplasma gondii:* Oocysts in water, soil and food. Food Waterborne Parasitol. 15, e00049. https://doi.org/10.1016/j.fawpar.2019.e00049

Stears, K., Schmitt, M.H., Turner, W.C., McCauley, D.J., Muse, E.A., Kiwango, H., Mathayo, D., Mutayoba, B.M., 2021. Hippopotamus movements structure the spatiotemporal dynamics of an active anthrax outbreak. Ecosphere 12. https://doi.org/10.1002/ecs2.3540

Taft, S.C., Nichols, T.L., Hines, S.A., Barnewall, R.E., Stark, G.V., Comer, J.E., 2020. Physiological responses to multiple low-doses of *Bacillus anthracis* spores in the rabbit model of inhalation anthrax. Pathogens 9, 877. https://doi.org/10.3390/pathogens9110877

Titcomb, G., Mantas, J.N., Hulke, J., Rodriguez, I., Branch, D., Young, H., 2021. Water sources aggregate parasites with increasing effects in more arid conditions. Nat. Commun. 12, 7066. https://doi.org/10.1038/s41467-021-27352-y

Towne, E.G., 2000. Prairie vegetation and soil nutrient responses to ungulate carcasses. Oecologia 122, 232–239. https://doi.org/10.1007/PL00008851

Turnbull, P.C.B., Bowen, J., Mann, J., 1996. Stubborn contamination with anthrax spores. Environ. Health 171–173.

Turner, W.C., Imologhome, P., Havarua, Z., Kaaya, G.P., Mfune, J.K.E., Mpofu, I.D.T., Getz, W.M., 2013. Soil ingestion, nutrition and the seasonality of anthrax in herbivores of Etosha National Park. Ecosphere 4, art13. https://doi.org/10.1890/ES12-00245.1

Turner, W.C., Kausrud, K.L., Beyer, W., Easterday, W.R., Barandongo, Z.R., Blaschke, E., Cloete, C.C., Lazak, J., Van Ert, M.N., Ganz, H.H., Turnbull, P.C.B., Stenseth, N.Chr., Getz, W.M., 2016. Lethal exposure: An integrated approach to pathogen transmission via environmental reservoirs. Sci. Rep. 6, 27311. https://doi.org/10.1038/srep27311

Turner, W.C., Kausrud, K.L., Krishnappa, Y.S., Cromsigt, J.P.G.M., Ganz, H.H., Mapaure, I., Cloete, C.C., Havarua, Z., Küsters, M., Getz, W.M., Stenseth, N.Chr., 2014. Fatal attraction: vegetation responses to nutrient inputs attract herbivores to infectious anthrax carcass sites. Proc. R. Soc. B Biol. Sci. 281, 20141785. https://doi.org/10.1098/rspb.2014.1785

Turner, W.C., Périquet, S., Goelst, C.E., Vera, K.B., Cameron, E.Z., Alexander, K.A., Belant, J.L., Cloete, C.C., du Preez, P., Getz, W.M., Hetem, R.S., Kamath, P.L., Kasaona, M.K., Mackenzie, M., Mendelsohn, J., Mfune, J.K.E., Muntifering, J.R., Portas, R., Scott, H.A., Strauss, W.M., Versfeld, W., Wachter, B., Wittemyer, G., Kilian, J.W., 2022. Africa's drylands in a changing world: Challenges for wildlife conservation under climate and land-use changes in the Greater Etosha Landscape. Glob. Ecol. Conserv. 38, e02221. https://doi.org/10.1016/j.gecco.2022.e02221

van Klink, R., Laar-Wiersma, J. van, Vorst, O., Smit, C., 2020. Rewilding with large herbivores: Positive direct and delayed effects of carrion on plant and arthropod communities. PLOS ONE 15, e0226946. https://doi.org/10.1371/journal.pone.0226946

VanderWaal, K.L., Ezenwa, V.O., 2016. Heterogeneity in pathogen transmission: mechanisms and methodology. Funct. Ecol. 30, 1606–1622. https://doi.org/10.1111/1365-2435.12645

Weinstein, S.B., Buck, J.C., Young, H.S., 2018. A landscape of disgust. Science 359, 1213–1214. https://doi.org/10.1126/science.aas8694

WHO, 2008. Anthrax in humans and animals, fourth. ed.

Zidon, R., Garti, S., Getz, W.M., Saltz, D., 2017. Zebra migration strategies and anthrax in Etosha National Park, Namibia. Ecosphere 8, e01925. https://doi.org/10.1002/ecs2.1925

CHAPTER THREE: Host range size and density, environmental variation, and pathogen persistence alter disease dynamics in an agent-based model of anthrax in Namibian wildlife

Contributing authors : Amélie C. Dolfi, Marie L. J. Gilbertson, Wendy C. Turner

PICTURE 3: Group of herbivores drinking at the Okaukuejo waterhole, in Etosha National Park, Namibia. We can see two springboks (*Antidorcas marsupialis*), two black-faced impalas (*Aepyceros melampus petersi*), one blue wildebeest (*Connochaetes taurinus*), and six plains zebra (*Equus quagga*). Photo by Amélie Dolfi, May 2022

3.1 Abstract

Anthrax, caused by the obligate-killer pathogen *Bacillus anthracis* (BA) kills a diversity of hosts in a multitude of ecosystems, from prairies to savannas to tundra. Mammalian herbivores are the most susceptible hosts and become infected when foraging at anthrax infectious sites. After host death, BA is deposited into the soil, where it can survive for decades in spore form. While these spores are hardy, their survival depends on the soil type and environmental conditions. Depending on the ecosystem, the disease dynamics can vary widely from endemic to epidemic outbreaks. It is assumed that epidemic outbreaks are density-dependent, such that host population must be large enough to sustain the outbreak. Understanding the factors driving the differences in outbreak dynamics is crucial to better respond to and manage the disease. In this study, we developed an agent-based model to determine how variations in host density, range sizes, rainfall conditions, and pathogen persistence alter anthrax dynamics in Etosha National Park, Namibia. Host range size, host density, and environmental conditions were the most important factors in altering the timing and intensity of outbreaks. When hosts had smaller than typical home ranges, the number of cases remained low over the simulation period due to a lower host-pathogen encounter rate. Under wetter conditions, large outbreaks occurred early on, with outbreak size depending on the initial host density, followed by a decline in host population density, and with it a decline in anthrax cases. This simulation model emphasized how modifications in environmental features, pathogen persistence, and host ecology alter the timing and intensity of anthrax outbreaks in an endemic savanna system. In particular, host movement was the main driver for understanding anthrax dynamics. Thus, our model emphasized the need to determine what drives host movements and how environmental conditions can modify those movements to better characterize anthrax outbreaks.

3.2 Introduction

Bacillus anthracis (BA), the causative agent of anthrax, is found in all inhabited continents (Carlson et al., 2019), with the disease dynamics being dependent on the ecosystem. BA is a multi-host obligate-killer bacterium, meaning it must kill its host and be released into the environment before transmitting to a new susceptible host. This pathogen has a broad spatial distribution and occurs in widely different environments, from Australian and African savannas (Durrheim et al., 2009; Muturi et al., 2018) to North American prairies (Mongoh et al., 2008), to Bangladeshi tropical floodplains (Hassan et al., 2015), to Siberian tundras (Ezhova et al., 2021). The large differences in the ecology of these locations and their available host species make it challenging to understand the key factors underlying variation in anthrax outbreak dynamics.

While anthrax mainly affects wild and domestic herbivores, cases in carnivores are reported, and it remains a risk for humans (Beyer and Turnbull, 2009; WHO, 2008). For livestock and wildlife, gastrointestinal exposure is the main transmission pathway and occurs when foraging or drinking (Hugh-Jones and de Vos, 2002; Turner et al., 2014). As a multi-host pathogen, BA infects a large diversity of herbivores, including those with different diets (grazers, mixed-feeders, browsers) and in varying environments. Among grazers, such as cattle (*Bos taurus*), hippopotamus (*Hippopotamus amphibious*), plains zebra (*Equus quagga*), or bison (*Bison bison*), anthrax is transmitted through ingesting contaminated grass or forage (Schild et al., 2006; Walker et al., 2020). For browsers such as white-tailed deer (*Odocoileus virginanus*) and greater kudus (*Tragelaphus strepsiceros*), anthrax is transmitted by ingestion of spore-contaminated browse (Clegg et al., 2007; Mullins et al., 2015). Leaves become contaminated from blowflies that feed on nearby anthrax-infected carcasses, rest on woody vegetation, and excrete BA (Basson et al., 2018; Blackburn et al., 2014). Depending on the season, anthrax infections may occur from either

exposure pathway for herbivores that consume both grass and browse (mixed-feeders), such as elk (*Cervus elaphus*) and impala (*Aepyceros melampus*). This diversity of host species and transmission routes highlights the extensive risk posed by anthrax, which can infect very different host species in many different ecosystems.

BA spores are highly resistant to biotic and abiotic factors and can survive for extended periods in the environment, usually decades (Barandongo et al., 2023; Dragon and Rennie, 1995; Manchee et al., 1981). However, the survival of spores depends on soil properties, temperature, relative humidity, and the genetic diversity of the pathogen (Dey et al., 2012; Govender, 2022; Smith et al., 2000). Heterogeneity in spore survival can have significant impacts on anthrax outbreak dynamics. Specifically, we can characterize anthrax outbreaks into two broad types: endemic and epidemic. In endemic systems, recurrent seasonal, usually small, outbreaks are observed, such as in Kenya (Muturi et al., 2018), Bangladesh (Hassan et al., 2015), or Türkiye (Bayir, 2023). In epidemic systems, massive outbreaks occur infrequently. For example, an anthrax outbreak in 2004 in Malilangwe Wildlife Reserve, Zimbabwe, killed nearly the entire kudu population and 70% of the nyala (*Tragelaphus angasii*) population (Clegg et al., 2007). In 2016, in Siberia, thousands of reindeer (*Rangifer tarandus*) died of anthrax, about 70 years after the last recorded epidemic (Ezhova et al., 2021). It is assumed that epidemic systems are strongly linked to the host density (De Vos and Bryden, 1996). Indeed, during these outbreaks, most of the host population is killed; thus, enough time is required between consecutive outbreaks for the host population to recover sufficiently to support another outbreak.

Anthrax outbreaks are seasonal, although the seasonality varies across locations (Pittiglio et al., 2022). In some ecosystems, outbreaks are associated with heavy rainfall and wet seasons (e.g. in Bangladesh [Hassan et al., 2015] or Tanzania [Mlengeya et al., 1998]) possibly due to the rainfall

unearthing spores (Durrheim et al., 2009), or increasing grass growth in preferred habitats, increasing pathogen exposure (Turner et al., 2014). In contrast, droughts are associated with anthrax outbreaks in Zimbabwe (Clegg et al., 2007), Ethiopia (Shiferaw et al., 2002), and Zambia (Turnbull et al., 1991). In these areas, drought conditions likely cause aggregation of herbivores close to waterholes, an increase in physiological stressors reducing host resistance to anthrax, or the ingestion of spores along with dry forage creating small lesions in the mouth that facilitate infections (Hugh-Jones and de Vos, 2002).

Due to the long persistence of anthrax spores in the environment, the multi-host nature of this disease, and the variation in environments and host ecology over different time scales, it can be challenging to link all ecological components together to understand the disease dynamics arising in different ecosystems (Huang et al., 2022). Mathematical models have been developed over time to better understand anthrax transmission risk and obtain the reproduction number of this disease (Blackburn et al., 2019; Dolfi et al., 2024). The use of differential equations is the main modeling framework that has been applied (Friedman and Yakubu, 2013; Furniss and Hahn, 1981; Osman et al., 2018; Saad-Roy et al., 2017), but these models often lack spatiotemporal components (e.g., assuming all hosts can encounter any reservoirs at any time of the simulation) which can be quite significant, especially for modeling ETP disease dynamics (Arab, 2015; Elliott and Wartenberg, 2004; Lawson, 2013). Similarly, individual-level variation in host behaviors and susceptibility can alter disease dynamics, and their inclusion into models can prove necessary for better understanding pathogen transmission risk (Craft, 2015; Paull et al., 2012).

Agent-based models (ABM) can capture the role of complex relationships between individual and landscape heterogeneity in disease emergence and dynamics (Scherer et al., 2020; White et al., 2018). By allowing agents to move independently in their environment and to respond to different

stimuli following a set of pre-defined rules, we can observe the emergence of broad-scale patterns without forcing them into the model (Grimm et al., 2020; Railsback and Grimm, 2019). Notably, one theoretical ABM inspired by anthrax dynamics (Dougherty et al., 2018) emphasized the importance of individual host movement decisions in understanding the risk of transmission by measuring the number of encounters between hosts and reservoirs. However, this model lacked host heterogeneity in susceptibility and was based on a theoretical landscape rather than an *in-situ* ecosystem.

Here, we developed an ABM to evaluate how modifications in host density and behavior, pathogen persistence, and rainfall patterns alter disease dynamics. While we focus our model on one specific location, Etosha National Park (hereafter Etosha) in Namibia, for which detailed knowledge about anthrax is available (see below), the objectives of this model were to broaden our understanding of what drives the timing and intensity of anthrax outbreaks. Etosha is an endemic system for anthrax, and we seek to understand how host species and behaviors, pathogen characteristics, seasonality and rainfall conditions interact to maintain Etosha as an anthrax-endemic system. These findings, and the ABM developed in this study, have the potential to be generalized to other anthrax systems to improve our general understanding of the drivers of anthrax outbreaks in different ecosystems.

3.3 Materials and Methods

3.3.1 Study area

3.3.1.a Environmental characteristics

Etosha is a 22,270 km^2 nature reserve situated in northern Namibia at the base of the Cuvelei basin (Turner et al., 2022). It is a sub-tropical, semi-arid savannah with two distinct seasons: the wet season (January–April) and the dry season (May-December). Etosha encompasses a 5,000 km^2 salt

pan seldom used by herbivores and was defined as a barrier to movement in our model. Etosha has a gradient of increasing rainfall from west to east, with annual rainfall of about 260mm (rainfall from 1983-2020, from the Etosha Ecological Institute, (EEI)) in the west, 400mm in the central region, and 520mm in the east. Natural water sources are primarily artesian or contact springs, mostly found south of the main salt pan, but boreholes are also present along tourist roads (Turner et al., 2022).

An extensive classification of Etosha's vegetation was done by Le Roux and collaborators (1988). For our model, we simplified the vegetation into four habitats: sweetgrass, sandveld, mopane (*Colophospermum mopane*) shrubland, and mopane woodland (habitats shown in figure 3.1). Common species in the sweetgrass habitat include highly palatable grass species such as *Enneapogon desvauxii* and *Eragrostis nindensis*, and dwarf shrubs such as *Leucosphaera bainesii*, *Cyathula hereroensis*, *Monechma* spp. Sweetgrass habitat, found southwest of the salt pan, is preferred by grazers in the wet season, although under pressure of migratory herds of grazing herbivores, this resource is depleted annually. The sandveld, found northeast of the salt pan, is favored by browsing herbivores and contains a variety of trees and shrubs, such as *Terminalia prunioides*, *T. sericea*, *Croton menyharthii*, and *Philenoptera nelsii*, as well as less palatable grasses, such as *Schmidtia kalahariensis*, and *Digitaria seriata*. The other two habitats are dominated by mopane, with differences defined by its growth form and height, driven by variations in soil characteristics and rainfall. Mopane shrubland is found primarily west of the salt pan, together with other woody shrubs such as *Catophractes alexandri*, and *L. bainesii*, as well as less palatable grasses such as *Aristida adscensionis* and *A. rhiniochloa.* Mopane woodland, found primarily southeast of the salt pan, also contains marula trees (*Sclerocarya birrea*), *Spirostachys africana, Combretum apiculatum, T. prunioides,* and acacias such as *Vachellia nilotica.* In those

woodlands, the herbaceous layer is composed of species such as *E. desvauxii*, *E. cenchroides*, and *A. adscensionis*.

3.3.1.b Anthrax in Etosha

Anthrax outbreaks in Etosha have been studied extensively for multiple decades (Barandongo et al., 2023; Cizauskas et al., 2014a; Ebedes, 1976; Huang et al., 2021; Lindeque and Turnbull, 1994; Turner et al., 2013). Anthrax is considered to have originated in southern Africa (Keim et al., 1997) and, in Etosha, this disease is unmanaged, making this park an excellent study area for understanding anthrax outbreaks in wildlife populations. Anthrax cases are recorded annually in Etosha, and, while sporadic cases can occur throughout the year, anthrax deaths peak at the end of the wet season (March-April) among grazers. The primary anthrax hosts in Etosha are grazers, specifically plains zebra (*Equus quagga*, hereafter zebra) and blue wildebeest (*Connochaetes taurinus*, hereafter wildebeest), representing respectively 50% and 16% of all confirmed cases between 1975 and 2020 (mortality data obtained from EEI). Mixed-feeding hosts are the next most common, especially springboks (*Antidorcas marsupialis*) which represent 14% of all cases, and African elephants (*Loxodonta africana*, hereafter elephant), which represent 16% of cases, with deaths peaking during the late dry season (around November). All other species, which include browsers, carnivores, and other herbivores infrequently detected, make up the remaining 4% of anthrax cases. Among the grazers, the main anthrax transmission pathway is through the ingestion of spores while grazing at infectious carcass sites. In Etosha, most cases are recorded in the central region, where grazing herbivores congregate on preferred sweetgrass habitat during the wet season. During dry seasons and drought years, this preferred habitat is depleted, and most grazers migrate along the Etosha salt pan toward less preferred foraging grounds (Huang et al., 2021; Zidon et al., 2017). This seasonal migration reduces the impact of this disease on grazing hosts,

providing a reprieve from anthrax with lower exposure risk in other habitats (Huang et al., 2021). However, BA spores can survive for up to 10 years in Etosha soils (Barandongo et al., 2023) and up to two years on grasses (Turner et al., 2014), allowing a continuation of infections once individuals return to the sweetgrass habitat. While anthrax cases can be observed year-round, reservoirs formed during the wet season are the main source of anthrax transmission in Etosha (Dolfi et al., 2024), emphasizing the seasonal dynamics of this disease. However, the transmission route is still unknown for elephants. Elephants are mixed feeders and are more likely to browse than graze during the season of highest anthrax mortality (Turner et al., 2013), and exposure from dust bathing or drinking is unlikely (Barandongo et al., 2023; Turner et al., 2016). Currently BA exposure for elephants is suspected to occur from osteophagia or mourning behaviors at elephant anthrax carcass sites (Joel, 2021).

3.3.2 Model description

We developed an ABM representing herbivore hosts moving within Etosha and being at risk of BA infection upon grazing at an infectious site. The model description following the ODD (Overview, Design concepts, Details) protocol for ABMs, as updated by Grimm et al. (2020), can be found in Appendix C. The model and analysis were done using R software (version 4.3.2. R Core Team, 2023).

In summary, the model includes two agents: herds of anthrax hosts and anthrax spore reservoirs. We used herd agents to limit the number of agents in the model, reducing its computational intensity. Empirically, individuals within a herd tend to stay close and move together, which would complicate the movement of simulated individual agents, as the movements of individuals from the same herds are non-independent (Allen et al., 2020; Fischhoff et al., 2007). The environment is defined using grid cells representing the geographical locations of Etosha.

The state variables for the herds of hosts (referred to as hosts hereafter) are the foraging type, the herd disease status ('S' for susceptible, 'I' for infected), and the number of infected individuals within the herd. The forage type is split into four categories: (i) non-selective grazers, called 'grazer1' in the model (e.g., representative of zebra), (ii) selective grazers, 'grazer2' (e.g., representative wildebeest), (iii) small-bodied mixed-feeders, 'mixed-feeder1' (e.g., representative of springbok), and (iv) large-bodied mixed-feeders, 'mixed-feeder2' (e.g., representative of elephant). The anthrax reservoir agents' state variable is the infectivity risk, defined as the probability of infection, given effective contact. The environmental grid cells are $250m^2$ and are composed of the vegetation type defined as five habitat categories: (i) sandveld, (ii) mopane woodland, (iii) mopane shrubland, (iv) sweetgrass, and (v) barrier (i.e., the salt pans). We also record if a grid cell contains a waterhole, and if not, we record the distance of all grid cells to the closest waterhole. The model runs for 5 years at a weekly time step (one time step = 7 days).

We initialized the model by creating the gridded environment and adding host agents and BA reservoirs (figure 3.1). All input data were drawn from long-term datasets collected by the EEI. We used the functional water points for the waterhole distribution as of 2006. To initialize the host spatial distribution, we used herd locations from the aerial survey of Etosha conducted in the dry season of 2015 (Kilian, 2015). Finally, we initialized infectious environment locations based on confirmed anthrax mortalities and their GPS locations recorded from 2000-2010.

The model includes seven sub-models, which proceed as follows: (i) rainfall; (ii) host movements within the landscape using a resource selection function (RSF); (iii) death of infected host and anthrax reservoir creation; (iv) probabilistic herd dissolution if death by anthrax occurred; (v) anthrax transmission; (vi) environmental anthrax risk decay; and (vii) new host creation. Each of these sub-models is described in the subsections that follow.

3.3.2.a Rainfall

Rainfall is a major source of heterogeneity in savanna ecosystems, as it can alter animal movements due to herd aggregation around water points during dry periods (VanderWaal et al., 2017). To determine if rainfall occurs during a time step, we make a binomial draw, weighted by $p_{rain,m}$, the probability of accumulating 10mm of rainfall per month m. We chose 10mm as this is the effective rainfall quantity to initiate grass growth in Etosha (du Plessis, 2001). We calculated this probability from the daily rainfall data from 1983-2020 from EEI, computing the proportion of weeks with at least 10mm of rainfall per month over the entire rainfall dataset.

When rain occurs, we consider that host herds do not need to visit a waterpoint during their weekly movement; we assume that ephemeral water is present in the environment (Naidoo et al., 2020; Schaffer-Smith et al., 2022), allowing hosts to satisfy their water requirements without long movements to perennial water.

3.3.2.b Movement

Resource-selection function

The movement of hosts is modeled using an RSF. Within one model time step (i.e., a 7-day period), herds can be found anywhere within their weekly home range. The weekly home range depends on the host foraging type and comprises η cells. Movements are determined by an RSF, which incorporates the habitat type, the distance to the nearest water points, and the distance to the seasonal migration zone. Two migration zones are defined: a migration zone toward the central region of Etosha, where forage grounds are better during the wet season, and a migration zone along the southern edge of the main salt pan during the dry season (see Appendix C figure C1; Zidon et al., 2017). We are assuming that grazers have a memory of the better foraging areas (Bracis and Mueller, 2017), and we therefore chose to facilitate the migration movement using the

distance to the migration zone. The probability of a host moving from its current location to a new location, *b*, is:

$$P = \frac{\omega_b}{\sum_{k=1}^{\eta}[\omega_k]} \quad (3.1)$$

Where ω_b and ω_k are RSFs governing a herd's movement preference for cells *b* and *k*, respectively. The RSF of any given cell *j* is:

$$\omega_j = \exp(\beta * Wood_j + \beta_1 * Sandveld_j + \beta_2 * Shrub_j + \beta_3 * Grass_j + \beta_4 * Barrier_j + \beta_5 * Water_{dist\,j} + \beta_6 * Migration_{dist\,j}) \quad (3.2)$$

with $Wood_j$, $Sandveld_j$, $Shrub_j$, $Grass_j$, and $Barrier_j$, representing the type of vegetation in cell *j*. Because a cell contains only one type of vegetation, only one of those five will equal 1, the rest will be 0. The associated β represent the strength of selection for the specific vegetation type. Coefficients vary per herd foraging type and season to represent different foraging preferences by host species and time of year (Table 3.1). $Water\_dist_j$ represents the distance to the closest water point in km, and $\beta 5$ is the strength of selection for that variable, which also varies by host foraging type and season. All four foraging types represented here are water-dependent, but the water requirements and how far they can move from water depends on the species (Veldhuis et al., 2019). For example, grazers are more water-dependent than mixed-feeders, which can obtain water from browsing on leaves. As a consequence, grazers will move longer distances from water as vegetation around waterholes is depleted (Redfern et al., 2003). $Migration_{dist,j}$ is the distance in km between cell *j* and the migration zone, for either the wet or dry season. The same coefficient β_6 regulates the strength of attraction toward the migration zones in both seasons; the higher β_6, the stronger the selection for a cell closer to the migration zone. The values attributed to each coefficient can be found in Appendix C, Table C1.

Polygon of host occurrence

Once the next step point is selected, we used the package ‘gdistance’ (version 1.6.4 [van Etten, 2017]) to calculate the shortest path between the two locations to ensure that individuals did not cross park fences to reach their destination. To account for uncertainty in herd movement during our 7-day time steps, we add a buffer of occurrence around the host movement path, σ, depending on the host foraging type (Table 3.1). This simplifying assumption allows us to reduce the computationally intensive resolution of the model by modeling weekly time steps instead of daily steps. The buffer also helps to account for the increased spatial extent of a single herd due to individual movements within the herd.

When rain occurs, we consider the movement to be as described above, as the presence of local ephemeral surface water does not constrain herds to go to a waterhole to drink (figure 3.2a). In contrast, if rainfall did not occur during the movement step (i.e., a week), we assume that the movement must incorporate a waterhole (figure 3.2b). For this, we selected the closest water point along the movement path and included it in the herd movement buffer. This approach allows us to explicitly include water dependency in our movement model, while also allowing agents to minimize travel distance to water sources. With the simulated occurrence buffers (hereafter referred to as polygons), we assumed that a herd could be exposed to infectious environments anywhere within its buffer.

3.3.2.c Infected host death and reservoir creation

Empirically, anthrax deaths occur within 2-5 days after infection (Easterday et al., 2020), so simulated herds with infected individuals create a new anthrax reservoir in the time step following infection. Using the occurrence polygon of hosts, we randomly select a location within which the infected individual dies, and the spore reservoir is established. The initial infectivity of an anthrax reservoir, denoted ρ, depends on the season (Dolfi et al., 2024) and represents the risk of infection

given effective contact. For a reservoir formed during the wet season, the initial probability is drawn within the truncated normal law with a mean of 7.5×10^{-4} and variance of 2.5×10^{-4}, and with a mean of 5×10^{-5} and variance of 1×10^{-5} for the dry season formed reservoirs. We make the simplifying assumption that the cell infectivity probability is directly proportional to the pathogen load in the environment.

3.3.2.d Herd dissolution

Upon the death of an individual, herds may dissolve and be removed from the simulation. We use binomial draws weighted by the herd dissolving probability, γ, which depends on the host type (Table C1). Each time a herd loses an individual, we repeat the binomial draw, so herds with more losses have a higher cumulative probability of dissolution than those with fewer losses. Parameterization of γ for grazer1 and mixed-feeder2 is designed to represent species with tight knit social structure, such that the death of an individual has a higher probability of inducing dissolution of their herd by destabilization than for the other foraging types. As an empirical example, if a matriarch dies in an elephant herd, the herd may become unstable, with reduced social cohesion and potential dispersion of some individuals (Lee et al., 2022; Wittemyer et al., 2005). Similarly, among zebras, if a stallion dies, there is an increased risk of herd fission (Penzhorn, 1984). For grazer2 and mixed-feeder1, the value of γ is lower to represent weaker social ties or structure; as such, the death of an individual may be less impactful on herd persistence.

3.3.2.e Infection

If there are BA reservoirs within a herd's occurrence distribution, there is a risk of infection. Infection depends on the combination of (1) effective contact between a herd and an infectious reservoir, and (2) the probability of infection, given that effective contact occurred. To determine if effective contact occurred, we made a binomial draw for each anthrax reservoir within an

occurrence polygon, weighted by the probability ξ of effectively interacting with that reservoir. ξ depends on the host forage type and season (Cunningham Jr. and Cunningham Sr., 2024; Havarua et al., 2014; Woolley et al., 2011). If an effective contact occurs with a reservoir, we perform another binomial draw, in this case, weighted by the reservoir infectivity ρ (determined by initial infectivity and decay rate; see 3.3.2.c and f). Within a time step, a reservoir can only infect one individual per herd. However, herds may encounter multiple reservoirs, leading to multiple independent infections during one time step.

3.3.2.f Anthrax risk decay

We allowed the infectivity of a cell to decay over time, assuming that the infectivity ρ of cell c, at time $t+1$, followed an exponential law:

$$\rho_{c,t+1} = \rho_{c,t} \cdot e^{-\mu} \quad (3.3)$$

where μ is the decay rate.

We removed reservoirs from the environment (cell infectivity returned to zero) when we considered their infectivity below a minimum level, ρ_{min}, defined as an infectivity of 5×10^{-7}, necessary for transmission (as in a minimum infectious dose).

3.3.2.g Reproduction

Reproduction occurs in an annual pulse every year during the week around March 15. Because our agents represent herds rather than individuals, we assume that herds can undergo fission (especially driven by yearlings) following birth events, resulting in new herds in the environment. We draw the number of new herds based on the number of herds present in the environment and the host foraging type using a truncated normal distribution (mean = δ, sd = δ_{sd}, min = δ_{min}, max = δ_{max}). As we assume that herds split from each other, each new herd initially takes the spatial coordinates of the herd from which it split.

3.3.3 Model scenarios and analysis

We aimed to determine what factors drive Etosha outbreak dynamics and which of the host density, host range sizes, pathogen decay rate, and rainfall conditions led to most modifications of the dynamic. We used the primary literature to parameterize an Etosha-like base model (hereafter, base Etosha model) that reproduces key observed anthrax dynamics in this system (see Table C1 for the fixed parameter values). In particular, we used Huang et al., (2023) to determine the herd movement variables, and Barandongo et al., (2023) and Dolfi et al., (2024) for the pathogen parameterization. Birth rates and herd dissolving rates were set to ensure the stability of host populations in our base model, as populations in Etosha have been relatively stable for the past 30 years (Turner et al., 2022). We validated our Etosha model by ensuring that the number of cases recorded yearly, per species, and per season matched observations made for the Etosha system.

Once our Etosha model was established, we varied certain parameters (Table 3.1) to determine their impact on outbreak dynamics. We included variations in the pathogen decay rate μ (rapid vs. slow), the density of herds (low vs. high density), the range size of herds, η and σ (small vs. large), and rainfall patterns—including their effect on host migration. For this latter condition, we included four rainfall scenarios: (1) regular rainfall as empirically observed in Etosha, with migration present along the salt pan during the dry season; (2) wetter conditions, leading to no migration and herd movement following the wet season parameters only; (3) drought conditions leading to no migration and herd movement following the dry season parameters only; and (4) a variable rainfall pattern. For this last scenario, the rainfall pattern of each year (regular, wetter, or drought) is drawn randomly, with each year having a 40% risk of being a drought, 35% of being a regular rainfall year, and 25% of being a wetter-than-average year.

We decided to vary these parameters by comparing Etosha and Kruger National Park (Kruger hereafter), the latter having epidemic anthrax outbreaks (Huang et al., 2022). Both parks contain similar host species, but in Kruger, anthrax outbreaks are assumed to be density-dependent (De Vos and Bryden, 1996), with a high density of hosts leading to large outbreaks. Host ranges are much smaller in Kruger than in Etosha (Huang et al., 2023), and herbivores in Kruger do not engage in seasonal migration as the large availability of water in the park allows hosts to satisfy their foraging and water demand without movement over long ranges (Redfern et al., 2003). Finally, anthrax persistence in both parks may differ due to differences in BA strains. Indeed, B-clade strains, which can be found in northern Kruger and a few other locations, survive less well than the A-clade strains, which are found in Kruger, Etosha, and globally (Govender, 2022; Smith et al., 2000).

We used a factorial design to determine the effects and interactions between our parameters, resulting in 72 scenarios. Each scenario was run ten times up to 5 years (i.e., 260-time steps) or until no anthrax reservoirs or infected hosts were present.

For each simulation, we extracted the number and seasonality of cases over time. To determine which of the four variables (pathogen decay, host density, movement ranges, and rainfall conditions) was the most important for shaping these outcomes, we conducted a variable importance analysis using random forests with the ‘party’ package (version 1.3.-14, [Strobl et al., 2008]).

3.4 Results

Under the Etosha base scenario (i.e., all parameters drawn from the Etosha system), we observed 40-60 anthrax cases per year over the simulation period, with seasonal increases in cases during simulated wet seasons (figures 3.3, 3.4). Cases were primarily among grazer1, with grazer2 and

the two mixed feeder foraging types infected infrequently (figure 3.3). These observed dynamics aligned with empirical observations from Etosha, where anthrax cases typically number between 10 and 100 per year, with most cases occurring in the wet season among zebras (figure 3.3). However, while our model reproduced coherent infection numbers for grazer1 (i.e., zebras in Etosha); it was not performing as well for the other hosts. Especially, elephants in Etosha exhibit more anthrax cases in the dry season, and we did not observe a similar peak for the corresponding foraging type ('mixfeeder2') in our simulations. However, elephant anthrax dynamics are driven by a few large outbreaks under drought conditions (Huang et al., 2022) which is unlikely to be observed in a relatively short simulation under average rainfall conditions.

Building off the base Etosha model, changing only a single parameter could cause widely different anthrax dynamics (figure 3.4), indicating that all the components we varied have key impacts on disease dynamics in this system. Notably, the number of cases recorded per simulation year decreased when we simulated a drought, a low density of hosts, a smaller host range, or a faster pathogen decay (figure 3.4a). In contrast, more infections were observed under wetter and more variable rainfall conditions, high host density, and slower pathogen decay (figure 3.4a). We observed a high degree of variability in outbreak sizes in the variable rainfall scenario, with stochasticity in rainfall conditions leading to few or no cases during drought compared to hundreds of cases under wetter conditions (figure 3.4, 3.5a).

In addition to their impact on outbreak size, we observed that simulated rainfall conditions strongly impacted outbreak seasonality (figure 3.4b), even to the extent of eliminating seasonality in anthrax cases. Under the Etosha base scenario, the majority of cases occurred from January to April (wet season), and a drop in cases was observed during the remainder of the year (figure 3.3, 3.5b). Under wetter conditions (i.e., wet season conditions year-round), anthrax cases were

consistently high across all months (figure 3.5b). Likewise, dry condition simulations (i.e., dry season conditions year-round) consistently produced few anthrax cases throughout simulation months (figure 3.5b). Under variable conditions, anthrax cases were higher across all months, potentially driven by the wetter-than-average years (figure 3.5b).

When examining the scenarios with multiple parameters differing from the Etosha base model, we observed that almost every scenario with small host range sizes produced fewer than 10 yearly infections (Figure 3.6). When host ranges were small, the number of cases recorded was similar to the base Etosha model only when host density was high, with an Etosha-like pathogen decay rate and wetter conditions. If the pathogen decay rate was slower, this scenario led to double the number of cases than the base Etosha model. When fast pathogen decay was modeled, a high host density was necessary to reproduce Etosha anthrax infection numbers. For scenarios with higher population density, the number of cases recorded was always higher than the corresponding scenarios with lower host densities (figure 3.6).

For every scenario, wetter conditions consistently led to more yearly infections (figure 3.6), and under small range sizes or fast pathogen decay parameters, scenarios showed the highest number of cases recorded within a year. However, the scenarios with an Etosha-based range size, and an Etosha-based or slower pathogen decay rate led to more cases recorded within a year under the variable rainfall conditions (figure 3.6b). Over all simulations, wetter conditions led to an initial explosion of cases, causing a large decrease in the grazer1 population (figure 3.5b) which subsequently limited the number of cases observed (i.e., compare years 4 and 5 for the ‘wetter’ scenario in figure 3.5a, figure C2). These large outbreaks happened earlier under high density scenario compared to the lower density scenarios.

From our variable importance analysis (figure C3), the size of the host ranges was the most important parameter in determining the median yearly outbreak sizes, with a lower range size leading to fewer overall encounters (figure C4) and thus fewer cases. The second most important parameter was the density of hosts, followed by the rainfall conditions. Higher density, wetter conditions and variable rainfall led to more simulated cases each year, as compared to low host density, Etosha base density and rainfall patterns, or drought conditions.

3.5 Discussion

We used an ABM to investigate key drivers of anthrax outbreak dynamics in Etosha National Park, Namibia. Our model reproduced anthrax outbreak dynamics consistent with observations from Etosha. In particular, the model correctly reproduced seasonal outbreaks in the wet season, with cases predominantly among plains zebra (i.e., grazer1 of our simulation). However, we could not correctly reproduce outbreak dynamics among the selective grazers and the two mix-feeders. The model's inability to capture the anthrax dynamic for other species than zebras may be due to the rarity of outbreaks for those species, making it difficult for the model to reproduce. Especially, most of the elephant cases recorded in Etosha occurred during outbreaks in the 1980s following droughts, after which few to no elephant cases were recorded per year (Huang et al., 2022). During the 10-year sample used to initialize the reservoir layer, only 32 elephant cases were recorded (EEI's mortality data). Ensuring that our Etosha model reproduced the dynamics observed among zebras, i.e., the primary host in this system, allowed us to compare the different simulation scenarios with the base Etosha model and make inferences about which parameters are the main drivers of the anthrax dynamics observed in Etosha. These results can then also inform which parameters may be key components to study further in other anthrax systems (e.g., as in model-guided fieldwork [Restif et al., 2012]).

Host range size was the most important parameter affecting the number of anthrax cases per simulation year, with very few cases under the small host range scenarios. To parameterize the different home range scenarios, we used information from Kruger National Park, South Africa as Kruger and Etosha contain similar anthrax host species but experience widely different outbreak dynamics. Our simulations showed that reducing range sizes can significantly reduce the number of encounters between a host and environmental reservoirs and thereby reduce the number of infections. The anthrax hosts in Etosha have much larger home ranges than the same species in Kruger, from 1.5 times larger for elephants, 1.6 times larger for kudus, 8.3 times for zebra, to 17.3 times for wildebeests (Huang et al., 2023). These differences in range size may explain the differences in anthrax outbreaks between the two parks. However, range size was not the sole predictor of anthrax infection, as elephants—which always had the largest ranges compared to other host species—were not the most frequently infected hosts in simulations. Elephants use a different habitat from the grazers, preferring woodlands (Harris et al., 2008; Loarie et al., 2009), and, by being a mixed-feeder, there is a trade-off between grazing and browsing which may lead to fewer BA encounters from grazing. Indeed, most anthrax cases occurred in the sweetgrass habitat of Etosha, while elephants spent more time in other habitats, such as the mopane woodland and sandveld. Increasing range size, and with it an increased number of possible encounters between hosts and reservoirs, is an important parameter to consider for anthrax outbreak prediction and understanding. Studying host range sizes in wildlife populations in other ecosystems afflicted by anthrax may help in estimating anthrax risk and understanding the variations in disease dynamics.

Host density is often a major component of disease dynamics, especially for directly transmitted pathogens, with higher density leading to more infections (Tarwater and Martin, 2001). Especially

for anthrax in Kruger, epidemic outbreaks are assumed to be density-dependent (De Vos and Bryden, 1996). Our simulation was in agreement with this, where higher densities of hosts led to the greatest number of infections observed within a year, and, in contrast, the lower density of hosts led to the lowest number of yearly infections. Notably, under the wetter simulation scenario, the number of anthrax cases per year increased over time until a large outbreak occurred, followed by large population declines which subsequently diminished annual cases of anthrax. In this case, host density contributed to the creation of epidemic-like outbreaks, as, after a large outbreak, host density was too low to maintain high ongoing transmission. While an increase in host density does not modify the rate at which hosts interact with the environment (e.g., the rate of foraging does not change), the increased number of hosts increases the cumulative probability that a host-pathogen encounter will occur in a given time step. This increases the number of hosts infected each time step, which consequently increases the number of environmental reservoirs. This positive feedback loop can then lead to large outbreaks where most of the hosts encounter reservoirs and become infected. Our model only simulated outbreaks over a five-year period which limits our ability to reproduce periodic, epidemic-like outbreaks. We suspect that with longer simulation periods, we may see periodic epidemics emerge as populations undergo large variations in population density as a response to anthrax deaths and eventual recovery (e.g., as observed in Kruger). Ultimately, density-dependence and the emergence of periodic epidemics likely depends on the balance between host density and movement (which govern exposure to infectious sites) and pathogen environmental decay (pathogen must survive long enough for host population to recover).

Our simulations also highlighted the importance of rainfall conditions in shaping anthrax dynamics in a savanna ecosystem. The simulated rainfall conditions impacted the movement and local density of hosts, notably by eliminating migration of hosts in the park. When using our model to

simulate wetter conditions, (i.e., when hosts could stay within the sweetgrass habitat for longer), normal seasonal patterns were reversed, with more cases during the dry than the wet season. This increased number of cases during the dry season was likely a result of the dry season being twice as long as the wet season, and the ability of hosts to stay in the preferred wet season habitat (where much of the environmental BA risk was concentrated) all year long. Empirically, the 2010 anthrax outbreak—which was the biggest outbreak in Etosha since the 1960s—killed at least 177 individuals (confirmed cases only) and was associated with higher-than-average rainfall. The rainfall led to better foraging conditions in the sweetgrass area earlier in the season and lasted for longer than usual, allowing the outbreak to start in February and to last until June (Huang et al., 2021). Together, our simulation results and these empirical observations indicate that wetter conditions can lead to more anthrax cases and can shift the seasonality of anthrax outbreaks by modifying hosts' movements on a landscape with heterogeneous exposure risk.

In contrast to wetter conditions, we observed far fewer anthrax cases in simulated drought conditions. In our simulations, the migration between preferred wet and dry season forage habitats was not present under droughts, and hosts tended to stay in the less preferred mopane woodlands in the southeast of Etosha which has lower risk of BA exposure. This agrees with prior empirical research on host movement ecology and anthrax case counts during severe drought. Indeed, Huang et al., (2021) showed that during a severe drought, zebras avoided the sweetgrass areas during the typical "wet season" months as there was insufficient rainfall for grass production, and zebras instead moved deeper into less preferred habitats, matching simulation results. As in our simulations, anthrax pressure in mopane woodlands is lower, leading to very few observed anthrax cases. Rainfall conditions, by altering hosts' movement, are therefore an important parameter for understanding anthrax outbreak dynamics. Studying the effect of abiotic conditions on host

movements—and their heterogeneity—is thus essential to capture host-pathogen encounter rates and predict their response to environmental change.

The simulated decay rate of anthrax in the environment, while less responsible for outbreak size than other parameters, may have a significant impact on the maintenance of the disease in a system. The lack of significance of this parameter in our outcomes likely resulted from the short duration of our simulations. For example, we did not observe any pathogen extinction as average BA reservoir survival was longer than the duration of simulations (reservoir survival was about seven years in the fast decay scenario). However, we did observe a reduction in cases and subsequent environmental reservoirs in the Etosha base scenario when shifting to a faster pathogen decay. We therefore expect that increased pathogen decay rates would ultimately result in increased pathogen extinction events over longer simulation periods. While the survival of BA in Etosha is similar over the entire park, soil properties and genetic diversity of BA are important properties for predicting the survival of BA at larger spatial scales. Multiple niche models have been developed for anthrax (e.g., Blackburn et al., 2017; Deka et al., 2022; Walsh et al., 2018), and they consider soil characteristics and other abiotic conditions as indicators of the suitability of an ecosystem for anthrax. However, these models typically do not include the role of soil, abiotic factors, or pathogen genetic diversity in shaping BA maintenance (but see Mwakapeje et al., 2019). Our model suggests that these factors—and the differences in pathogen decay rates they produce—may be limiting the ability of BA to persist due to variable outbreak dynamics in an ecosystem. More research is needed on the heterogeneity in the survival of anthrax in different environmental conditions, from different soil properties to different abiotic conditions and for the different clades of BA genetic diversity. This information may be crucial to understand the differences in anthrax dynamics across diverse ecosystems.

Climate change is predicted to have significant impacts on Etosha in the coming decades, by reducing rainfall and increasing temperatures (Engelbrecht et al., 2015; Turner et al., 2022). We assumed that drought only affected the movement decisions of hosts and the initial quantity of pathogen released at death. However, droughts can have major impacts on population health. For example, persistent droughts can increase natural death rates as individuals die of hunger or thirst, and consequently reduce host density (Walker et al., 1987). As evidenced by our simulations, these effects could further alter or even reduce anthrax persistence in the system. Alternatively, host susceptibility to pathogens may be enhanced during droughts (Filipe et al., 2020), which could also increase susceptibility to anthrax. However, in Etosha, co-infections with gastrointestinal helminths, which are of higher prevalence and infection intensity during the wet season, were linked to a heightened susceptibility to BA (Cizauskas et al., 2014b). Drought conditions—especially increased surface temperature, reduced rainfall and increased evaporative water loss from soils—may also impact BA directly by altering sporulation and survival rates (Hugh-Jones and Blackburn, 2009). In a long-term study of BA survival at environmental reservoirs in Etosha, the 2019 drought is suspected to have shortened the lifespan of spore reservoirs due to lack of vegetation and extreme exposure to ultraviolet radiation (Barandongo et al., 2023). The effects of temperature and rainfall are similarly apparent in the observed seasonality of anthrax reservoir formation: in Etosha, infected hosts dying during the dry season led to lower concentrations of BA spores at the site of death and had a very low risk of infecting new hosts (Barandongo et al., 2023; Dolfi et al., 2024). Future work incorporating natural host death and interactions between environmental conditions, host susceptibility, and anthrax decay rates could lead to a better understanding of anthrax dynamics under drought conditions, which are expected to occur more regularly in Etosha and many other anthrax systems in the future.

We incorporated seasonal variability in host movements and contact with infectious sites, but additional layers of complexity could be included in future research. For example, the host species that dies of anthrax can affect the infectiousness of the resulting carcass site (Bengis, 2010; Joel, 2021). While we used a fixed parameter for initial infectiousness of anthrax reservoirs, this could be modified in the future to specifically investigate the effect of heterogeneity in initial infectiousness on broader outbreak dynamics. Similarly, we only modeled the grazing transmission pathway in Etosha, as this is the primary route for anthrax transmission in Etosha. However, this route can be of lesser importance in other systems. For example, anthrax transmission due to blowflies appears to be much more important in ecosystems where browsers are the primary hosts, such as in Kruger (Basson et al., 2018; Braack and De Vos, 1990), Malilangwe, Zimbabwe (Clegg et al., 2007), and in Texas, United States (Blackburn et al., 2014). This difference could even contribute to the occurrence of epidemic anthrax outbreaks in these sites, as compared to the endemicity observed in Etosha. After feeding on infectious body fluids, blowflies can deposit between 5-60 droplets on one leaf and each droplet may contain about 500 spores (Braack and De Vos, 1990). This means one leaf could contain about 10^5 spores (Jiranantasak et al., 2022). Among grazers, the lethal dose of anthrax is around 10^7 to 10^8 spores ingested (Dolfi et al., 2024; Turner et al., 2016; WHO, 2008). As such, a browser consuming only a few leaves may ingest enough spores to be lethally infected. This last point emphasizes that the blowfly pathway may increase pathogen exposure of browsers and lead to epidemic-type systems: blowflies can increase the spatial extent of transmission risk to most of the surrounding vegetation, rather than remaining within a small, localized grazing site (Dolfi et al., 2024; Turner et al., 2014), thereby exposing more susceptible individuals (Clegg et al., 2007). Testing how the blowfly pathway alters disease dynamics may be an important future direction to determine how different transmission pathways

(e.g., grazing versus browsing) interact with herbivore community composition to shape anthrax dynamics and endemicity.

One key simplification in our model was the 7-day time step. This decision was made to reduce the computational intensity of the ABM, however, this choice can impact host-pathogen encounter rates (Dougherty et al., 2018). Indeed, by having a weekly time step, our model could not reproduce the daily cycle of movements observed among herbivores in a savanna ecosystem. For example, our movement model did not include directed movements between different habitats, movements linked to drinking events (which usually occur every 1-3 days, [Gaylard et al., 2003]), foraging movements, or resting events. To account for these daily movements, we used a buffer to approximate a herd's occurrence distribution. We also assumed that the movement within the occurrence distribution was random. This assumption could misrepresent host-pathogen encounter rates if hosts are attracted to or actively avoid anthrax reservoir sites. For example, water sources could act as attractants—and consequently generate anthrax "hotspots"—especially under drought conditions. Future climate risk analysis could, therefore, include water dependence and host aggregation at water sources to understand how these factors may affect anthrax dynamics. More generally, including more complex movement with a higher temporal resolution (e.g., using GPS collar data) could be a useful improvement of our model, though such modifications would significantly increase the already high running time of the model.

Our objective was to determine the drivers of anthrax outbreaks in Etosha, and to understand under which conditions we could alter the patterns observed. We found that host range size, host density, and rainfall conditions were critical for shaping outbreak size and seasonality. Rainfall conditions were especially important due to their interactions with host movements. Alteration of the migration pattern observed in Etosha led to widely different outbreaks, from a significant increase

of cases under wetter conditions to a large drop in cases under droughts, patterns driven by an increase or decrease, respectively, of local host density in the sweetgrass habitat. Host range size was also a major contributor to the disease dynamics, as lower range size significantly reduced the number of reservoirs a host may encounter, which ultimately reduced the number of cases observed. These findings have important implications for understanding differences in outbreak dynamics in different ecosystems. The ABM developed in this study may be adaptable to other ecosystems and could allow comparison of systems with different anthrax dynamics. Taken together, the results of this study highlight the need to further explore the interactions between host movement and environmental conditions, and how these dynamics shape transmission of anthrax, with extension to other ETPs.

3.6 Acknowledgments

We thank N. Owen-Smith for his input in the parameterization of the model. We greatly appreciate the scientific staff and managers at the Etosha Ecological Institute for logistical support and assistance in obtaining all the datasets used to parameterize this model, particularly to W. Kilian, C. Cloete, and G. Shatumbu. We thank all of those who assisted with data collection, in particular H. Joel. We acknowledge the Center for High Throughput Computing at the University of Wisconsin-Madison for providing resources that contributed to the research results reported in this paper (https://chtc.cs.wisc.edu/). This work was funded by the U.S. National Science Foundation grant DEB-1816161/DEB2106221 and the Department of Agriculture, National Institute of Food and Agriculture grant 2022-05138, both through the NSF-NIH-USDA Ecology and Evolution of Infectious Diseases program. Any use of trade, firm, or product names is for descriptive purposes only and does not imply endorsement by the US Government.

3.7 Tables

Table 3-1: Anthrax agent-based model parameters, scenario variations, and rationale for the scenarios. The numbers in bold represent the parameterization most representative of the observed Etosha National Park, Namibia system.

Variable	Values	Hypothesis
Pathogen decay rate (μ)	0.005; **0.1**; 0.2	Soil properties and genetic group of *Bacillus anthracis* can impact the survival of the pathogen, and so the transmissibility over time (Govender, 2022; Smith et al., 2000)
Overall initial host density	349; **698;** 1396	Epidemic anthrax outbreaks are assumed to be linked to higher density of host populations (Furniss and Hahn, 1981)
Host movement range (in km): Daily movement η Wet - Dry season (buffer σ)	Grazer 1: 5**0 - 30 (16.5)** 9 - 18 (7) Grazer 2: 1**8 - 19 (9.5)** 3 - 7.5 (3) Mixed-feeder1: **24 - 18 (7.5)** 3 - 4.5 (2.25) Mixed-feeder2: **70 - 50 (16)** 48 - 23.5 (12)	Host home range can affect the number of encounters with reservoirs, affecting the disease dynamics. In Etosha, home ranges are larger than over systems, which may explain differences in anthrax dynamics (Huang et al., 2023)
Rainfall conditions	**Regular: Observed rainfall and migration**	Grazers migrate along the pan during the dry season due to forage depletion in the

	Wetter period: no migration and wet season parameters Drought: no migration and dry season parameters Variable: Drought (Risk of 40%); Regular (35%); Wetter (25%)	wet season habitat (Zidon et al., 2017). During drought, grazers stay in the 'dry' season area which reduces the risk of anthrax (Huang et al., 2021)

3.8 Figures

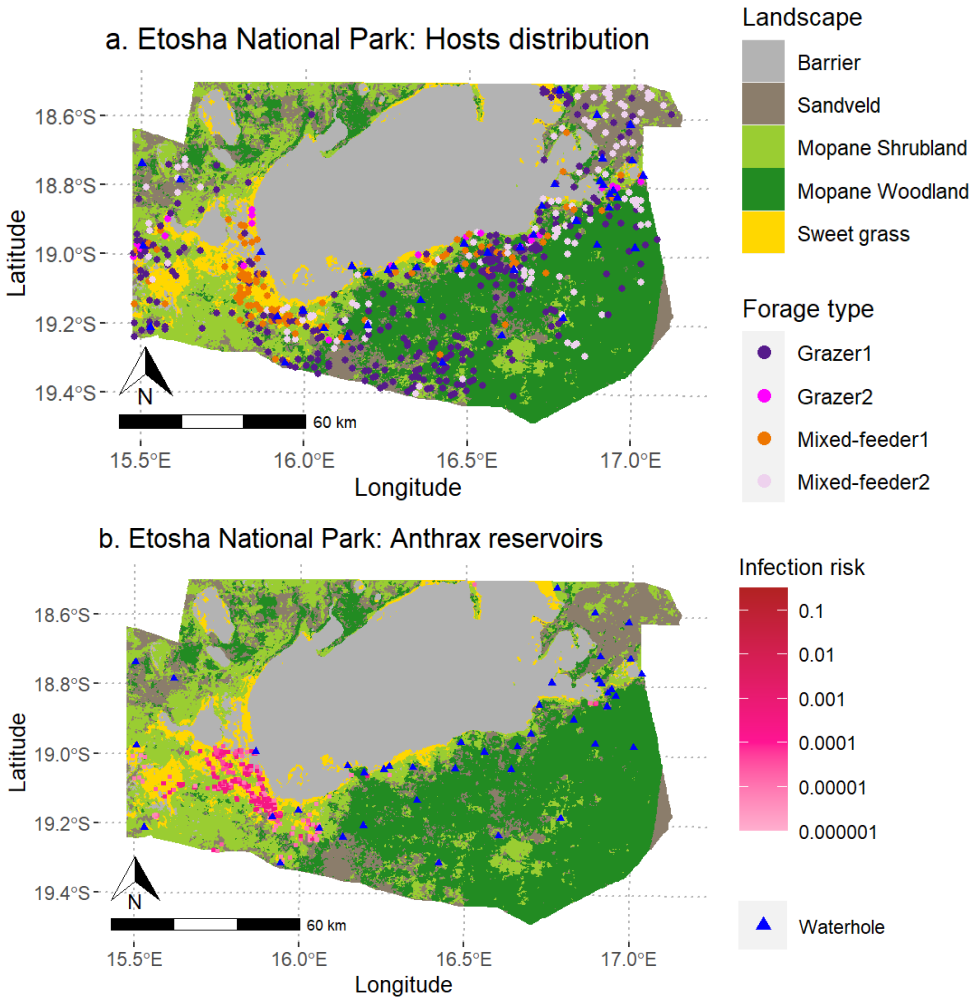

FIGURE 3.1: Initialization maps of Etosha National Park, Namibia; gridded at a 250m^2 resolution. The landscape features of the park are split into five habitats: barrier, sandveld, mopane shrubland, mopane woodland and sweetgrass. The barrier represents the salt pans, which herbivores seldom use. Blue triangles represent waterholes. In (a), host initial spatial distribution was obtained using aerial survey data from 2015. Each point represents a herd, and the color represents the four foraging types used in the model: grazer1 (non-selective, e.g. plains zebra (*Equus quagga*)), grazer2 (selective, e.g. blue wildebeest (*Connochaetes taurinus*)), mixed-feeder1 (small bodied, e.g. springboks (*Antidorcas marsupialis*)), and mixed-feeder2 (large bodied, i.e., African elephant (*Loxodonta africana*)). In (b), anthrax initial spatial distribution was obtained from mortality data

(2000-2010), and the infection risk depends on the age of the reservoir, and the simulated decay rate.

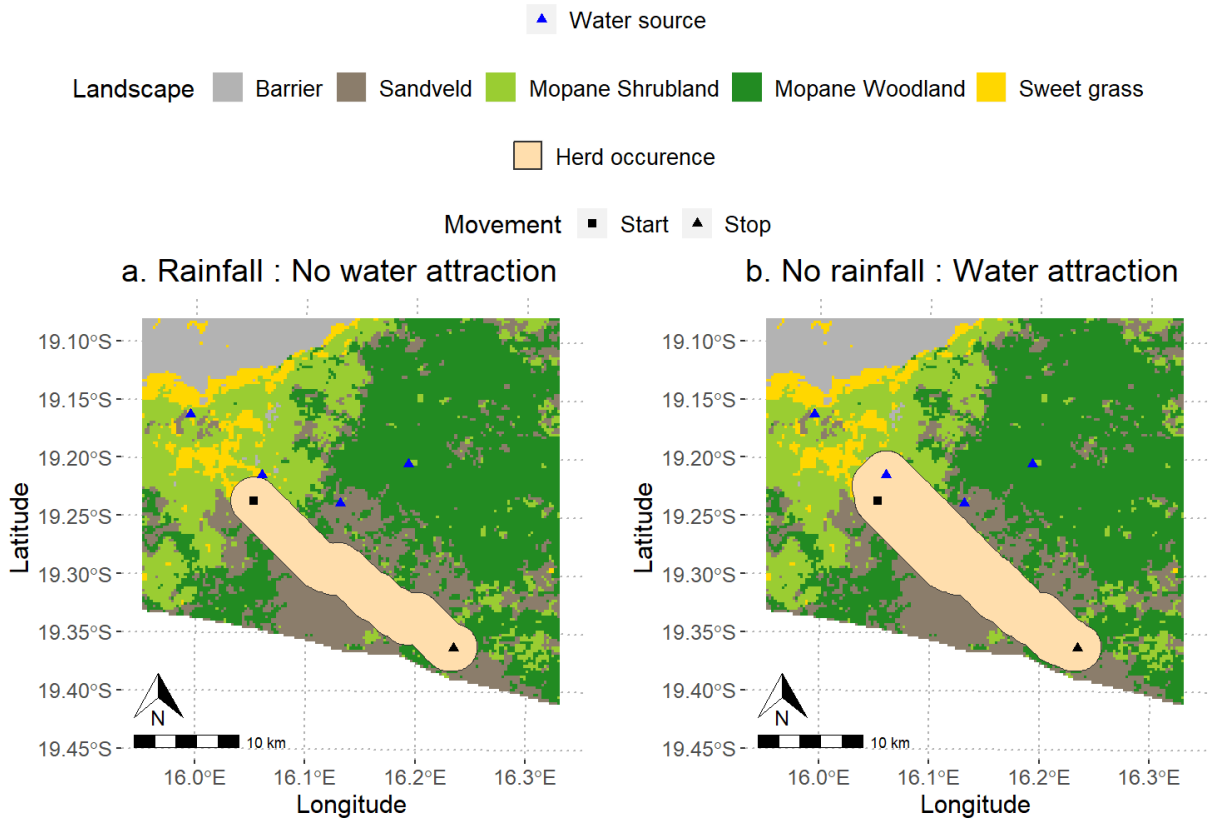

FIGURE 3.2: An example of the movement of one host herd depending on rainfall occurring during a weekly time step. In (a), rainfall occurred, so no attraction toward the nearest waterhole was necessary due to local ephemeral surface water. In (b), no rainfall occurred, rendering it necessary to include the closest water source along the movement path. The beige polygon represents the entire environment where individuals from the herd could be found during this time step. In this example, the buffer around the path is 2km. The paths do not appear as a straight line due to the gridding of the environment.

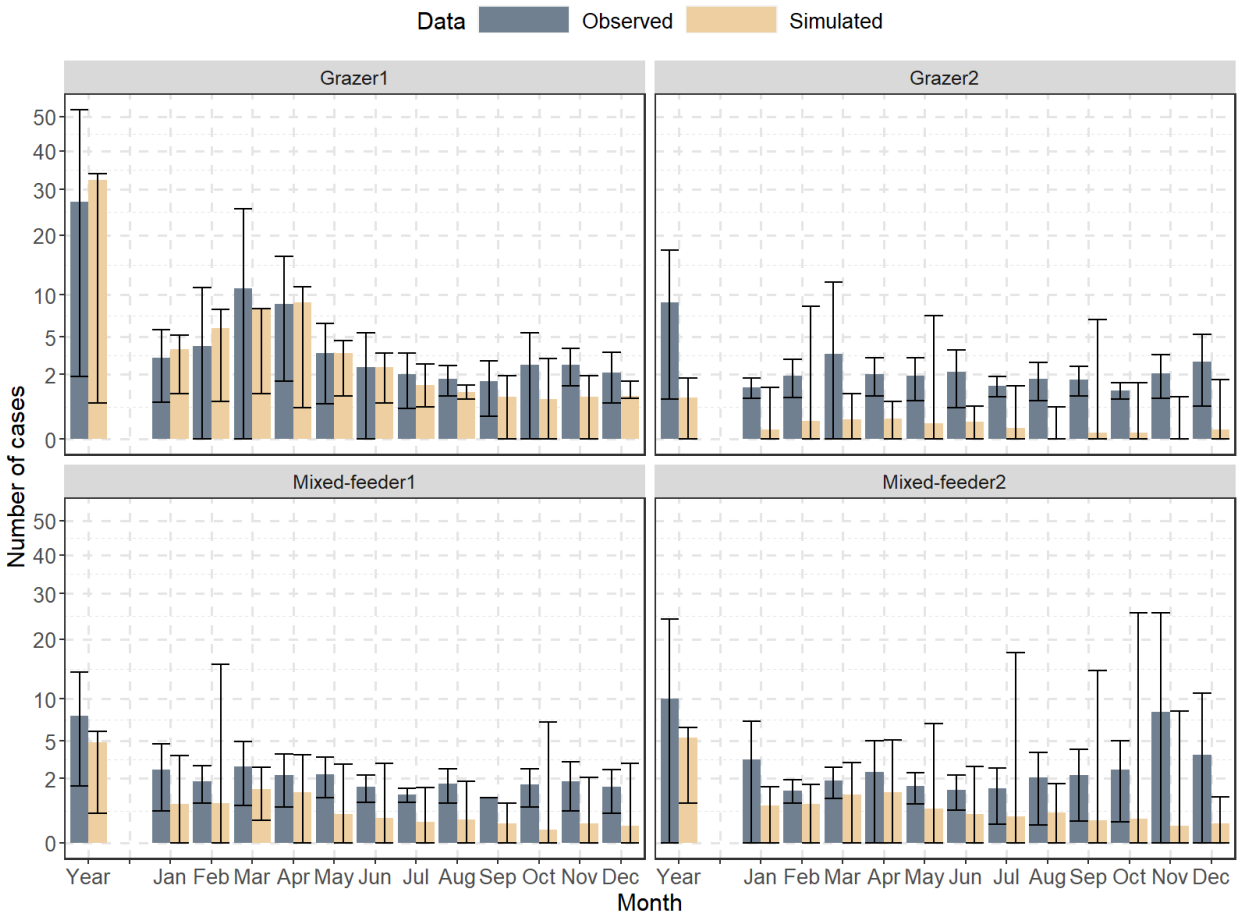

FIGURE 3.3: Average number of anthrax cases recorded in Etosha National Park, Namibia (mortality data from Etosha Ecological Institute from 1973-2020) and cases recorded in a five-year simulation of an agent-based model for Etosha. Each panel represents the host foraging type: grazer1 represents non-selective grazer1 (e.g., plains zebras (*Equus quagga*)); grazer2 are selective grazers (e.g. blue wildebeest (*Connochaetes* taurinus)); mixed-feeder1 are small-bodied mixed feeder (e.g. springbok, (*Antidorcas marsupialis*)) and mixed-feeder2 are large-bodied mixed feeder (e.g. African elephant (*Loxodonta africana*)). The leftmost bar represents the average number of cases per year; the others represent the average number per month. The y-axis is square root transformed to facilitate visualization. Error bars represent the standard deviations.

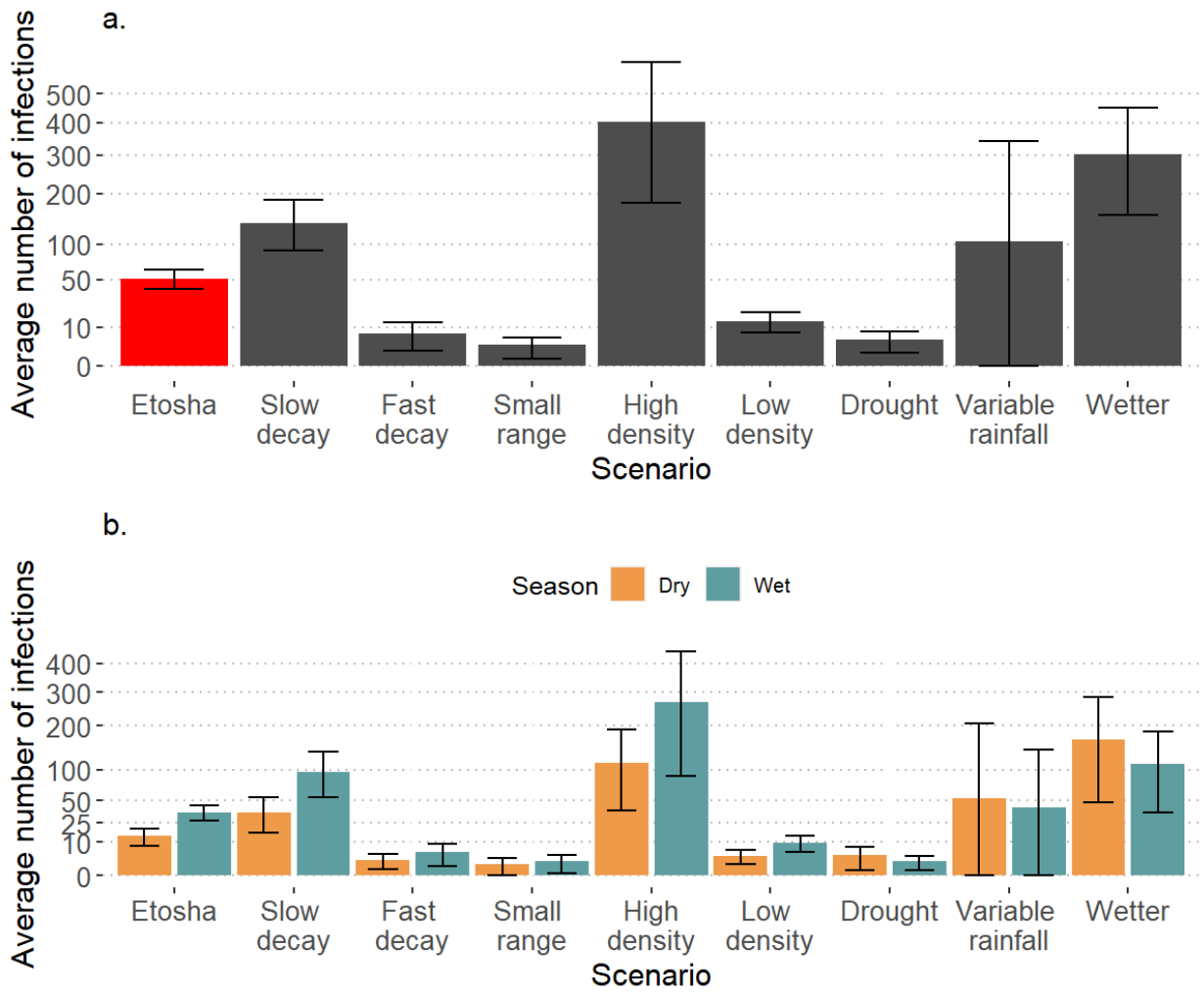

FIGURE 3.4: Average numbers of simulated anthrax cases in an agent-based model for Etosha National Park, Namibia. a. Yearly average number of cases by simulated scenario; and b. Seasonal average number of cases recorded over five-year simulations, based on the simulated scenario. The Etosha scenario (leftmost) in both panels represents the 'base' scenario that we compare to all others. In all other scenarios, only one parameter was modified from the Etosha scenario. Error bars represent the standard deviations.

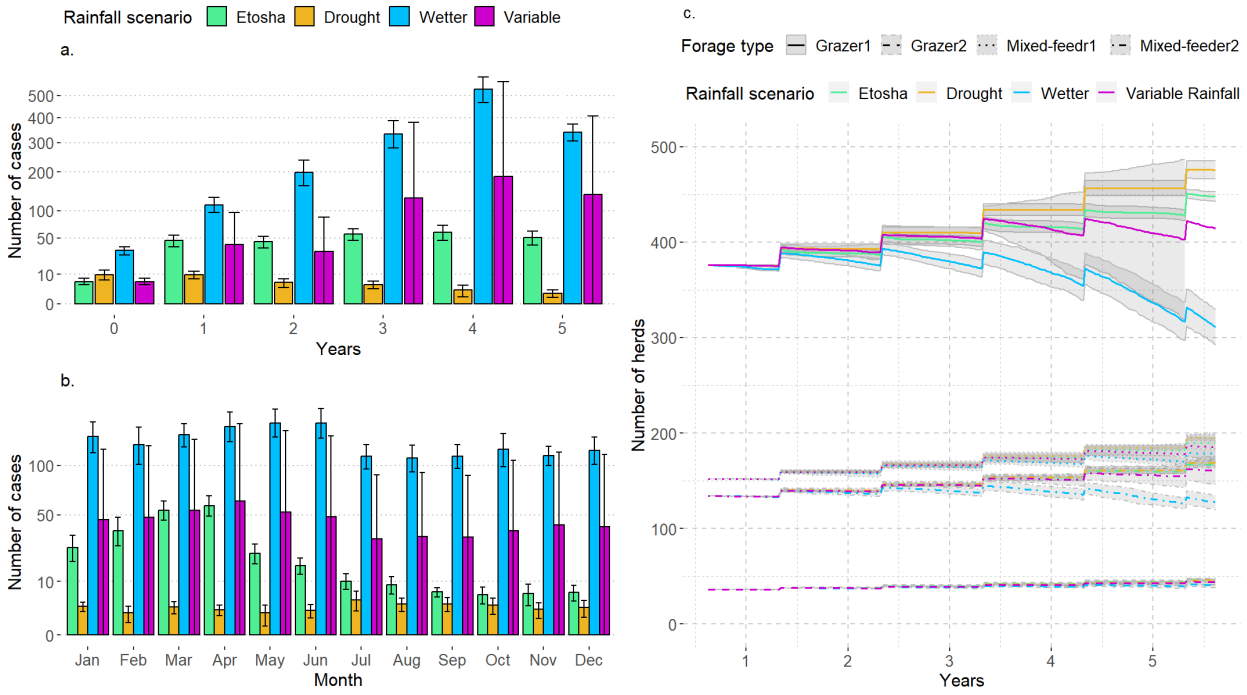

FIGURE 3.5: Anthrax case numbers and host population sizes from an agent-based model for anthrax transmission in Etosha National Park, Namibia, over a five-year simulation. Results are shown for four scenarios, which vary only in the simulated rainfall conditions: Etosha base scenario ('Etosha', green; simulations representative of observed conditions); wetter conditions (blue); drought conditions (yellow); and variable conditions (purple)). In (a) we show the yearly median number of cases over the simulation period; in (b) we show the monthly median number of cases; and in (c) we show population sizes of the four foraging types of our host agents over time. Grazer1 represents non-selective grazer1 (e.g., plains zebras (*Equus quagga*)); grazer2 are selective grazers (e.g. blue wildebeest (*Connochaetes taurinus*)); mixed-feeder1 are small-bodied mixed feeder (e.g. springbok, (*Antidorcas marsupialis*)) and mixed-feeder2 are large-bodied mixed feeder (e.g. African elephant (*Loxodonta africana*)). Note that cases in (a) and (b) represent individuals, but population sizes in (c) represent counts of herds. Error bars in (a) and (b) and the grey ribbon in (c) represent the standard deviations. The y-axis in (a) was square transformed to facilitate the visualization of smaller numbers.

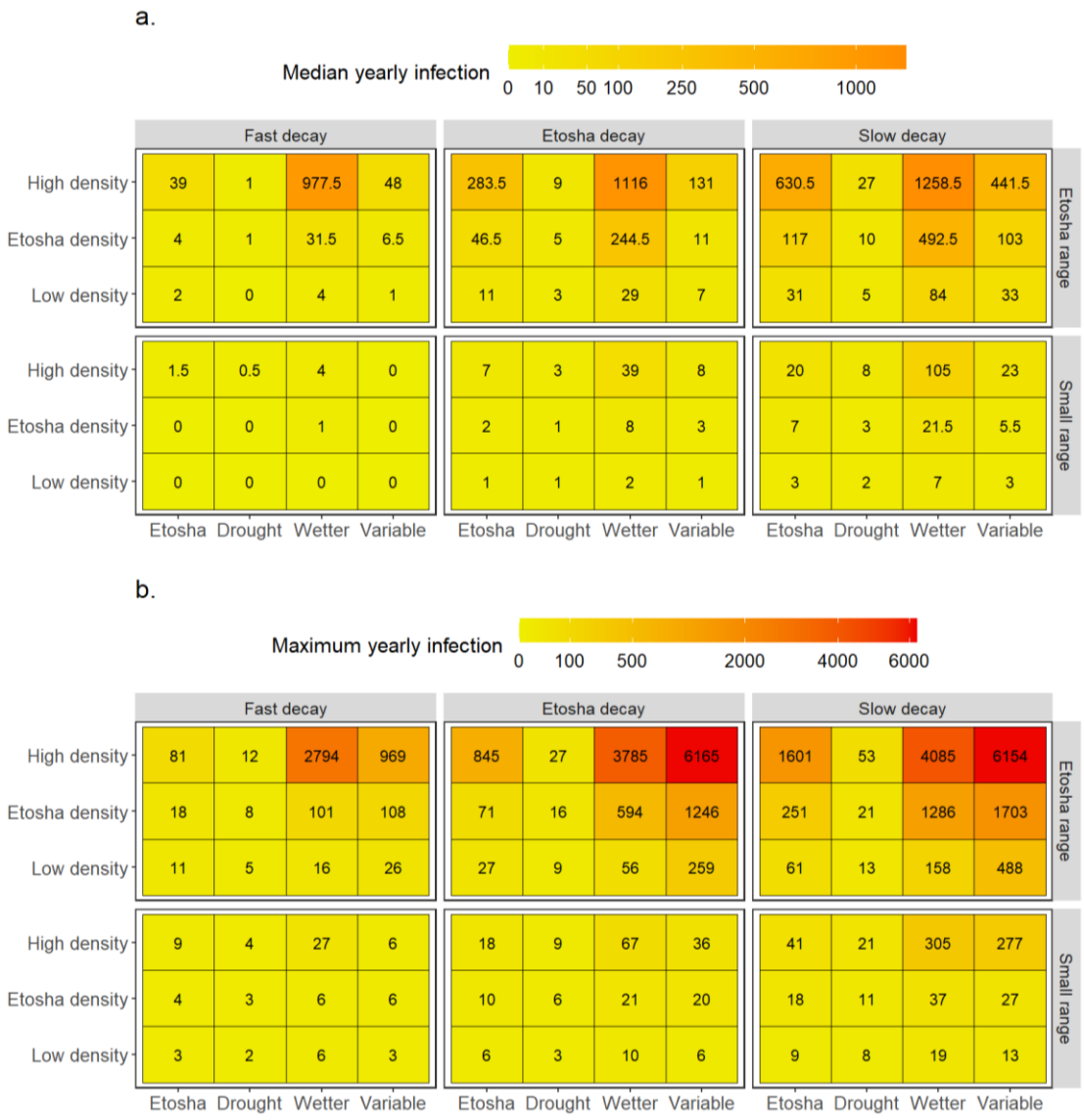

FIGURE 3.6: Simulated anthrax cases across the range of parameter space used in an agent-based model for anthrax transmission in Etosha National Park, Namibia. Heatmaps show (a) the median number of yearly infections and (b) the maximum number of infections recorded for each of the scenarios, over five-year simulations. The x-axis represents the rainfall conditions parameter, the y-axis represents the host density parameter ("hosts" were herds of susceptible herbivores). The panel rows are divided by the home range sizes of the hosts, and the columns by the decay rate of the pathogen in the environment. The 'Etosha' parameters are representative of observed conditions in Etosha. The redder the tiles, the higher the number of cases recorded.

3.9 References

Allen, C.R.B., Brent, L.J.N., Motsentwa, T., Weiss, M.N., Croft, D.P., 2020. Importance of old bulls: leaders and followers in collective movements of all-male groups in African savannah elephants (*Loxodonta africana*). Sci. Rep. 10, 13996. https://doi.org/10.1038/s41598-020-70682-y

Arab, A., 2015. Spatial and Spatio-Temporal Models for Modeling Epidemiological Data with Excess Zeros. Int. J. Environ. Res. Public. Health 12, 10536–10548. https://doi.org/10.3390/ijerph120910536

Barandongo, Z.R., Dolfi, A.C., Bruce, S.A., Rysava, K., Huang, Y.-H., Joel, H., Hassim, A., Kamath, P.L., van Heerden, H., Turner, W.C., 2023. The persistence of time: the lifespan of *Bacillus anthracis* spores in environmental reservoirs. Res. Microbiol. 104029. https://doi.org/10.1016/j.resmic.2023.104029

Basson, L., Hassim, A., Dekker, A., Gilbert, A., Beyer, W., Rossouw, J., Van, H.H., 2018. Blowflies as vectors of *Bacillus anthracis* in the Kruger National Park. Koedoe Afr. Prot. Area Conserv. Sci. 60, 1–6. https://doi.org/10.4102/koedoe.v60i1.1468

Bayir, T., 2023. Seasonal variation and spatial-temporal pattern analysis of anthrax among livestock in Türkiye, 2005-2019. Pak. Vet. J. https://doi.org/10.29261/pakvetj/2023.059

Bengis, R., 2010. Anthrax everywhere. NAVC Conference

Beyer, W., Turnbull, P.C.B., 2009. Anthrax in animals. Mol. Aspects Med., Anthrax 30, 481–489. https://doi.org/10.1016/j.mam.2009.08.004

Blackburn, J.K., Ganz, H.H., Ponciano, J.M., Turner, W.C., Ryan, S.J., Kamath, P., Cizauskas, C., Kausrud, K., Holt, R.D., Stenseth, N.C., Getz, W.M., 2019. Modeling R0 for pathogens with environmental transmission: animal movements, pathogen populations,

and local infectious zones. Int. J. Environ. Res. Public. Health 16, 954. https://doi.org/10.3390/ijerph16060954

Blackburn, J.K., Matakarimov, S., Kozhokeeva, S., Tagaeva, Z., Bell, L.K., Kracalik, I.T., Zhunushov, A., 2017. Modeling the ecological niche of *Bacillus anthracis* to map anthrax risk in Kyrgyzstan. Am. J. Trop. Med. Hyg. 96, 550–556. https://doi.org/10.4269/ajtmh.16-0758

Blackburn, J.K., Van Ert, M., Mullins, J.C., Hadfield, T.L., Hugh-Jones, M.E., 2014. The necrophagous fly anthrax transmission pathway: Empirical and genetic evidence from wildlife epizootics. Vector-Borne Zoonotic Dis. 14, 576–583. https://doi.org/10.1089/vbz.2013.1538

Braack, L.E., De Vos, V., 1990. Feeding habits and flight range of blow-flies (*Chrysomyia* spp.) in relation to anthrax transmission in the Kruger National Park, South Africa. Onderstepoort J. Vet. Res. 57, 141–142.

Bracis, C., Mueller, T., 2017. Memory, not just perception, plays an important role in terrestrial mammalian migration. Proc. R. Soc. B Biol. Sci. 284, 20170449. https://doi.org/10.1098/rspb.2017.0449

Carlson, C.J., Kracalik, I.T., Ross, N., Alexander, K.A., Hugh-Jones, M.E., Fegan, M., Elkin, B.T., Epp, T., Shury, T.K., Zhang, W., Bagirova, M., Getz, W.M., Blackburn, J.K., 2019. The global distribution of *Bacillus anthracis* and associated anthrax risk to humans, livestock and wildlife. Nat. Microbiol. 4, 1337–1343. https://doi.org/10.1038/s41564-019-0435-4

Cizauskas, C.A., Bellan, S.E., Turner, W.C., Vance, R.E., Getz, W.M., 2014a. Frequent and seasonally variable sublethal anthrax infections are accompanied by short-lived immunity

in an endemic system. J. Anim. Ecol. 83, 1078–1090. https://doi.org/10.1111/1365-2656.12207

Cizauskas, C.A., Turner, W.C., Wagner, B., Küstersrs, M., Vance, R.E., Getz, W.M., 2014b. Gastrointestinal helminths may affect host susceptibility to anthrax through seasonal immune trade-offs. BMC Ecol. 14, 27. https://doi.org/10.1186/s12898-014-0027-3

Clegg, S.B., Turnbull, P.C.B., Foggin, C.M., Lindeque, P.M., 2007. Massive outbreak of anthrax in wildlife in the Malilangwe Wildlife Reserve, Zimbabwe. Vet. Rec. 160, 113–118. https://doi.org/10.1136/vr.160.4.113

Craft, M.E., 2015. Infectious disease transmission and contact networks in wildlife and livestock. Philos. Trans. R. Soc. B Biol. Sci. 370, 20140107. https://doi.org/10.1098/rstb.2014.0107

Cunningham Jr., P.L., Cunningham Sr., P.L., 2024. Seasonal changes in herd size and time budget of springbok (*Antidorcas marsupialis*) in southern Namibia. Afr. J. Ecol. 62, e13216. https://doi.org/10.1111/aje.13216

De Vos, V., Bryden, H., 1996. Anthrax in the Kruger National Park: temporal and spatial patterns of disease occurrence. Salisb. Med. Bull. 87, 26–30.

Deka, M.A., Vieira, A.R., Bower, W.A., 2022. Modelling the ecological niche of naturally occurring anthrax at global and circumpolar extents using an ensemble modelling framework. Transbound. Emerg. Dis. 69, e2563–e2577. https://doi.org/10.1111/tbed.14602

Dey, R., Hoffman, P.S., Glomski, I.J., 2012. Germination and amplification of anthrax spores by soil-dwelling amoebas. Appl. Environ. Microbiol. 78, 8075–8081. https://doi.org/10.1128/AEM.02034-12

Dolfi, A.C., Kausrud, K., Rysava, K., Champagne, C., Huang, Y.-H., Barandongo, Z.R., Turner, W.C., 2024. Season of death, pathogen persistence and wildlife behaviour alter number of anthrax secondary infections from environmental reservoirs. Proc. R. Soc. B Biol. Sci. 291, 20232568. https://doi.org/10.1098/rspb.2023.2568

Dougherty, E.R., Seidel, D.P., Carlson, C.J., Getz, W.M., 2018. Using movement data to estimate contact rates in a simulated environmentally-transmitted disease system. https://doi.org/10.1101/261198

Dragon, D.C., Rennie, R.P., 1995. The ecology of anthrax spores: tough but not invincible. Can. Vet. J. 36, 295–301.

du Plessis, W.P., 2001. Effective rainfall defined using measurements of grass growth in the Etosha National Park, Namibia. J. Arid Environ. 48, 397–417. https://doi.org/10.1006/jare.2000.0752

Durrheim, D.N., Freeman, P., Roth, I., Hornitzky, M., 2009. Epidemiologic questions from anthrax outbreak, Hunter Valley, Australia. Emerg. Infect. Dis. 15, 840–842. https://doi.org/10.3201/eid1505.081744

Easterday, W.R., Ponciano, J.M., Gomez, J.P., Van Ert, M.N., Hadfield, T., Bagamian, K., Blackburn, J.K., Stenseth, N.Chr., Turner, W.C., 2020. Coalescence modeling of intrainfection *Bacillus anthracis* populations allows estimation of infection parameters in wild populations. Proc. Natl. Acad. Sci. 117, 4273–4280. https://doi.org/10.1073/pnas.1920790117

Ebedes, H., 1976. Anthrax epizotics in Etosha National Park. Madoqua 10, 99–118.

Elliott, P., Wartenberg, D., 2004. Spatial epidemiology: Current approaches and future challenges. Environ. Health Perspect. 112, 998–1006. https://doi.org/10.1289/ehp.6735

Engelbrecht, F., Adegoke, J., Bopape, M.-J., Naidoo, M., Garland, R., Thatcher, M., McGregor, J., Katzfey, J., Werner, M., Ichoku, C., Gatebe, C., 2015. Projections of rapidly rising surface temperatures over Africa under low mitigation. Environ. Res. Lett. 10, 085004. https://doi.org/10.1088/1748-9326/10/8/085004

Ezhova, E., Orlov, D., Suhonen, E., Kaverin, D., Mahura, A., Gennadinik, V., Kukkonen, I., Drozdov, D., Lappalainen, H.K., Melnikov, V., Petäjä, T., Kerminen, V.-M., Zilitinkevich, S., Malkhazova, S.M., Christensen, T.R., Kulmala, M., 2021. Climatic factors influencing the anthrax outbreak of 2016 in Siberia, Russia. EcoHealth 18, 217–228. https://doi.org/10.1007/s10393-021-01549-5

Filipe, J.F., Herrera, V., Curone, G., Vigo, D., Riva, F., 2020. Floods, Hurricanes, and Other Catastrophes: A Challenge for the Immune System of Livestock and Other Animals. Front. Vet. Sci. 7. https://doi.org/10.3389/fvets.2020.00016

Fischhoff, I.R., Sundaresan, S.R., Cordingley, J., Larkin, H.M., Sellier, M.-J., Rubenstein, D.I., 2007. Social relationships and reproductive state influence leadership roles in movements of plains zebra, *Equus burchellii*. Anim. Behav. 73, 825–831. https://doi.org/10.1016/j.anbehav.2006.10.012

Friedman, A., Yakubu, A.-A., 2013. Anthrax epizootic and migration: Persistence or extinction. Math. Biosci. 241, 137–144. https://doi.org/10.1016/j.mbs.2012.10.004

Furniss, P.R., Hahn, B.D., 1981. A mathematical model of an anthrax epizootic in the Kruger National Park.

Gaylard, A., Owen-Smith, N., Redfern, J.V., 2003. Surface water availability: implications for heterogeneity and ecosystem processes, in: The Kruger Experience. JT Toit, KH Rogers, HC Biggs. Island Press, Washington, District of Columbia, USA., pp. 171–188.

Govender, K., 2022. Investigation of *Bacillus anthracis* spore survival in soils from Kruger National Park in South Africa and Etosha National Park in Namibia.

Grimm, V., Railsback, S.F., Vincenot, C.E., Berger, U., Gallagher, C., DeAngelis, D.L., Edmonds, B., Ge, J., Giske, J., Groeneveld, J., Johnston, A.S.A., Milles, A., Nabe-Nielsen, J., Polhill, J.G., Radchuk, V., Rohwäder, M.-S., Stillman, R.A., Thiele, J.C., Ayllón, D., 2020. The ODD protocol for describing agent-based and other simulation models: A second update to improve clarity, replication, and structural realism. J. Artif. Soc. Soc. Simul. 23, 7. https://doi.org/10.18564/jasss.4259

Harris, G.M., Russell, G.J., Aarde, R.I. van, Pimm, S.L., 2008. Rules of habitat use by elephants *Loxodonta africana* in southern Africa: insights for regional management. Oryx 42, 66–75. https://doi.org/10.1017/S0030605308000483

Hassan, J., Ahsan, M., Rahman, M., Chowdhury, S., Parvej, M., Nazir, K.N.H., 2015. Factors associated with repeated outbreak of anthrax in Bangladesh: Qualitative and quantitative study. J. Adv. Vet. Anim. Res. 2. https://doi.org/10.5455/javar.2015.b72

Havarua, Z., Turner, W.C., Mfune, J.K.E., 2014. Seasonal variation in foraging behaviour of plains zebra (*Equus quagga*) may alter contact with the anthrax bacterium (*Bacillus anthracis*). Can. J. Zool. 92, 331–337. https://doi.org/10.1139/cjz-2013-0186

Huang, Y., Kausrud, K., Hassim, A., Ochai, S.O., Van Schalkwyk, O.L., Dekker, E.H., Buyantuev, A., Cloete, C.C., Kilian, J.W., Mfune, J.K.E., Kamath, P.L., Van Heerden, H., Turner, W.C., 2022. Environmental drivers of biseasonal anthrax outbreak dynamics in two multihost savanna systems. Ecol. Monogr. 92, e1526. https://doi.org/10.1002/ecm.1526

Huang, Y.-H., Joel, H., Küsters, M., Barandongo, Z.R., Cloete, C.C., Hartmann, A., Kamath, P.L., Kilian, J.W., Mfune, J.K.E., Shatumbu, G., Zidon, R., Getz, W.M., Turner, W.C., 2021. Disease or drought: environmental fluctuations release zebra from a potential pathogen-triggered ecological trap. Proc. R. Soc. B Biol. Sci. 288, 20210582. https://doi.org/10.1098/rspb.2021.0582

Huang, Y.-H., Owen-Smith, N., Henley, M.D., Kilian, J.W., Kamath, P.L., Ochai, S.O., Van Heerden, H., Mfune, J.K.E., Getz, W.M., Turner, W.C., 2023. Variation in herbivore space use: comparing two savanna ecosystems with different anthrax outbreak patterns in southern Africa. Mov. Ecol. 11, 46. https://doi.org/10.1186/s40462-023-00385-2

Hugh-Jones, M., Blackburn, J., 2009. The ecology of *Bacillus anthracis*. Mol. Aspects Med., Anthrax 30, 356–367. https://doi.org/10.1016/j.mam.2009.08.003

Hugh-Jones, M.E., de Vos, V., 2002. Anthrax and wildlife. Rev. Sci. Tech. Int. Off. Epizoot. 21, 359–383. https://doi.org/10.20506/rst.21.2.1336

Jiranantasak, T., Benn, J.S., Metrailer, M.C., Sawyer, S.J., Burns, M.Q., Bluhm, A.P., Blackburn, J.K., Norris, M.H., 2022. Characterization of Bacillus anthracis replication and persistence on environmental substrates associated with wildlife anthrax outbreaks. PLOS ONE 17, e0274645. https://doi.org/10.1371/journal.pone.0274645

Joel, H., 2021. Effects of elephant carcasses on vegetation cover, herbivore behaviour, and potential anthrax transmission in central Etosha National Park. University of Namibia.

Keim, P., Kalif, A., Schupp, J., Hill, K., Travis, S.E., Richmond, K., Adair, D.M., Hugh-Jones, M., Kuske, C.R., Jackson, P., 1997. Molecular evolution and diversity in *Bacillus anthracis* as detected by amplified fragment length polymorphism markers. J. Bacteriol. 179, 818–824. https://doi.org/10.1128/jb.179.3.818-824.1997

Kilian, J.W., 2015. Aerial Survey of Etosha National Park: Internal Report to the Ministry of Environment and Tourism.

Lawson, A.B., 2013. Statistical methods in spatial epidemiology. John Wiley & Sons.

Le Roux, C.J.G., Grunow, J.O., Bredenkamp, G.J., Morris, J.W., Scheepers, J.C., 1988. A classification of the vegetation of the Etosha National Park. South Afr. J. Bot. 54, 1–10. https://doi.org/10.1016/S0254-6299(16)31355-2

Lee, P.C., Moss, C.J., Njiraini, N., Poole, J.H., Sayialel, K., Fishlock, V.L., 2022. Cohort consequences of drought and family disruption for male and female African elephants. Behav. Ecol. 33, 408–418. https://doi.org/10.1093/beheco/arab148

Lindeque, P.M., Turnbull, P.C.B., 1994. Ecology and epidemiology of anthrax in the Etosha National Park, Namibia.

Loarie, S.R., van Aarde, R.J., Pimm, S.L., 2009. Elephant seasonal vegetation preferences across dry and wet savannas. Biol. Conserv. 142, 3099–3107. https://doi.org/10.1016/j.biocon.2009.08.021

Manchee, R.J., Broster, M.G., Melling, J., Henstridge, R.M., Stagg, A.J., 1981. *Bacillus anthracis* on Gruinard Island. Nature 294, 254–255. https://doi.org/10.1038/294254a0

Mlengeya, T., Mbise, A.N., Kilewo, M., Mlengeya, M., Gereta, E., Moshy, W.E., Mtui, P.F., Kaare, M., Mlengeya, T., Mbise, A.N., Kilewo, M., Mlengeya, M., Gereta, E., Moshy, W.E., Mtui, P.F., Kaare, M., 1998. Anthrax epizootics in Tanzania's National Parks with special interest in a recent anthrax outbreak in Serengeti National Park. Bull. Anim. Health Prod. Afr. 46, 65–73.

Mongoh, M.N., Dyer, N.W., Stoltenow, C.L., Khaitsa, M.L., 2008. Risk Factors Associated with Anthrax Outbreak in Animals in North Dakota, 2005: A Retrospective Case-Control

Study. Public Health Reports® 123, 352–359. https://doi.org/10.1177/003335490812300315

Mullins, J.C., Van Ert, M., Hadfield, T., Nikolich, M.P., Hugh-Jones, M.E., Blackburn, J.K., 2015. Spatio-temporal patterns of an anthrax outbreak in white-tailed deer, *Odocoileus virginanus*, and associated genetic diversity of *Bacillus anthracis*. BMC Ecol. 15, 23. https://doi.org/10.1186/s12898-015-0054-8

Muturi, M., Gachohi, J., Mwatondo, A., Lekolool, I., Gakuya, F., Bett, A., Osoro, E., Bitek, A., Thumbi, S.M., Munyua, P., Oyas, H., Njagi, O.N., Bett, B., Njenga, M.K., 2018. Recurrent anthrax outbreaks in humans, livestock, and wildlife in the same locality, Kenya, 2014–2017. Am. J. Trop. Med. Hyg. 99, 833–839. https://doi.org/10.4269/ajtmh.18-0224

Mwakapeje, E.R., Ndimuligo, S.A., Mosomtai, G., Ayebare, S., Nyakarahuka, L., Nonga, H.E., Mdegela, R.H., Skjerve, E., 2019. Ecological niche modeling as a tool for prediction of the potential geographic distribution of *Bacillus anthracis* spores in Tanzania. Int. J. Infect. Dis. 79, 142–151. https://doi.org/10.1016/j.ijid.2018.11.367

Naidoo, R., Brennan, A., Shapiro, A.C., Beytell, P., Aschenborn, O., Du Preez, P., Kilian, J.W., Stuart-Hill, G., Taylor, R.D., 2020. Mapping and assessing the impact of small-scale ephemeral water sources on wildlife in an African seasonal savannah. Ecol. Appl. 30, e02203. https://doi.org/10.1002/eap.2203

Osman, S., Makinde, O.D., Theuri, D.M., 2018. Mathematical modelling of transmission dynamics of anthrax in human and animal population. Mathematical Theory and Modeling.

Paull, S.H., Song, S., McClure, K.M., Sackett, L.C., Kilpatrick, A.M., Johnson, P.T., 2012. From superspreaders to disease hotspots: linking transmission across hosts and space. Front. Ecol. Environ. 10, 75–82. https://doi.org/10.1890/110111

Penzhorn, B.L., 1984. A long-term study of social organisation and behaviour of Cape Mountain zebras *Equus zebra zebra*. Z. Für Tierpsychol. 64, 97–146. https://doi.org/10.1111/j.1439-0310.1984.tb00355.x

Pittiglio, C., Shadomy, S., El Idrissi, A., Soumare, B., Lubroth, J., Makonnen, Y., 2022. Seasonality and ecological suitability modelling for anthrax (*Bacillus anthracis*) in Western Africa. Animals 12, 1146. https://doi.org/10.3390/ani12091146

R Core Team, 2023. R: A language and environment for statistical computing. R Foundation for Statistical Computing, Vienna, Austria.

Railsback, S.F., Grimm, V., 2019. Agent-based and individual-based modeling: a practical introduction, Second Edition. Princeton University Press.

Redfern, J.V., Grant, R., Biggs, H., Getz, W.M., 2003. Surface-water constraints on herbivore foraging in the Kruger National Park, South Africa. Ecology 84, 2092–2107. https://doi.org/10.1890/01-0625

Restif, O., Hayman, D.T.S., Pulliam, J.R.C., Plowright, R.K., George, D.B., Luis, A.D., Cunningham, A.A., Bowen, R.A., Fooks, A.R., O'Shea, T.J., Wood, J.L.N., Webb, C.T., 2012. Model-guided fieldwork: practical guidelines for multidisciplinary research on wildlife ecological and epidemiological dynamics. Ecol. Lett. 15, 1083–1094. https://doi.org/10.1111/j.1461-0248.2012.01836.x

Saad-Roy, C.M., van den Driessche, P., Yakubu, A.-A., 2017. A mathematical model of anthrax transmission in animal populations. Bull. Math. Biol. 79, 303–324. https://doi.org/10.1007/s11538-016-0238-1

Schaffer-Smith, D., Swift, M., Killea, A., Brennan, A., Naidoo, R., Swenson, J.J., 2022. Tracking a blue wave of ephemeral water across arid southern Africa. Environ. Res. Lett. 17, 114063. https://doi.org/10.1088/1748-9326/ac98d9

Scherer, C., Radchuk, V., Franz, M., Thulke, H.-H., Lange, M., Grimm, V., Kramer-Schadt, S., 2020. Moving infections: individual movement decisions drive disease persistence in spatially structured landscapes. Oikos 129, 651–667. https://doi.org/10.1111/oik.07002

Schild, A.L., Sallis, E.S.V., Soares, M.P., Ladeira, S.R.L., Schramm, R., Priebe, A.P., Almeida, M.B., Riet-Correa, F., 2006. Anthrax in cattle in southern Brazil: 1978-2006. Pesqui. Veterinária Bras. 26, 243–248. https://doi.org/10.1590/S0100-736X2006000400009

Shiferaw, F., Abditcho, S., Gopilo, A., Laurenson, M.K., 2002. Anthrax outbreak in Mago National Park, southern Ethiopia. Vet. Rec. 150, 318–320. https://doi.org/10.1136/vr.150.10.318

Smith, K.L., DeVos, V., Bryden, H., Price, L.B., Hugh-Jones, M.E., Keim, P., 2000. *Bacillus anthracis* diversity in Kruger National Park. J. Clin. Microbiol. 38, 3780–3784. https://doi.org/10.1128/jcm.38.10.3780-3784.2000

Strobl, C., Boulesteix, A., Kneib, T., Augustin, T., Zeileis, A., 2008. Conditional variable importance for random forests. BMC Bioinformatics 9. https://doi.org/10.1186/1471-2105-9-307

Tarwater, P.M., Martin, C.F., 2001. Effects of population density on the spread of disease. Complexity 6, 29–36. https://doi.org/10.1002/cplx.10003

Turnbull, P., Bell, R., Saigawa, K., Munyenyembe, F., Mulenga, C., Makala, L., 1991. Anthrax in wildlife in the Luangwa Valley, Zambia. Vet. Rec. 128, 399–403. https://doi.org/10.1136/vr.128.17.399

Turner, W.C., Imologhome, P., Havarua, Z., Kaaya, G.P., Mfune, J.K.E., Mpofu, I.D.T., Getz, W.M., 2013. Soil ingestion, nutrition and the seasonality of anthrax in herbivores of Etosha National Park. Ecosphere 4, art13. https://doi.org/10.1890/ES12-00245.1

Turner, W.C., Kausrud, K.L., Beyer, W., Easterday, W.R., Barandongo, Z.R., Blaschke, E., Cloete, C.C., Lazak, J., Van Ert, M.N., Ganz, H.H., Turnbull, P.C.B., Stenseth, N.C., Getz, W.M., 2016. Lethal exposure: An integrated approach to pathogen transmission via environmental reservoirs. Sci. Rep. 6, 27311. https://doi.org/10.1038/srep27311

Turner, W.C., Kausrud, K.L., Krishnappa, Y.S., Cromsigt, J.P.G.M., Ganz, H.H., Mapaure, I., Cloete, C.C., Havarua, Z., Küsters, M., Getz, W.M., Stenseth, N.Chr., 2014. Fatal attraction: vegetation responses to nutrient inputs attract herbivores to infectious anthrax carcass sites. Proc. R. Soc. B Biol. Sci. 281, 20141785. https://doi.org/10.1098/rspb.2014.1785

Turner, W.C., Périquet, S., Goelst, C.E., Vera, K.B., Cameron, E.Z., Alexander, K.A., Belant, J.L., Cloete, C.C., du Preez, P., Getz, W.M., Hetem, R.S., Kamath, P.L., Kasaona, M.K., Mackenzie, M., Mendelsohn, J., Mfune, J.K.E., Muntifering, J.R., Portas, R., Scott, H.A., Strauss, W.M., Versfeld, W., Wachter, B., Wittemyer, G., Kilian, J.W., 2022. Africa's drylands in a changing world: Challenges for wildlife conservation under climate and land-use changes in the Greater Etosha Landscape. Glob. Ecol. Conserv. 38, e02221. https://doi.org/10.1016/j.gecco.2022.e02221

van Etten, J., 2017. R Package gdistance: Distances and routes on geographical grids. J. Stat. Softw. 76, 1–21. https://doi.org/10.18637/jss.v076.i13 <https://doi.org/10.18637/jss.v076.i13>

VanderWaal, K., Gilbertson, M., Okanga, S., Allan, B.F., Craft, M.E., 2017. Seasonality and pathogen transmission in pastoral cattle contact networks. R. Soc. Open Sci. 4, 170808. https://doi.org/10.1098/rsos.170808

Veldhuis, M.P., Kihwele, E.S., Cromsigt, J.P.G.M., Ogutu, J.O., Hopcraft, J.G.C., Owen-Smith, N., Olff, H., 2019. Large herbivore assemblages in a changing climate: incorporating water dependence and thermoregulation. Ecol. Lett. 22, 1536–1546. https://doi.org/10.1111/ele.13350

Walker, B.H., Emslie, R.H., Owen-Smith, R.N., Scholes, R.J., 1987. To Cull or Not to Cull: Lessons from a Southern African Drought. J. Appl. Ecol. 24, 381–401. https://doi.org/10.2307/2403882

Walker, M.A., Uribasterra, M., Asher, V., Ponciano, J.M., Getz, W.M., Ryan, S.J., Blackburn, J.K., 2020. Ungulate use of locally infectious zones in a re-emerging anthrax risk area. R. Soc. Open Sci. 7, 200246. https://doi.org/10.1098/rsos.200246

Walsh, M.G., de Smalen, A.W., Mor, S.M., 2018. Climatic influence on anthrax suitability in warming northern latitudes. Sci. Rep. 8, 9269. https://doi.org/10.1038/s41598-018-27604-w

White, L.A., Forester, J.D., Craft, M.E., 2018. Disease outbreak thresholds emerge from interactions between movement behavior, landscape structure, and epidemiology. Proc. Natl. Acad. Sci. 115, 7374–7379. https://doi.org/10.1073/pnas.1801383115

WHO, 2008. Anthrax in Humans and Animals. World Health Organization.

Wittemyer, G., Douglas-Hamilton, I., Getz, W.M., 2005. The socioecology of elephants: analysis of the processes creating multitiered social structures. Anim. Behav. 69, 1357–1371. https://doi.org/10.1016/j.anbehav.2004.08.018

Woolley, L.-A., Page, B., Slotow, R., 2011. Foraging strategy within African elephant family units: Why body size matters. Biotropica 43, 489–495. https://doi.org/10.1111/j.1744-7429.2010.00733.x

Zidon, R., Garti, S., Getz, W.M., Saltz, D., 2017. Zebra migration strategies and anthrax in Etosha National Park, Namibia. Ecosphere 8, e01925. https://doi.org/10.1002/ecs2.1925

APPENDIX A: Supplementary material for Chapter one

A1. ODD protocol

The model description follows the ODD (Overview, Design concepts, Details) protocol for describing individual- and agent-based models, as updated by Grimm et al. (Grimm et al., 2020).

A1.1 Purpose and patterns

The purpose of this model was to simulate the effect of environmental pathogen transmission mode on the spatial distribution of the pathogen in a landscape within a fully susceptible host population. The model addressed the role of host movement decisions, pathogen dynamics, and resource quality and fragmentation in spatial disease distribution. The model examined three transmission modes, with pathogens being released into the environment either *(i)* at host death, Obligate-killer scenario (OK), *(ii)* shed over the infectious period, Continuous-shedder scenario (CS), or *(iii)* both shed over time and at host death, Shedder-Killer scenario (SK). We varied multiple parameters in the model to test the role of the environment, host, and pathogen (Table A1).

The simulations were evaluated by analyzing the disease dynamic and spatial distribution of the pathogen in the environment.

A1.2 Entities, state variables, and scales

The entities included in this model are composed of two agents, the hosts and the pathogen reservoirs, which exist on cells within a two-dimensional environment grid.

The state variables of the hosts were their infectious status (‘S’ for susceptible and ‘I’ for infected) and their coordinates.

The pathogen reservoir state variables were the location coordinate, the time step at which they were created, and their infectivity. The infectivity of the reservoir referred to the probability of infection when a host had effective contact with it.

The environmental grid cell was composed of 33 x 33 static square cells. The environment represented a binary resource, i.e., grid cells are either high (1) or medium (0) resource quality. Four landscapes were created and used throughout the simulations (figure A1). Within a simulation, the landscape was fixed for the entire simulation duration.

The model included time, defined as discrete steps of one day. This simulation model is theoretical; thus, the resolution of the spatial scale was not fixed but rather species-specific. It assumes that host movement to a neighboring cell and infections could occur within one time step. The environment was toroidal to avoid edge effects.

Parameters were inspired by known environmentally transmitted pathogens (e.g., anthrax, gastrointestinal nematode, chronic-wasting disease). Due to the persistence potential of some pathogens in the environment, the simulations were run for 10,000 steps, representing about 27 years of duration per simulation.

A1.3 Process overview and scheduling

The model was developed to cover the transmission dynamics of ETPs among their mobile hosts. It was structured in four processes: one related to the host (movement), two related to the interaction between hosts and pathogen (transmission and pathogen reservoir creation), and one related to the reservoir only (pathogen reservoir dynamics) (figure 1.1).

All the processes took place during each time step following a specific order. First, every host moved within the environment simultaneously. If susceptible hosts were present on a pathogen

reservoir cell, the probability of infection was calculated using the infectivity of the reservoir site, given that contact was established. When infection occurred, the host status changed from susceptible to infected. After the infection, all previously infected hosts could release pathogens in their cells (either by shedding or upon death). When a host dies or recovers from infection (i.e., given the probability of survival), it is removed from the simulation. Finally, the infectivity of each pathogen reservoir decayed over time, following an exponential decay. Once the simulation was finished, output files were written. We recorded the number of susceptible and infected hosts and the number of reservoir cells for each time step, as well as the spatial distribution of the reservoir cells and their infectivity every 150 steps.

Host movement and infection processes occurred before the reservoir's formation and decay, as creating a new reservoir may modify the movement decisions of hosts and, thus, the disease dynamics. We also had all hosts moving and being infected simultaneously, as the hosts did not interact with each other.

A simulation was considered successful if at least five hosts were infected. We ran each parameter set until we obtained either 100 successful simulations or 10,000 failed simulations.

A1.4 Design concept

Basic principles: The model addressed the role of host movement behavior, pathogen reservoir dynamics, and resource quality and fragmentation on disease dynamic and spatial distribution of ETPs. By simulating multiple parameter sets, the model aimed to infer which parameters specific to the host, pathogen, or landscape features mostly influenced disease dynamic outcomes.

Emergence: The main outcomes of the model were the number of susceptible and infected individuals in the population over time as well as the spatiotemporal distribution of the reservoir sites in the landscape.

Adaptation: The model included one direct object seeking adaptive behavior: host agents moved in reaction to their environment. Their movement was influenced by both the habitat quality and the presence of reservoir sites in their surroundings.

Objectives: No direct object-seeking behavior was present in the model.

Learning: There was no learning in the model.

Predictions: There were no explicit predictions. Movement of hosts implies the implicit predictions that moving to a high quality habitat is better for the individuals (the intensity being regulated by model parameters) and that avoidance or attraction toward reservoir site will be beneficial to the hosts (which of avoidance or attraction is better depends on the model simulations).

Sensing: Hosts could perfectly sense their environments within a one-cell radius around them and make decisions according to the presence/absence of reservoirs and the habitat quality.

Interaction: One direct interaction was modeled between the host and the pathogen reservoir. While the reservoir agent was not impacted by the interaction, the host agent may become infected. Interactions occurred at the daily time step resolution. Disease transmission happened from single contact between the host and the reservoir. The host did not build immunity over multiple contacts, and reservoir infectivity was not impacted by the presence of the host.

Stochasticity: Stochasticity was used multiple times in the model. At initialization, hosts were randomly placed across the landscape, and one host was randomly selected to be infected. Both

host movement and infection relied on stochasticity. Host movement followed a resource selection function, which included randomness in the cell selection. For the infection risk, the probability of contact between a host and the given reservoir cell was randomly drawn, and if contact occurred, the probability of being infected was drawn based on the probability of infection at the reservoir site.

Collectives: There were no collectives in the model.

Observation: The model aimed to determine how pathogen transmission mode, host movement and behavior, pathogen dynamics, and resource distribution on the landscape affected disease outbreak and spatial reservoir distribution. For each simulation, we recorded the number of susceptible and infected individuals and the number of pathogen reservoirs in the environment at each time step. We also recorded the spatial distribution of the pathogen reservoirs and their infectivity every 150 steps.

A1.5 Initialization

The model's initialization consisted of placing the individual agents within the landscape and selecting the first agent to be infected. The 'Landscape' parameter selected the environmental layer, referring to four specific landscapes pre-created.

Host agents: We added a fixed number, *N*, of susceptible host agents in the environment. Each host was given a random location, and their status was set to 'S'. Then, we randomly selected one individual and changed their status to 'I'. No reservoir agents are created during the initialization.

A1.6. Input data

The landscape layer was given at the beginning of each simulation. Four different binary landscapes were generated using the midpoint displacement algorithm (Turner and Gardner, 2015).

The landscapes varied in their proportion of high-quality resources available (p) and their degree of aggregation (Hurst exponent, H). Four 33x33 cell landscapes were generated and used for simulations (i) medium resource availability with low aggregation: p = 0.5; H = 0.5; (ii) high resource availability with low aggregation: p = 0.8, H = 0.5; (iii) medium resource availability with high aggregation: p = 0.5, H = 0.8, and (iv) high resource availability with high aggregation: p = 0.8, H = 0.8 (figure A1). The landscapes assumed a torus shape (i.e., wrapped boundaries) to avoid movement edge effects.

A1.7 Sub-models

See the detailed description of the sub-models in the Materials and Method section of the main text of Chapter one.

A2. Supplementary tables

TABLE A1: Variable importance analysis for all parameters tested within the model. Values represent the mean decrease in accuracy. The top three variables of importance are in bold, and the number of starts shows their order of important *** = most important parameter, ** = 2nd most important, and * = 3rd most important. Values have been scaled for each variable to facilitate their visualization. OK = Obligate-killer; CS = Continuous-shedder; SK = Shedder-Killer. p represents the proportion of high-resource habitat; H is the aggregation of the high-resource habitat; N is the initial population size; β and β_1 are respectively the strength of selection for high-resource habitat and reservoir presence for the resource-selection function; ξ_1 and ξ_0 are the probability of effective contact in high and low habitat quality respectively; γ is the infection duration; μ is the pathogen decay rate; and ρ_D and ρ_S are the initial infectivity at pathogen release at death and shed respectively.

Variable	Scenario	p	H	N	β	β1	ξ1	ξ0	ϒ	μ	ρD	ρS
Proportion of successful simulations	OK	-0.90	-0.89	-0.42	-0.55	**1.77*** **	-0.38	-0.38	-0.54	**1.30***	**1.69****	
	CS	-0.91	-0.95	-0.45	-0.52	**2.40*** **	-0.42	-0.46	0.29	**1.54***		**1.90****
	SK	-0.93	-0.95	-0.61	-0.72	**0.92*** **	-0.61	-0.60	-0.70	**0.60****	**0.27***	0.23
Simulations with disease fade out	OK	-0.64	-0.61	-0.37	-0.41	**0.02****	-0.41	-0.40	-0.18	**2.41*** **	**-0.14***	
	CS	-0.55	-0.64	-0.20	-0.28	**0.60****	-0.31	-0.29	-0.24	**3.75*** **		**0.10***
	SK	-0.61	-0.66	-0.31	-0.37	**-0.05****	-0.34	-0.34	-0.41	**2.38*** **	**-0.24***	**-0.24***
Simulations with susceptible	OK	-1.13	-1.17	-0.62	-0.47	**1.54*** **	-0.56	-0.56	-0.55	**1.38****	**0.92***	
	CS	-1.14	-1.19	-0.50	-0.48	**0.72***	-0.70	-0.66	0.42	**1.33*** **		**0.73****

population extinction	SK	-0.89	-1.13	-0.42	-0.06	**1.84****	-0.55	-0.54	-0.20	**2.38*****	**0.92***	0.91
Period of continuous non-infection	OK	-0.87	-1.06	-0.06	-0.57	**1.40****	-0.44	-0.41	-0.61	**0.88***	**1.73*****	
	CS	-0.92	-1.04	-0.03	-0.46	**1.30****	-0.60	-0.60	0.10	**3.30*****		**1.27***
	SK	-0.98	-1.08	-0.43	-0.33	**0.73*****	-0.60	-0.61	-0.28	0.28	**0.50***	**0.43****
Period of continuous infection	OK	-0.90	-1.01	**0.39***	-0.70	**2.18*****	-0.61	-0.61	-0.35	-0.25	**1.41****	
	CS	-0.79	-1.01	0.34	-0.60	**2.66*****	-0.51	-0.51	**1.12***	0.08		**1.70****
	SK	-0.96	-1.02	0.28	-0.75	**1.43*****	-0.70	-0.70	-0.14	-0.25	**0.45****	**0.35***
Proportion of infected population	OK	-0.76	-0.88	-0.32	-0.58	**2.41*****	-0.38	-0.39	-0.54	**0.13***	**1.70****	
	CS	-0.66	-0.88	-0.24	-0.48	**2.79*****	-0.43	-0.41	**0.43***	0.34		**1.88****
	SK	-0.87	-0.91	-0.50	-0.70	**1.31*****	-0.59	-0.59	-0.61	-0.05	**0.38***	**0.39****
Proportion of infected cells	OK	-0.93	-0.93	**-0.42****	-0.84	**-0.53***	-0.81	-0.80	-0.65	-0.72	**-0.09*****	
	CS	-0.80	-0.85	**0.61***	-0.20	0.41	-0.35	-0.37	**3.08*****	0.25		**1.48****
	SK	-0.77	-0.85	**1.06****	-0.16	0.49	-0.37	-0.39	**2.54*****	0.22	0.81	**0.87***
Median Moran'I	OK	-0.71	-0.85	-0.41	-0.63	**0.89*****	-0.64	-0.64	-0.67	**0.10****	**0.02***	
	CS	-0.61	-0.79	-0.02	-0.24	**3.60*****	-0.32	-0.32	1.17	**1.43***		**1.62****
	SK	-0.77	-0.83	-0.34	-0.64	**1.70*****	-0.60	-0.61	-0.36	**0.56****	**-0.06***	**-0.06***
Number of high-infectivity clusters	OK	-0.70	-0.76	**-0.64****	-0.70	**-0.68***	-0.75	-0.74	-0.73	**-0.61*****	-0.71	
	CS	-0.34	-0.50	1.34	0.77	**2.09***	0.28	0.32	**2.70****	**2.75*****		1.10
	SK	**-0.11***	-0.60	-0.16	-0.31	**-0.04****	-0.59	-0.57	**-0.03*****	-0.16	-0.49	-0.49
	OK	-0.59	-0.69	-0.03	-0.12	**1.04***	-0.23	-0.21	0.30	**1.45****	**3.92*****	
	CS	-0.68	-0.77	-0.73	-0.71	**-0.57****	-0.77	-0.77	-0.75	**-0.63***		**-0.32*****

Mean relative cluster infectivity	SK	-0.16	-0.53	-0.33	-0.39	**0.60***	-0.45	-0.42	0.32	0.34	**1.43****	**1.44*****
Mean cluster size	OK	-0.92	-1.08	-0.55	0.18	**3.01*****	-0.19	-0.27	**1.70****	0.55	**0.71***	
	CS	-1.19	-1.25	-0.11	-0.74	-0.52	-0.85	-0.85	**1.19*****	**0.26****		**0.09***
	SK	-0.69	-0.93	**0.75****	-0.34	-0.06	-0.59	-0.60	**2.16*****	**0.65***	-0.32	-0.33

A3. Supplementary figures

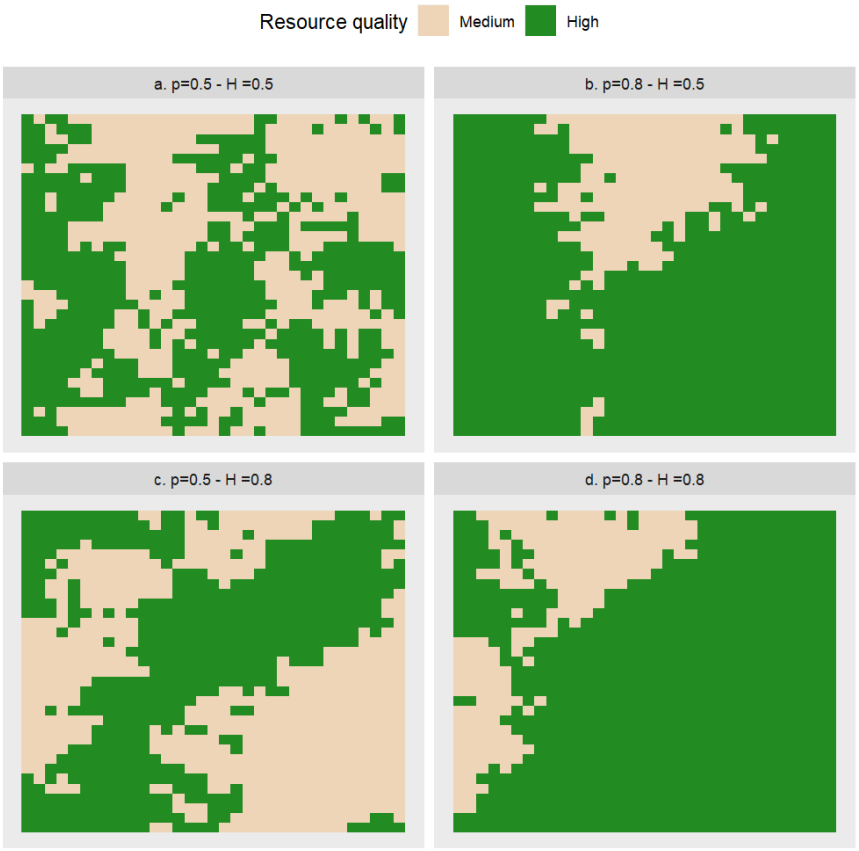

FIGURE A1: Spatially explicit 33 x 33 gridded binary landscape used for the simulations. The four landscape varied in their proportion of high-quality resources available (p) and their degree of resource aggregation (H) a. Medium resource availability with low aggregation: p = 0.5; H = 0.5; (b) High resource availability with low aggregation : p = 0.8, H = 0.5; (c) Medium resource availability with high aggregation: p = 0.5, H = 0.8, and (d) High resource availability with high aggregation : p = 0.8, H = 0.8. Green represents high-quality resources, and beige represents medium-quality resources.

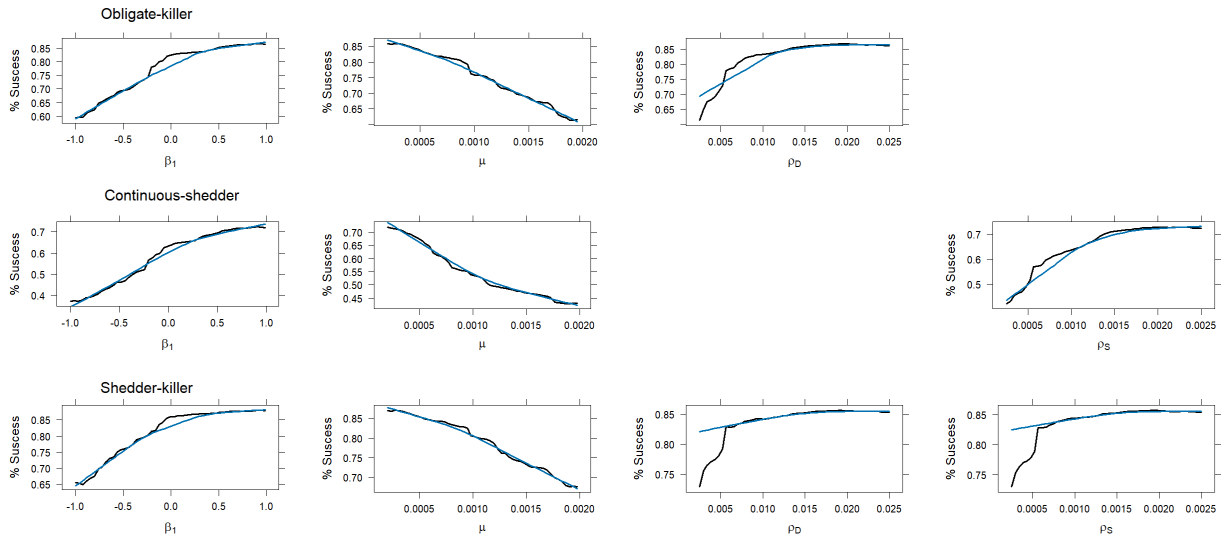

FIGURE A2: Partial dependence plot of the three most important parameters for the proportion of simulation success. The top row represents the Obligate-killer scenario, the middle row is the Continuous-shedder, and the bottom row is the Shedder-killer. Parameters β_1 represents the effect of environmental reservoirs on the resource-selection movement function, μ is the pathogen decay rate, ρ_D, and ρ_S are the initial infectivity of a reservoir created respectively by a death event or by continuous shedding.

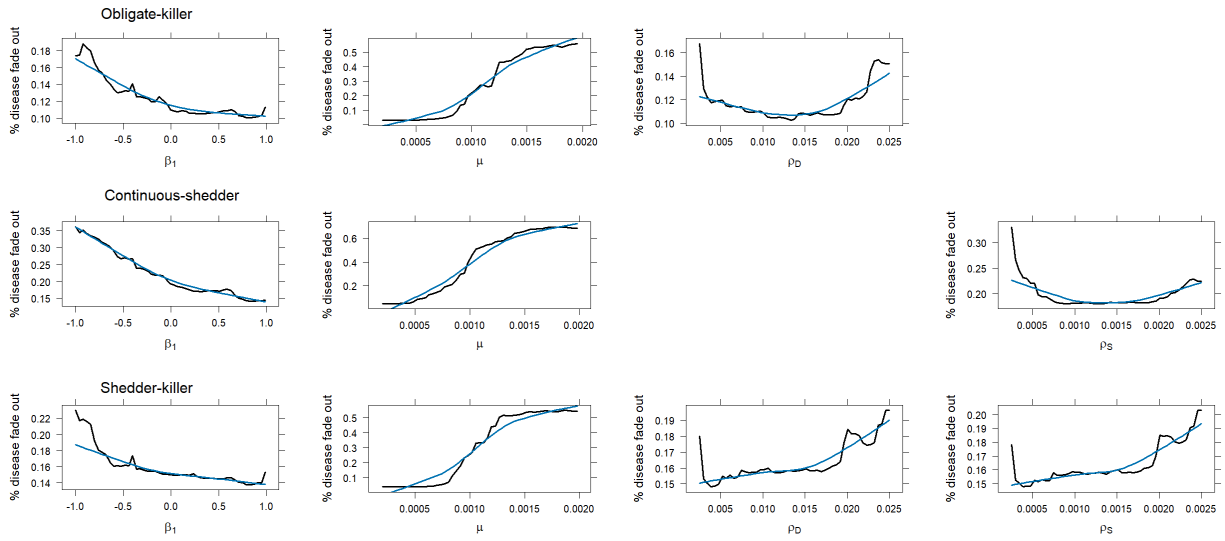

FIGURE A3: Partial dependence plot of the three most important parameters for the proportion of simulation with disease disappearing. The top row represents the Obligate-killer scenario, the middle row is the Continuous-shedder, and the bottom row is the Shedder-killer. Parameters β_1 represents the effect of environmental reservoirs on the resource-selection movement function, μ is the pathogen decay rate, ρ_D, and ρ_S are the initial infectivity of a reservoir created respectively by a death event or by continuous shedding.

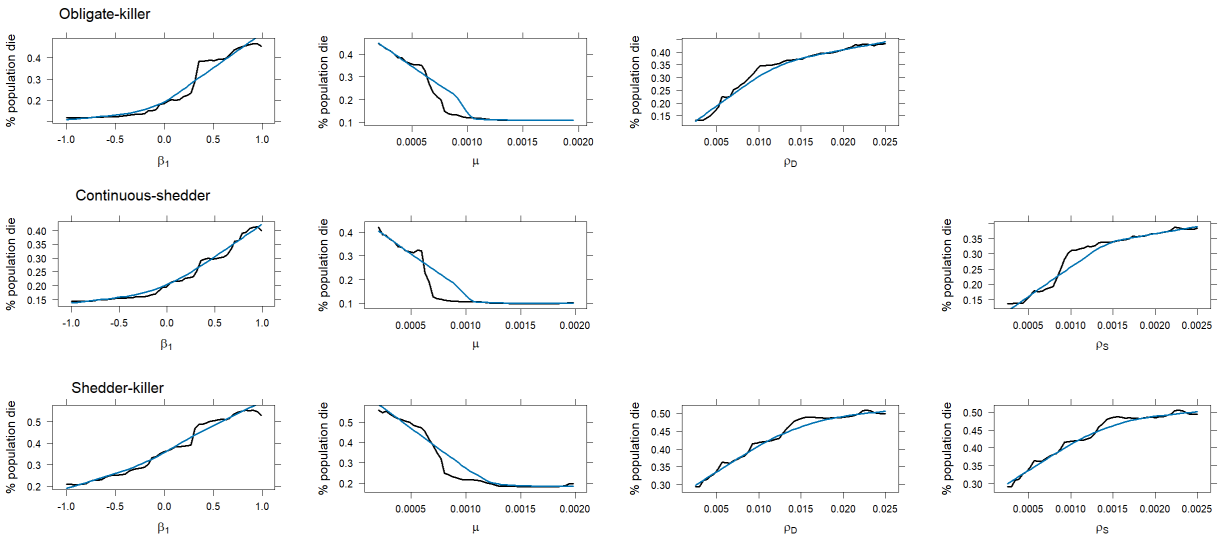

FIGURE A4 : Partial dependence plot of the three most important parameters for the proportion of simulation with the population dying off / being fully immune. The top row represents the Obligate-killer scenario, the middle row is the Continuous-shedder, and the bottom row is the Shedder-killer. Parameters β_1 represents the effect of environmental reservoirs on the resource-selection movement function, μ is the pathogen decay rate, ρ_D, and ρ_S are the initial infectivity of a reservoir created respectively by a death event or by continuous shedding.

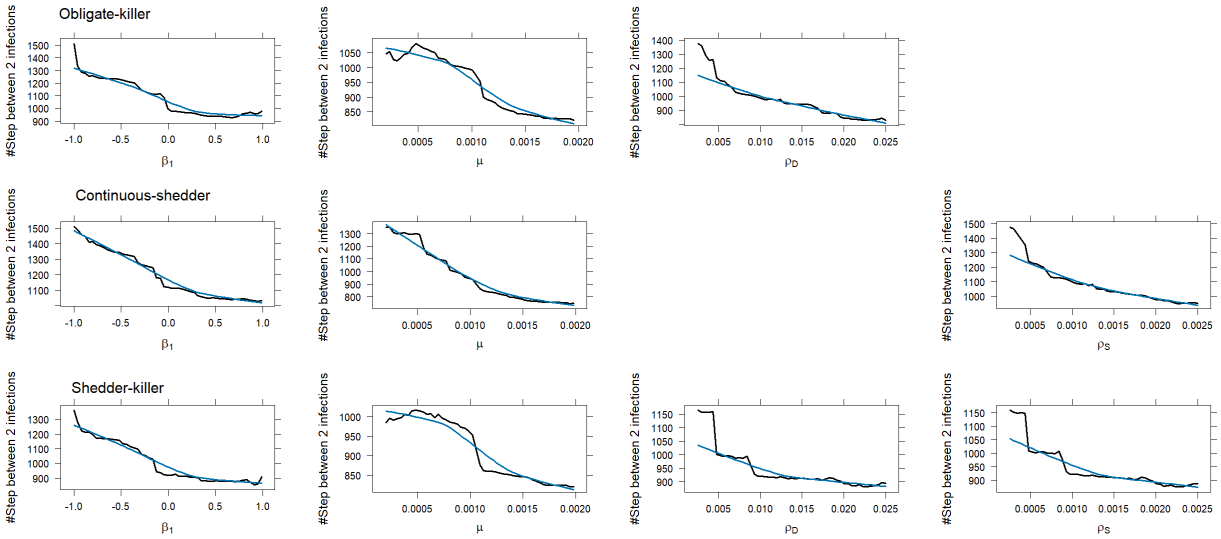

FIGURE A5: Partial dependence plot of the three most important parameters for the maximal number of temporal steps between two infections. The top row represents the Obligate-killer scenario, the middle row is the Continuous-shedder, and the bottom row is the Shedder-killer. Parameters β_1 represent the effect of environmental reservoirs on the resource-selection movement function, μ is the pathogen decay rate, ρ_D, and ρ_S are the initial infectivity of a reservoir created respectively by a death event or by continuous shedding.

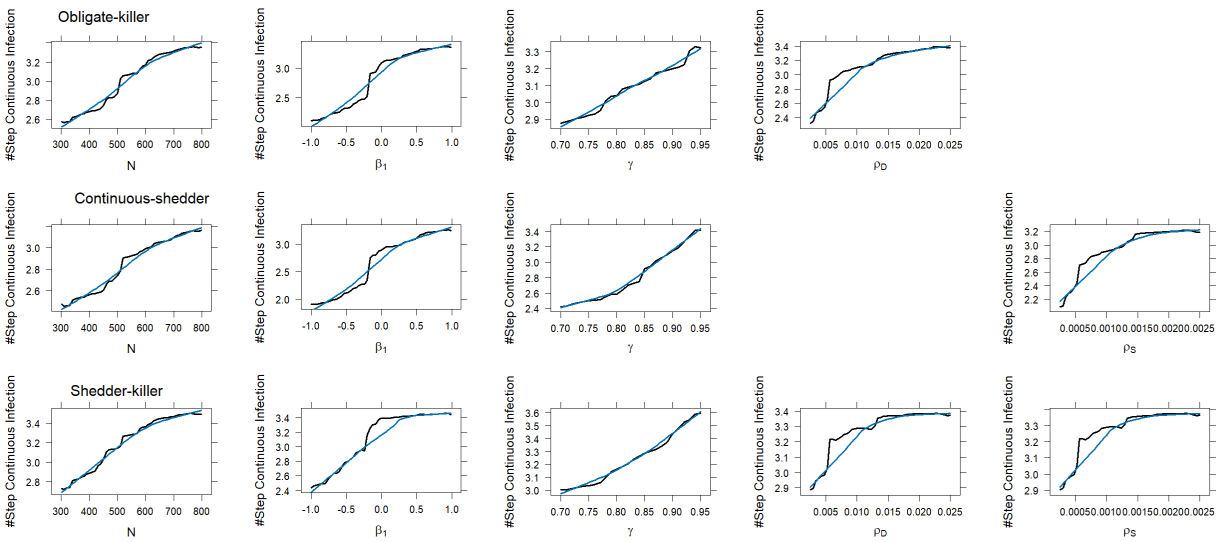

FIGURE A6: Partial dependence plot of the four most important parameters for the maximal number of temporal steps with continuous infections. The top row represents the Obligate-killer scenario, the middle row is the Continuous-shedder, and the bottom row is the Shedder-killer. Parameter N is the number of hosts at the start of the simulation, β_1 represents the effect of environmental reservoirs on the resource-selection movement function, γ is the infection duration, ρ_D, and ρ_S are the initial infectivity of a reservoir created respectively by a death event or by continuous shedding.

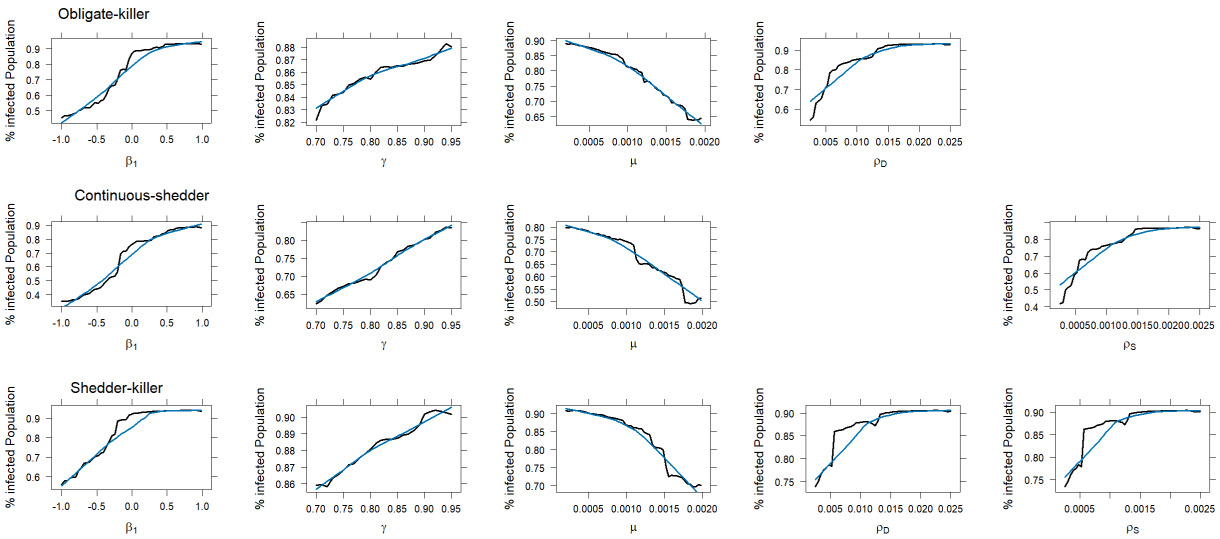

FIGURE A7: Partial dependence plot of the four most important parameters for the proportion of the population being infected by the end of a simulation. The top row represents the Obligate-killer scenario, the middle row is the Continuous-shedder, and the bottom row is the Shedder-killer. Parameters β_1 represents the effect of environmental reservoirs on the resource-selection movement function, γ is the infection duration, μ is the pathogen decay rate, ρ_D, and ρ_S are the initial infectivity of a reservoir created respectively by a death event or by continuous shedding.

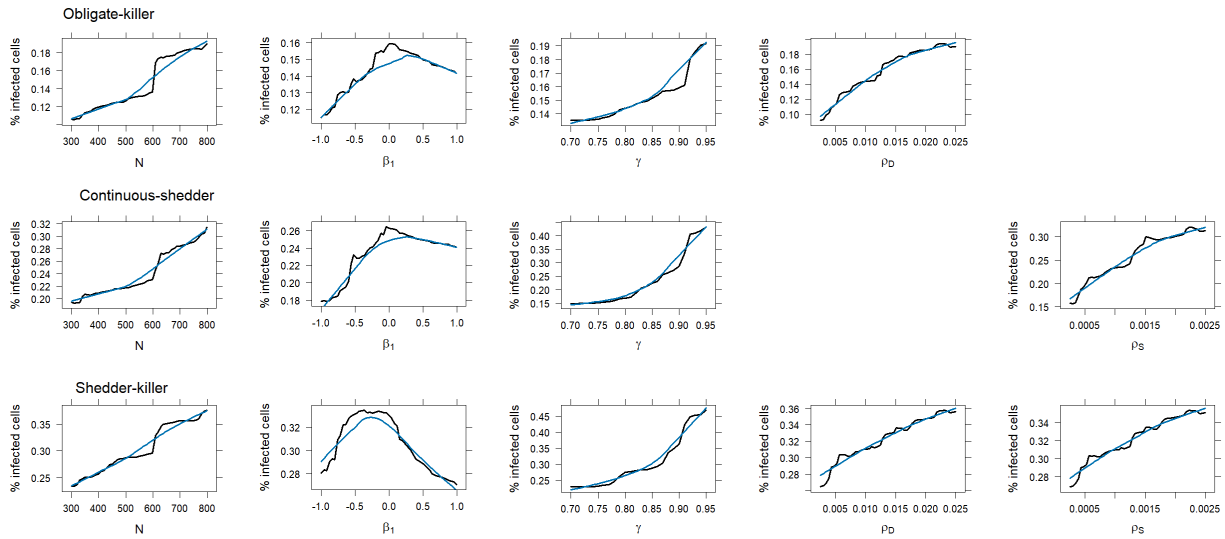

FIGURE A8: Partial dependence plot of the five most important parameters for the proportion of environmental cells infected. The top row represents the Obligate-killer scenario, the middle row is the Continuous-shedder, and the bottom row is the Shedder-killer. Parameter N is the number of hosts at the start of the simulation, β_1 represents the effect of environmental reservoirs on the resource-selection movement function, γ is the infection duration, ρ_D, and ρ_S are the initial infectivity of a reservoir created respectively by a death event or by continuous shedding.

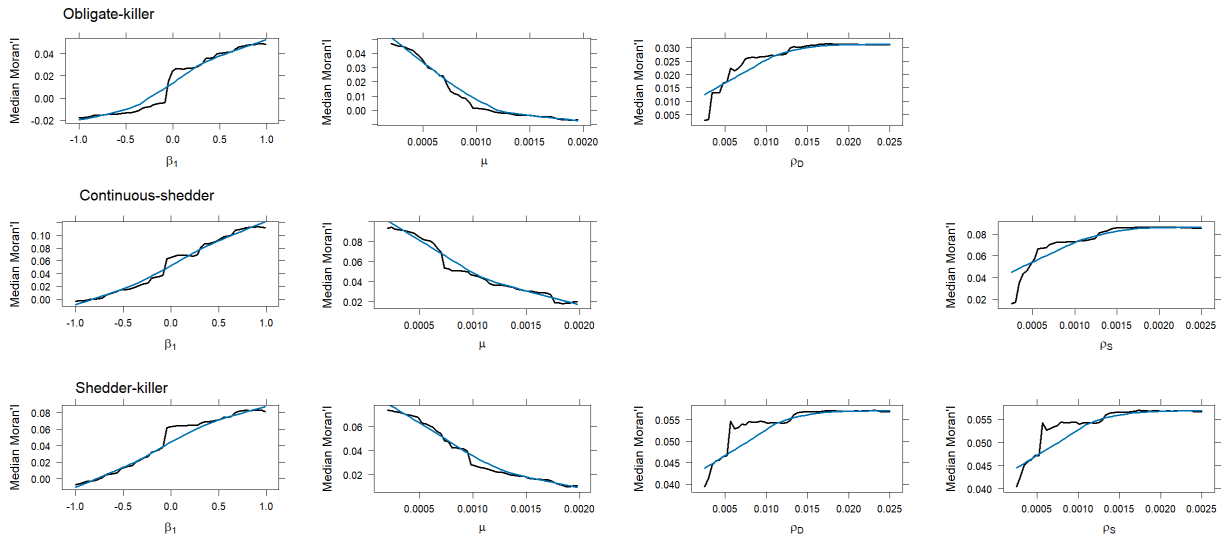

FIGURE A9: Partial dependence plot of the three most important parameters for the median Moran'I index value. The top row represents the Obligate-killer scenario, the middle row is the Continuous-shedder, and the bottom row is the Shedder-killer. Parameters β_1 represent the effect of environmental reservoirs on the resource-selection movement function, μ is the pathogen decay rate, ρ_D, and ρ_S are the initial infectivity of a reservoir created respectively by a death event or by continuous shedding.

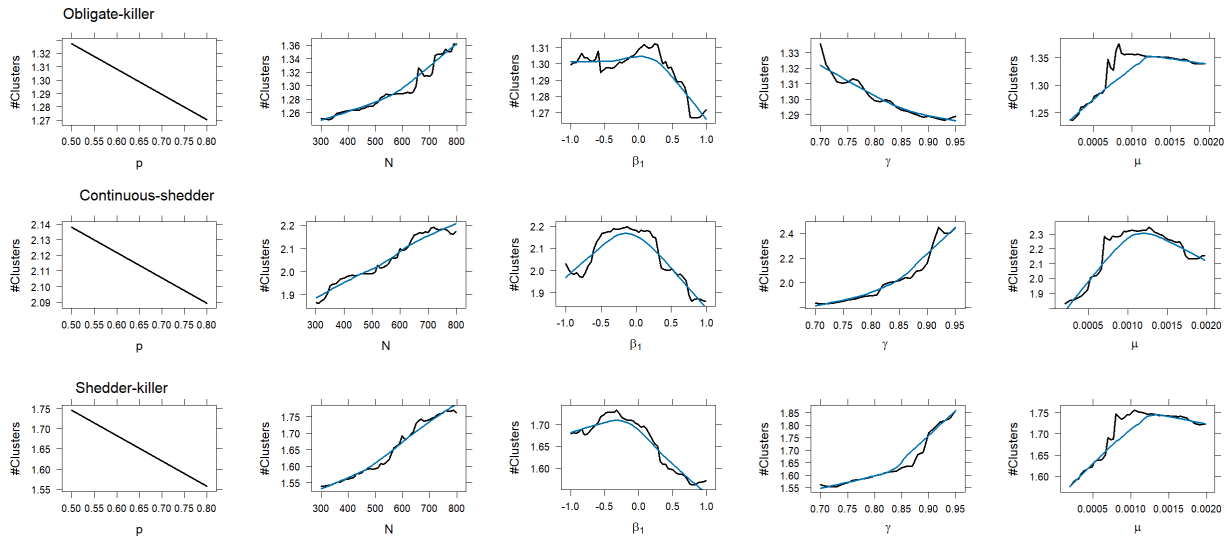

FIGURE A10: Partial dependence plot of the six most important parameters for the number of unique high-infectious risk clusters created during a simulation. The top row represents the Obligate-killer scenario, the middle row is the Continuous-shedder, and the bottom row is the Shedder-killer. Parameters p is the proportion of high-resource habitat in the landscape, N is the number of hosts at the start of the simulation, β is the attractivity of high-quality habitat resource, and β_1 the effect of environmental reservoirs on the resource-selection movement function, γ is the infection duration, and μ is the pathogen decay rate.

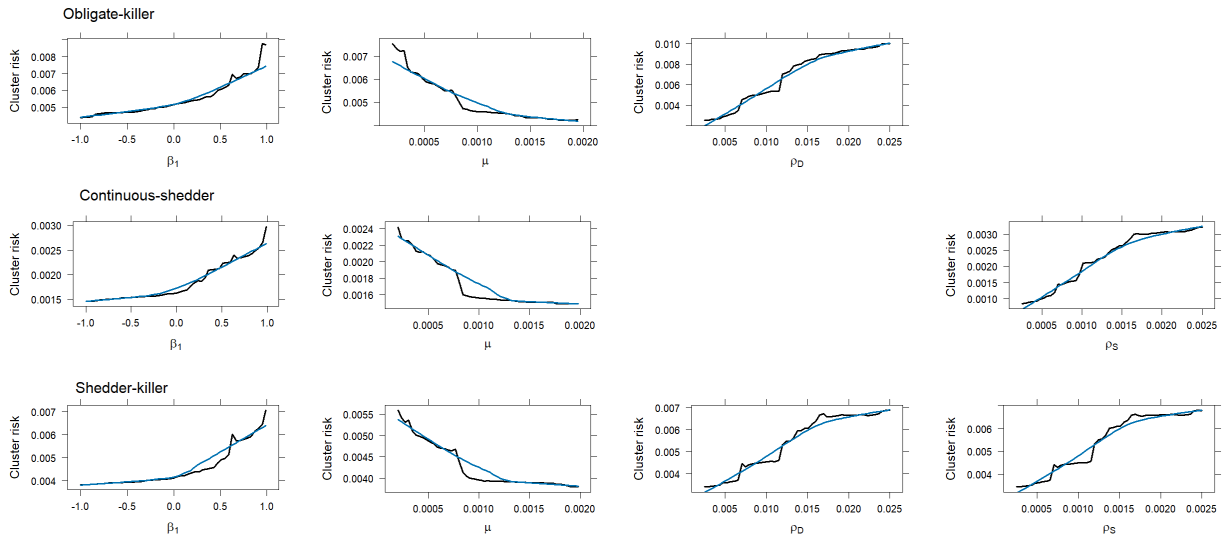

FIGURE A11: Partial dependence plot of the five most important parameters for the mean peak of relative infectivity risks within clusters. The top row represents the Obligate-killer scenario, the middle row is the Continuous-shedder, and the bottom row is the Shedder-killer. β_1 represents the effect of environmental reservoirs on the resource-selection movement function, μ is the pathogen decay rate, ρ_D, and ρ_S are the initial infectivity of a reservoir created respectively by a death event or by continuous shedding.

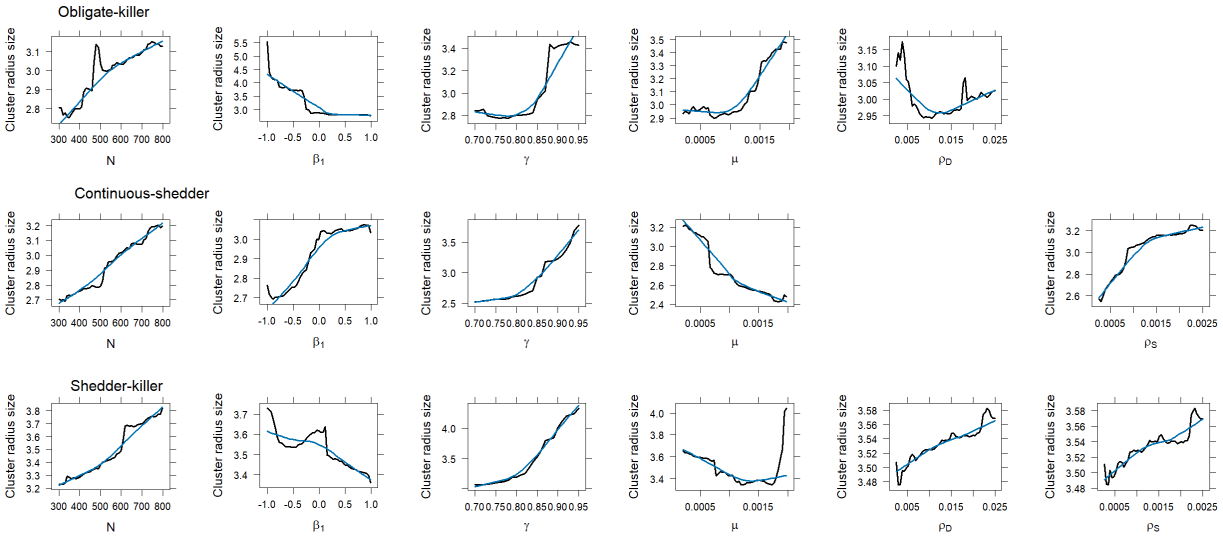

FIGURE A12: Partial dependence plot of the four most important parameters for the size of high infectivity clusters created during a simulation. The top row represents the Obligate-killer scenario, the middle row is the Continuous-shedder, and the bottom row is the Shedder-killer. Parameter N is the number of hosts at the start of the simulation, β_1 represents the effect of environmental reservoirs on the resource-selection movement function, γ is the infection duration, μ is the pathogen decay rate, ρ_D, and ρ_S are the initial infectivity of a reservoir created respectively by a death event or by continuous shedding.

A4. References

Grimm, V., Railsback, S.F., Vincenot, C.E., Berger, U., Gallagher, C., DeAngelis, D.L., Edmonds, B., Ge, J., Giske, J., Groeneveld, J., Johnston, A.S.A., Milles, A., Nabe-Nielsen, J., Polhill, J.G., Radchuk, V., Rohwäder, M.-S., Stillman, R.A., Thiele, J.C., Ayllón, D., 2020. The ODD Protocol for describing agent-based and other simulation models: A second update to improve clarity, replication, and structural realism. J. Artif. Soc. Soc. Simul. 23, 7. https://doi.org/10.18564/jasss.4259

Turner, M.G., Gardner, R.H., 2015. Landscape ecology in theory and practice: Pattern and process. Springer New York, New York, NY. https://doi.org/10.1007/978-1-4939-2794-4

APPENDIX B: Supplementary material for Chapter two

B1. Supporting Method

B1.1 Camera trap photo animal identification

Coat striping patterns were used to identify individual zebra between sequential pictures and triggers, though this was only assessed for triggers proximate in time. Wildebeest had fewer individuals in photos than did zebra and following one individual through the picture sequences was more straightforward and could be done based on size, age, sex, and position in the field of view. To determine sex and age, specific cues were used. For both species, the presence of mammary glands, vulva, penis sheath, or penis was used. When these were not visible, we used other cues. Male zebras are about 10 % larger than females and tend to have thicker necks and legs (Skinner and Chimimba, 2005). For wildebeest, male horns are more prominent and extend beyond the ears, with a large, well-developed boss. Females have a round stomach, while males have a more angular shape. For the age, sub-adult zebras have a body height similar to adults but look thinner, and their backs can still be furry. For wildebeest, the sub-adults have their adult darker coat, except between their eyes where brown coat can be present. Their bodies are smaller than adults, and, for juveniles, horns start appearing small and straight.

B1.2 Camera trap data statistical analysis

Generalized linear models were used to analyse (i) the number of monthly visitations, (ii) the monthly proportion of grazing events and (iii) the time spent grazing. The monthly visitation and proportion of grazing were obtained by summing the number of visits per month, site ID, and treatment by age and sex. Juveniles were not included due to the relatively small number recorded and the difficulty of determining their sex. Because each camera was not functioning the whole time it was set up (flat battery, SD card failure, knocked down by animals, etc), we only kept the

months for which at least 20 days of recording were available for both cameras in a camera pair to limit bias due to unequal sampling across months. In total, 273 months of data were recorded at paired camera sites (control and carcass), totaling 546 individual cameras-months of data. Of the 273 samplings, 219 met our 20 day-cutoff, representing 438 individual camera-months of recording. Of those 438 samples, 78% had 0-1 days of missing data (340), and if days were missing, it represented an average of 2.5 days (figure B2 represents the number of missing days per camera used in the analysis). Considering this, choosing a 20-day cutoff allowed us to limit the bias arising from missing data as most of our data had a low number of missing days, without dismissing too much of the data collected. A cutoff of 20 days also allowed to have a similar number of months observed per season (156 for hot wet season, 134 for cool dry and 148 for hot dry season). A total of 8 fixed variables were tested; a description of each variable and their hypothesized role in visitation and grazing are presented in Table B1. Sixteen models were tested for each species and for each of the three response variables, as presented in Table B2.

The number of monthly visitations was analysed using a zero-truncated negative-binomial generalized linear mixed model to understand which factors affected the number of individuals visiting a site, when we know that individuals are present. The proportion of monthly grazing events was analysed using a binomial generalized linear mixed model. Finally, the time spent grazing was analysed using a log transformation and a linear mixed model. Site ID was included as a random effect in all models.

B1.3 Probability Distribution Functions (PDFs)

The PDFs for the number of individuals visiting sites were estimated by dividing our dataset by age, sex, year after death, season, treatment, and, for zebra, distance from perennial water, or for wildebeest, distance from the Etosha main pan. For the probability of grazing, we divided our

dataset by age, sex, treatment, and year after death. Finally, for the time spent grazing, we divided by age, sex, and season. For each variable, we manually selected the appropriate bandwidth, i.e., the smoothness of the functions using the entire dataset, that best kept the variability of each variable, without over-smoothing them. See figures B3 to B8 for the visual representation of the PDFs.

B2. Supplementary results

Selected models for zebra and wildebeest:

Number of visits, zebra:

```
Family: Zero-truncated negative binomial

Link function: Log

Formula: NV ~ Treatment + Age + Sex + NDVI + Season + Water + Water:Season + (1 |
ID)

     AIC          BIC        logLik     Deviance    Df.resid

   2432.7       2485.6      -1204.3      2408.7         594

Random effects:

          Name          Variance       Std Dev
 ID       (Intercept)   0.3119         0.5585


Number of obs: 606, groups: ID, 13

Dispersion parameter for truncated_nbinom2 family (): 1.21

Fixed effects:

                        Estimate      Std Error    Z value       Pr(>|z|)
 (Intercept)            0.31916       0.43207      0.739         0.4601
 Treatment              -0.21524      0.10001      -2.152        0.0314    *
 AgeSA                  -1.72172      0.12345      -13.947       < 2e-16   ***
 SexM                   -0.62605      0.10037      -6.237        4.46e-10  ***
 NDVI                   4.44984       0.95215      4.673         2.96e-06  ***
 SeasonCool_dry         0.21739       0.26334      0.825         0.4091
 SeasonHot_dry          1.13777       0.22884      4.972         6.63e-07  ***
 Water                  -0.08032      0.04024      -1.996        0.0459    *
 SeasonCool_dry:Water   0.04965       0.04370      1.136         0.2558
 SeasonHot_dry:Water    -0.09585      0.04268      -2.246        0.0247    *

Signif. codes:  0 ‘***’ 0.001 ‘**’ 0.01 ‘*’ 0.05 ‘.’ 0.1 ‘ ’ 1
```

The best model explaining the number of zebras visiting a site was composed of Treatment, Age, Sex, NDVI, Season, distance to closest waterhole and an interaction between the distance to closest waterhole and season. The number of visits varied with the site ID with a variance of 0.31 and a standard deviation of 0.56.

Number of visits, wildebeest

```
Family : Zero-truncated negative binomial

Link function: Log

Formula : NV ~ Treatment + Age + Sex + NDVI + Season + Pan + MAD + Treatment:MAD +
(1 | ID)

   AIC       BIC     logLik   Deviance  Df.resid
  792.3     833.1    -384.1     768.3       209


Random effects:

       Name           Variance      Std Dev
 ID    (Intercept)    5.787e-10     2.406e-05


Number of obs: 221, groups: ID, 12

Dispersion parameter for truncated_nbinom2 family (): 1.57

Fixed effects:

                     Estimate      Std Error    Z value      Pr(>|z|)
 (Intercept)         1.233513      0.637571     1.935        0.05303    .
 Treatment           0.981996      0.391218     2.510        0.01207    *
 AgeSA               -1.038030     0.208159     -4.987       6.14e-07   ***
 SexM                -0.788549     0.170821     -4.616       3.91e-06   ***
 NDVI                -0.043934     1.741772     -0.025       0.97988
 SeasonCool_dry      0.239400      0.268689     0.891        0.37293
 SeasonHot_dry       -0.007464     0.270472     -0.028       0.97799
 Pan                 -0.066754     0.025215     -2.647       0.00811    **
 MAD                 0.006732      0.016048     0.419        0.67485
 Treatment:MAD       -0.060981     0.024025     -2.538       0.01114    *


Signif. codes:  0 ‘***’ 0.001 ‘**’ 0.01 ‘*’ 0.05 ‘.’ 0.1 ‘ ’ 1
```

The best model explaining the number of wildebeests visiting a site was composed of Treatment, Age, Sex, NDVI, Season, distance to the main Etosha salt pan, the number of months after death and an interaction between the treatment and the number of months after death. This interaction was negative, meaning the older the carcass site, the fewer visitations by wildebeest. The number

of visits did not vary much with the site ID, the variance and standard deviation being very low (5.87×10^{-10}, 2.4×10^{-5}, respectively).

Probability of grazing, zebra

```
Family : Binomial
Link function: logit
Formula: PG ~ Treatment + Age + Sex + NDVI + Season + MAD + Treatment:MAD + (1|ID)

   AIC      BIC    logLik   Deviance   Df.resid
 1450.4   1494.4   -715.2    1430.4      596

Scaled residuals:
   Min       1Q      Median      3Q       Max
 -2.8965   -0.7590   -0.3875   0.8788    5.4567


Random effects:
       Name           Variance       Std Dev
 ID    (Intercept)    0.6473         0.8045

Number of obs: 606, groups: ID, 13
Fixed effects:
                      Estimate      Std Error    Z value      Pr(>|z|)
 (Intercept)          -1.696246     0.382801     -4.431       9.37e-06     ***
 Treatment            1.282767      0.2180068    5.882        4.04e-09     ***
 AgeSA                -0.316267     0.136973     -2.309       0.02095      *
 SexM                 -0.517314     0.103004     -5.022       5.11e-07     ***
 NDVI                 3.321061      0.808653     4.107        4.01e-05     ***
 SeasonCool_dry       0.325422      0.152003     2.141        0.03228      *
 SeasonHot_dry        -0.030392     0.148745     -0.204       0.83810
 MAD                  0.016980      0.009666     1.757        0.07897      .
 Treatment:MAD        -0.040494     0.012557     -3.225       0.00126      **

Signif. codes:  0 ‘***’ 0.001 ‘**’ 0.01 ‘*’ 0.05 ‘.’ 0.1 ‘ ’ 1
Correlation of Fixed Effects:
            (Intr)   Tr       AgeSA    SexM     NDVI     SeasonCD  SeasonHW  MAD
 Trt        -0.309
 AgeSA      -0.027   -0.011
 SexM       -0.016   -0.050   -0.027
 NDVI       -0.637   0.067    -0.042   -0.105
 SeasonCD   -0.465   0.080    0.000    0.017    0.428
 SeasonHD   -0.485   0.037    -0.036   0.001    0.515    0.706
 MAD        -0.426   -0.545   0.038    -0.050   0.080    0.126     0.062
 Trt:MAD    0.290    -0.896   -0.003   0.040    -0.085   -0.108    -0.070    -0580
```

The best model explaining the probability of grazing for zebras was composed of Treatment, Age, Sex, NDVI, Season, the number of months after death and an interaction between the treatment and the number of months after death. This interaction was negative, meaning the older the carcass site, the lower the probability of grazing on the site. The probability of grazing at a site varied with the site ID, with a variance of 0.65 and a standard deviation of 0.80.

Probability of grazing wildebeest

```
Family : Binomial

Link function : logit

Formula: PG ~ Treatment + Age + Sex + NDVI + Season + Water + Water:Season + (1|ID)

   AIC       BIC     logLik   Deviance  Df.resid
  537.0     574.4    -257.5     515.0      210

Scaled residuals:

   Min       1Q      Median      3Q       Max
 -4.0573   -0.9547   -0.1487   0.8651    3.0612

Random effects:

       Name           Variance       Std Dev
 ID    (Intercept)    0.1542         0.3926

Number of obs: 221, groups: ID, 12

Fixed effects:
                        Estimate      Std Error    Z value     Pr(>|z|)
 (Intercept)            -0.63765      0.96116      -0.923      0.356225
 Treatment              0.69894       0.17977      3.888       0.000101      ***
 AgeSA                  0.16699       0.23465      0.712       0.476680
 SexM                   -0.29730      0.19225      -1.546      0.122004
 NDVI                   5.09456       2.23084      2.284       0.022389      *
 SeasonCool_dry         -0.62510      0.65865      -0.949      0.342586
 SeasonHot_dry          -1.05349      0.46330      -2.274      0.022973      *
 Water                  -0.23850      0.07111      -3.354      0.000797      ***
 SeasonCool_dry:Water   0.39657       0.17034      2.328       0.019908      *
 SeasonHot_dry:Water    0.27184       0.07825      3.474       0.000512      ***

Signif. codes:  0 ‘***’ 0.001 ‘**’ 0.01 ‘*’ 0.05 ‘.’ 0.1 ‘ ’ 1

Correlation of Fixed Effects:

          (Intr)   Trt      AgeSA    SexM     NDVI     SnCD     SsHD     W        SnCD:W
 Trt      -0.011
 AgeSA    -0.124   -0.035
 SexM     -0.027   0.045    -0.030
 NDVI     -0769    -0.099   0.122    -0.105
 SnCD     -0.428   0.028    -0.096   0.022    0.192
 SnHD     -0.589   -0.083   -0.039   0.004    0.197    0.482
 W        -0.277   -0.085   -0.014   0.007    -0.273   0.299    0.560
 SnCD:W   0.103    -0.072   0.106    -0.001   0.056    -0.886   -0.224   -0.270
 SnHD:W   0.123    0.098    0.057    -0.042   0.309    -0.276   -0.715   -0.800   0.257
```

The best model explaining the probability of grazing for wildebeests was composed of Treatment, Age, Sex, NDVI, Season, the distance to the closest waterhole and of an interaction between the season and the distance to the closest waterhole. This interaction was positive, meaning that, during

the dry season, the probability of grazing at a site farther from water was higher than during the wet season. The probability of grazing at a site varied slightly with the site ID, with a variance of 0.15 and a standard deviation of 0.39.

Time spent grazing, zebra

```
Linear mixed model fit by REML

Formula :log(TG) ~ Treatment + Age + Sex + Season + (1 | ID)

REML criterion at convergence: 2726.7

Scaled residuals:

   Min       1Q      Median      3Q       Max
 -2.4804   -0.6704   -0.0442   0.6346    3.2851


Random effects:

           Name          Variance      Std Dev
 ID        (Intercept)   0.1135        0.3368
 Residual                1.4866        1.2193


Number of obs: 834, groups: ID, 13

Fixed effects:

                   Estimate      Std Error  df           t value   Pr(>|t|)
 (Intercept)       2.04155       0.14332    31.62995     14.245    2.61e-15  ***
 Treatment         -0.03081      0.08611    825.32101    -0.358    0.720556
 AgeSA             -0.26195      0.12674    821.65220    -2.067    0.039054  *
 SexM              -0.14706      0.09556    823.39532    -1.539    0.124215
 SeasonCool_dry    0.70483       0.11860    787.76400    5.943     4.20e-09  ***
 SeasonHot_dry     0.38290       0.11369    806.15437    3.368     0.000793  ***


Signif. codes:  0 ‘***’ 0.001 ‘**’ 0.01 ‘*’ 0.05 ‘.’ 0.1 ‘ ’ 1


Correlation of Fixed Effects:

              (Intr)     Trt        AgeSA        SexM      SsnCD
 Trt          -0.261
 AgeSA        -0.100     -0.014
 SexM         -0.258     -0.027     0.008
 SsnCD        -0.438     -0.076     0.000        0.111
 SsnHD        -0.433     -0.032     -0.064       0.096     0.596
```

The best model explaining the time spent grazing for zebras was composed of Treatment, Age, Sex, and Season. The time spent grazing at a site varied slightly with the site ID, with a variance of 0.11 and a standard deviation of 0.34.

Time spent grazing, wildebeest

```
Linear mixed model fit by REML

Formula :log(TG) ~ Treatment + Age + Sex + Season + (1 | ID)

REML criterion at convergence: 1176.7

Scaled residuals:

   Min       1Q      Median      3Q       Max
 -2.2491   -0.6499   -0.0644   0.6163    4.1016


Random effects:

           Name          Variance       Std Dev
 ID        (Intercept)   0.000          0.000
 Residual                1.611          1.269


Number of obs: 353, groups: ID, 11

Fixed effects:

                   Estimate      Std Error  df           t value   Pr(>|t|)
 (Intercept)       1.9259        0.1970     347.000      9.778     < 2e-16   ***
 Treatment         0.1239        0.1428     347.000      0.867     0.386
 AgeSA             0.1901        0.1767     347.000      1.076     0.283
 SexM              0.1144        0.1564     347.000      0.732     0.465
 SeasonCool_dry    0.8046        0.1877     347.000      4.287     2.35e-05  ***
 SeasonHot_dry     0.2623        0.2056     347.000      1.276     0.203

Signif. codes:  0 ‘***’ 0.001 ‘**’ 0.01 ‘*’ 0.05 ‘.’ 0.1 ‘ ’ 1


Correlation of Fixed Effects:

           (Intr)       Trt         AgeSA     SexM      SsnCD
 Trt       -0.496
 AgeSA     -0.115       0.032
 SexM      -0.341       0.055       0.049
 SsnCD     -0.717       -0.020      -0.082    0.171
 SsnHD     -0.698       0.160       -0.103    0.030     0.663


optimizer (nloptwrap) convergence code: 0 (OK)

boundary (singular) fit: see help('isSingular')
```

The best model explaining the time spent grazing for zebras was composed of Treatment, Age, Sex, and Season. The time spent grazing at a site did not vary the site ID (variance = 0, Standard deviation = 0).

B3. Supplementary tables

TABLE B1: Description of model variables used in the statistical analysis, and their hypothesized role in visitation and grazing of plains zebra (*Equus quagga*) and blue wildebeest (*Connochaetes taurinus*) at carcass and control sites

Variable	Description	Hypothesis		Source
		Plains zebra	**Blue wildebeest**	
ID	Name of site. Each site comprises a carcass and control pair	Differences are expected both in term of utilization (overall number of times a site is used) and in the number of individuals recorded due to the different spatial location.		
Treatment	Control (non-infectious) or Carcass (infectious)	No differences in the number of individual visiting but higher probability of grazing and longer time spent grazing expected on carcass sites		Turner et al., 2014
MAD (Month After Death)	Number of months after infected animal death	More grazing events expected within the first 12 months after death and up to 30 months. Longer time spent grazing at carcass site within the first 12 months, mainly during the cool and hot dry seasons		Turner et al., 2014
NDVI	Normalized Difference Vegetation Index, recorded every 8 days at a 250 m resolution per ID	Expect more individual on greener areas (younger and more palatable forage, and more movement in high NDVI landscapes Expect higher probability of grazing in high NDVI but time of grazing maxed at average NDVI.		Boyers et al., 2019; Hopcraft et al., 2014

Season	Hot wet (Jan-Apr) Cool dry (May-Aug) Hot dry (Sep-Dec)	More visitation expected in Cool and Hot dry due to the decrease in forage availability. Higher intensity of grazing events in the hot wet season due to increased food availability. Grazing time is expected to be higher during the cool dry season as during the hot wet, the high availability would lead to lower time spent on one spot, while in hot dry, not enough food available at one spot.		Havarua et al., 2014
Water	Distance to the closest perennial water source	Water dependent animals expected close to the water, mostly during dry season		Hopcraft et al., 2014
Pan	Smallest distance to the main Etosha salt pan's edge	Not expected to be affected by the distance to the main Etosha pan's edge	Observed close to, and crossing the main Etosha pan's edge	Author observation (AD, WT)
Age	Adult (> 2 years) Sub-adult (1-2 years)	More adults are expected on each site due to the higher density of adults in the environment. Adult being bigger, they might need to forage more often and for longer than sub-adult.		
Sex	Female Male	More females are expected to graze due to the higher physiological requirement of lactating females, but same time spent grazing as they take more bites per minutes.	Males are bigger than females, but do not feed during the rut (i.e., end of wet season) so we expect more females grazing during the end of the wet season, then no sex differences.	Havarua et al., 2014; Neuhaus and Ruckstuhl, 2002

TABLE B2: The 16 candidate models for each of the three response variables. Only the fixed effect is indicated. A random effect representing the site ID was included in each model. The ':' denotes an interaction between the parameters. NDVI: Normalized Difference Vegetation Index; MAD: Month After Death. Water and Pan represent the distance between from the cameras and the closest waterhole or the main Etosha salt pan's edge.

Models
Treatment + Age + Sex
Treatment + Age + Sex + Season
Treatment + Age + Sex + NDVI
Treatment + Age + Sex + MAD + MAD:Treatment
Treatment + Age + Sex + NDVI + MAD + MAD:Treatment
Treatment + Age + Sex + Season + Water + Pan
Treatment + Age + Sex + NDVI + Season
Treatment + Age + Sex + NDVI + Season + MAD + MAD:Treatment
Treatment + Age + Sex + NDVI + Season + Pan
Treatment + Age + Sex + NDVI + Season + Water
Treatment + Age + Sex + NDVI + Season + Water + Pan + Water:Season
Treatment + Age + Sex + Season + Water + Pan + Water:Season
Treatment + Age + Sex + NDVI + MAD + Season + Water + Pan + Water:Season + MAD:Treatment
Treatment + Age + Sex + NDVI + MAD + Season + Water + Water:Season + MAD:Treatment
Treatment + Age + Sex + NDVI + Season + Water + Water:Season
Treatment + Age + Sex + NDVI + MAD + Season + Pan + MAD:Treatment

B4. Supplementary figures

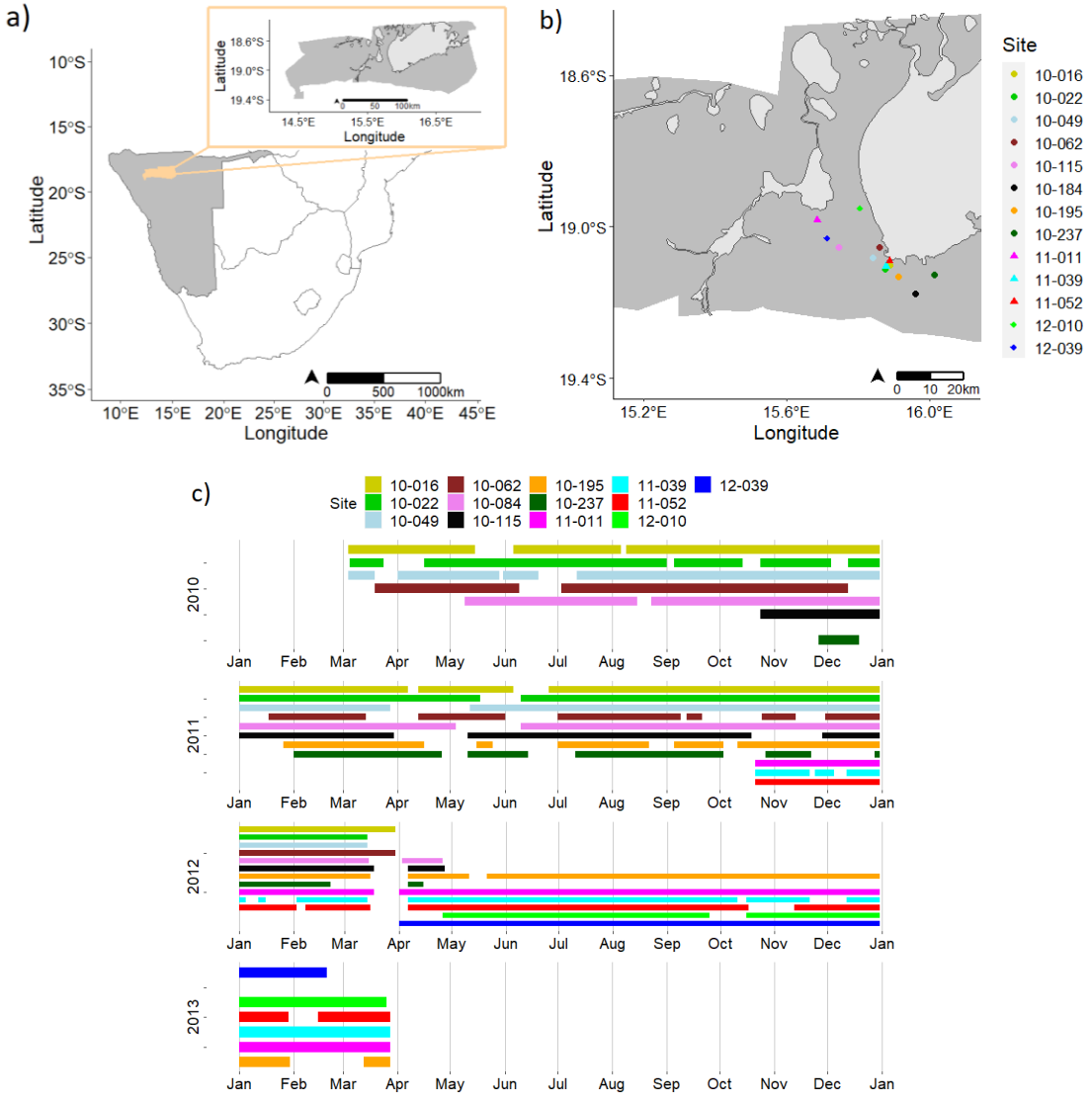

FIGURE B1: Study area and camera trap data collection in Etosha National Park, Namibia. a) Map of Southern Africa with Namibia in grey and Etosha National Park in beige, with an inset of the park. b) Locations of camera sites in the central part of Etosha. Each site was composed of a pair of cameras (carcass and control) situated 100 m from each other. The colour represents the site ID and the shapes the year of death, round is 2010, triangle 2011 and diamond 2012. c) Timetable of site data collection. Pairs of cameras were installed in the field between March 2010 and March 2013. The time represented here indicates that both cameras at a site were functioning.

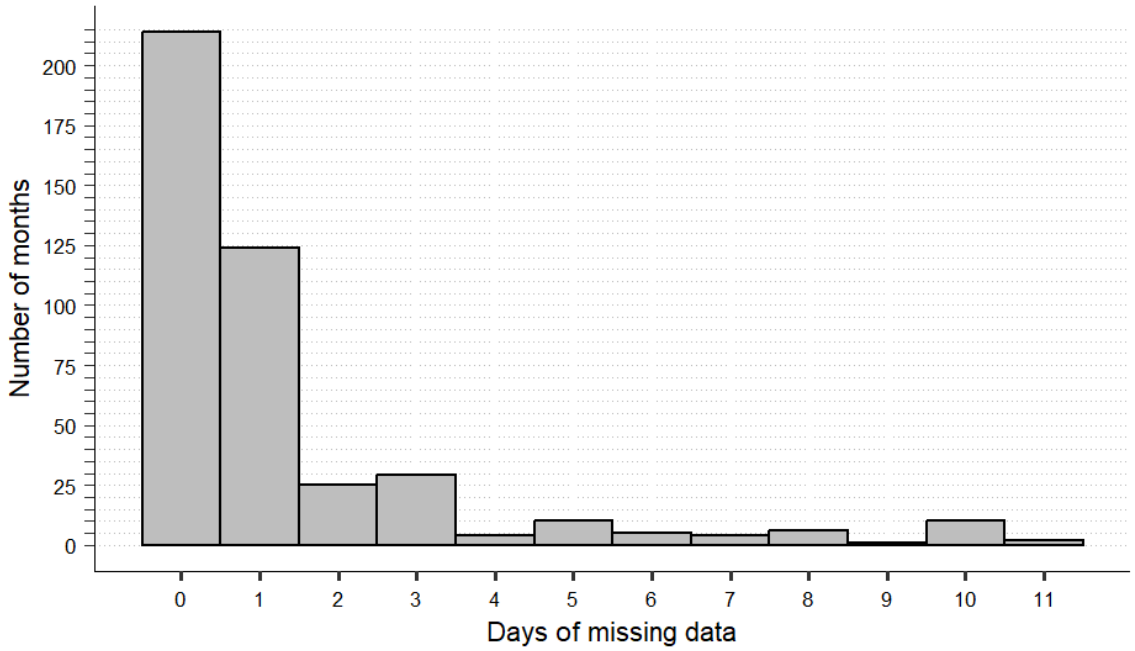

FIGURE B2: Number of days of missing data from a camera per month on recording, for data included in statistical analyses. In total, 219 months of paired recording (carcass and control cameras at a site) were used in the camera trap study analysis, representing 438 months of data from individual cameras. Of those, 340 cameras had 0 or 1 missing day of data. Camera-months with more missing data were excluded from analyses.

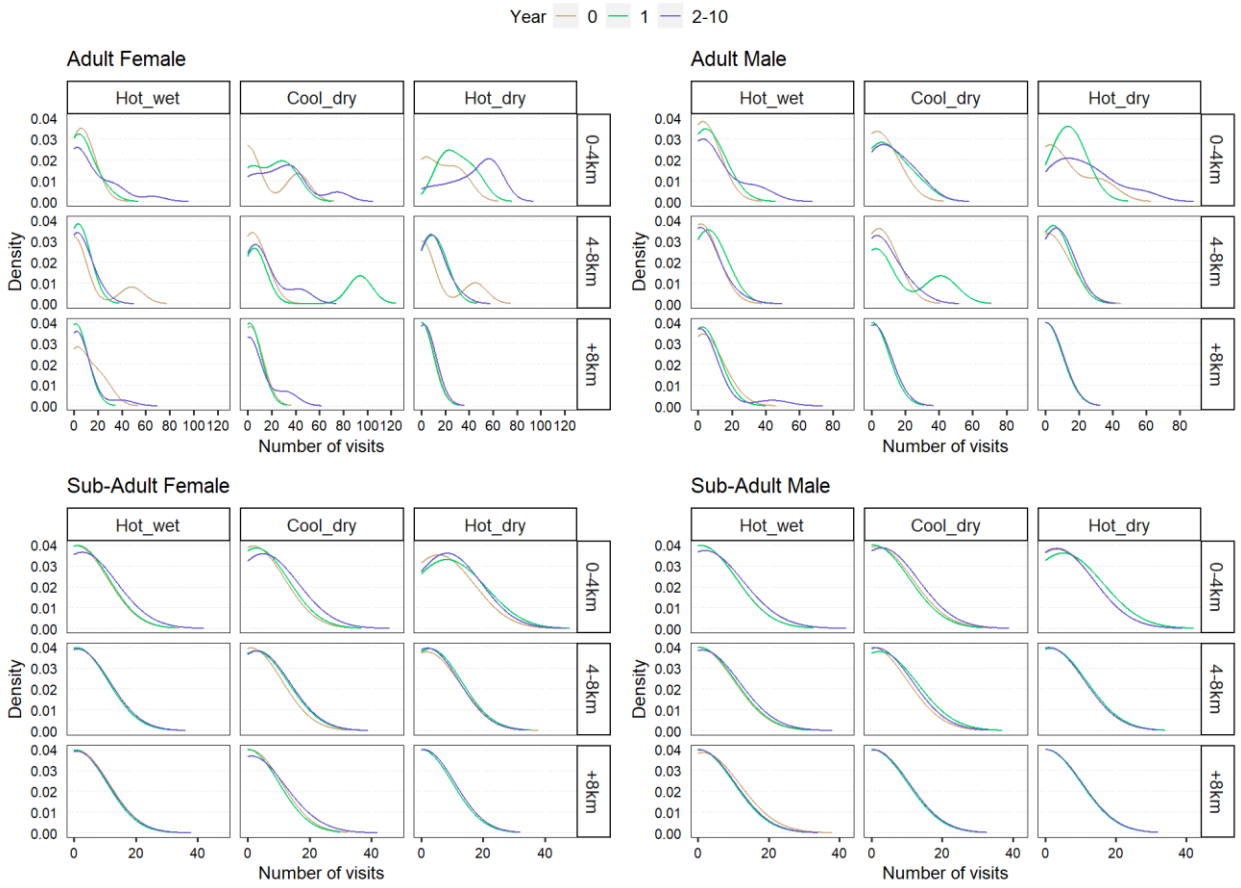

FIGURE B3: Probability density function (PDF) to draw the number of plains zebra (*Equus quagga*) visiting an infectious site. The PDF were constructed using the camera trap dataset and were separated by year after death, season, distance to the closest waterhole, age, and sex based on results of the statistical analysis. We grouped years after death into three categories (years 0, 1 and 2-10) since we found a statistical difference in the number of visits within the first 24 months of death only.

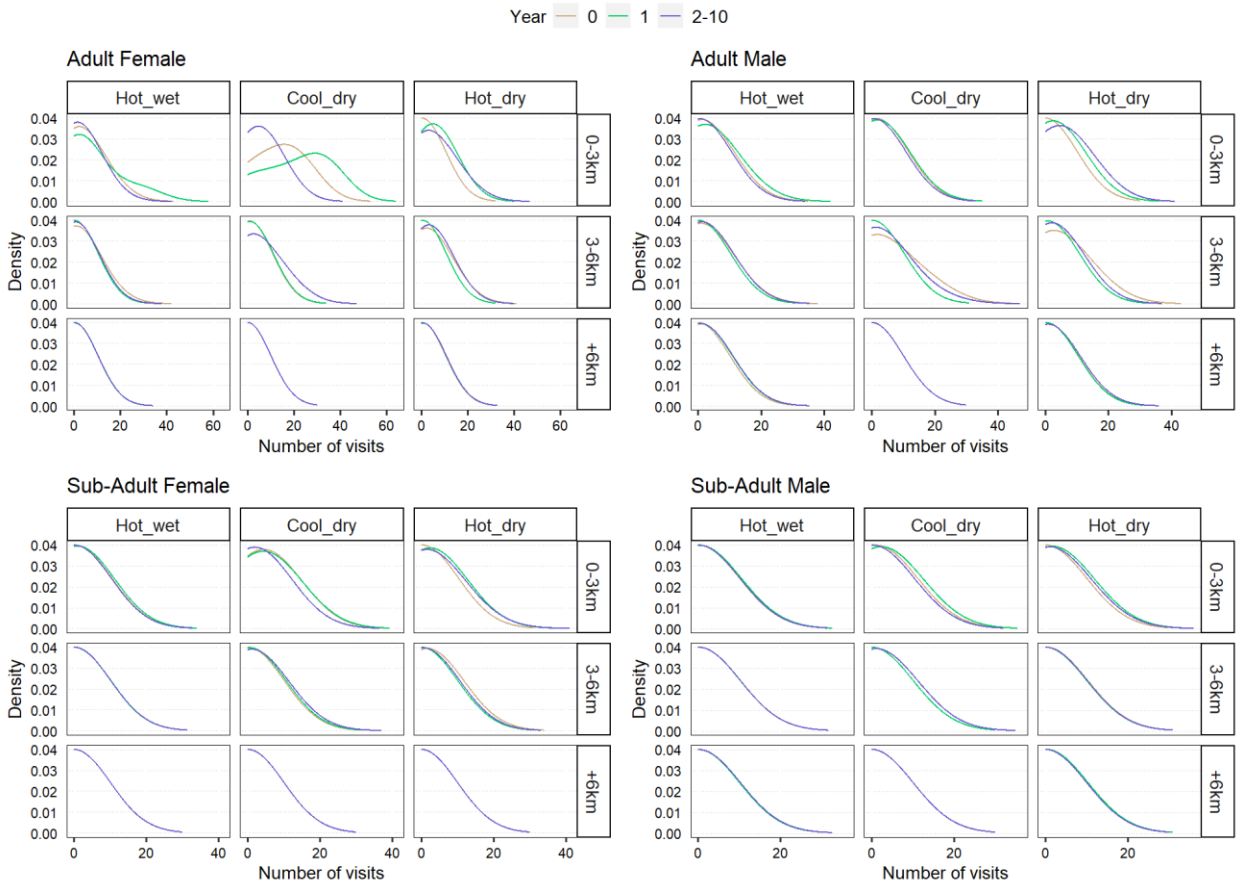

FIGURE B4: Probability density function (PDF) to draw the number of blue wildebeest (*Connochaetes taurinus*) visiting an infectious site. The PDF were constructed using the camera trap dataset and were separated by year after death, season, distance to the salt pan's edge, age, and sex based on results of the statistical analysis. We grouped years after death into three categories (years 0, 1 and 2-10) since we found a statistical difference in the number of visits within the first 24 months of death only.

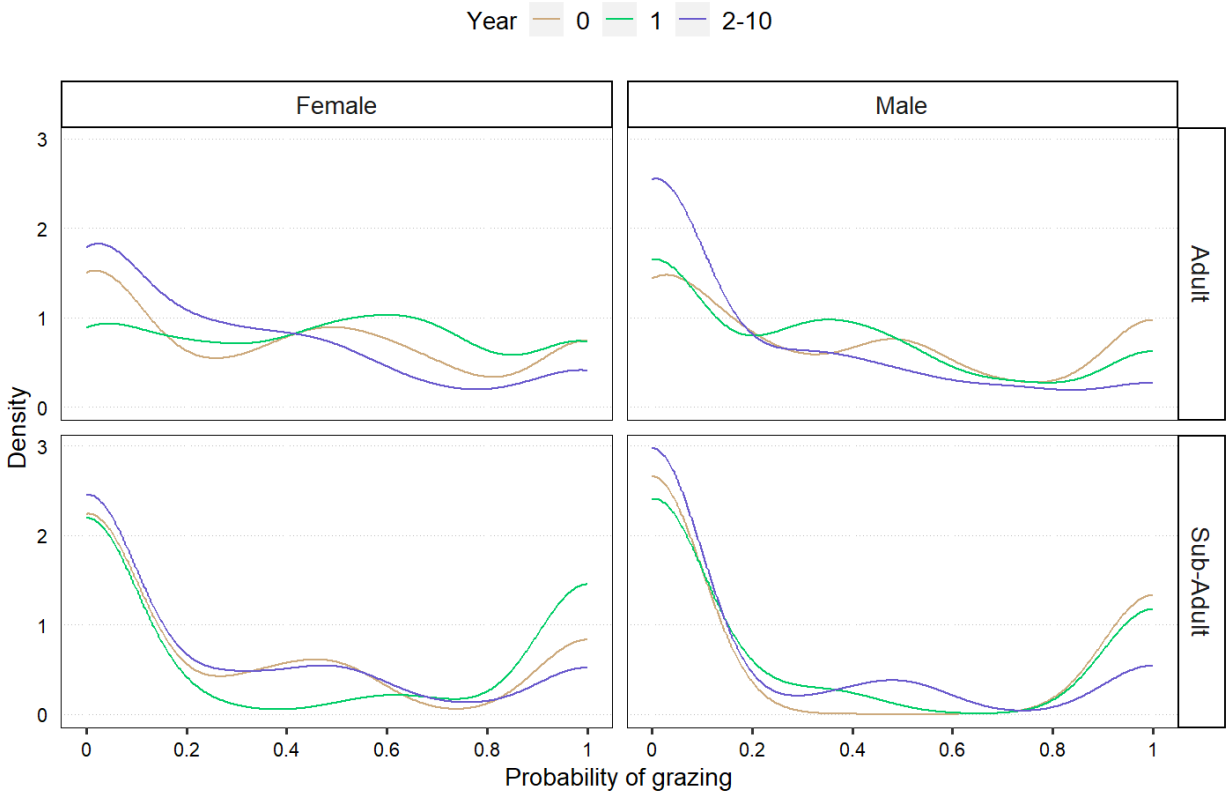

FIGURE B5: Probability density functions (PDF) used to draw the probability of grazing at a site for plains zebra (*Equus quagga*). The PDF were constructed using the camera trap dataset and separated by year after death, age, and sex based on results of the statistical analysis. We grouped years after death into three categories (years 0, 1 and 2-10) since we found a statistical difference in the number of visits within the first 24 months of death only.

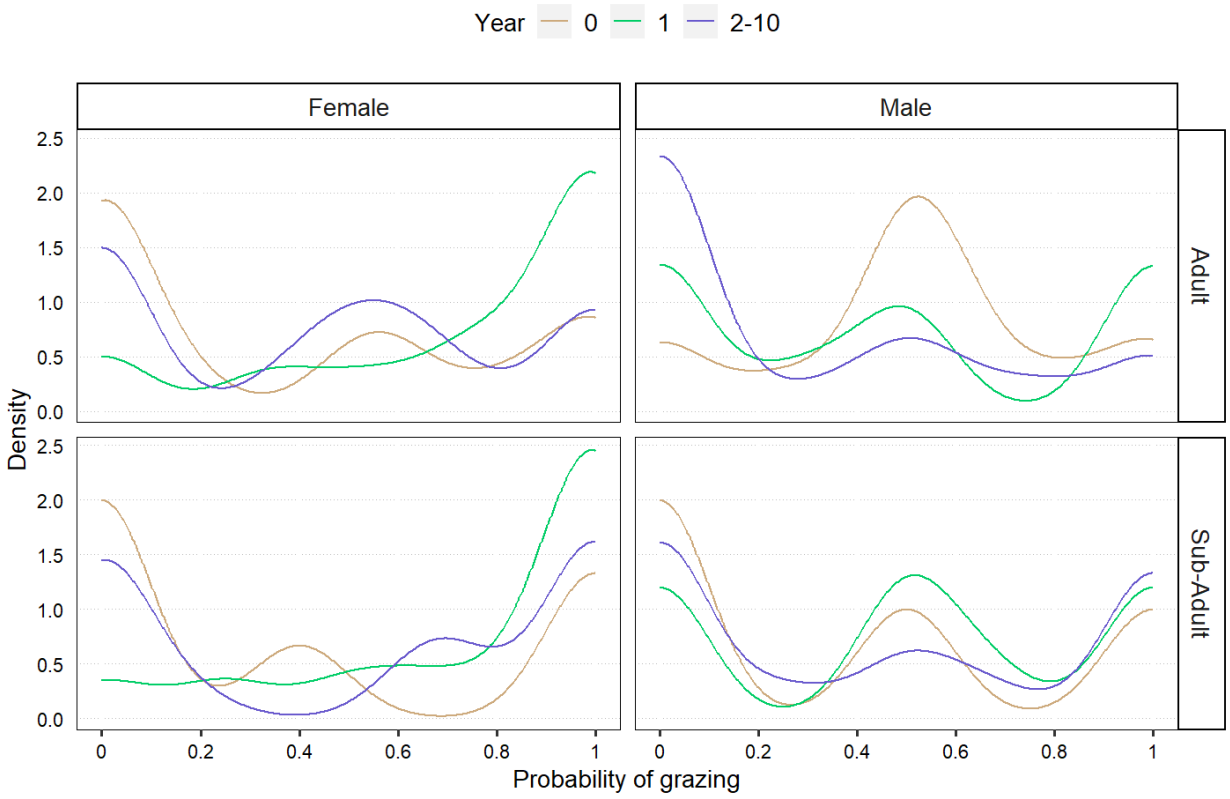

FIGURE B6: Probability density functions (PDF) used to draw the probability of grazing at a site for blue wildebeest (*Connochaetes taurinus*). The PDF were constructed using the camera trap dataset and separated by year after death, age, and sex based on results of the statistical analysis. We grouped years after death into three categories (years 0, 1 and 2-10) since we found a statistical difference in the number of visits within the first 24 months of death only.

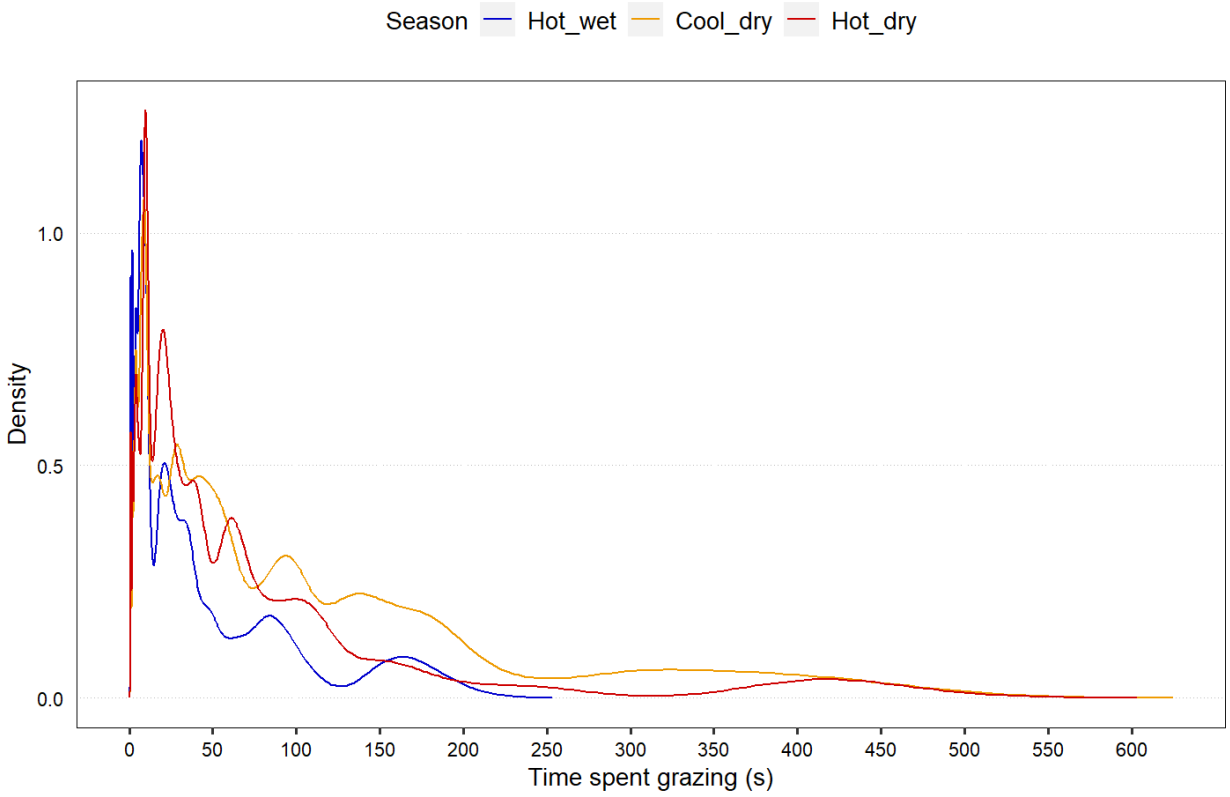

FIGURE B7: Probability density functions (PDF) used to draw the time spent grazing at a site for plains zebra (*Equus quagga*). The PDFs are separated by season. The PDFs were constructed using the camera trap dataset. We chose to construct three PDFs due to significant effects of season detected in the statistical analysis.

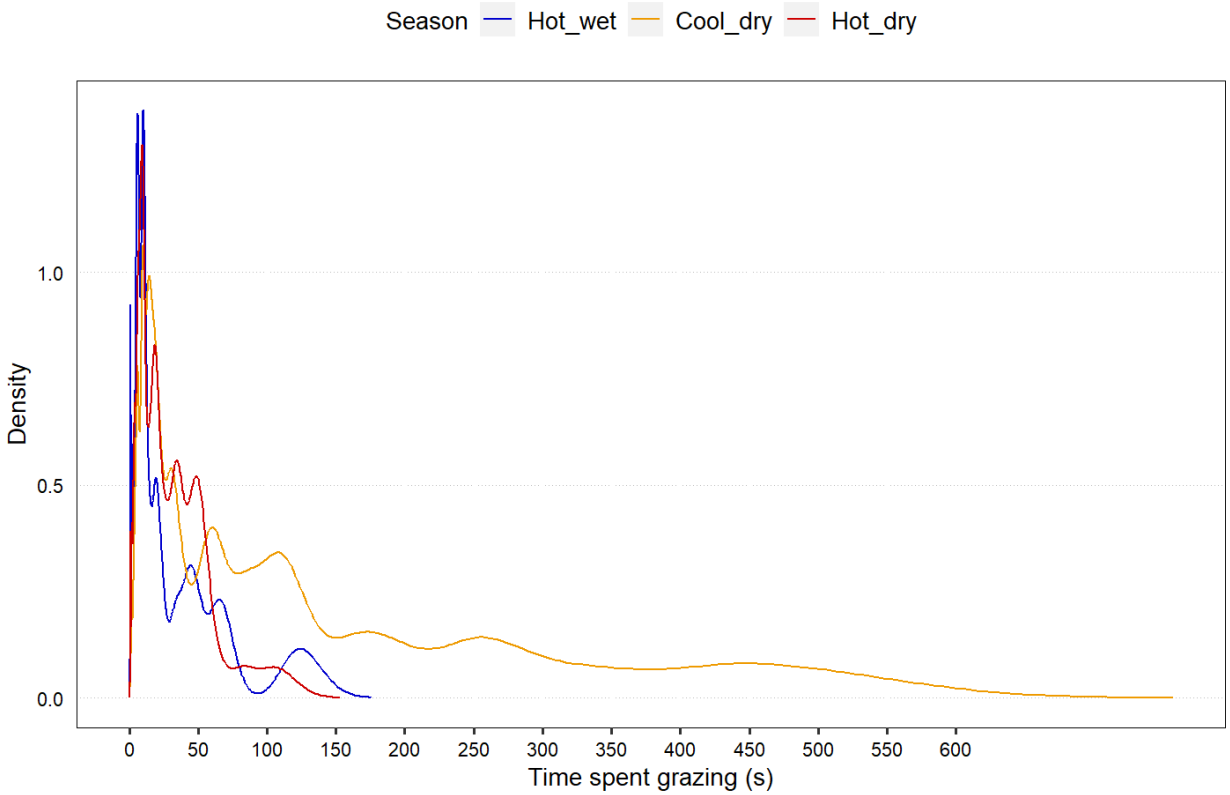

FIGURE B8: Probability density functions (PDF) used to draw the time spent grazing at a site for blue wildebeest (*Connochaetes taurinus*). The PDFs are separated by season. The PDFs were constructed using the camera trap dataset. We chose to construct three PDFs due to significant effects of season detected in the statistical analysis.

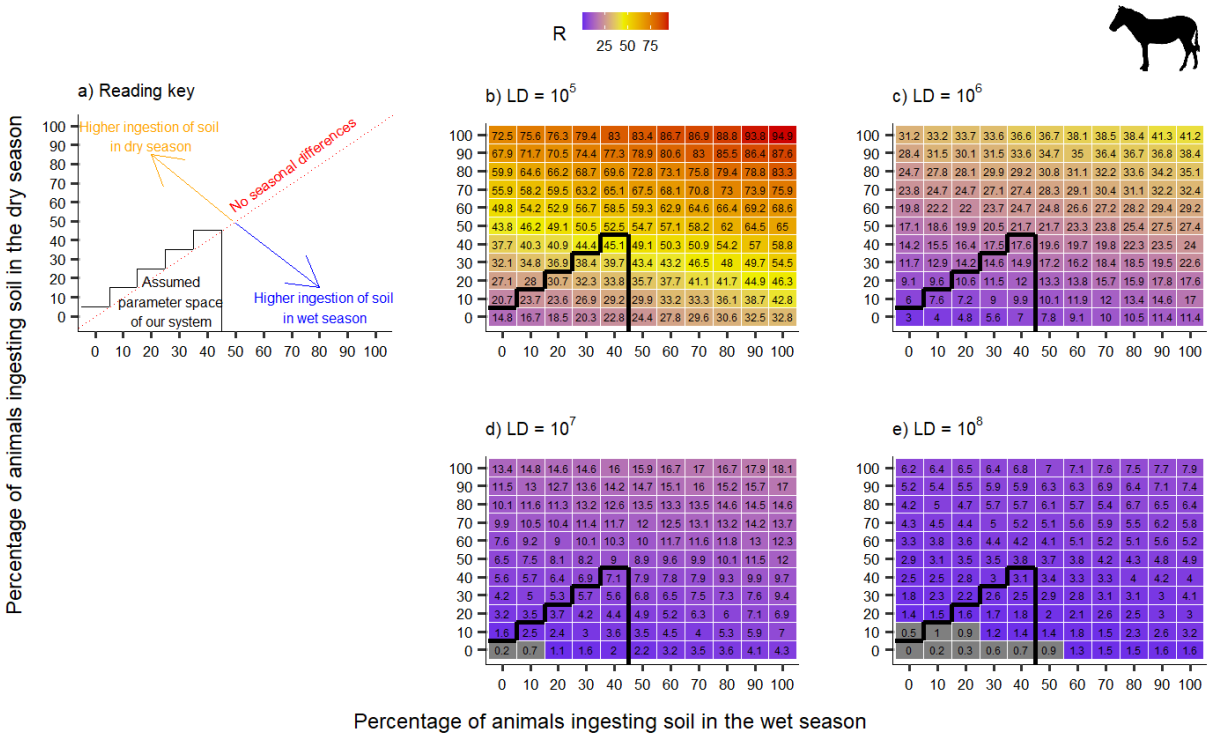

FIGURE B9: Variation in the reproductive number, *R*, of anthrax carcass sites for plains zebras (*Equus quagga*), based on differences in lethal dose (LD) thresholds of *Bacillus anthracis* spores, and percentage of individuals ingesting soil during grazing, estimated over the 10-year lifetime of a reservoir site. The percentage of animals ingesting soil while grazing is varied from 0-100%. In all cases, animals are ingesting 10% soil, 90% grass (by weight) if soil is consumed. Soil contact during foraging is considered for two seasons, wet season (numbers below the diagonal) and dry season (numbers above the diagonal). The *R* values falling along the diagonal represent no difference in soil exposure by season. The black line represents the most likely parameter space for the study system. The grey tiles represent a $R<1$, then a colour gradient is used for $R>1$. a= reading key, bcde = zebra *R* for lethal dose thresholds of 10^5, 10^6, 10^7, 10^8, respectively.

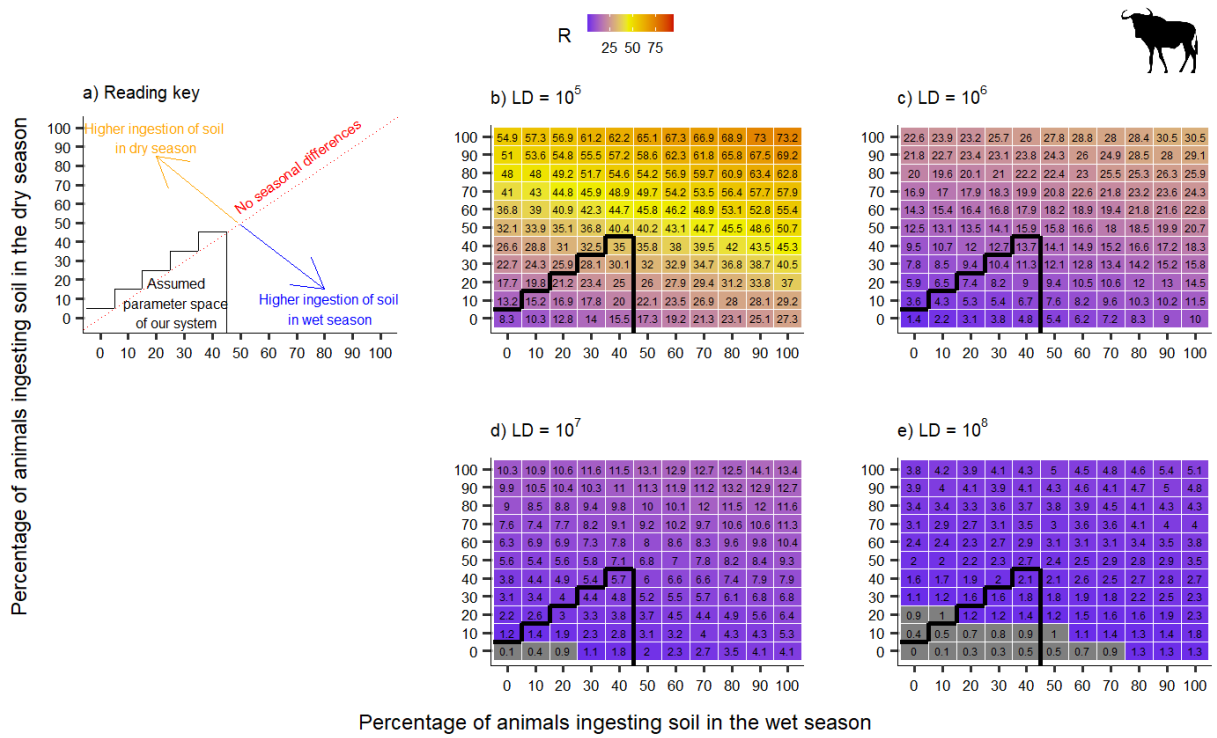

FIGURE B10: Variation in the reproductive number, *R*, of anthrax carcass sites for blue wildebeest (*Connochaetes taurinus*), based on differences in lethal dose (LD) thresholds of *Bacillus anthracis* spores, the percentage of individuals ingesting of soil during grazing, estimated over the 10-year lifetime of a reservoir site. The percentage of animals ingesting soil while grazing is varied from 0-100%. In all cases, animals are ingesting 10% soil, 90% grass (by weight) if soil is consumed. Soil contact during foraging is considered for two seasons, wet season (numbers below the diagonal) and dry season (numbers above the diagonal). The *R* values falling along the diagonal represent no difference in soil exposure by season. The black line represents the most likely parameter space for this disease system. The grey tiles represent a $R<1$, then a colour gradient is used for $R>1$. a= reading key, bcde = wildebeest *R* for lethal dose thresholds of 10^5, 10^6, 10^7, 10^8, respectively.

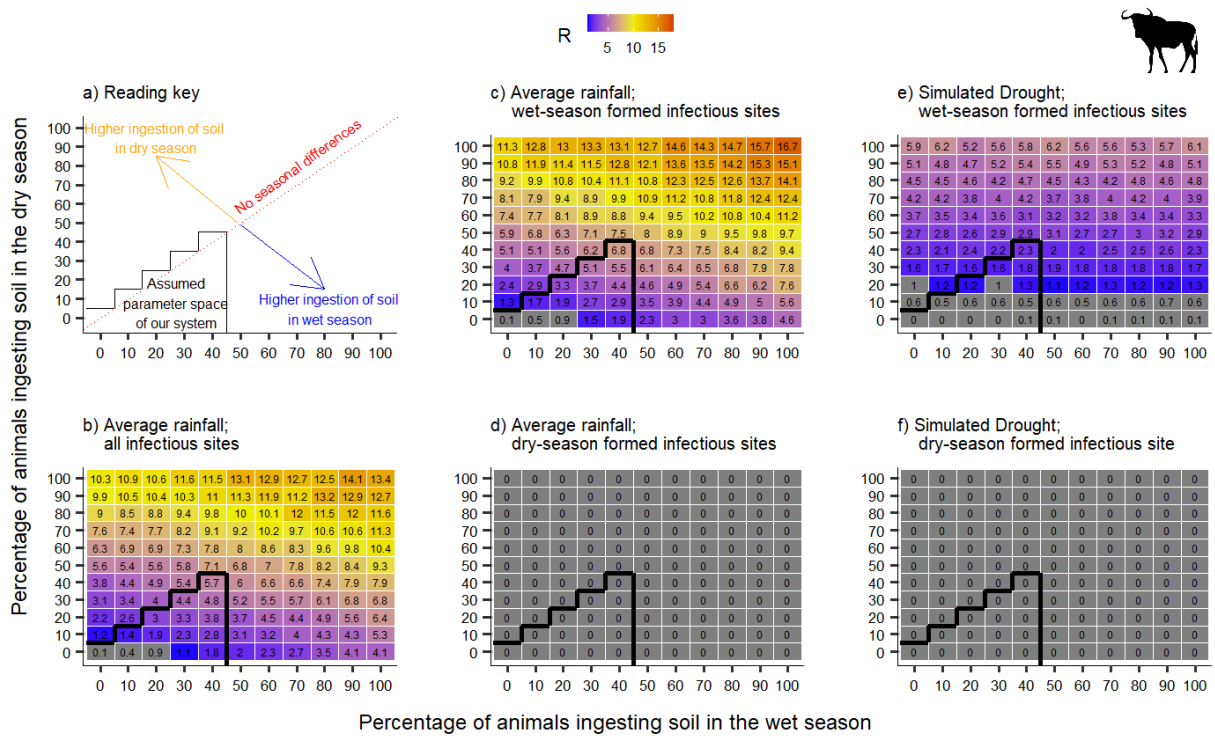

FIGURE B11: Variation in the reproductive number, *R*, for blue wildebeest (*Connochaetes taurinus*) at anthrax carcass sites, for a lethal dose threshold of 10^7 *Bacillus anthracis* spores based on differences in seasonality of host visitation, season of reservoir formation, and percentage of individuals ingesting soil during grazing, estimated over the 10-year lifetime of a *Bacillus anthracis* reservoir site. The percentage of animals ingesting soil while grazing is varied from 0-100%. In all cases, animals are ingesting 10% soil, 90% grass (by weight) if soil is consumed. Soil contact during foraging is considered for two seasons, wet season (numbers below the diagonal) and dry season (numbers above the diagonal). The *R* values falling along the diagonal represent no difference in soil exposure by season. The black line represents the most likely parameter space for the study system. The grey tiles represent a $R<1$, then a colour gradient is used for $R>1$. a= Reading key, b= all host and reservoir data, c = visitation rates under good rainfall, wet season reservoir, d= visitation rates under good rainfall, dry season reservoir, e= visitation rates under

simulated drought, wet season reservoir, f= visitation rates under simulated drought, dry season reservoir.

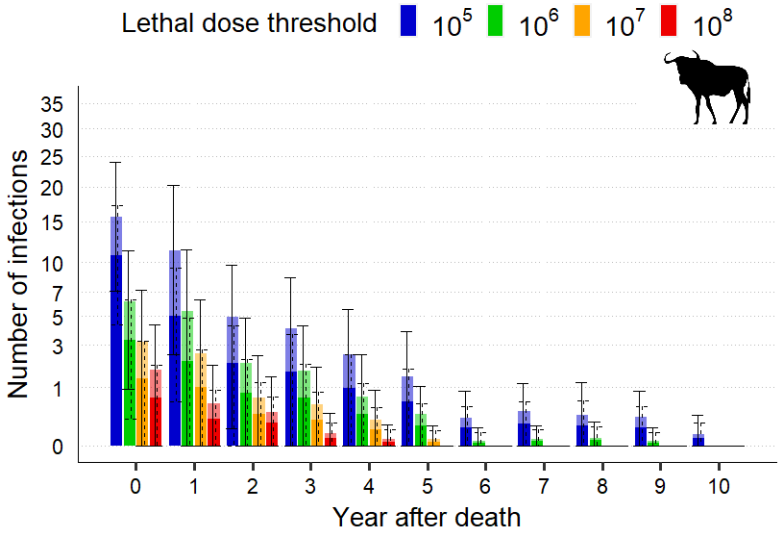

FIGURE B12: Variation in the average number of blue wildebeest (*Connochaetes taurinus*) secondary anthrax mortalities occurring per year after death at a carcass site, depending on the lethal dose threshold of *Bacillus anthracis* spores ingested. The opaque colour and dotted error bars represent the average number of infections within the assumed parameter space of our system, i.e., the percentage of animals ingesting soil while grazing is varied from 0-40%. The transparent bar and solid error bar represent the average number of infections for the entire parameter space, i.e., the percentage of animals ingesting soil while grazing is varied from 0-100%. The y-axis is square root transformed to better visualize small numbers. Error bars representant the standard deviation of the outputs.

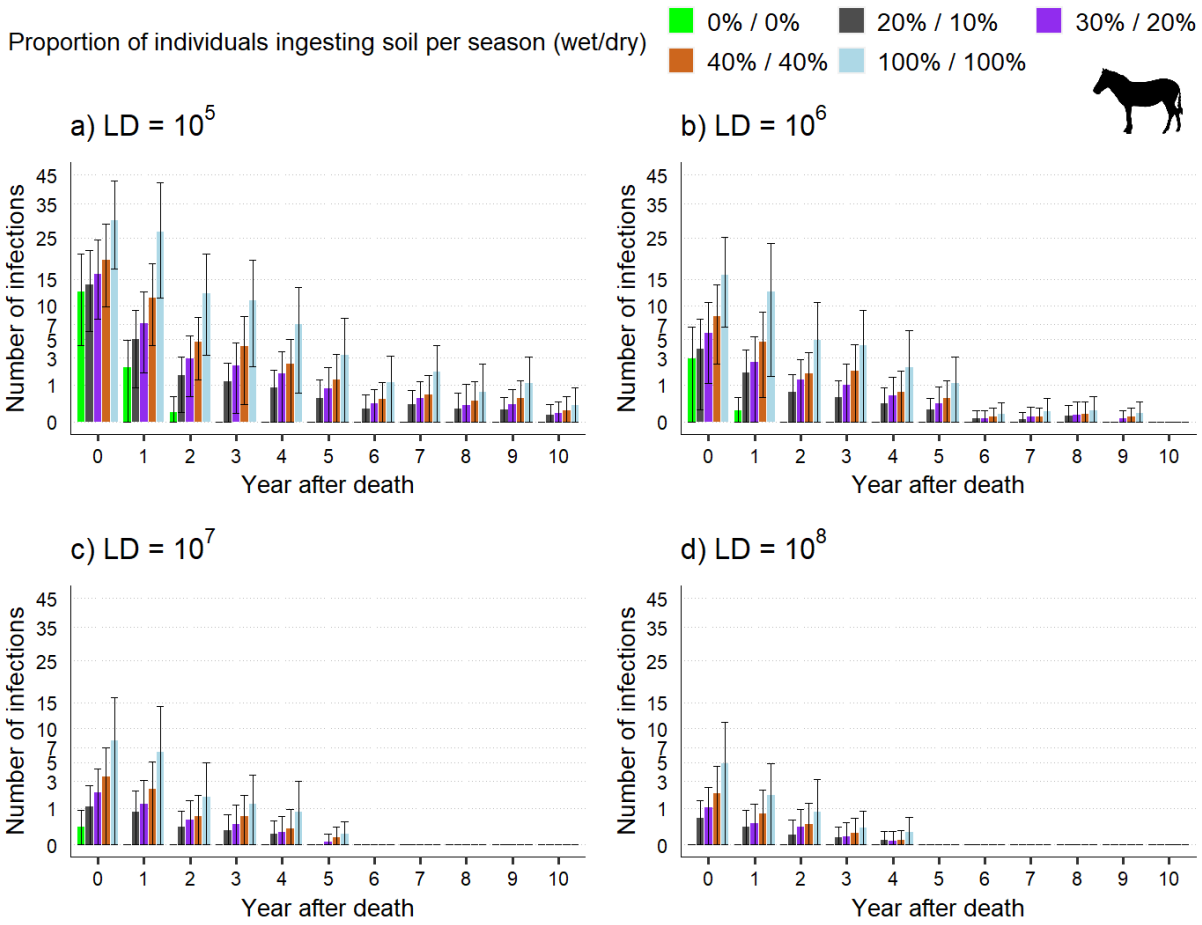

FIGURE B13: Variation in the number of secondary anthrax infections in plains zebra (*Equus quagga*) over time, depending on the lethal dose threshold of *Bacillus anthracis* spores and the proportion of individuals ingesting soil when grazing (set at 10% of intake mass) during the wet (ω_{wet}) and dry (ω_{dry}) seasons. When no soil is ingested ($\omega_{wet} = 0\%$ / $\omega_{dry} = 0\%$), no lethal infections are recorded after three years. When the proportion of individuals ingesting soil increases, the number of infections increases, as well as the period during which an infectious site can infect new host. The y-axis is square root transformed to better visualize small numbers.

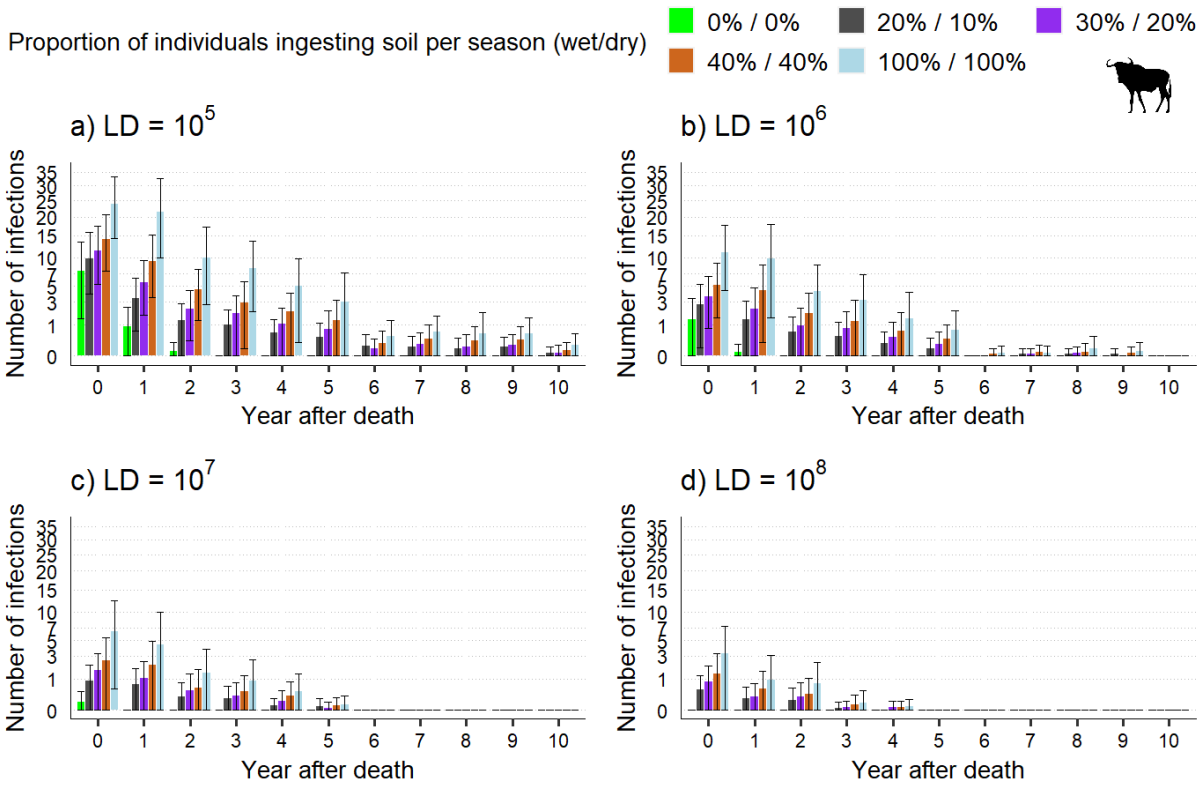

FIGURE B14: Variation in the number of secondary anthrax infections in blue wildebeest (*Connochaetes taurinus*) over time, depending on the lethal dose threshold of *Bacillus anthracis* spores and the proportion of individuals ingesting soil when grazing (set at 10% of intake mass) during the wet (ω_{wet}) and dry (ω_{dry}) seasons. When no soil is ingested (ω_{wet} = 0% / ω_{dry} = 0%), no lethal infections are recorded after three years. When the proportion of individuals ingesting soil increases, the number of infections increases, as well as the period during which an infectious site can infect new host. The y-axis is square root transformed to better visualize small numbers.

B5. References

Boyers, M., Parrini, F., Owen-Smith, N., Erasmus, B.F.N., Hetem, R.S., 2019. How free-ranging ungulates with differing water dependencies cope with seasonal variation in temperature and aridity. Conserv. Physiol. 7, coz064. https://doi.org/10.1093/conphys/coz064

Havarua, Z., Turner, W.C., Mfune, J.K.E., 2014. Seasonal variation in foraging behaviour of plains zebra (*Equus quagga*) may alter contact with the anthrax bacterium (*Bacillus anthracis*). Can. J. Zool. 92, 331–337. https://doi.org/10.1139/cjz-2013-0186

Hopcraft, J.G.C., Morales, J.M., Beyer, H.L., Borner, M., Mwangomo, E., Sinclair, A.R.E., Olff, H., Haydon, D.T., 2014. Competition, predation, and migration: individual choice patterns of Serengeti migrants captured by hierarchical models. Ecol. Monogr. 84, 355–372. https://doi.org/10.1890/13-1446.1

Neuhaus, P., Ruckstuhl, K.E., 2002. The link between sexual dimorphism, activity budgets, and group cohesion: the case of the plains zebra (*Equus burchelli*). Can. J. Zool. 80, 1437–1441. https://doi.org/10.1139/z02-126

Skinner, J.D., Chimimba, C.T., 2005. The mammals of the Southern African sub-region, 3rd ed. Cambridge University Press, Cambridge. https://doi.org/10.1017/CBO9781107340992

Turner, W.C., Kausrud, K.L., Krishnappa, Y.S., Cromsigt, J.P.G.M., Ganz, H.H., Mapaure, I., Cloete, C.C., Havarua, Z., Küsters, M., Getz, W.M., Stenseth, N.Chr., 2014. Fatal attraction: vegetation responses to nutrient inputs attract herbivores to infectious anthrax carcass sites. Proc. R. Soc. B Biol. Sci. 281, 20141785. https://doi.org/10.1098/rspb.2014.1785

APPENDIX C: Supplementary materials for Chapter three

C1. ODD Protocol

The model description follows the ODD (Overview, Design concepts, Details) protocol for describing individual- and agent-based models, as updated by Grimm et al., (2020). The model was coded using R software (version 4.3.2, R Core Team, 2023).

C1.1 Purpose and patterns

The model's purposes are to understand what drives the seasonality and endemicity of anthrax outbreaks in Etosha National Park, Namibia (hereafter Etosha). Specifically, we are interested in how host movement and population dynamics, anthrax persistence in the environment, and environmental rainfall conditions affect anthrax outbreaks in this landscape.

First, we built our base model representing Etosha anthrax outbreaks; then we varied key parameters and assessed the role of each parameter in shaping the resulting outbreaks, both in terms of seasonality and size.

C1.2 Entities, state variables, and scales

The model includes two agents: herds of anthrax hosts, and anthrax reservoirs. The environment is defined using grid cells representing the geographical locations of Etosha at a $250m^2$ spatial resolution.

The herds of hosts' (referred to as hosts hereafter) state variables are:

- The foraging type, split into four categories (i) Non-selective grazers (e.g., plains zebra (*Equus quagga*)); (ii) Selective grazers (e.g., blue wildebeest (*Connochaetes taurinus*)); (iii) Small-bodied mix-feeders (e.g., springbok (*Antidorcas marsupialis)*); (iv) Large-bodied mix-feeders (e.g., African elephant (*Loxodonta africana*))

- The herd grid cell location
- The herd disease status: ‘S’ for susceptible, ‘I’ for infected,
- The number of infected individuals within the herd

The anthrax reservoir agents' state variables are:

- The reservoir grid cell location
- The reservoir's infectivity risk, defined as the probability of infection given effective contact

The grid cells’ state variables are:

- The landscape type, defined as five categories: (i) Sandveld, (ii) Mopane woodland, (iii) Mopane shrubland, (iv) Sweetgrass, and (v) Barrier
- The distance to the closest water point
- The distance to the migration zones (wet and dry season migration zones, see below)

The model runs at a weekly time step (7-days’ time step) for five years.

C1.3 Process overview and scheduling

Processes: The base Etosha model is developed to reproduce outbreaks akin to those empirically observed in the park. Seven processes are used in the model: one related to host movement, two related to host population dynamics, one related to anthrax transmission to hosts, three related to the anthrax infectivity and persistence in the environment (decay of anthrax risk over time, creation of new anthrax reservoirs at host death, the effect of rainfall on anthrax reservoir disappearance), and one related to the environment (seasonal change in environmental quality).

The agents update their state variable at each time step. New agents are created once a year (i.e., every 52 weeks).

Schedule: The simulation starts at a fixed date (July 1st 2010). The environment is initialized, and the host herds and anthrax reservoir agents are placed. Then the sub-models proceed as follows (see Chapter three Material and Method section for the description of each sub-model):

1) Rainfall
2) Hosts movement within the landscape using a resource selection function (RSF)
3) Death of infected hosts and anthrax reservoir creation/ accumulation
4) Probabilistic herd dissolution if death by anthrax occurred
5) Anthrax transmission
6) Environmental anthrax exponential decay
7) Reproduction: New host herd creation; occurs in a single pulse once per year

C1.4 Design concept

Basic principles: The model addressed the role of host movement behavior, anthrax persistence and transmission pathways, and landscape features on the dynamics of anthrax outbreaks in an endemic ecosystem.

Emergence: The main outcomes of the model were the emergent properties of anthrax outbreak size and seasonality among the different hosts' foraging types.

Adaptation: Direct and indirect objective-seeking adaption are present in the model pertaining to host movement. For all hosts, movement decisions depend on vegetation and the distance to water. Indirect memory is included by allowing grazer hosts to migrate along the Etosha Pan's edge during the dry season, and to return to the central region of Etosha during the wet season. GPS tags have empirically shown (personal observations) that wildebeests seldom cross the main Etosha pan, and on the few occasions when they do so, complete the long-distance crossing within

about 2-3 days. Thus, if a simulated host moves into the pan, the model causes them to use a direct, straight movement to cross the pan within a single one-week time step.

Objectives: No objectives

Learning: No learning

Predictions: Host movement is driven by the implicit prediction that vegetation and the distance to water are the primary driver of hosts movement and they are able to optimize their movement choice given the vegetation type and distance to water.

Sensing: Host herds can fully perceive the environment within their 7-day travel distance. They also know the closest waterpoint present within their movement path.

Interaction: No interaction between hosts. Interaction occurs between hosts and anthrax reservoirs. Hosts may become infected upon contact with an anthrax reservoir; the reservoirs are not modified by the hosts. The vegetation is not modified by host presence or foraging.

Stochasticity: Initialization is fixed in the model, but stochasticity arises across the entire model. Rainfall probabilities are drawn using a binomial distribution at every time step. Host movement follows an RSF which is inherently stochastic. The probability of effective contact and transmission risk are stochastic, each following a binomial distribution. The location where infected hosts die and create a new reservoir is drawn using a uniform law within the host movement range. Reproduction is also stochastic and follows a truncated normal distribution.

Collectives: No collectives

Observation: For each simulation, we record three outcomes at each time step. First the environment, host, and reservoir dynamics: Rain (0=No, 1=Yes), number of susceptible and infected hosts per foraging type, and the number of reservoirs. Then, we record the spatial location

of each host herd (i.e., the movement over time); and finally, we record the spatial location and infectivity associated with each reservoir site.

C1.5 Initialization

The model initialization consisted of creating the gridded environment for Etosha and adding host agents to it.

Environmental layer: The environmental layer comprised the vegetation and waterholes at a 250m^2 spatial resolution. Values are initialized using the input environment layer data (see C1.6). We modeled the anthrax prone areas of Etosha where most of our knowledge is based, i.e., everywhere on the east side of Longitude 15.5 East.

Hosts agents: Host agents are placed into the environment using locations from census input data (see C1.6) from Etosha. Each host starts the simulation as '*Susceptible'*.

Anthrax agent: We used the anthrax mortality data from Etosha (see C1.6) to initialize the anthrax layer in the landscape.

C1.6 Input data

All input data related to Etosha were shared by Etosha Ecological Institute (EEI).

Landscape: We used Etosha vegetation and functioning waterholes files to initialize the environments in which the model takes place. We used the vegetation characterization from Le Roux et al., (1988) and compiled the different layers into five distinct categories: (i) mopane woodland, (ii) mopane shrubland, (iii) sandveld, (iv) sweetgrass, and (v) barrier (i.e., the pans). We used EEI's records of functional waterpoints for the waterhole distribution as of 2006.

Rainfall: We used daily rainfall data from 1990-2013 to obtain our monthly rain probability. We summed the rainfall per week for each week, and if the rainfall was above 10mm, we considered the rain enough to create ephemeral surface water usable by the hosts to satisfy their weekly water

requirements. We then calculated the probability of a random week in a given month having rainfall above 10mm (i.e., within a month, all weeks were assumed to have equal probability of >10mm of rainfall). While there is a marked rainfall gradient in ENP from east to west (average of 260mm in the east and 520mm in the west, EEI), we used the same rainfall parameterization for the entire park, as most of the simulated landscape was a subset of Etosha with generally similar annual rainfall (most of the simulated park falls within the 400mm-450mm rainfall range [Le Roux et al., 1988]).

Host spatial distribution: We used the July, 2015 aerial census (Kilian, 2015) to initialize the spatial location of our host herds. We collapsed the different anthrax host species in Etosha into classes based on foraging preferences and typical movement capacity (i.e., small versus large home ranges): (i) non-selective grazers being 'Grazer1', (ii) selective grazer being 'Grazer2', (iii) small-bodied mixed-feeder being 'Mixed-feeder1', and (iv) large-bodied mixed-feeder being 'Mixed-feeder2'. The census recorded the location and number of individuals of each species observed during transect observations. As we are working with herds, we assumed that each census point represented a herd in our model.

Anthrax cases: Anthrax mortalities and their locations were obtained from 1988-2020. As we know that anthrax persist for about 10 years in Etosha (Barandongo et al., 2023), we used all anthrax cases recorded from January 2000 to June 2010, and started our simulation on July 2010.

C1.7 Sub-models

See the detailed description of the sub-models in the Materials and methods section of the main text in Chapter three. Each sub-model used different parameters; the values of fixed parameters are given in Table C1.

C2. Supplementary Tables

TABLE C1: Agent-based model parameters for anthrax transmission in Etosha National Park, Namibia. All parameters in this table are fixed for all scenarios tested (see Chapter three Matrial and Method).

		Grazer1	Grazer2	Mixed-feeder1	Mixed-feeder2
Resource selection function parameters					
Sandveld (β)	Wet	0.3	0.3	1	0.5
	Dry	0.5	0.5	0.5	1
Mopane Woodland (β_1)	Wet	0.4	0.4	0	0.5
	Dry	1	1	1	0.8
Mopane Shrubland (β_2)	Wet	0.8	0.7	1	1
	Dry	0.7	0.6	0.7	0.8
Sweet grass (β_3)	Wet	0.9	1	1.5	1
	Dry	0.7	0.6	0.5	0.5
Barrier (β_4)	Wet	-3	-2	-3	-3
	Dry	-3	-1	-3	-3
Distance to water (β_5)	Wet	-2	-2	-2	-2
	Dry	-1	-1	-1	-1.5
Distance to migrating zone (β_6)	Wet-zone	1	1	1	1
	Dry-zone	1	1	1	1
Contact risk					
Probability of grazing on a reservoir (ξ)	Wet	0.3	0.3	0.3	0.2
	Dry	0.15	0.15	0.15	0.1
Population dynamics					
Birth rate ($\delta \pm$ sd)		0.05	0.05	0.05	0.05
Minimum and maximum birth rate (δ_{min} - δ_{max})		0.01-0.1	0.01-0.1	0.01-0.1	0.01-0.1
Dissolving rate (γ)		0.15	0.1	0.1	0.12

C3. Supplementary figures

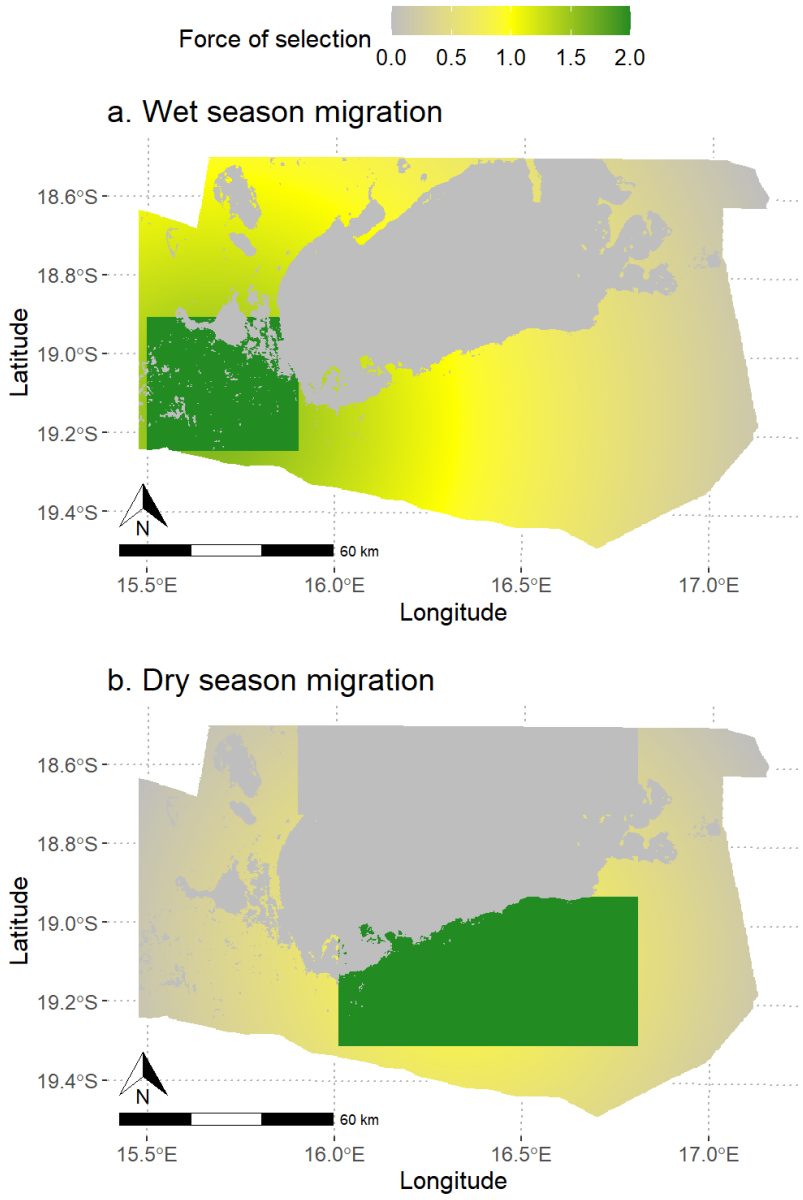

FIGURE C1: Migration zones and associated strength of selection for an agent-based model of anthrax transmission in Etosha National Park, Namibia (dark green = strong selection for a location; grey = strong avoidance of a location). a. Migration zone during the wet season and b. Migration during the dry season.

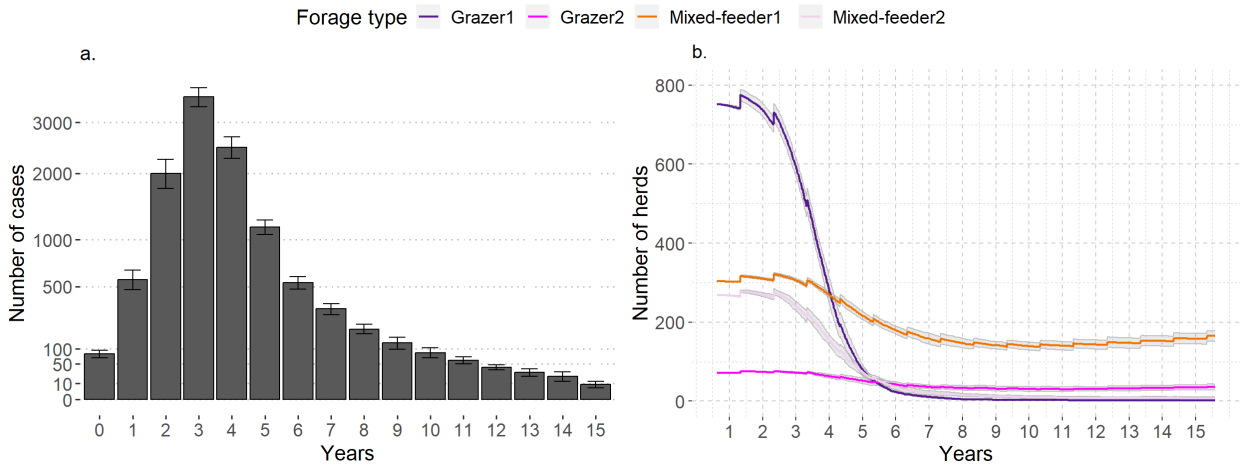

FIGURE C2: Anthrax case numbers and host population sizes from an agent-based model for anthrax transmission in Etosha National Park, Namibia, over a fifteen-years simulation. Results are shown for the scenario with a high density of hosts under wetter conditions, an Etosha-like pathogen decay rate and host range size. In (a) we show the yearly median number of cases over the simulation period; in (b) we show population sizes of the four foraging types of our host agents over time. Grazer1 represents non-selective grazer1 (e.g., plains zebras (*Equus quagga*)); grazer2 are selective grazers (e.g. blue wildebeest (*Connochaetes taurinus*)); mixed-feeder1 are small-bodied mixed feeder (e.g. springbok, (*Antidorcas marsupialis*)) and mixed-fedder2 are large-bodied mixed feeder (e.g. African elephant (*Loxodonta africana*)). Error bars in (a) and the grey ribbon in (b) represent the standard deviations. The y-axis in (a) was square transformed to facilitate the visualization of smaller numbers.

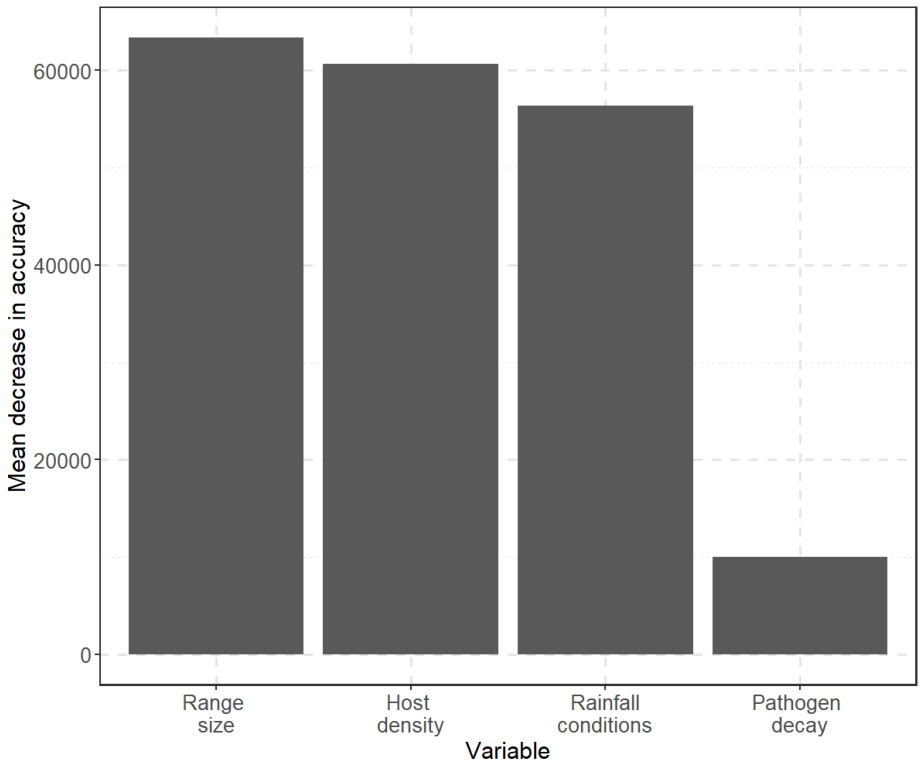

FIGURE C3: Variable importance analysis of the number of yearly median cases generated by an agent-based model of anthrax transmission in Etosha National Park, Namibia. Four main parameters were varied in the simulation: the host range sizes, the host density, the rainfall conditions, and the pathogen decay rate. The y-axis represents the mean decrease in accuracy, a higher number meaning a higher importance of the associated parameter

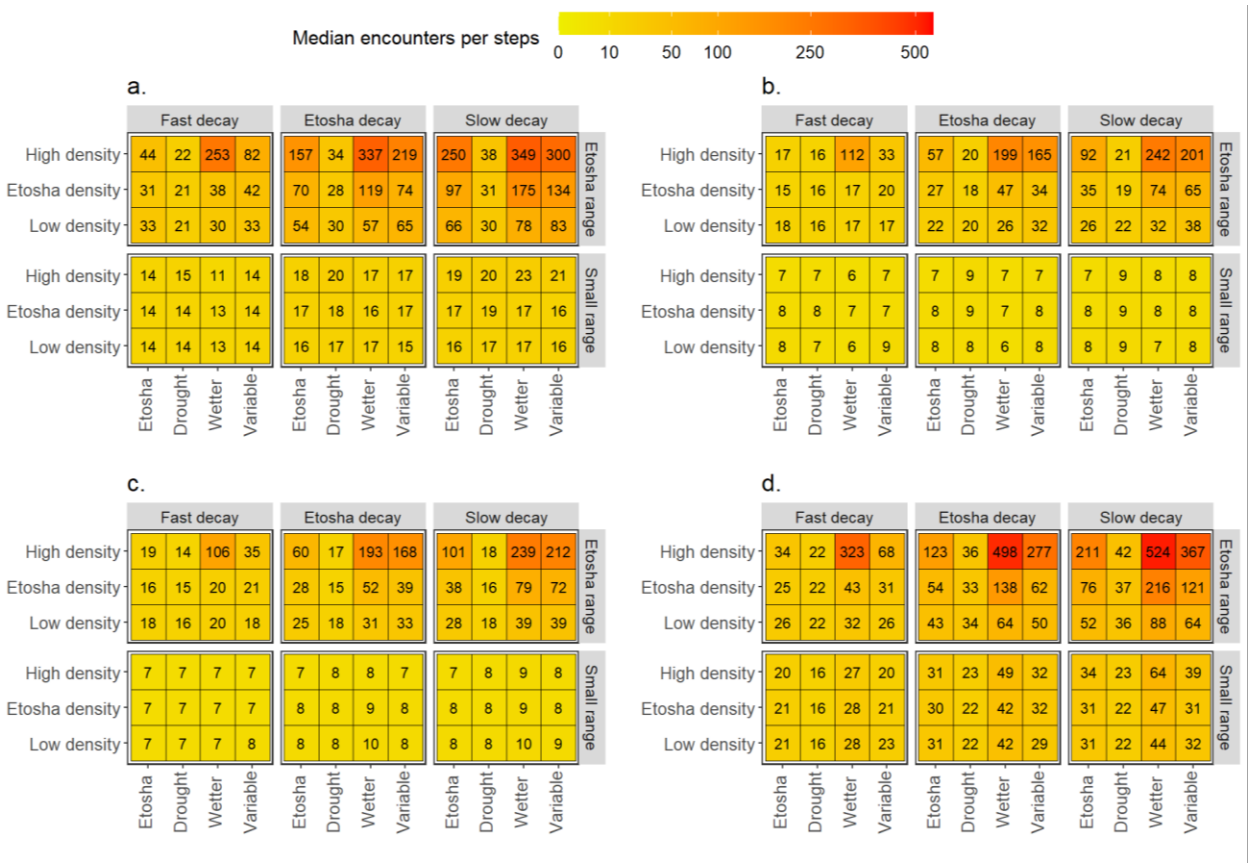

FIGURE C4: Average number of encounters between a host herd and anthrax reservoirs in a five-year simulation of an agent-based model of anthrax transmission in Etosha National Park, Namibia. (a) represents Grazer1, i.e., non-selective grazers such as plains zebra (*Equus quagga*). (b) represents Grazer2, i.e., selective grazers such as blue wildebeest (*Connochaetes taurinus*). (c) represents Mixed-feeder1, i.e., small-bodied mixed-feeders such as springbok (*Antidorcas marsupialis*). (c) represents Mixed-feeder2, i.e., large-bodied mixed-feeders such as African elephant (*Loxodonta africana*). The x-axis represents the rainfall conditions parameter, the y-axis represents the host density parameter. The panel rows are divided by the home range sizes of the hosts, and the columns by the decay rate of the pathogen in the environment. The 'Etosha' parameters are representative of observed conditions in Etosha. The redder the tiles, the higher the number of encounters.

C4. References

Barandongo, Z.R., Dolfi, A.C., Bruce, S.A., Rysava, K., Huang, Y.-H., Joel, H., Hassim, A., Kamath, P.L., van Heerden, H., Turner, W.C., 2023. The persistence of time: the lifespan of *Bacillus anthracis* spores in environmental reservoirs. Res. Microbiol., Insights into the Bacillus anthracis cereus thuringiensis 2022 conference 174, 104029. https://doi.org/10.1016/j.resmic.2023.104029

Grimm, V., Railsback, S.F., Vincenot, C.E., Berger, U., Gallagher, C., DeAngelis, D.L., Edmonds, B., Ge, J., Giske, J., Groeneveld, J., Johnston, A.S.A., Milles, A., Nabe-Nielsen, J., Polhill, J.G., Radchuk, V., Rohwäder, M.-S., Stillman, R.A., Thiele, J.C., Ayllón, D., 2020. The ODD protocol for describing agent-based and other simulation models: A second update to improve clarity, replication, and structural realism. J. Artif. Soc. Soc. Simul. 23, 7. https://doi.org/10.18564/jasss.4259

Kilian, J.W., 2015. Aerial survey of Etosha National Park: Internal report to the Ministry of Environment and Tourism.

Le Roux, C.J.G., Grunow, J.O., Bredenkamp, G.J., Morris, J.W., Scheepers, J.C., 1988. A classification of the vegetation of the Etosha National Park. South Afr. J. Bot. 54, 1–10. https://doi.org/10.1016/S0254-6299(16)31355-2

R Core Team, 2023. R: A language and environment for statistical computing. R Foundation for Statistical Computing, Vienna, Austria.